

This electronic thesis or dissertation has been downloaded from the King's Research Portal at <https://kclpure.kcl.ac.uk/portal/>



## Understanding local respiratory toxicity and bioavailability of inhaled pesticides in an occupational exposure setting

Enlo-Scott, Zachary

*Awarding institution:*  
King's College London

The copyright of this thesis rests with the author and no quotation from it or information derived from it may be published without proper acknowledgement.

### END USER LICENCE AGREEMENT



Unless another licence is stated on the immediately following page this work is licensed

under a Creative Commons Attribution-NonCommercial-NoDerivatives 4.0 International

licence. <https://creativecommons.org/licenses/by-nc-nd/4.0/>

You are free to copy, distribute and transmit the work

Under the following conditions:

- Attribution: You must attribute the work in the manner specified by the author (but not in any way that suggests that they endorse you or your use of the work).
- Non Commercial: You may not use this work for commercial purposes.
- No Derivative Works - You may not alter, transform, or build upon this work.

Any of these conditions can be waived if you receive permission from the author. Your fair dealings and other rights are in no way affected by the above.

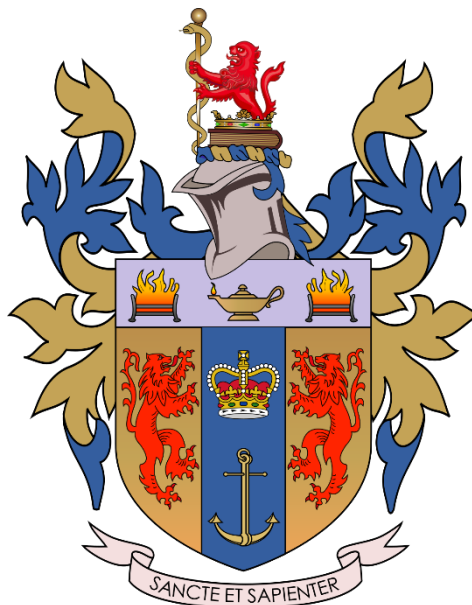
### Take down policy

If you believe that this document breaches copyright please contact [librarypure@kcl.ac.uk](mailto:librarypure@kcl.ac.uk) providing details, and we will remove access to the work immediately and investigate your claim.

# **Understanding local respiratory toxicity and bioavailability of inhaled pesticides in an occupational exposure setting.**

**Zachary Enlo-Scott**

**A thesis submitted in partial fulfilment  
of the requirement for the degree of  
Doctor of Philosophy (PhD)**



**Institute of Pharmaceutical Science**

**King's College London**

**September 2021**

## Abstract

**Background:** Occupational exposure to xenobiotic aerosols may occur within different settings, with a common example being the unintentional inhalation of pesticide aerosols sprayed to protect various crops. Current regulatory guidelines do not exploit emerging *in vitro* toxicity models and make the unvalidated assumption that 100% of the inhaled pesticide is absorbed into systemic circulation, in stark contrast to oral or dermal routes of exposure, which use established evidence-based *in vitro* and *in silico* methods, in addition to *in vivo* models. The assumption of 100% respiratory bioavailability overlooks several established clearance mechanisms, such as mucociliary clearance and lung metabolism. Data-driven approaches for predicting toxicity and estimating respiratory bioavailability based on experimental evidence are therefore urgently needed and have important implications for future risk assessments. This body of work is focused on (i) the suitability of *in vitro* respiratory models, (ii) the use of *in vitro* and *in silico* data for toxicokinetic predictions and (iii) NMR metabolomics as a sensitive measure of changes to lung cell phenotype following pesticide exposure at subtoxic concentrations.

**Methods:** To address these knowledge gaps regarding regional respiratory toxicity throughout the airway and bioavailability of xenobiotics in an occupational exposure setting, several experimental methods were employed alongside *in silico* modelling approaches. Epithelial cell models (RPMI-2650, Calu-3, 16HBE14o-, BEAS-2B, TT1 and A549), reflecting different regions of the airway were utilised to investigate the toxicity, permeability and metabolism of a range of pesticides. The results from these respiratory models were compared against the gastrointestinal epithelial cell line Caco-2, which has been more widely employed in the field. Techniques used included various cytotoxicity assays, Phase I and II metabolism studies to highlight enzyme activity in the different models, NMR metabolomics to assess the changes to lung cell phenotype at subtoxic xenobiotic concentrations, and permeability studies using various Transwell models (Calu-3, Caco-2, PAMPA and lung lipid extract), alongside *in vitro* protein binding assays. Additionally, *in vitro* data was paired with *in silico* predictions for lung deposition and pharmacokinetics to predict the bioavailability of inhaled xenobiotics in an occupational exposure scenario.

**Results:** Significant differences were found in the suitability of the different biological models for assessing toxicity, metabolism and permeability within the lungs. The effect of the physicochemical properties of different xenobiotics on the predicted bioavailability following

inhalation was also shown to be substantial. Finally, in addition to cytotoxicity, several changes to cell phenotype were observed following realistic (and non-cytotoxic) pesticide exposure concentrations of 1-10  $\mu\text{M}$ . Cytotoxicity, mitochondrial inhibition, CYP1A1 induction and increased intracellular glutathione were observed at within this concentration range for various pesticides, whilst chlorothalonil 20  $\mu\text{M}$  was found to be capable of causing epithelial damage to Calu-3 cells cultured at air-liquid interface.

**Conclusion:** This study confirmed that the assumption of 100% bioavailability for inhaled pesticides is often an overestimate and regional airway models may better predict the actual dose fraction reaching the systemic circulation. These *in vitro* data combined with *in silico* approaches highlight the potential to improve predictions of respiratory toxicity and bioavailability and improve future occupational risk assessments for respiratory exposure to xenobiotics.

## **Declaration**

The work in this thesis is based on research performed within the Institute of Pharmaceutical Science, Faculty of Life Sciences and Medicine, King's College London, UK.

I hereby declare that no part of this thesis has previously been submitted in substance for any other degree or qualification, and it is the result of my own work unless otherwise stated in the text.

## Publications

1. Jarvis, I.W., Enlo-Scott, Z., Nagy, E., Mudway, I.S., Tetley, T.D., Arlt, V.M. and Phillips, D.H., 2018. Genotoxicity of fine and coarse fraction ambient particulate matter in immortalised normal (TT1) and cancer-derived (A549) alveolar epithelial cells. *Environmental and molecular mutagenesis*, 59(4), pp.290-301.
2. Mantaj, J., Abu-Shams, T., Enlo-Scott, Z., Swedrowska, M. and Vllasaliu, D., 2018. Role of the basement membrane as an intestinal barrier to absorption of macromolecules and nanoparticles. *Molecular Pharmaceutics*, 15(12), pp.5802-5808.
3. Enlo-Scott, Z., Swedrowska, M. and Forbes, B., 2021. Epithelial permeability and drug absorption in the lungs. In *Inhaled Medicines* (pp. 267-299). Academic Press.
4. Enlo-Scott, Z., Bäckström, E., Mudway, I. and Forbes, B., 2021. Drug metabolism in the lungs: opportunities for optimising inhaled medicines. *Expert Opinion on Drug Metabolism & Toxicology*, pp.1-15.
5. Enlo-Scott, Z., Mudway, IS., and Forbes, B., 2021. Comparison of permeability, drug metabolism and sensitivity to toxicity in human respiratory epithelial cell lines, for the risk assessment of inhaled xenobiotics. (In preparation)
6. Enlo-Scott, Z., Akhmemokhan, P., Charlton, A., Best, M., Avdeef, A., Olsson, B., Mudway, IS. and Forbes, B., 2021. Exposure prediction for inhaled pesticides using data-informed mechanistic pharmacokinetic modelling. (In preparation)
7. Enlo-Scott, Z., Horrocks, V., Charlton, A., Best, M., Mason, AJ., Mudway, IS. and Forbes, B., 2021. NMR metabolomic analysis of changes in respiratory cell phenotype for assessment of inhaled pesticide toxicity. (In preparation)

## Conference Presentations

1. Enlo-Scott, Z., Swedrowska, M., Charlton, A., Merolla, L., Mudway, IS. and Forbes, B., 2018. "Understanding respiratory transepithelial bioavailability and comparative toxicology for human exposure assessments". Poster presentation. *The Joint Pharmaceutical Analysis Group Research Symposium, London, UK.*
2. Enlo-Scott, Z., Swedrowska, M., Charlton, A., Merolla, L., Mudway, IS. and Forbes, B., 2018. "Comparison of human cell lines for risk assessment of aerosolised pesticides". Poster presentation. *Drug Delivery to the Lungs (DDL) Conference, Edinburgh, UK.*
3. Enlo-Scott, Z., Swedrowska, M., Charlton, A., Merolla, L., Mudway, IS., and Forbes, B., 2019. "Comparison of human cell lines for risk assessment of aerosolised pesticides". Poster presentation. *Institute of Pharmaceutical Science, Postgraduate Research Symposium, King's College London, London, UK.*
4. Enlo-Scott, Z., Akhuemokhan, P., Tetley, TD., Mudway, IS., and Forbes, B., 2019. "Comparison of PAMPA to human respiratory epithelial cell lines for the estimation of xenobiotic permeability in the lungs". Poster presentation. *The Joint Pharmaceutical Analysis Group Research Symposium, London, UK.*
5. Enlo-Scott, Z., Akhuemokhan, P., Tetley, TD., Mudway, IS., and Forbes, B., 2019. "Comparison of PAMPA to human respiratory epithelial cell lines for the estimation of xenobiotic permeability in the lungs". Poster presentation. *Drug Delivery to the Lungs (DDL) Conference, Edinburgh, UK.*
6. Z. Enlo-Scott, 2019. "Development of *in vitro* models for assessing the toxicity and bioavailability of inhaled pesticides". Oral presentation. *Association of Inhalation Toxicologists, Brighton, UK.*
7. Enlo-Scott, Z., Avdeef, A., Olsson, B., Mudway, IS., and Forbes, B., 2020. "Computational prediction of xenobiotic respiratory bioavailability in an occupational exposure setting". Oral presentation. *Institute of Pharmaceutical Science, Postgraduate Research Symposium, King's College London, UK (Virtual).*

8. Enlo-Scott, Z., Avdeef, A., Olsson, B., Mudway, IS., and Forbes, B., 2020. "Computational prediction of xenobiotic respiratory bioavailability in an occupational exposure setting". Poster presentation. *The Joint Pharmaceutical Analysis Group Research Symposium, London, UK (Virtual)*.
9. Enlo-Scott, Z., Mudway, IS., and Forbes, B., 2021. "Identification of functional xenobiotic metabolising enzymes in human lung in vitro models". Oral & Poster presentation. *Drug Metabolism Discussion Group, (Virtual)*.
10. Enlo-Scott, Z., 2021. "A combined *in vitro-in silico* approach for the toxicokinetic prediction of inhaled pesticides". Oral presentation. *Association of Inhalation Toxicologists, (Virtual)*.

## Awards

1. CN Davies Award, 2018. "Respiratory bioavailability and comparative toxicology following inhalation of pesticide aerosols". *The Aerosol Society*.
2. Best Scientific Poster, 2018. "Understanding respiratory transepithelial bioavailability and comparative toxicology for human exposure assessments". *The Joint Pharmaceutical Analysis Group Research Symposium*.
3. Best Scientific Poster, 2019. "Comparison of human cell lines for risk assessment of aerosolised pesticides". *Institute of Pharmaceutical Science, Postgraduate Research Symposium, King's College London*.
4. Best 3 minute Thesis Heat, 2020. "Computational prediction of xenobiotic respiratory bioavailability in an occupational exposure setting". *Institute of Pharmaceutical Science, Postgraduate Research Symposium, King's College London*.
5. Best Scientific Poster, 2020. "Computational prediction of xenobiotic respiratory bioavailability in an occupational exposure setting". *The Joint Pharmaceutical Analysis Group Research Symposium, The Royal Society of Chemistry*.
6. Student Prize (Best Poster/Presentation), 2021. "Identification of functional xenobiotic metabolising enzymes in human lung in vitro models". *The Drug Metabolism Discussion Group (DMDG) Open Meeting*.



## Acknowledgements

This thesis would not have been possible without the support and contributions of those around me, who I would like to wholeheartedly extend my thanks.

Firstly, I would like to thank my supervisors, for their support, encouragement and patience. Especially for their belief in my potential, allowing me to take responsibility for this project and guiding my growth as a researcher.

I would like to thank Professor Ben Forbes for his conscious guidance towards focusing on the bigger picture and the impact of my research, whilst still making time to discuss the minutiae of particular experiments. I truly appreciate the countless opportunities he has provided me with, the freedom he has given me to pursue my own research interests and his continued guidance.

I would like to thank Dr Ian Mudway, for his endless support, as well as encouraging me both prior to and during the PhD. It is this that helped me to still be hopeful in the face of the most challenging experiments, confident in my ability and excited by what might be accomplished.

I could not have asked for better supervisors, they have shown me the best aspects of research in academia, allowing passion and independence within my research whilst guiding me around the stumbling blocks.

Secondly, I would like to sincerely thank my thesis progression committee and industrial supervisors; Dr Simon Pitchford, Dr James Mason, Dr Driton Vlassaliu, Dr Alex Charlton and Dr Mark Best for their insightful comments and suggestions, which both enriched my research and widened my perspective. For the technical support with NMR metabolomics, I would like to thank Vicky Horrocks and Dr Adrien Le Guennec. Additional or informal support during my time at King's has also proved to be invaluable, and for that I would like to thank many of those within the Institute of Pharmaceutical Science, particularly Dr Jane Preston and Dr Bahijja Raimi-Abraham for their kind guidance and generous advice.

I would like to thank my friends within King's College London, for keeping me sane and for filling the lab and office with laughter - Precious, Altin, Delaram and Makiko! Magda and Wachirun within our research group, as well as Laura, Sajeel, Osamah, Sevda & Simona.

Finally, a special thank you to my mum, Alice Enlo-Scott for her unconditional and unwavering support and belief in me. It is through her education, perseverance and love that I have been guided through the significant milestones which have shaped who I am today.

# Table of Contents

ABSTRACT .....	- 2 -
DECLARATION .....	- 4 -
PUBLICATIONS.....	- 5 -
CONFERENCE PRESENTATIONS .....	- 6 -
ACKNOWLEDGEMENTS .....	- 8 -
TABLE OF CONTENTS .....	- 9 -
LIST OF TABLES.....	- 13 -
LIST OF FIGURES .....	- 13 -
LIST OF EQUATIONS .....	- 17 -
LIST OF ABBREVIATIONS.....	- 17 -
<b>CHAPTER 1.....</b>	<b>- 21 -</b>
INTRODUCTION .....	- 22 -
1.1 GENERAL INTRODUCTION .....	- 22 -
1.2 RESPIRATORY SYSTEM ANATOMY & PHYSIOLOGY .....	- 23 -
1.3 XENOBIOTIC EXPOSURE (INCLUDING PESTICIDE EXPOSURE).....	- 26 -
1.4 FATE OF THE INHALED AEROSOL.....	- 27 -
1.5 AEROSOL DEPOSITION.....	- 28 -
1.5.1 <i>Dissolution</i> .....	- 30 -
1.5.2 <i>Absorption</i> .....	- 31 -
1.5.3 <i>Metabolism</i> .....	- 36 -
1.5.4 <i>Local toxicity</i> .....	- 38 -
1.6 <i>IN VIVO, EX VIVO, IN VITRO AND IN SILICO</i> MODELS OF THE RESPIRATORY TRACT .....	- 40 -
1.6.1 <i>In vivo models</i> .....	- 40 -
1.6.2 <i>Ex vivo models</i> .....	- 41 -
1.6.3 <i>In vitro models</i> .....	- 44 -
1.6.4 <i>In silico models</i> .....	- 51 -
1.7 AIMS AND SCOPE OF THESIS .....	- 55 -
1.8 RESEARCH QUESTIONS AND OBJECTIVES .....	- 55 -
<b>CHAPTER 2.....</b>	<b>- 57 -</b>
EVALUATION OF <i>IN VITRO</i> RESPIRATORY PERMEABILITY AND TOXICITY MODELS. ....	- 57 -
2.1 INTRODUCTION.....	- 57 -
2.2 AIMS AND OBJECTIVES.....	- 60 -

2.3 METHODS .....	- 61 -
2.3.1 Evaluating common in vitro toxicity models .....	- 61 -
2.3.2 Evaluating common in vitro permeability models .....	- 64 -
2.3.3 Evaluation of commonly used in vitro xenobiotic metabolism models.....	- 71 -
2.4 RESULTS.....	- 77 -
2.4.1 MTT cytotoxicity assay.....	- 77 -
2.4.2 Mechanistic toxicity assay.....	- 79 -
2.4.3 Transepithelial Electrical resistance (TEER).....	- 82 -
2.4.4 Zonula Occludens-1 imaging.....	- 83 -
2.4.5 Permeability assays with fluorescent permeability markers .....	- 84 -
2.4.6 Lipid based permeability models.....	- 85 -
2.4.7 Permeability comparison with all models.....	- 86 -
2.4.8 P-glycoprotein activity .....	- 87 -
2.4.9 Optimisation of resorufin-based metabolism assay .....	- 88 -
2.4.10 EROD assay as a measure of CYP1A1 induction in live 16HBE14o- cells.....	- 89 -
2.4.11 GST induction/inhibition in snap frozen 16HBE14o- cells .....	- 91 -
2.4.12 Comparative xenobiotic metabolism studies.....	- 92 -
2.5 DISCUSSION .....	- 94 -
2.5.1 MTT and mechanistic toxicity assays.....	- 94 -
2.5.2 Permeability .....	- 96 -
2.5.3 Metabolism .....	- 99 -
2.6 CONCLUSION .....	- 102 -
<b>CHAPTER 3.....</b>	<b>- 104 -</b>
TOXICOKINETIC PREDICTION OF PESTICIDES INHALED DURING OCCUPATIONAL EXPOSURE.....	- 104 -
3.1 INTRODUCTION.....	- 104 -
3.2 AIMS AND OBJECTIVES.....	- 106 -
3.3 METHODS .....	- 106 -
3.3.1 Pesticide selection .....	- 106 -
3.3.2 Exposure scenario .....	- 106 -
3.3.3 Respiratory tract model & aerosol deposition prediction .....	- 107 -
3.3.4 Preliminary in vitro assays .....	- 108 -
3.3.5 Radiochemicals and fungicide method quantification.....	- 109 -
3.3.6 $P_{app}$ measurement in vitro.....	- 109 -
3.3.7 $P_{app}$ prediction in silico.....	- 110 -

3.3.8 Protein binding experiments .....	- 110 -
3.3.9 Toxicokinetic prediction .....	- 111 -
3.3.10 Predicted in situ metabolism and toxicokinetic implications .....	- 113 -
3.4 RESULTS .....	- 114 -
3.4.1 Respiratory tract model and aerosol deposition prediction.....	- 114 -
3.4.2 Preliminary in vitro assays .....	- 117 -
3.4.3 Quantification of radiolabelled fungicides .....	- 118 -
3.4.4 $P_{app}$ prediction in vitro and in silico .....	- 120 -
3.4.5 Protein binding assays .....	- 123 -
3.4.6 Toxicokinetic prediction .....	- 126 -
3.4.7 Predicted in situ metabolism and toxicokinetic implications .....	- 132 -
3.5 DISCUSSION .....	- 137 -
3.6 CONCLUSION .....	- 142 -
<b>CHAPTER 4.....</b>	<b>- 143 -</b>
A METABOLOMIC INVESTIGATION INTO RESPIRATORY EPITHELIAL CELL RESPONSES TO PESTICIDE EXPOSURES. .	-
143 -	
4.1 INTRODUCTION.....	- 143 -
4.2 AIMS AND OBJECTIVES.....	- 147 -
4.3 METHODS .....	- 147 -
4.3.1 Experimental design.....	- 147 -
4.3.2 Cell culture conditions.....	- 149 -
4.3.3 Sample generation .....	- 150 -
4.3.4 Alamar Blue cytotoxicity assay .....	- 151 -
4.3.5 NMR metabolomics sample preparation .....	- 151 -
4.3.6 NMR data acquisition.....	- 151 -
4.3.7 Metabolomic data processing and analysis.....	- 152 -
4.4 RESULTS.....	- 154 -
4.4.1 Alamar Blue cytotoxicity assay .....	- 154 -
4.4.2 NMR metabolomics.....	- 157 -
4.5 DISCUSSION .....	- 176 -
4.5.1 Comparison of general metabolomic responses between cell lines .....	- 177 -
4.5.2 Metabolites of interest & potential modes of action for toxicity.....	- 178 -
4.6 CONCLUSION .....	- 181 -
<b>CHAPTER 5.....</b>	<b>- 182 -</b>

GENERAL DISCUSSION .....	- 182 -
5.1 ORIGINAL PREMISE .....	- 182 -
5.2 LOCAL RESPIRATORY TOXICITY AND BIOAVAILABILITY OF INHALED PESTICIDES .....	- 183 -
5.3 CONTRIBUTION TO KNOWLEDGE .....	- 186 -
5.4 EXPERIMENTAL LIMITATIONS.....	- 188 -
5.5 FUTURE WORK .....	- 189 -
5.6 CONCLUSION .....	- 191 -
REFERENCES .....	- 192 -
<b>APPENDIX .....</b>	<b>- 219 -</b>
SUPPLEMENTARY DATA (I).....	- 219 -
SUPPLEMENTARY DATA (II).....	- 225 -
SUPPLEMENTARY DATA (III).....	- 231 -

## List of Tables

Table 1.1. Common drug transporters expressed in the human respiratory tract.....	- 35 -
Table 1.2. A summary of regulatory bodies that require or use acute inhalation data. ....	- 39 -
Table 1.3. Summary of commonly used human cell lines to represent different regions of the respiratory tract. ....	- 48 -
Table 2.1. Cell seeding densities and cell medium composition for the MTT assay.....	- 62 -
Table 2.2.. The substrate and inhibitor combinations and concentrations used for enzyme activity assays for CYP, esterase and GST enzymes in vitro. ....	- 72 -
Table 2.3. Details for human lung S9 fraction donor information .....	- 74 -
Table 2.4. Representative confocal images of ZO-1 fluorescently stained with AlexaFluor 488 (green) and cell nuclei stained with DAPI (blue).....	- 83 -
Table 3.1. Chlorothalonil representative spray application scenarios and inhalation exposures.....	- 107 -
Table 3.2. Predicted vs calculated inputs for Mimetikos Preludium.....	- 125 -
Table 3.3. Summary of key toxicokinetic data predicted using Mimetikos Preludium, for the three fungicides and 3 different models. ....	- 131 -
Table 4.1. A comparison of NMR and LC-MS metabolomic methods .....	- 146 -
Table 4.2. Cell line, passage number and seeding density for the metabolomic experiments..	- 150 -
Table 4.3. Assignments of extracellular metabolites identified by NMR.....	- 158 -
Table 4.4. Summary of OPLS-DA analysis of NMR metabolomics data.....	- 161 -
Table 5.1. Summary of possible future research considerations .....	- 190 -
Table 0.1. Details for MTT calibration curves, including passage number, linear range and R <sup>2</sup> value .....	- 219 -
Table 0.2. Human lung S9 fraction information. Donor details, serology information and enzyme activities.....	- 220 -
Table 0.3. Summary of certificate of analysis data for the radiolabelled pesticides used within Chapter 3. ....	- 226 -
Table 0.4. Summary of key toxicokinetic data predicted using Mimetikos Preludium, for the three fungicides and 3 different models. Data shown is based on for an 8 h exposure during mixing & loading (MMAD = 13.5 µm). ....	- 230 -

## List of Figures

Figure 1.1. Diagram of branching airways, based on the Weibel model. ....	- 24 -
Figure 1.2. Different epithelial cell types and the secretion of surfactant/lung lining fluid. -	- 25 -
Figure 1.3. Aerodynamic diameter .....	- 28 -
Figure 1.4. Different pathways for drug absorption across the respiratory epithelial monolayer. ....	- 31 -
Figure 1.5. Potential non-absorptive clearance mechanisms,.....	- 34 -
Figure 1.6. Summary of substrate promiscuity, for common CYP450 enzymes. ....	- 36 -
Figure 2.1. Chemical reduction of MTT to formazan by mitochondrial dehydrogenases in viable cells. ....	- 61 -
Figure 2.2. An illustration showing the structure of a Transwell insert .....	- 66 -

Figure 2.3. Resorufin based substrates that may be used to measure the activity of xenobiotic metabolism for CYP, esterase or NQO1 activity. ....	71 -
Figure 2.4. GST mediated reaction, using CDNB as a substrate that forms a colorimetric glutathione conjugate. ....	73 -
Figure 2.5. The 96-well plate map and position of each of the S9 fraction samples, for all xenobiotic metabolism reactions ....	76 -
Figure 2.6. Comparison of pesticide LC <sub>50</sub> values between the different respiratory epithelial cell lines ....	77 -
Figure 2.7. Pesticide cytotoxicity as assessed by the MTT assay ....	78 -
Figure 2.8. Mechanistic toxicity assay in the bronchial cell line 16HBE14o- ....	79 -
Figure 2.9. Bubble plot showing mechanistic toxicity assay in the bronchial cell line 16HBE14o- ....	80 -
Figure 2.10. Dose response curve using the mechanistic toxicity assay with 16HBE14o- cells for (A) abamectin, (B) azoxystrobin, (C) chlorothalonil and (D) isopyrazam ....	81 -
Figure 2.11. Transepithelial electrical resistance over 0-22 days for A549, Calu-3, Caco-2, TT1 and RPMI-2650 ....	82 -
Figure 2.12. Transepithelial electrical resistance over 12 days, for TT1 cultured on Transwells precoated with basement membrane extract (BME), co-cultured with 3T3 cells (basolateral side of membrane) or supplemented with synthetic lung fluid (SLF). ....	82 -
Figure 2.13. Interdependence between TEER values for each cell line and P <sub>app</sub> values for (A) sodium fluorescein, (B) rhodamine-123 and (C) FITC-Dextran 4000. ....	84 -
Figure 2.14. P <sub>app</sub> values corresponding to (A) sodium fluorescein and (B) rhodamine-123 transport across Transwells coated with either dodecane (negative control), PAMPA or rat lung lipid extract. ....	85 -
Figure 2.15. Comparative P <sub>app</sub> values for (A) sodium fluorescein, (B) rhodamine-123 and (C) FITC-Dextran 4000, using the permeability barriers created by A549, Calu-3, RPMI-2650, TT1, PAMPA and rat lung lipid extract models. ....	86 -
Figure 2.16. Rhodamine-123 bidirectional transport across (A) A549 or (B) TT1 cell layers, cultured at air-liquid interface on Transwells. ....	87 -
Figure 2.17. Comparative emission values at (A) 595 nm and (B) 635 nm are shown, in addition to (C) relative fluorescence of resorufin subtracted from background fluorescence from ethoxyresorufin. ....	88 -
Figure 2.18. Resorufin calibration curves quantified by fluorescence for the different enzyme assays used to assess functional enzyme expression. ....	89 -
Figure 2.19. EROD activity as a measure of CYP1A1 induction in the bronchial epithelial cell line 16HBE14o-, following a 24 h exposure to 10 µM of a range of pesticides. ....	89 -
Figure 2.20. EROD activity as a measure of CYP1A1 induction in the bronchial epithelial cell line 16HBE14o-, following a 48h exposure to (A) Propiconazole (1.25-10 µM) or (B) β-Naphthoflavone (2.5-20 µM). ....	90 -
Figure 2.21. CDNB-GSH conjugation as a measure of GST activity in the bronchial epithelial cell line 16HBE14o-, following a 24 h exposure to 10 µM of a range of pesticides. ....	91 -
Figure 2.22. Heatmap showing differences between cell lines for % inhibition of NQO1, GST and the CYP isozymes; CYP1A1, CYP1A2, CYP2B6, CYP3A4, CYP3A5. ....	92 -
Figure 2.23. Radar graphs illustrating the xenobiotic metabolism profile of each of the cell lines. ....	93 -
Figure 3.1. Regional lung deposition dependent on median mass aerodynamic diameter. ....	114 -

Figure 3.2. Predicted regional deposition for pesticide aerosols inhaled during occupational exposure. ....	114 -
Figure 3.3. Size distribution of deposited pesticide aerosol (A) 13.5 $\mu\text{m}$ and (B) 35 $\mu\text{m}$ , in relation to region of deposition. ....	115 -
Figure 3.4. Comparison of Syngenta vs Mimetikos Preludium respiratory tract deposition models. ....	116 -
Figure 3.5. TEER values for Calu-3 during a 6 h exposure to azoxystrobin, chlorothalonil, propiconazole 10 $\mu\text{M}$ or DMSO control. ....	117 -
Figure 3.6. FITC-Dextran MW 4000 permeability, across Calu-3 following 6 h apical exposure	117 -
Figure 3.7. Calibration curve using $^{14}\text{C}$ -labelled azoxystrobin, chlorothalonil and propiconazole in HBSS transport medium, 0-5000 nM. ....	118 -
Figure 3.8. Calibration curve using $^{14}\text{C}$ -labelled (A) azoxystrobin, (B) chlorothalonil and (C) propiconazole in the sample matrices used for protein binding experiments, 0-5000 nM. -	119 -
Figure 3.9. Transepithelial electrical resistance over 14 and 21 days, for Calu-3 (Passages 10-12) and Caco-2 (Passages 20-22). ....	120 -
Figure 3.10. $\text{LogP}_{\text{app}}$ data for the three fungicides measured using in vitro models. ....	120 -
Figure 3.11. One-Way ANOVA was used to compare (A) inter-model variability and (B) intra-model variability. ....	121 -
Figure 3.12. Fungicide binding to membrane as a percentage of the total mass applied. -	122 -
Figure 3.13. % Protein binding to (A) Synthetic airway surface liquid or (B) human plasma. ....	123 -
Figure 3.14. Fraction unbound to plasma. ....	124 -
Figure 3.15. Comparison of blood toxicokinetic profiles predicted using Mimetikos Preludium	127 -
Figure 3.16. Azoxystrobin, chlorothalonil and propiconazole blood toxicokinetic profiles following inhalation	128 -
Figure 3.17. Predicted fungicide toxicokinetics in the respiratory epithelium using in vitro Calu-3 $\text{P}_{\text{app}}$ , ASL and plasma protein binding data. ....	129 -
Figure 3.18. Oral bioavailability has been included for the comparison of blood toxicokinetic profiles predicted using Mimetikos Preludium with in silico (pCEL-X) or in vitro data (Caco-2 & Calu-3) ....	130 -
Figure 3.19. Metabolic pathway for azoxystrobin metabolites potentially formed within the lung	132 -
Figure 3.20. Metabolic pathway for potential chlorothalonil metabolites formed within the lung	133 -
Figure 3.21. Metabolic pathway for potential propiconazole metabolites formed within the lung	134 -
Figure 3.22. Caco-2 $\text{P}_{\text{app}}$ values predicted in silico using pCEL-X, for the parent compounds azoxystrobin, chlorothalonil and propiconazole and their respective metabolites. ....	135 -
Figure 3.23. Predicted Caco-2 $\text{P}_{\text{app}}$ and $\text{LogP}$ values using pCEL-X	136 -
Figure 4.1. Diagram indicating the number of original research articles related to metabolomics and pesticide exposure	145 -
Figure 4.2. Categories for the different respiratory epithelial cell lines selected for inclusion in NMR metabolomics studies. ....	148 -
Figure 4.3. Selected fungicides (including mode of action) arranged based on GHS classification. ....	148 -



Figure 4.4. Heatmap showing Alamar Blue cytotoxicity data for A549, TT1, BEAS-2B, 16HBE14o- and Calu-3, following exposure to various fungicides. ....	154 -
Figure 4.5. Individual graphs for (A) A459, (B) TT1, (C) BEAS-2B, (D) 16HBE14o- and (E) Calu-3, showing % cell viability as assessed by the Alamar Blue assay following 24 h fungicide exposure. ....	156 -
Figure 4.6. Example NMR spectra, comparing fresh medium with spent A549 medium..	157 -
Figure 4.7. Oxidative dimerisation of L-cysteine to cystine.....	159 -
Figure 4.8. PCA plot comparing NMR metabolomic spectra for (1) Fresh medium, (2) A549, (3) TT1, (4) BEAS-2B, (5) 16HBE14o- and (6) Calu-3.....	160 -
Figure 4.9. OPLS-DA plots illustrating discrimination of NMR metabolomics spectra for DMSO control in blue vs chlorothalonil 1 $\mu$ M groups .....	161 -
Figure 4.10. Differences in basal metabolism for the different cell lines, normalised against a fresh medium control.....	162 -
Figure 4.11. Boxplots showing differences in normalised extracellular lactate concentration (n=4).....	163 -
Figure 4.12. Differences in A549 metabolism following 24 h exposure to the different fungicides, normalised against the A549 DMSO control. ....	164 -
Figure 4.13. Boxplots showing differences in A549 extracellular pyruvate and lactate concentration .....	165 -
Figure 4.14. Differences in TT1 metabolism following 24 h exposure to the different fungicides.....	166 -
Figure 4.15. Boxplot showing increased acetate production by TT1 following 24 h to isopyrazam.....	167 -
Figure 4.16. Boxplot showing differences in TT1 extracellular pyruvate and lactate concentration .....	168 -
Figure 4.17. Boxplot showing reduced alanine consumption in TT1 following 24 h to chlorothalonil .....	169 -
Figure 4.18. Differences in BEAS-2B metabolism following 24 h exposure to the different fungicides.....	170 -
Figure 4.19. Boxplot showing increased acetate production by BEAS-2B following 24 h to isopyrazam.....	171 -
Figure 4.20. Differences in 16HBE14o- metabolism following 24 h exposure to the different fungicides.....	172 -
Figure 4.21. Boxplot showing increased acetate production by 16HBE14o- following 24 h to isopyrazam.....	173 -
Figure 4.22. Differences in Calu-3 metabolism following 24 h exposure to the different fungicides.....	174 -
Figure 4.23. Boxplot showing increased acetate production by Calu-3 following 24 h to isopyrazam.....	175 -
Figure 4.24. Boxplot showing increased alanine consumption by Calu-3 following 24 h to chlorothalonil 10 $\mu$ M.....	176 -
Figure 0.1. Calibration curves, plotting UV absorbance against cell number for (A) A549 or (B) RPMI-2650, following a 4 h incubation with MTT.....	219 -
Figure 0.2. Bicinchoninic acid (BCA) assay calibration curve .....	220 -
Figure 0.3. (A) CYP1A1 and (B) CYP1A2 functional activity using the EROD and MROD assay, respectively. ....	221 -
Figure 0.4. (A) CYP2B6 and (B) CYP3A4 functional activity using the PROD and BROD assay, respectively. ....	222 -

Figure 0.5. (A) CYP3A5 and (B) NQO1 functional activity using the BROD and resorufin assay, respectively. ....	- 223 -
Figure 0.6. GST functional activity using CDNB assay with and without the GST inhibitor ethacrynic acid 20 $\mu$ M. ....	- 224 -
Figure 0.7. Predicted regional lung deposition data for the generations of the tracheobronchial tree .....	- 225 -
Figure 0.8. Predicted maximum fungicide concentration in (A) lumen or (B) epithelium of the extrathoracic region. ....	- 227 -
Figure 0.9. Predicted maximum fungicide concentration in (A) lumen or (B) epithelium of the tracheobronchial region. ....	- 227 -
Figure 0.10. Predicted maximum fungicide concentration in (A) lumen or (B) epithelium of the bronchiolar region. ....	- 228 -
Figure 0.11. Predicted maximum fungicide concentration in (A) lumen or (B) epithelium of the alveolar region. ....	- 228 -
Figure 0.12. % Mucociliary clearance, predicted using Mimetikos Preludium .....	- 229 -
Figure 0.13. Maximum fungicide concentration in the blood, following an 8 h exposure to either an aerosol with an MMAD of 13.5 or 35 $\mu$ m (GSD=1.5). ....	- 229 -
Figure 0.14. Principal component analysis (PCA) plot comparing NMR metabolomics samples- 231 -	
Figure 0.15. OPLS-DA plots illustrating discrimination between the metabolomic profiles of the DMSO control groups for the different cell lines. ....	- 232 -

## List of Equations

Equation 2.1. % Cell viability .....	- 63 -
Equation 2.2. Transepithelial electrical resistance (TEER) .....	- 65 -
Equation 2.3. Apparent permeability coefficient. ....	- 68 -
Equation 2.4. Efflux ratio .....	- 70 -
Equation 3.1 Rapid equilibrium dialysis, % unbound .....	- 111 -
Equation 3.2 Rapid equilibrium dialysis, % recovery .....	- 111 -
Equation 3.3 Aerosol exposure dose per minute .....	- 112 -
Equation 4.1. % Cell viability (Alamar Blue) .....	- 151 -

## List of Abbreviations

2D	Two-dimensional
3D	Three-dimensional
ADME	Absorption, Distribution, Metabolism & Excretion
ADMET	Absorption, Distribution, Metabolism, Excretion & Toxicity
AhR	Aryl hydrocarbon receptor
AI	Active Ingredient
ALI	Air-Liquid Interface
AOP	Adverse Outcome Pathway
API	Active Pharmaceutical Ingredient
ARDS	Acute respiratory distress syndrome
ASL	Airway surface liquid
BaP	Benzo[a]pyrene
BCRP	Breast cancer resistant protein
BCS	Biopharmaceutics Classification System
BROD	7-benzyloxy-resorufin-O-deethylase
CAR	Constitutive androstane receptor
CDNB	2,4-Dinitrochlorobenzene
CES	Carboxylesterase
CFD	Computational fluid dynamics
CFTR	Cystic fibrosis transmembrane conductance regulator
COPD	Chronic Obstructive Pulmonary Disease
cpm	Counts per minute
CYP	Cytochrome P450
DAPI	4',6-diamidino-2-phenylindole
DMEM	Dulbecco's Modified Eagle Medium
DMF	Dimethyl formamide
DMPK	Drug metabolism and pharmacokinetics
DMSO	Dimethyl sulfoxide
DNA	Deoxyribonucleic acid
dpm	Disintegrations per minute
DPPC	Dipalmitoyl phosphatidylcholine
EDTA	Ethylenediamine tetra-acetic acid

EFSA	European Food Safety Authority
EGF	Epidermal growth factor
EPA	Environmental Protection Agency
EROD	7-ethoxy-resorufin-O-deethylase
ex/em	excitation/emission
F	Bioavailability
FBS	Foetal bovine serum
FD-4	FITC dextran-4000
FDA	Food and Drug Administration
FITC	Fluorescein isothiocyanate
FMO	Flavin-containing monooxygenase
F <sub>oral</sub>	Oral bioavailability
FRC	Forced residual capacity
F <sub>ue</sub>	Fraction unbound to ASL
f <sub>up</sub>	fraction unbound to plasma
GHS	Globally Harmonized System
GIT	Gastrointestinal tract
GSD	Geometric standard deviation
GSH	Glutathione
GSSG	Glutathione disulphide
GST	Glutathione-S-Transferase
HBSS	Hanks balanced salt solution
HC	Hydrocortisone
iBCS	Inhaled Biopharmaceutics Classification System
IPL	Isolated perfused lung
iPSCs	Induced pluripotent stem cells
ITS-X	Insulin, transferrin, selenium & ethanolamine
KBq	Kilobecquerel
KE	Key event
K <sub>p</sub>	fraction bound to tissue
k <sub>p</sub>	Tissue-plasma partition ratio
LC <sub>50</sub>	Lethal concentration at which 50% of the sample population is killed
LC-MS	Liquid chromatography-Mass spectrometry

LD <sub>50</sub>	Lethal dose at which 50% of the sample population is killed
LOD	Limit of detection
LogD	Logarithm of the distribution coefficient
LogP	Logarithm of the partition coefficient
LogS <sub>w</sub>	Intrinsic water solubility
LOQ	Limit of quantification
MBq	Megabecquerel
MCIB	Monochlorobimane
MDR	Multi-drug resistant
MIE	Molecular initiating event
mRNA	messenger ribonucleic acid
MROD	7-methoxy-resorufin-O-deethylase
MRP	Multi-drug resistance associated protein
MTT	3-(4,5-dimethylthiazol-2-yl)-2,5-diphenyl tetrazolium bromide
MW	Molecular Weight
MWCO	Molecular weight cut-off
NADP <sup>+</sup>	Nicotinamide adenine dinucleotide phosphate
NADPH	Nicotinamide adenine dinucleotide phosphate (reduced)
NaF	Sodium fluorescein
NAT	N-acetyl transferase
NC3Rs	National Centre for Replacement, Reduction and Refinement of Animals in Research
NEAA	Non-essential amino acids
NHBE	Normal human bronchial epithelial (cells)
NMR	Nuclear magnetic resonance
NQO1	NAD(P)H dehydrogenase (quinone 1)
OAT	Organic anion transporter
OATP	Organic anion transporting polypeptide
OCT	Organic cation transporter
OPEX	Occupational exposure
OPLS-DA	Orthogonal Projections to Latent Structures Discriminant Analysis
P/S	Penicillin-streptomycin
PAH	Polycyclic aromatic hydrocarbon
PAMPA	Parallel artificial membrane permeability assay

P <sub>app</sub>	Apparent permeability
PAPS	3'-Phosphoadenosine-5'-phosphosulfate
PBPK	Physiologically-based pharmacokinetic
PBS	Phosphate buffered saline
PCA	Principal component analysis
PCB	Polychlorinated biphenyl
PEPT	Peptide transporter
P-gp	P-glycoprotein
PK	Pharmacokinetic
PK <sub>a</sub>	-Log <sub>10</sub> K <sub>a</sub> , where K <sub>a</sub> is the acid dissociation constant
POPC	1-palmitoyl-2-oleoyl-sn-glycero-3-phosphocholine
POR	Cytochrome P450 reductase
PPP	Plant protection product
PQN	Probabilistic Quotient Normalization
PROD	7-pentoxo-resorufin-O-deethylase
PXR	Pregnane X receptor
RA	Retinoic acid
Rh-123	Rhodamine 123
ROS	Reactive Oxygen Species
RPM	Revolutions per minute
SD	Standard deviation
SDS	Sodium dodecyl sulphate
SLC	Solute carrier
SLF	Simulated lung fluid
SP	Sodium pyruvate
SULT	Sulfotransferase
TEER	Trans-epithelial electrical resistance
TK	Toxicokinetic
TMRM	Tetramethylrhodamine
UGT	UDP-glucuronosyltransferase
V <sub>d</sub>	Volume of distribution
XME	Xenobiotic metabolising enzyme
ZO-1	Zonula occludens-1

# Chapter 1

## Introduction

### 1.1 General introduction

The inhalation of xenobiotics represents a major route of administration in the field of drug delivery and exposure in the fields of environmental or occupational toxicology. Xenobiotics are commonly inhaled as aerosols, with a pertinent example being anthropogenic aerosols created and unintentionally inhaled whilst pesticides or plant protection products (PPPs) are sprayed to protect various crops.

Whilst common within the pharmaceutical industry, there is limited use of human-based biological models to assess local respiratory toxicity or xenobiotic bioavailability following inhalation during occupational exposure. This is exemplified by the current lack of *in vitro* experimental models accepted by the regulatory bodies, of which the two main ones are the European Food Safety Authority (EFSA) and the US Environmental Protection Agency (EPA). Despite this, within the EU in 2014 it was estimated that ~400,000 tonnes of PPPs were sold (Rani and Shanker, 2018), with the spray application of these PPPs likely leading to widespread respiratory exposure among agricultural workers. In addition to the large quantity of fungicides, insecticides and herbicides sprayed there is also an increasing variety of PPPs used, with 1457 different active ingredients registered with EFSA of which 455 are currently approved for use (EFSA, 2021).

Additionally, from a general respiratory exposure perspective, there are estimated to be over 10,000 chemicals in commercial production (Timbrell, 1999, Lee, 2012), many of which may potentially be aerosolised, in addition to the wide variety of environmental air pollutants (Wei et al., 2009). Whilst, air pollutants represent an example of chronic exposure and generally reflect lower exposure concentrations than occupational exposure scenarios, air pollution has been identified as one of the main threats to public health in Europe (Annesi-Maesano, 2017) and is undoubtedly a global concern contributing to a wide range of adverse effects on health (Zhao et al., 2021b, Mudway et al., 2020).

With regards to regulatory toxicology, which may span considerations for both drug development, occupational exposure or public health and the environment, there is burgeoning interest in the use of physiologically-based toxicokinetic (PBTK) models,

particularly to enable animal-free risk assessment and obtain information with increased relevance to human exposures (Tonnelier et al., 2012, Armitage et al., 2021, Bessems et al., 2014). Whilst there have been many recent advances to PBTK models, significantly more work is needed to approach the point of widespread regulatory approval (Cohen Hubal et al., 2019), additionally extensive validation is required.

Due to the large requirement for *in vitro* respiratory toxicity testing along with pharmacokinetic/toxicokinetic prediction of inhaled xenobiotic disposition, there is increasing interest in methods for *in vitro* respiratory ADMET experimental methods that may be combined with physiologically-based pharmacokinetic models for the improved evaluation of inhaled exposures.

This thesis outlines the relevant background material in **Chapter 1**, establishing the significant considerations such as respiratory system anatomy and physiology, xenobiotic/pesticide exposure, fate of inhaled aerosols (lung deposition & toxicokinetics), local toxicity mechanisms and common experimental methods to predict and understand local respiratory toxicity and bioavailability. The subsequent chapters, **Chapters 2-4**, outline the investigation and development of experimental approaches to determining xenobiotic respiratory toxicokinetics.

## **1.2 Respiratory system anatomy & physiology**

The respiratory system may be divided into several sections, comprising of the nasal/oral cavity, pharynx, larynx, trachea, bronchi, bronchioles and alveoli, spanning the extrathoracic and thoracic region of the body. The upper respiratory tract is often described as the “conducting zone” in which the nose, pharynx, larynx and trachea may filter, warm and moisten inhaled air before it reaches the lungs. The lower respiratory tract or the “respiratory zone” which consists of the respiratory bronchioles, alveolar ducts and alveoli is the region in which gaseous exchange occurs, with the alveoli predominantly being the site for this process. Gaseous exchange occurs between the external environment at the epithelial surface of the alveoli and the internal pulmonary capillaries (Maina, 2002), and it is this region of the respiratory tract in which xenobiotics are most readily absorbed, due to the large surface area (70-100 m<sup>2</sup>), thin epithelial barrier (<1 µM) and high perfusion (Stone et al., 1992, Wiebe and Laursen, 1995, Mariassy, 1992).

The respiratory tract may be further classified by generations of airways, from the trachea to the alveoli, best illustrated though the Weibel model (Weibel et al., 1963) (**Figure 1.1**).



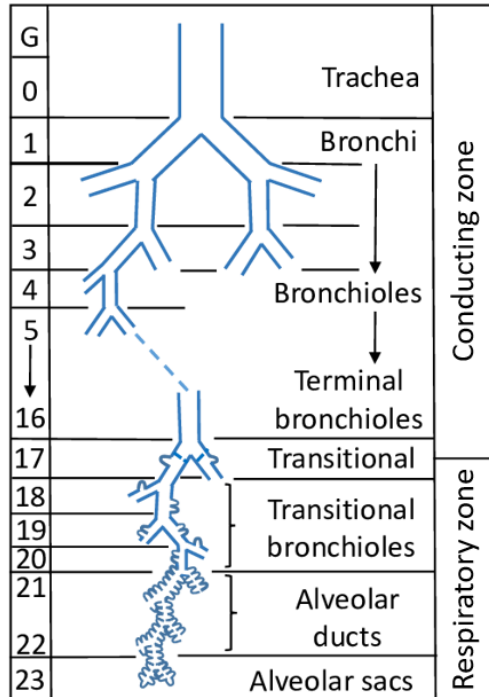


**Figure 1.1.** Diagram of branching airways, based on the Weibel model. The first 16 generations are within the conducting zone and do not greatly contribute to gaseous exchange, the final generation of the respiratory zone are the alveolar sacs which are the predominant site of gaseous exchange. Figure reproduced from Han and Hirahara (2016).

This series of airways starting with the trachea as a single tube, before undergoing serial bifurcations to reach the alveolar sacs, with the 23<sup>rd</sup> generation estimated to comprise of 8.38 million branches. Various equations have been applied to described the “optimal branching ratio” and the implications on flow, with the most common being the Hess-Murray Law, with equations such as these later being used to predict airway geometry and airway flow (Sciubba, 2016).

The respiratory tract is lined by epithelial cells which vary in morphology and function depending on the region (**Figure 1.2**). The upper airways are lined with a ciliated pseudostratified columnar epithelium, comprising of multiple cell types, before transitioning to a simple cuboidal epithelium and finally a simple squamous epithelium within the alveolar ducts/sacs (Junqueira and Mescher, 2013). Whilst the lung consists of over 40 different cell types (Franks et al., 2008), the major cell types within the respiratory epithelium are ciliated cells, goblet cells, club cells and airway basal cells. Ciliated cells and club cells are the predominant cell type within the bronchioles, where the epithelium varies from columnar to cuboidal (Miller et al., 2010). Within the alveolar region, alveolar type I cells comprise of 95% of the alveolar surface area and contribute to gaseous exchange, whereas alveolar type II cells

are cuboidal cells which serve to secrete surfactant to reduce alveolar surface tension and are also capable of differentiation into type I cells.

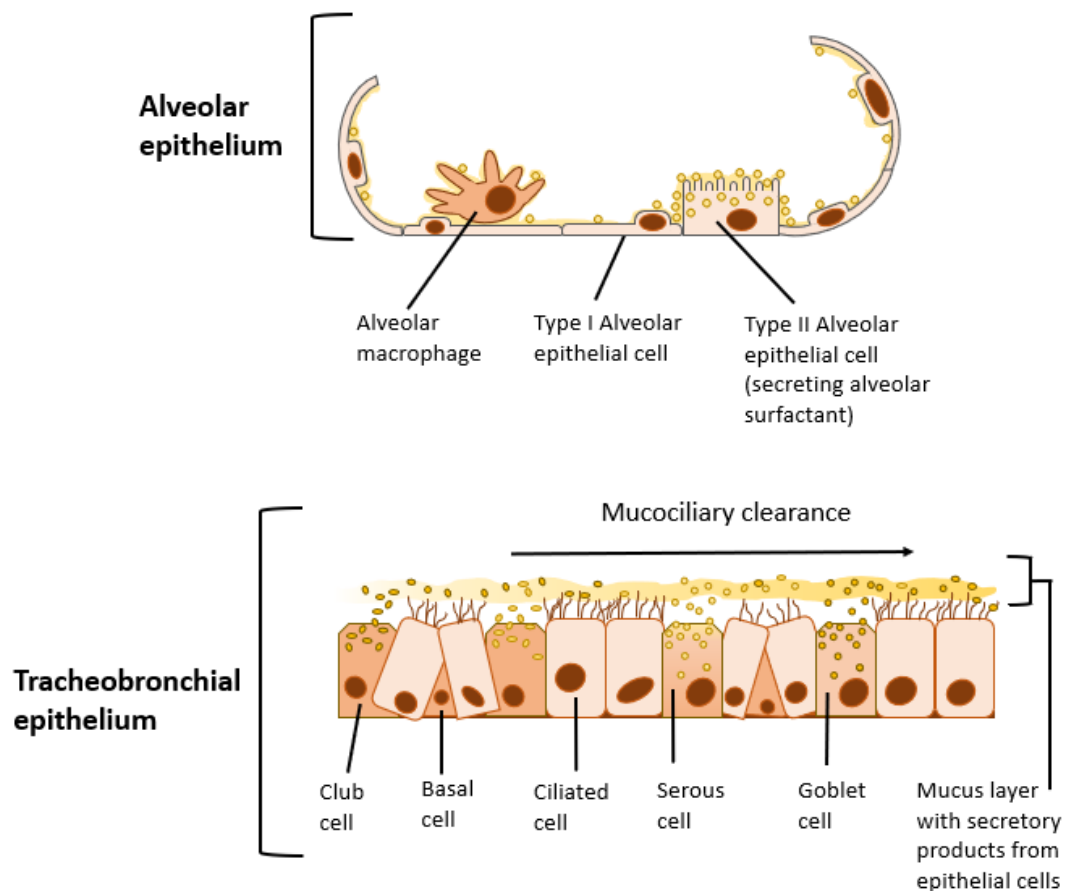


**Figure 1.2. Different epithelial cell types and the secretion of surfactant/lung lining fluid.**  
*Figure adapted from Enlo-Scott et al. (2021b)*

Moisture is maintained within the respiratory tract, by the continuous secretion of “airway surface liquid” (ASL) or lung lining fluid, which serves multiple protective functions. Physically, this thin film of fluid prevents the cells from drying out and in the alveolar region reduces surface tension that would otherwise result in atelectasis (collapse of the alveoli). Chemically, lung lining fluid provides protection from the environment, in the form of antioxidants such as glutathione, ascorbate and urate (Cantin et al., 1987, Hassoun et al., 2018). The fluid has been shown to also comprise of lipids such as cholesterol, dipalmitoylphosphatidylcholine, dipalmitoylphosphatidylglycerol, proteins such as albumin, Immunoglobulin G and electrolytes and mucins (Bicer et al., 2012, Kim, 2012). In the majority of the respiratory tract, this fluid consists of two layers, a watery layer or “periciliary liquid layer” which is in direct contact with the cells and above it is the more viscous gel layer of mucus. This fluid that contributes to the

extracellular environment is created through the secretions of goblet cells and mucosal glands, and further dispersed by the cilia of the ciliated cells (Enlo-Scott et al., 2021b). In the alveolar region, a less viscous lining fluid comprising of antioxidants, lung surfactant proteins and phospholipids is secreted by type II alveolar cells. As well as being less viscous, the alveolar surface lining fluid has a depth of approximately 0.07  $\mu\text{m}$  which is significantly thinner than the ASL in either the nasal cavity, large airways or bronchioles, which have a depth of 100, 11 and 6  $\mu\text{m}$  respectively (Bair, 1994).

### **1.3 Xenobiotic exposure (including pesticide exposure)**

Xenobiotics are chemicals not naturally produced or expected to occur within a particular organism and are therefore foreign substances. Whilst, xenobiotics are commonly thought of as artificial or anthropogenic chemicals such as synthesised pharmaceuticals, pesticides, environmental pollutants or food additives, many are naturally occurring compounds such as polyphenols or other phytochemicals we are exposed to through our diet or the diverse mixture of natural air pollutants (Sonwani and Saxena, 2016, Visioli, 2015).

Xenobiotic exposure is most likely to occur in the sites at which the organism comes into direct contact with the external environment, with this most commonly representing the gastrointestinal system, integumentary system and the respiratory system. With regards to the respiratory system, it is estimated that the volume of air breathed daily is 14  $\text{m}^3$  for males and 10  $\text{m}^3$  for females (Nazaroff and Singer, 2004), and each breath will contain some air contaminants whether inert or biologically active. It is due to this that the respiratory tract has several protective mechanisms, which are discussed in detail below.

With regards to xenobiotic inhalation, it may occur via the inhalation of vapours or gases in addition to aerosols (particulate matter or liquid droplets suspended in air) and depending on the scenario the exposure may be acute, sub-chronic or chronic.

A specific example of this is with pesticide exposure, which may occur through occupational exposure in which a worker is either mixing and loading or spraying a pesticide and the aerosol created may be unintentionally inhaled. Additionally, bystander or resident exposure may occur, for those located within or near the area of the pesticide spray application during or recently after spraying, or those who may live, work or attend school in a nearby area (EFSA, 2014b). Whilst operators/workers are likely to have personal protective equipment, bystanders and residents are unlikely to take any action to avoid/control exposure, furthermore, whilst occupational exposure is well regulated in Europe, in other countries

where these products are sprayed adequate personal protective equipment is not always available or used. For example one study found that globally on average only 43.2% of pesticide handlers wore a face mask/nose cover, compared to 84.2% in North America, with this being linked to several socioeconomic reasons (Sapbamrer and Thammachai, 2020). Similarly, a study amongst Mexican agricultural workers, representing 99 workers, 59 commercial pesticide brands and 33 active ingredients found that the correct usage of PPE was 2% (Blanco-Muñoz and Lacasaña, 2011). High pesticide inhalation exposures have also been shown in South Africa and Egypt (Msibi et al., 2021). Additionally, with the use of fog spraying (10-30  $\mu\text{m}$ ) or aerosol spraying (30-50  $\mu\text{m}$ ), the effect of spray drift must also be considered, with bystanders, residents or occupational workers who have removed PPE shortly after spraying potentially being (re)exposed whilst small droplets are still suspended in the air (Yarpuz-Bozdogan, 2018). Furthermore, even in Europe where pesticides are well regulated, a recent study of 50 operators found that 60% performed pesticide applications with predicted exposures greater than the Acceptable Operator Exposure Level (AOEL) (Wong et al., 2018). Therefore, it is clear that whether due to lack of compliance with regulation, lack of availability of PPE or several other considerations, significant pesticide exposure by inhalation is a hazard likely to occur for occupational workers.

Thus, appropriate risk assessments are needed, with respiratory toxicity and bioavailability being a key concern. This relates both to the development and registration of safer pesticides and to stricter regulatory control of those with known respiratory toxicity. Within Europe, this is the responsibility of the European Food Safety Authority (EFSA) which assess the pesticide, and require the compilation of an assessment report, whilst in the US this is performed by the Environmental Protection Agency (EPA).

#### **1.4 Fate of the inhaled aerosol**

Following xenobiotic exposure and inhalation, there are two key considerations, toxicokinetics and toxicodynamics. Toxicokinetics describes the effect that the body has on the xenobiotic, in terms of absorption, metabolism, distribution and excretion, whilst toxicodynamics describes the toxicological effect of the xenobiotic on the body, both with regards to mechanism of action and potency. The fate of the inhaled xenobiotic aerosol is ultimately determined by the regional deposition in the respiratory tract, and kinetic processes that occur, including dissolution, diffusion, permeation, protein binding, metabolism, distribution and excretion.

## 1.5 Aerosol deposition

With regards to the fate of the inhaled aerosol, the first consideration is aerosol particle deposition within the respiratory tract. Deposition is effectively determined by the aerosol properties, in addition to the respiratory anatomy/structure and airflow velocity.

Whilst aerosols may vary in terms of physical composition and may either represent airborne liquid droplets or solid particles, the most commonly used descriptors in relation to aerosol deposition are the median mass aerodynamic diameter (MMAD) and geometric standard deviation (GSD). Aerodynamic diameter, describes the “equivalent diameter” of an airborne particle which settles in the air at the same velocity as a standard particle with a known geometric diameter that is spherical in shape and has the density of water ( $1 \text{ g/cm}^3$ ) this is illustrated in **Figure 1.3**.

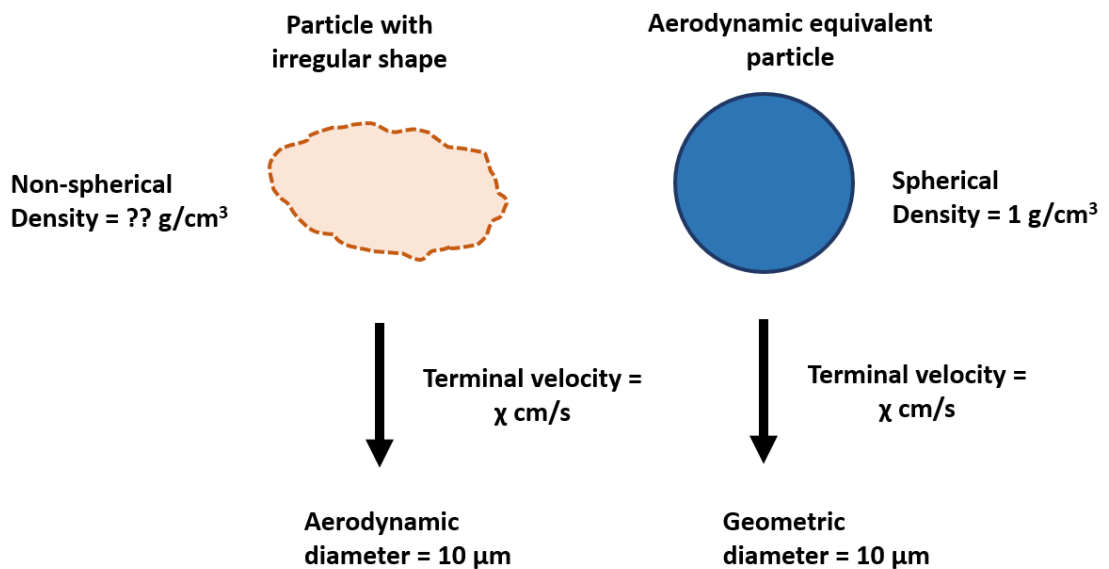


**Figure 1.3.** Aerodynamic diameter is determined by shape/density influencing terminal velocity for settling in the air rather than geometric diameter.

Mass median aerodynamic diameter, describes the aerodynamic diameter which represents the median value of the total particle population from the recovered aerosol mass, i.e. 50% of particles in the aerodynamic size distribution (based on mass) are above or below that diameter (Muralidharan et al., 2015). Geometric standard deviation is used to describe the particle size distribution and is useful in highlighting how polydisperse the aerosol is. A GSD of 1.22 is most commonly used as the upper limit for monodispersity and may be achieved within the medicines development field (Lourenço and Cotromanes, 1982, Biddiscombe et al., 2003),

whereas GSD values are generally higher for environmental or occupational aerosols, reflecting their wider particle size distribution (Pauluhn, 2005, Koehler et al., 2009, Cheng et al., 2005). Indeed, for occupational risk assessments the GSD value is commonly set at between 1.5-3.0 by the EPA and Society of Toxicology (Pauluhn, 2008).

Overall MMAD and GSD are useful descriptors of the physical aerosol, as they may be used to predict regional deposition within the respiratory tract. In relation to this there are several mechanisms for aerosol deposition, including; impaction, sedimentation, diffusion, and interception (Taulbee and Yu, 1975, Darquenne, 2020).

During nasal breathing, air is first filtered by the nasal concha/turbinates and an inhaled aerosol may deposit here or in any other region of the upper respiratory tract or within any of the generations in the tracheobronchial tree and alveoli. The predominant aerosol deposition mechanism in the nasal cavity, upper airways and bifurcations in the conducting region, is via inertial impaction.

Inertial impaction, is the main deposition mechanism for particles with an aerodynamic diameter  $\geq 5 \mu\text{m}$ , as these particles fail to follow the air stream, they may “impact” or collide against the airway walls particularly where there are steep curves/abrupt changes in direction in the airways and due to the particle’s size and momentum it is unable to follow the direction of the airflow (Darquenne, 2020). Due to the structure of the airways, significant deposition via impaction occurs in the nasal turbinates, along the nasopharyngeal bend and also at sites where the bronchi segment (Sosnowski et al., 2006, Phalen et al., 1991, Shi et al., 2007). Whilst many inhaled medicines are formulated to produce respirable particles with aerodynamic diameters in the size range  $0.5\text{-}5 \mu\text{m}$  that may reach the lower airways (Ali, 2010), environmentally and occupationally generated aerosols are likely to include particles that are larger in diameter and more polydisperse (Bémer et al., 2007, Cheng et al., 2005, Dorrian and Bailey 1995), with this corresponding to a greater proportion depositing in the upper airways. A second mechanism of deposition is gravitational sedimentation, which occurs for inhaled droplets/particles that are  $1\text{-}8 \mu\text{m}$ . Gravitational sedimentation describes the settling of particles due to gravity. This deposition mechanism is most common in the lower airways and alveoli, where the particle residence time is high, and due to the airways being narrower the distance travelled by the particles before touching the airway walls is less. Additionally, as it is gravity-driven, this means that this mechanism significantly contributes to deposition on horizontal airway surfaces, but is negligible for vertical surfaces (Rostami, 2009).

Finally, in cases where the particle size is small i.e.  $< 1 \mu\text{m}$ , and therefore largely avoids the previously described deposition mechanisms such as inertial impaction and gravitational sedimentation, the predominant deposition mechanism is Brownian diffusion (Balásházy et al., 2008, Darquenne, 2020). This deposition mechanism is particularly common in the lower or distal airways, and is driven by small inhaled particles colliding with gas molecules while suspended in slow moving air. The particles move randomly as they collide with gas molecules (Brownian motion) and deposit when they encounter ASL.

In addition, to the common deposition mechanisms above, interception may also occur. Interception may occur when a particle touches the edge of the airway wall as it travels along the airstream, and is different to impaction whereby the particle directly collides against the wall, it is common for elongated particles/inhaled fibres (Darquenne, 2020).

Whilst not strictly a deposition mechanism, another consideration is the effect of turbulent flow/mixing, particularly in the upper airways. This occurs predominantly due to the anatomy of the upper airway where a relatively high airflow velocity and the constriction of flow across nasal turbinates, or around the area of the larynx and glottis, creates turbulence. This has been suggested to be of equal importance to inertial impaction, and contributes significantly to deposition in the upper airways and early generations of the tracheobronchial tree (Matida et al., 2006, Parker et al., 2008).

### **1.5.1 Dissolution**

Following deposition, an inhaled xenobiotic may be effectively trapped in mucus secreted by goblet cells, or airway surface liquid. Solid particles may dissolve in the surrounding fluid, with this process being termed dissolution, before molecules in solution diffuse in ASL eventually coming into contact with the respiratory epithelium. The *in vitro* dissolution profile of a xenobiotic within the respiratory tract may be of interest for inhaled drug delivery because it may aid the prediction of *in vivo* drug performance, a rapid dissolution rate increases bioavailability and reduces the proportion of mucociliary clearance that might occur before this happens (Forbes et al., 2015). Based on the importance of dissolution to the performance of inhaled medicines, a range of *in vitro* dissolution techniques have been explored, including with the use of biorelevant media (Son and McConville, 2009, Radivojev et al., 2019, Hassoun et al., 2019). Diffusivity of inhaled xenobiotics in ASL may be calculated using computational modelling (Zhao et al., 2003, Hayduk and Laudie, 1974), and there is evidence to suggest that rather than just the solvent but also the lung surfactant proteins and lipids are capable of influencing the rate of xenobiotic diffusion in ASL (Widdicombe, 1997).

### 1.5.2 Absorption

Following deposition in the different regions of the respiratory tract and dissolution/diffusion across the mucus or airway surface liquid, xenobiotics come into direct contact with the respiratory epithelium where they may permeate across the epithelial barrier into underlying tissue, or nearby capillaries at which point it will be within the systemic circulation.

In order to permeate across the epithelial barrier, there are several different mechanisms of xenobiotic transport (**Figure 1.4**) involving passive diffusive processes or active transport across the respiratory tract (Selo et al., 2019).

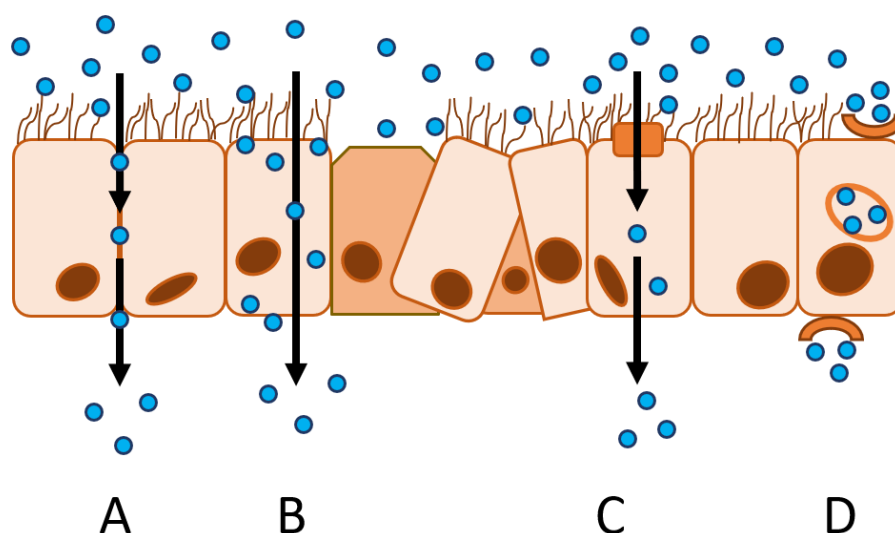


*Figure 1.4. Different pathways for drug absorption across the respiratory epithelial monolayer. Passive diffusion can occur via (A) the paracellular or (B) the transcellular route, (C) active transport and (D) transcytosis. Reproduced from Enlo-Scott et al. (2021b).*

#### 1.5.2.1 Paracellular transport

In paracellular transport, diffusion occurs through intercellular gaps between cells where the tight junctions are located. Paracellular transport is common for low molecular weight, hydrophilic and charged molecules (e.g.  $\text{Na}^+$ ,  $\text{Ca}^{2+}$ ,  $\text{Mg}^{2+}$ ,  $\text{Cl}^-$ ,  $\text{K}^+$ ,  $\text{H}_2\text{O}$ ,  $\text{PO}_4^{3-}$ ) which diffuse paracellularly across the respiratory epithelium as part of the normal absorption and secretion processes according to concentration gradients (Tang and Goodenough, 2003).

The tight junctions and tight junction-associated proteins include the occludins, claudins, cadherins, catenins, junction adhesion molecules (JAMs) and actin-binding proteins, overall representing both cytoplasmic and transmembrane proteins (Liu et al., 2000, Slifer and Blikslager, 2020, Mitchell et al., 2015). In the healthy and functional respiratory epithelium, xenobiotic transport via the paracellular route is low due both to the restrictive geometry of



tight junctions and also as the intercellular gaps between cells are only ~0.1% of the overall surface area of the epithelial layer (Boegh et al., 2013). Despite this, there is evidence of small hydrophilic molecules and even small peptides passing through the paracellular pores of the epithelium (Patton and Byron, 2007).

#### **1.5.2.2 Transcellular transport (via diffusion)**

Diffusion of xenobiotics may occur across the cell membrane. This is a passive transcellular process by which the compound permeates through/partitions into the apical membrane, passes through the cytoplasm and then exits the basolateral membrane. This is common for lipophilic molecules which are uncharged/non-ionised at physiological pH which is generally considered to be pH 7.4 but can be as low as pH 6.6 for the respiratory lining fluid (Zajac et al., 2021, Fischer and Widdicombe, 2006). Simple diffusion across the plasma membrane represents one of the predominant modes of transport for xenobiotics.

#### **1.5.2.3 Transcellular transport (via transcytosis)**

Vesicle-mediated endocytosis and transcytosis, is another mode of transcellular xenobiotic transport, particularly for macromolecules or large hydrophilic molecules (Patton and Byron, 2007, Detampel et al., 2019). Invagination of the plasma membrane, creates a xenobiotics-containing membrane vesicle or “caveoli”, which may transport the contents to the basolateral side of the cell, before the vesicle fuses with the basolateral plasma membrane and releases the contents extracellularly/basolaterally. There is evidence of this occurring in the upper airways for large macromolecules such as IgG via receptor-mediated transcytosis (Patton and Byron, 2007). In the case of proteins, this mechanism of uptake may protect proteins from intracellular or lysosomal degradation or proteolysis (Forbes and Ehrhardt, 2005), with transcytosis by caveolae and clathrin-coated pits believed to be the main route of alveolar epithelial protein transport (Olsson et al., 2011). Interestingly, it has recently been proposed that exposure to cigarette smoke dysregulates this process, with clathrin-mediated endocytosis impaired and calveolin-mediated endocytosis upregulated in primary small airway cells (Duffney et al., 2020), which is suggested to lead to increased respiratory infections in smokers.

#### **1.5.2.4 Transcellular transport (via active transport)**

Xenobiotics may also be transported transcellularly by drug transporters and active transport may include either uptake or efflux (Selo et al., 2019). Uptake may be performed through the

exchange of an extracellular xenobiotic for a readily available endogenous compound, with one being transported intracellularly essentially as the other is transported extracellularly (secondary active transport). Alternatively, efflux drug transporters may remove the xenobiotic through the use of ATP (primary active transport). As there are a limited number of binding sites for each transporter, active transport may become saturated with high xenobiotic concentrations (i.e. there is a maximum rate of transport). Additionally transporter activity may be reduced by selective inhibitors or activity may be reduced if there is insufficient ATP (e.g. due to mitochondrial inhibition).

Common uptake transporters include the solute-linked carriers (SLC), organic anion transporters (OATS), organic anion transporting polypeptides (OATPs), organic cation transporters (OCT) and peptide transporters (PEPT). Uptake transporters are more commonly researched with regard to hepatic or renal tissues, and regulatory bodies such as the European Medical Authority (EMA) and the USA Food and Drug Administration (FDA) currently recommend the investigation of carrier-mediated drug-drug interactions for OATP1B1, OATP1B3, OAT1, OAT3, OCT2 and OCT1 (Sudsakorn et al., 2020, Wang and Urban, 2014).

However, there is increasing focus on the impact of drug transporters on drug disposition and respiratory pharmacokinetics (Ehrhardt et al., 2017, Gustavsson et al., 2016).

In particular, the uptake transporters OCT1, OCT3, OCTN1, OCTN2 and PEPT2 have been found in primary lung tissue and cell lines (Bosquillon, 2010, Endter et al., 2009), whilst an even wider range of uptake transporters have been identified in human nasal epithelium (Agu et al., 2011, Anand et al., 2014, Al-Ghabeish et al., 2015). Within the respiratory tract, uptake transporters have substrates that include environmental xenobiotics such as aflatoxin B1 and inhaled drugs such as budesonide and salbutamol (Fardel et al., 2012, Gustavsson et al., 2016). There is also evidence that uptake of inhaled cationic bronchodilators such as formoterol and salbutamol may be partially mediated by OCTN1 and OCTN2 (Horvath et al., 2007).

Despite the likelihood of significant paraquat inhalation being low due to both the aerosol properties and its highly regulated use, paraquat accumulation in the lung is a common example of the role of uptake transporters in xenobiotic toxicokinetics. Orally ingested paraquat may accumulate in the lung, leading to concentrations 6-10 times higher than in the plasma, due to uptake predominantly by club cells and type II alveolar cells via the polyamine transport system for naturally occurring amines; spermine, spermidine and putrescine (Foth, 1995, Dinis-Oliveira et al., 2008). Conversely, the respiratory epithelium also contains efflux drug transporters such as P-glycoprotein (P-gp), multidrug resistance associated proteins (MRP1 and MRP2) and breast cancer resistance protein (BCRP), which have a relatively high

substrate promiscuity and may significantly contribute to the intracellular removal of inhaled xenobiotics (Sakamoto et al., 2015, Bosquillon, 2010). These transporters effectively work to reduce the intracellular xenobiotic concentration and limit xenobiotic absorption by removing them from the exposed cells (**Figure 1.5**).

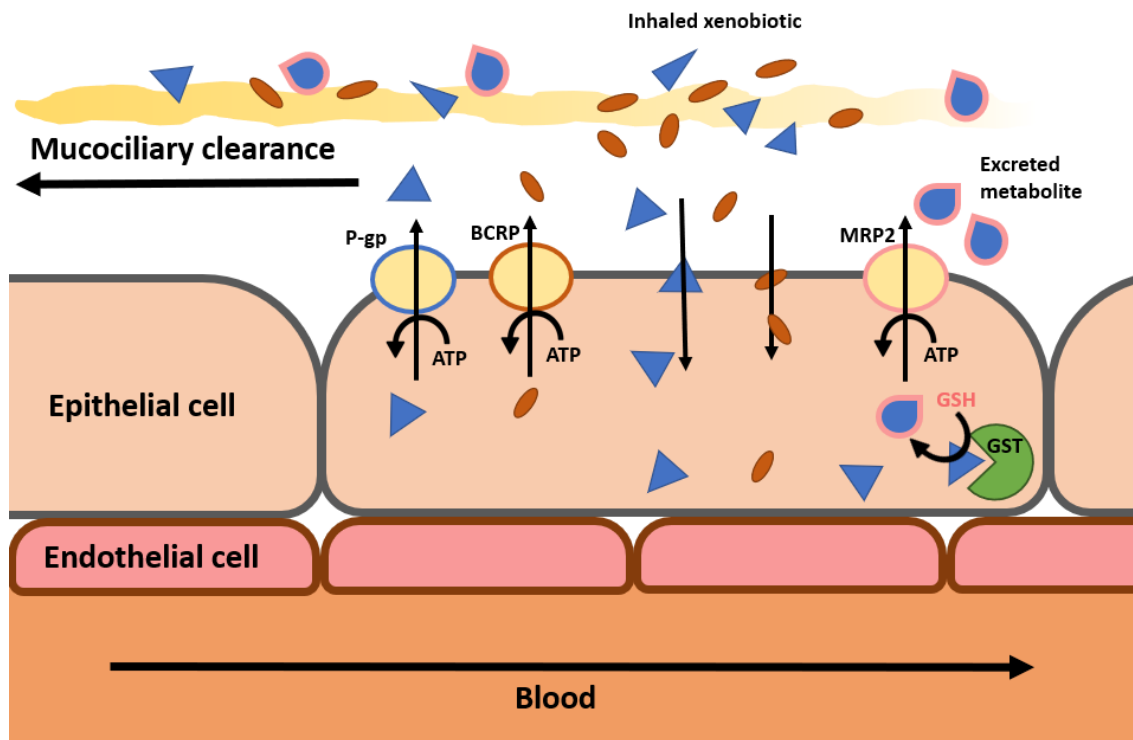


*Figure 1.5. Potential non-absorptive clearance mechanisms, including efflux by P-glycoprotein, BCRP or MRP2 drug transporters, in situ metabolism by metabolically active epithelial cells (glutathione-S-transferase is included as an example enzyme), and mucociliary clearance.*

Efflux transporters may also work alongside other non-absorptive clearance mechanisms, for example xenobiotic metabolism, i.e. glutathione-s-transferases may conjugate glutathione to the xenobiotic and MRP1 or MRP2 may identify the glutathione conjugate as a substrate for efflux (Mairinger et al., 2020, Selo et al., 2021). Whilst MRP1 is located on the basolateral membrane of respiratory epithelial cells and MRP2 is localised to the apical membrane, both may transport hydrophobic or anionic molecules in addition to glutathione and glucuronide conjugates (Br  chet et al., 1998, Olsson et al., 2011). Another example of interaction between xenobiotic metabolism and active transport is with CYP3A4/5 and P-glycoprotein, which are often found in the same cell types, induced by the same compounds and may act on the same substrates (Kim, 2002).

Although more research is needed, particularly to characterise functional activity of various drug transporters in respiratory epithelial tissue (Ehrhardt et al., 2017), a multitude of drug transporters have been shown to be expressed within the respiratory tract based on analysis of primary tissue and cell lines (Endter et al., 2009, Al-Ghabeish et al., 2015, Bosquillon, 2010), as illustrated in **Table 1.1**.

**Table 1.1. Common drug transporters expressed in the human respiratory tract. ✓ represent positive results based on reported data from mRNA microarrays or quantitative targeted absolute proteomics (Endter et al., 2009, Al-Ghabeish et al., 2015, Ehrhardt et al., 2017, Bosquillon, 2010).**

Transporter Family	Transporter	Nasal	Tracheal	Bronchial	Alveolar
ABCB1	MDR1/P-gp	✓		✓	✓
ABCC	MRP1	✓	✓	✓	✓
	MRP2			✓	
	MRP3	✓		✓	
	MRP4	✓	✓	✓	✓
	MRP5	✓	✓	✓	✓
	MRP6	✓	✓	✓	✓
	MRP7	✓			
ABCG2	BCRP			✓	✓
SLC15A2	PEPT1	✓			
	PEPT2	✓		✓	
SLC22	OCT1	✓	✓	✓	
	OCT2		✓	✓	✓
	OCT3	✓		✓	
	OCTN1	✓	✓	✓	✓
	OCTN2	✓			
	OATP1A2	✓		✓	
	OAT3A1	✓		✓	
	OATB1B3		✓	✓	
	OATP2B1		✓	✓	✓
	OATP3	✓		✓	
	OAT3	✓		✓	
SLC29	ENT1	✓			
	ENT2	✓			

### 1.5.3 Metabolism

Intracellular drug-metabolising enzymes are capable of chemically altering inhaled xenobiotics, often to increase their hydrophilicity and make it more easily excreted (Ding and Kaminsky, 2003). This may represent either Phase I metabolism, consisting of redox reactions, hydrolysis and hydroxylation, often followed by Phase II metabolism in which the xenobiotic is conjugated with a charged or hydrophilic molecule such as glucuronic acid, glutathione, sulphate or acetyl group. The main drug metabolising enzymes, have a high substrate promiscuity, which is central to their ability to metabolise a wide range of compounds, including therapeutic drugs, dietary phytochemicals, environmental pollutants and pesticides (Hayes et al., 2014, Nath and Atkins, 2008, Atkins, 2020). This is exemplified through the wide range of substrates that undergo CYP-mediated phase I xenobiotic metabolism (**Figure 1.6**).

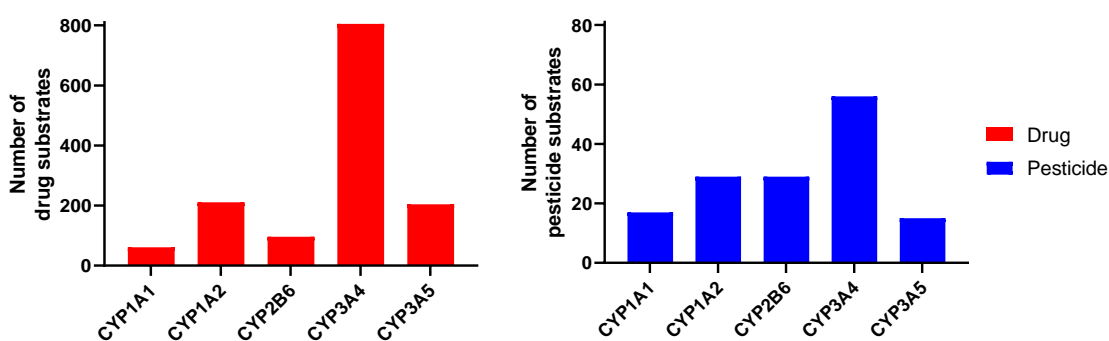


*Figure 1.6. Summary of substrate promiscuity, for common CYP450 enzymes. CYP-mediated pesticide metabolism has been less extensively studied and subsequently less substrates have been identified. Graphs generated from literature data (Abass et al., 2012, Law et al., 2014).*

Although often metabolism serves to detoxify the xenobiotic, there are also examples of bioactivation whereby the metabolite formed is more toxic than the original parent compound. A common example of this is the polycyclic aromatic hydrocarbon (PAH), benzo[a]pyrene, which is a commonly found air pollutant and known procarcinogen. Once inhaled, benzo[a]pyrene may sequentially be metabolised by CYP1A1/1A2/1B1 enzymes and epoxide hydrolase within alveolar cells, to form the active metabolite and carcinogen BPDE which may form DNA adducts (Jarvis et al., 2018, Barnes et al., 2018). Similar examples, of potential bioactivation of environmental toxins include CYP2A13/2F1-mediated metabolism of naphthalene toxicity in nasal and lung mucosa (Zubrod et al., 2019, Li et al., 2017) or the pulmonary “pro-toxin” 4-ipomeanol which is bio-transformed by CYP4B1 metabolism in rat club cells to a reactive electrophilic metabolite (Parkinson et al., 2016). Another study

demonstrated that pesticide-exposed fruit growers in Taiwan with GSTP1 and CYP3A5 polymorphisms that led to increased enzyme activity, were found to be at greater risk of DNA damage, suggesting bioactivation rather than detoxification (Liu et al., 2006). The particular pesticide(s) responsible could not be identified in the study, in part due to a mixture of ~30 different compounds including organophosphates, carbamates, pyrethroid insecticides, various fungicides being used by the workers. However, bioactivation of organophosphates has been shown to occur *in vitro* by CYP3A5 metabolism (Mutch et al., 1999). As GST metabolism has been highlighted as a detoxification pathway for organophosphates (Fujioka and Casida, 2007), the mechanism behind increased GSTP1 activity being associated with higher risk of DNA damage is not clear but was replicated in a separate study with organophosphate exposed workers in India (Singh et al., 2011). It has been suggested, that this particular polymorphism increases activity for the commonly used *in vitro* substrate of GST activity such as 1-chloro-3,4-dinitrobenzene by 3-fold, but actually reduces GSTP1 specific activity by 7-fold for PAHs, and perhaps in this case also organophosphates (Hu et al., 1997, Watson et al., 1998). If this is the case, whilst overall activity appears to be increased, in reality those with the polymorphism are less likely to rapidly detoxify environmental/occupational pollutants.

Indeed, there are numerous examples of biotransformation reactions for inhaled chemicals that ultimately change their toxicity profile (Uppstad et al., 2010, Boyd, 1980, Castell et al., 2005, Minchin and Boyd, 1983). Although xenobiotic metabolism in the respiratory tract is lower than in the liver, it is significant enough to impact the fate of inhaled drug and environmental pollutants and may have implications for *in situ* toxicity or pharmacological action. Traditionally, significant CYP450 metabolism has been deemed to be isolated to a few cell types within the lung, i.e. club cells, type II alveolar epithelial cells and alveolar macrophages (Steimer et al., 2005). Interestingly, no cell line model exists currently for human club cells, and whilst the type II alveolar epithelial cell line A549 has been used in several xenobiotic metabolism studies, the THP-1 cell line that is sometimes used as an alveolar macrophage model has not been thoroughly explored for CYP450 activity (Huang et al., 2014, Jakob et al., 1995, Oesch et al., 2019). Despite this, there is *ex vivo* and *in vitro data* to suggest that CYP450, esterase, NQO1 and GST metabolism are more widespread within the respiratory tract than just for these three cell types (Courcot et al., 2012, Zhang et al., 2006, Oesch et al., 2019). Xenobiotic metabolism in the respiratory tract is discussed in a recent review (Enlo-Scott et al., 2021a), explored *in vitro* within **Chapter 2** and considered from the standpoint of implications for local toxicity, permeability and efflux identified *in silico* within **Chapter 3**.

#### 1.5.4 Local toxicity

Xenobiotics may exert toxic effects on the cells they come into direct contact with once inhaled, however recent research predicting acute *in vivo* toxicity through lung surfactant studies alone highlights that chemical interactions between the xenobiotic and airway surface liquid are also of importance (Larsen et al., 2020, Sørli et al., 2018).

Acute toxicity in the respiratory tract, may manifest via various mechanisms; general cytotoxicity, plasma membrane disruption, dysregulation of energy production (e.g. mitochondrial inhibition), nucleotide or protein synthesis inhibition, oxidative stress or antioxidant depletion, and several other biochemical/cellular mechanisms (Vinken and Blaauboer, 2017, Clippinger et al., 2018b). The resulting effects are equally as varied, including but not limited to respiratory dyskinesia, dyspnoea, oedema, acute respiratory distress syndrome (ARDs), localised necrosis or metaplasia (Clippinger et al., 2018a, Kilgour et al., 2002a). Chronic exposure may be similarly harmful, and long-term effects may range from cancer to COPD or fibrosis.

As inhalation represents a major exposure route (along with dermal exposure and ingestion), acute toxicity data is often obtained for various environmental and occupational xenobiotics, whilst safety data is obtained as part of the preclinical studies within drug development (Parasuraman, 2011). The list of regulatory agencies that use acute inhalation data is extensive and varied (**Table 1.2**), highlighting the importance of this data in the regulation of medicines, agrochemicals, environmental and occupational chemicals. The commonly performed acute inhalation studies use a rodent inhalation model for which LC<sub>50</sub> values are reported, in addition to histopathology or necropsy data. This data, is useful in identifying the severity of the toxicity, and highlighting respiratory irritants, localised necrosis, tissue metaplasia, hyperplasia and other effects of the xenobiotic such as irregular respiration/tremors. Generally, the data is used for quantitative risk assessment (which requires a concentration-response relationship to be identified) or for classification and labelling purposes for which test guidelines (TGs) are listed by the Organization for Economic Cooperation and Development (OECD). For acute inhalation studies, this includes OECD TG 403, OECD TG 436 and OECD TG 433, which vary in the number of animals used, the former two using lethality as an endpoint, in contrast the latter one is more refined and uses a fixed concentration along with clinical signs of toxicity as an endpoint (OECD, 2017, Arts et al., 2008, Clippinger et al., 2018b).

However, for reducing, replacing and refining the use of animal models, and also to better understand the mechanistic toxicity of the xenobiotic, alternative approaches are useful and

will continue to increase in importance both for regulatory and non-regulatory data requirements (Clippinger et al., 2018b).

**Table 1.2. A summary of regulatory bodies that require or use acute inhalation data. Adapted from Clippinger et al. (2018b).**

<b>Region</b>	<b>Regulatory body</b>	<b>Acronym</b>
Australia	Australian Pesticides and Veterinary Medicines Authority	APVMA
Brazil	Brazilian Agência Nacional de Vigilância Sanitária (The National Health Surveillance Agency)	ANVISA
Canada	Canadian Healthy Environments and Consumer Safety Branch	HECSB
	Canadian Pest Management Regulatory Agency	PMRA
China	Chinese Association of International Chemical Manufacturers	ACICM
	Chinese Institute for the Control of Agrochemicals, Ministry of Agriculture	ICAMA
	Chinese Ministry of Environmental Protection	MEP
	Chinese State Administration of Work Safety	SAWS
Europe	European Chemicals Agency	ECHA
	European Food Safety Authority	EFSA
India	Indian Central Insecticide Board & Registration Committee,	CIBRC
Japan	Japanese Ministry of Agriculture, Forestry and Fisheries	MAFF
Nigeria	National Agency for Food and Drug Administration and Control	NAFDA
South Korea	South Korean Ministry of Agriculture, Food and Rural Affairs	MAFRA
	South Korean Ministry of Environment	MOE
United States of America	Environmental Protection Agency	EPA
	Food and Drug Administration	FDA
	Occupational Safety and Health Administration	OSHA
United Kingdom	United Kingdom Medicines & Healthcare Products Regulatory Agency	MHRA

Non-animal approaches, which make use of *in vitro* and *in silico* methods may be of particular use for the determination of adverse outcome pathways (AOPs), whereby molecular initiating events are identified *in vitro* and subsequent measurable key events are linked to clear adverse outcomes downstream (Rim, 2020). In general, this approach may start at a molecular level, but the focus expands to a cellular or tissue level, followed by contextualisation at an



organ or organism level. This framework is useful for organising existing knowledge, applying it to future chemicals, and linking *in vitro* data to adverse toxicological outcomes that are of clear relevance to chemical safety and regulation (Villeneuve et al., 2014). It also highlights the need for a suite of appropriate experimental models, representing both *in vivo*, *in vitro* and *in silico* techniques, that are capable of generating human relevant data.

## **1.6 *In vivo*, *ex vivo*, *in vitro* and *in silico* models of the respiratory tract**

Differences in the purpose of experiments and requirements of various regulatory bodies, mean that there are significant differences in the experimental models used to assess respiratory pharmacokinetics/toxicokinetics and local toxicity. However, there remains considerable overlap in the models used between the fields of pharmaceutical sciences, environmental sciences and occupational exposure. Common experimental methods seek to represent processes in the human airways with regards to pulmonary kinetics or local toxicity, and this includes the use of *in vivo*, *ex vivo*, *in vitro* set ups as well as *in silico* models.

### **1.6.1 *In vivo* models**

Animal models may be used to study both xenobiotic biological activity (i.e. toxicology, pharmacology) and also xenobiotic kinetics following inhalation. Rodent models (rats or mice) are most commonly used, due to reduced research costs (i.e. animal housing facilities), ease of handling and reduced mass of test compound required, in comparison to larger animal species, such as rabbits, dogs, sheep and primates (e.g. cynomolgus monkeys) which are used less frequently both due to practicality and for ethical reasons. Additionally, for acute inhalation toxicity testing (e.g. for GHS classification, EFSA or EPA), rodents may present an advantage due to being obligate nasal breathers, whilst for pre-clinical drug development this may be a disadvantage for studying what would be an orally inhaled medicine. In the latter case, tracheal cannulation may be used, to bypass nasal filtering. Overall, there are many aerosol delivery methods used, including whole body passive inhalation, nose-only passive inhalation (for which the aerosol may be nebulised), or direct delivery via endotracheal intubation/cannulation. Whole body passive inhalation may more accurately model an unintentional exposure scenario, but creates challenges in determining the inhaled dose, and so direct delivery may be preferred. Direct delivery methods used may vary significantly in complexity, ranging from a simple syringe to more advanced systems such as the PreciseInhale® which allows for precision dosing by tailoring the aerosol, setting the exact dose and properties of the aerosol used (concentration, aerodynamic particle size distribution), to

increase reproducibility and the correlation between *in vivo* rodent and human testing (Selg et al., 2012, Fioni et al., 2017).

Toxicity testing usually involves the monitoring of the animal post-inhalation and the histological analysis of tissues to identify any associated pathology in accordance with the OECD guidelines which were highlighted above.

Post-inhalation xenobiotic kinetic data may be obtained by sampling blood, urine and bile (via bile duct cannulation) at multiple intervals over a set time period, along with harvesting terminal tissue samples once the animal has been sacrificed. Through the use of LC-MS bioanalysis, the toxicokinetic profile in blood may be established, along with the identification of potential metabolites in the biological samples. Alternatively, radiolabelled compounds may be used to simplify the analysis if these are available and suitable. Despite inter-species differences, data obtained in this way provides a useful insight into the potential toxicity or xenobiotic kinetic profile in humans, and is often part of regulatory requirements.

As *in vivo* experiments allow the whole body system to be studied, toxicokinetic data from one species may translate to being predictive in human in cases where interspecies differences are not significant. However, due to the rodent respiratory tract being significantly different in structure to that of humans, aerosol deposition itself is markedly different (Kolanjiyil et al., 2019, Hofmann et al., 1989). Additionally, rodent xenobiotic metabolism is generally greater than human xenobiotic metabolism in the lungs and liver (Baillie and Rettie, 2010, Oesch et al., 2019). Despite these challenges, for certain pharmacokinetic parameters, the use of interspecies allometric scaling and combining *in vivo* rodent data with *in vitro* human data may be sufficient to be predictive (Lavé et al., 1999).

Overall, the shortcomings with the available *in vivo* models include ethical considerations, interspecies differences and the inherent challenges of using a physiologically complex system to answer specific mechanistic research questions (i.e. specifically comparing drug dissolution rates in the airway, whilst excluding the effect of pulmonary absorption).

### **1.6.2 *Ex vivo* models**

*Ex vivo* models may be particularly beneficial for elucidating the effect of specific physiological processes within the respiratory tract, by using a controlled environment with reduced confounding factors. The isolation of specific tissues such as the nasal mucosa, or whole organs such as the isolated perfused lung model, allows the physiology and native architecture of the biological system to be maintained whilst partially eliminating variability and simplifying experimental conditions. Although less useful for local toxicity studies due to the time

limitations associated with tissue viability once the animal is sacrificed, *ex vivo* models are especially valuable for xenobiotic absorption/permeability studies as well as the assessment of xenobiotic metabolism (Rubin et al., 2020, Olsson et al., 2011).

The isolated perfused lung (IPL) model is a well-established *ex vivo* model to assess xenobiotic absorption in the lung (Tronde et al., 2008, Mehendale et al., 1981). IPL models commonly use rat or guinea pig lungs, although it has also been adapted for rabbits and explored using human lungs (Linder et al., 1996, Uhlig and Wollin, 1994, Tate et al., 1982, Sakagami et al., 2006). The model preserves the structural integrity and function of the permeability barriers, including physical tight junctions but also the biological activity of drug transporters, without damaging the vascular barriers as might be the case in other *ex vivo* models that use lung slices or excised tissues (Mehendale et al., 1981). IPL begins with the surgical removal of the lungs from the host species. Surgical skill is required to quickly (within 10-15 minutes) isolate the lung without significantly delaying the setup of artificial ventilation and perfusion after the surgery has been initiated. The perfusion medium is designed to mimic physiological conditions i.e. pH 7.4 and 37°C, supplemented with glucose and equilibrated with oxygen and carbon dioxide (Tronde et al., 2008). Once the compound of interest is administered to the lungs, samples of the perfusate are taken at regular intervals to allow the time dependent analysis of xenobiotic concentration in the medium which perfuses the pulmonary circulation (and indicates systemic absorption of the xenobiotic from the lungs). The methodology involved in IPL provides several benefits over *in vivo* methods, in terms of controlled ventilation/perfusion rates, direct delivery of the xenobiotic, the removal of first pass metabolism considerations and the method has found use both within the pharmaceutical industry and for predicting bioavailability in environmental risk assessments (Chen et al., 1995, Mehendale et al., 1981). A major benefit of this approach is that by isolating the lung, the influence of other factors related to systemic pharmacokinetics are removed, and the data obtained relates solely to absorption, distribution and metabolism via the respiratory system (Tronde et al., 2008). However, the complexity of the experiment also creates limitations. A significant limitation is the need for specialist perfusion equipment and the relatively short time for which organ viability may be maintained, which is typically 3-5 hours. There has also been reported to be a high variability between individual lung samples and species selection is important due to interspecies differences in lung structure/branching patterns. Additionally, whilst mouse inhalation models may be commonly used *in vivo*, they present a challenge using IPL due to their small size (Tronde et al., 2008).

In the case of xenobiotics that rapidly cause acute toxicity, the IPL method has been used to explore mechanisms of toxicity (Ryrfeldt et al., 1990, Mark Lafranconi and Huxtable, 1984, Roth, 1995, Tate et al., 1982), however depending on the mechanism of toxicity more informative and refined *in vitro* models exist, that also allow for the reduction or replacement of the *ex vivo* model with regards to toxicity testing (Yaquib et al., 2021, Primavessy et al., 2021). Overall the IPL model, is most suited to absorption and metabolism studies, with a focus on xenobiotic kinetics and respiratory bioavailability rather than local respiratory toxicity (Tronde et al., 2008, Mehendale et al., 1981, Olsson et al., 2011), data obtained from the IPL model also complements *in vivo* whole animal studies and may inform *in silico* modelling approaches.

Another commonly used *ex vivo* model, is precision-cut lung slices, which are slightly higher throughput than the IPL model, preserve the native 3D architecture of the lung and may be used for metabolism and toxicity studies. The slices are commonly obtained from either rat or human tissue. Early studies have suggested that tissue viability may be maintained for 8-24 h (Nave et al., 2007, Umachandran et al., 2004), whilst other researchers have more recently suggested viability may be maintained for 15-21 days by adjusting the culturing conditions (Bailey et al., 2019, Neuhaus et al., 2017). Along with longer maintenance times than IPL, the generation of multiple slices from a lung sample offers improvements with regards to toxicity testing and the identification of xenobiotic metabolites formed within the lungs is facilitated by the increased xenobiotic incubation times compared to the IPL. Precision-cut rat lung slices have been used extensively to study xenobiotic metabolism within the lung (Nave et al., 2006, Yilmaz et al., 2019, Oesch et al., 2019), polyamine transport relevant to paraquat toxicity (Morin et al., 2013), and more generally to study inflammation and respiratory diseases such as COPD or idiopathic pulmonary fibrosis (Liu et al., 2019). Precision-cut lung slices are particularly useful as an *ex vivo* alternative to *in vivo* testing, and may be used for biomechanical, physiological and toxicological testing (Morin et al., 2013). However, limitations include; tissue availability, heterogeneity between samples from different locations within a single lobe, donor-to-donor variability, medium-to-low throughput and the need for more specialised techniques to maintain tissue viability and prevent airway remodelling or the loss of native 3D architecture or optimal cell function, both biochemical and structural (Liu et al., 2019, Neuhaus et al., 2017). An additional consideration is that by slicing lung tissue, cells that would not be present apically may be directly exposed to the xenobiotic and this may contribute to misleading results.

### **1.6.3 *In vitro* models**

Generally, *in vitro* models provide several advantages over *in vivo* and *ex vivo*, in terms of ease of use, versatility of experimental design, reduced cost and higher throughput. Additionally, in accordance with the NC3Rs, *in vitro* models are a vital part of the strategy to replace, refine and reduce the use of animal models (Burden et al., 2015, Prescott and Lidster, 2017). This is critical not just for ethical reasons associated with *in vivo* experiments, but also to improve the scientific data generated by using more human relevant models and avoiding pitfalls associated with interspecies differences. The use of non-animal approaches to respiratory absorption, metabolism and toxicity data continues to increase and improve, particularly in the development of *in vitro* models that better represent or replicate the human *in vivo* system, this includes the use of data rich or high throughput modelling strategies, along with the advances in 3D *in vitro* models (Balogh Sivars et al., 2018, Hoffmann et al., 2018).

#### **1.6.3.1 *In vitro* models using primary cells**

The use of primary epithelial cells for absorption, metabolism and toxicity studies is well established, in addition to their use to study mucociliary clearance. Primary epithelial cell models for have been described for each region of the respiratory tract, representing various cell types from the nasal cavity, trachea, bronchioles and alveoli (Fuchs et al., 2003, BéruBé et al., 2010, Murgia et al., 2017, Dahl and Hadley, 1991, Bleier et al., 2013). Additionally, non-epithelial cell models have also been used, such as primary alveolar macrophages to study xenobiotic toxicity or the role of these cells in the clearance of inhaled macromolecules (Yıldız-Peköz and Ehrhardt, 2020, Lombry et al., 2004, Kilgour et al., 2002b). Changes to macrophage phenotype such as pulmonary alveolar proteinosis (PAP) or phospholipidosis may be indicative of drug toxicity, and in some cases relate to chronic inflammation, tissue damage, neoplasia and fibrosis. Therefore the testing of alveolar macrophage responses *in vitro* may be useful for non-clinical toxicology risk assessments (Forbes et al., 2014).

The source and type of primary respiratory epithelial cell used in current research, is highly variable and includes both commercially available sources such as heterogenous human bronchial epithelial primary cells or the non-commercially available isolation and use of specific cell populations i.e. club cells or goblet cells (Rostami et al., 2021, Rayner et al., 2019). Overall, primary cells present several benefits over *in vivo* and *ex vivo* models, with the main one being that human cells and therefore human relevant data, may be more easily obtained. Additionally, the culturing of these cells means that cell viability may be preserved, significantly longer than for many of the *ex vivo* models, allowing for a greater range of

experiments to be performed, which is of particular benefit to toxicity or metabolism studies for which long or repeated exposures are of interest or xenobiotic metabolic clearance rate is low. The great diversity of assays that can be performed, particularly in a microplate format is a key advantage, along with the maintenance of normal cell phenotype, including beating cilia, mucus production, functional enzyme expression and permeability characteristics such as normal tight junction and drug transporter activity (Yıldız-Peköz and Ehrhardt, 2020, Forbes and Ehrhardt, 2005, Olsson et al., 2011). In addition to the inherent properties of the primary cells, several researchers have highlighted that these models may be improved to better represent the *in vivo* situation by either altering the culturing conditions or the extracellular matrices e.g. collagen coating, 3D hydrogels or the use of basement membrane extract. (Mantaj et al., 2018, Burgstaller et al., 2018, Saforo et al., 2019). Furthermore, the introduction of “lung-on-a-chip” models have highlighted that the use of biomechanical forces or microfluidics to simulate respiratory forces and perfusion, respectively, may be important to maintaining or modelling optimal primary epithelial cell phenotype *in vitro* (Doryab et al., 2016, Stucki et al., 2015, Nawroth et al., 2021).

Despite the great advantages and research opportunities offered by the use of primary cells, these models are not without their limitations. Primary cells undergo cell senescence and are generally unable to be cultured long term over many passages. One of the key advantages of primary cells are that they differentiate to form a polarised epithelial barrier with properties similar to those found in the *in vivo* epithelium, with regards to mucus secretion, beating cilia, functional enzymes/drug transporters/tight junction expression. However, over time in culture or after a few passages these characteristics may be lost, which may not be detected in cases where overall cell viability appears to have been maintained. Additionally, in the case of monocultures, some primary cells do not have the ability to actively divide and differentiate, as is the case with alveolar type I cells which *in vivo* are generated through the differentiation of alveolar type II cells (Rothen-Rutishauser et al., 2012, Evans and Lee, 2020). Obtaining the primary cells either commercially or within the lab is costly, and experimental results from these models may be complicated or ambiguous due to donor genetic variability limiting the reproducibility of certain experiments.

Some of the issues traditionally associated with respiratory epithelial primary cells have been overcome by newer models, including 3D complex models or induced pluripotent stem cells (iPSCs).

Although not currently available for every region of the respiratory tract, the companies Epithelix and MatTek Life Sciences, do currently provide 3D lung cell models (MucilAir and EpiAirway, respectively), which make use of primary cells and can be cultured long term for  $\geq 3$  months allowing for chronic exposure testing e.g. 30-90 day repeated dosing (Sakagami, 2020). Conversely, the model is not particularly high throughput in comparison to primary cells or bronchial cell lines. EpiAirway in particular was found to have a significantly greater paracellular permeability and poorer tight junction functionality, which may reduce its use for xenobiotic permeability studies (Furubayashi et al., 2020). Although the uptake of these models by researchers may be limited due to cost and genetic variation between donors remains a concern for the reproducibility of results, these models continue to become better characterised in terms of their suitability to represent the physiology *in vivo* and correspond to an improvement within the field.

Stem cell-derived lung epithelial cells, remain a potential method for the generation of various lung cell types, if the right differentiation protocol can be established. Data has shown that for alveolar cells generated via this method the epithelial barrier formed is not completely consistent with that *in vivo* and paracellular permeability is moderately higher than what has been reported with normal primary alveolar cells (Ghaedi et al., 2014, Van Haute et al., 2009). However, improvements in this area continue to be made and the use of iPSC lung models has been described recently for toxicity assessments and as a physiologically relevant model for studying SARS-CoV-2 infection (Armstrong, 2018, Djidrovksi et al., 2021). With further research confirming the phenotype of iPSC models to represent primary cell function with regards to permeability, drug transporters and xenobiotic metabolism, this may be a promising alternative for *in vivo* testing.

#### **1.6.3.2 *In vitro* models using cell lines**

Established cell lines offer alternative or complementary *in vitro* models to those that use primary cells. Cell lines do not readily undergo cell senescence and therefore may be sub-cultured or passaged continuously. Most cell lines are either cancer-derived or immortalised/"transformed" by other means e.g. transfection of viral genes that partially deregulate the cell cycle. The benefits, include continuous use, experimental flexibility, reduced cost and improved experimental (inter-lab and intra-lab) reproducibility due to the elimination of donor-to-donor genetic variability (Forbes and Ehrhardt, 2005, Sakagami, 2006). Furthermore, as cell lines may be continuously sub-cultured and overall cell number greatly expanded over several population doublings, these models are more amenable to high-

throughput than primary cells for which donor tissue (and cost) may be a limiting factor. Despite this, the use of cell lines are not without disadvantages, the main one being that through the immortalisation process, the cells may lose some of the phenotypic characteristics of normal/primary cells, which may result in reduced tight junction functionality, increased proliferation rate, altered drug transporter activity, altered xenobiotic metabolising enzyme activity or reduced sensitivity to chemical toxicity (Geraghty et al., 2014, Kaur and Dufour, 2012). To ensure that cell lines are appropriate models of the respiratory epithelium for particular purposes, they require careful validation and characterisation. Additionally, within and between labs there is the increased need for good cell culture practices to be maintained, for example to avoid cell line cross contamination or to prevent over-passaging cells which may result in “genetic drift” (Hughes et al., 2007). Genetic drift, or the gradual changes to the cell genotype (and subsequently cell phenotype), due to accumulative mutations, has been shown to significantly change cell function and toxicant sensitivity (Gutbier et al., 2018) and therefore low passage numbers should be maintained where possible between experiments to ensure reproducible results and the maintenance of the characterised cell phenotype. Additionally, mycoplasma contamination represents a major issue with the culturing of cell lines, estimated to affect 15-35% of cell lines (Uphoff and Drexler, 2002), and whilst it may go undetected it has been shown to significantly alter cell phenotype (Shin and Van Diggelen, 1978). Despite this if good practices are maintained and the models used are authenticated and well-characterised, then these *in vitro* models offer great opportunities and may be used to replace or provide complementary data to *in vivo* models. An example of this is that permeability data from the intestinal cell line Caco-2 is currently accepted by regulatory bodies such as the US FDA, in some circumstances as a replacement to *in vivo/ex vivo* oral permeability data (Jarc et al., 2019, Larregieu and Benet, 2013). The success of the Caco-2 *in vitro* cell line model, which has now been used for drug development applications for over 35 years, can be attributed to good characterisation in terms of tight junctions, drug transporter activity and xenobiotic metabolising enzyme functionality (Sambuy et al., 2005, Kuncharoenwirat et al., 2021).

Currently, there is no single respiratory epithelial cell line, that is comparable to the intestinal cell line Caco-2, with regards to widespread use, characterisation and acceptance from regulatory bodies in lieu of *in vivo* data (Gordon et al., 2015).

**Table 1.3** summarises some of the cell lines that have been explored as models for various regions of the respiratory tract, many of which have been used to study toxicity, permeability or metabolism.



**Table 1.3. Summary of commonly used human cell lines to represent different regions of the respiratory tract. ✓ = extensive use, ? = limited or contradictory data, X = extensive data showing the model to be unsuitable, N/A = no available data or not applicable.**

Cell type	Cell line	Experimental use/suitability			Reference
		Toxicity	Permeability	Metabolism	
Nasal	RPMI-2650	✓	?	?	(Mercier et al., 2018, Kreft et al., 2015b)
Pharyngeal	FaDu	✓	N/A	N/A	(Rangan, 1972)
Laryngeal	Hep-2	✓	N/A	N/A	(Den Beste et al., 1966)
Tracheal	9HTE16o-	✓	✓	N/A	(Steimer et al., 2005)
(Tracheo-) bronchial	BEAS-2B	✓	X	✓	(Forbes and Ehrhardt, 2005, Sakagami, 2020)
	16HBE14o-	✓	✓	?	(Selo et al., 2021, Steimer et al., 2005, Forbes and Ehrhardt, 2005)
	NuLi-1	✓	✓	N/A	(Sporty et al., 2008, Mroz and Harvey, 2019)
	Calu-3	✓	✓	✓	(Forbes and Ehrhardt, 2005, Sakagami, 2020)
	NCI-H441	✓	✓	?	(Selo et al., 2021, Salomon et al., 2014, Steimer et al., 2005)
Alveolar	A549 (Type II)	✓	X	✓	(Selo et al., 2021, Steimer et al., 2005, Forbes and Ehrhardt, 2005)
	TT1 (Type I)	✓	X	?	(van den Bogaard et al., 2009, Jarvis et al., 2018)
	hAELVi (Type I)	✓	✓	?	(Kletting et al., 2018, Selo et al., 2021)
	NCI-H441	✓	✓	?	(Selo et al., 2021, Salomon et al., 2014, Steimer et al., 2005)
Alveolar Macrophage	THP-1	✓	N/A	N/A	(Kletting et al., 2018, Forbes et al., 2014)

Whilst Calu-3, A549, 16HBE14o- and BEAS-2B cells are commonly used models (Sakagami, 2006, Forbes and Ehrhardt, 2005) with a well-established history, there are also newer or less well characterised cell lines. For example, the non-cancer derived TT1 an alveolar type-I like cell line may be a better model of the alveolar region than the cancer-derived alveolar type-II like cell line A549 (van den Bogaard et al., 2009, Jarvis et al., 2018). Neither of these models has been shown to form suitable permeability barriers, but A549 has been extensively tested for this, whilst only one published study has explored whether the epithelial barrier of TT1 may be improved to better represent normal alveolar permeability by optimising seeding density or culturing conditions (van den Bogaard et al., 2009). It may be worthwhile to pursue this as poor results in early permeability studies with the distal lung *in vitro* model NCI-H441, have been significantly improved upon through the optimisation of seeding densities, growth at air-liquid interface and the addition of various supplements (Selo et al., 2021). There is also early data to suggest that the TT1 model may also be a more sensitive model of genotoxicity than A549, in addition to expressing xenobiotic metabolising enzymes such as CYP1A1, CYP1B1 and NQO1 (Jarvis et al., 2018). In contrast, the newer alveolar model hAELVi, is also non-cancer derived and forms physiologically relevant permeability barriers (Kletting et al., 2018, Selo et al., 2021), although it has been less well studied in terms of toxicity and metabolism. Uptake of the hAELVi model may be limited by its relatively high cost in comparison to other *in vitro* models.

Although each cell line is most commonly used as a monoculture, the combination of these cell lines as co-culture models has also been explored and may be of value improving the physiological relevance of the system being studied. Examples include the pairing of alveolar macrophage cell line THP-1 with the alveolar cell lines TT1 or A549 (McKenzie et al., 2015, Yanamala et al., 2016, Danielsen et al., 2009), or the use of dendritic, endothelial or fibroblast cells basolaterally (Lehmann et al., 2011, Blom et al., 2016, Hermanns et al., 2004). These models, have primarily focused on either inflammatory models, or improving permeability barrier function. It is notable that whilst many of the respiratory epithelial cell lines currently used are homogenous monocultures, intestinal Caco-2 cell cultures represent a heterogeneous cell population which has led to significant divergence and lab-to-lab variation over time but also may better represent the heterogeneous cell population of the intestinal environment (Lea, 2015, Vachon and Beaulieu, 1992, Walter and Kissel, 1995). A heterogeneous bronchial epithelial cell line, or one that has the capacity of basal and club cells to not only multiply but also differentiate into other cell types, may better replicate the diverse cell type and functionality of the respiratory epithelium, particularly in relation to modelling xenobiotic

absorption, metabolism and toxicity in a way that is physiologically relevant or comparable to the *in vivo* situation.

### **1.6.3.3 Synthetic or non-biological *in vitro* models**

Sometimes deemed *in chemico* models, there are a few examples of non-biological *in vitro* models for permeability and toxicity. The Parallel Artificial Membrane Permeability Assay (PAMPA), relies on an artificial lipid infused membrane that replicates the permeability barrier that would typically be created by lipid bilayer/biological membrane of epithelial cells for intestinal, dermal, respiratory permeability or by endothelial cells for the blood-brain barrier (Mensch et al., 2010, Sun et al., 2017). As it is based on chemical constituents, there is no active transport and it only models transport by diffusion, so it is often complementary to typical *in vivo* or *in vitro* models. However, the relatively low cost, reduced experimental set-up time, amenability to high-throughput screening, simplicity and correlation with cell-based models have contributed to increased use of PAMPA and popularity within industry (Avdeef, 2005, Zhu et al., 2002). Various lipid formulations have been used, including to the validation through lipid extraction from *ex vivo* epithelial tissues (Seo et al., 2006, Bicker et al., 2016, Avdeef, 2005). To date, however, PAMPA has not been extensively explored as an alternative *in vitro* model for lung permeability. A PAMPA formulation developed within the Forbes group was used in this thesis to assess xenobiotic transport and compared to commonly used respiratory epithelial models. Additionally, a similar assay was developed using rat lung lipid extract, which to the best of the author's knowledge is the only example of this as a respiratory permeability model but is comparable to reported approaches to using brain lipid extract as a model of the blood brain barrier (Kansy et al., 2004, Mensch et al., 2010).

Whilst it does not currently exist for the respiratory epithelium, *in chemico* skin sensitisation assays based on covalent binding to proteins/small peptides or the "direct peptide reactivity assay", now form parts of an accepted alternative to animal testing, based on new OECD guidelines (Natsch et al., 2021, Kolle et al., 2021, Kolle et al., 2020). In the future, similar assays might be used with regards to lung toxicity, e.g. depletion/binding assays to antioxidants/proteins found within airway surface liquid. The use of such models in the right context may be prudent; Sørli et al. (2018) has highlighted that *in vitro* inhibition of lung surfactant properties is in some cases predictive of acute inhalation toxicity observed with *in vivo* mouse models. With the development of synthetic lung fluid (Hassoun et al., 2018, Kumar et al., 2017) and the use of chemical based models that replicate the physicochemical

environment of the respiratory lumen/epithelium, there is scope for other chemical based assays that may complement or replace existing *in vivo* or *in vitro* assays.

#### **1.6.4 *In silico* models**

Currently *in vivo*, *ex vivo* and *in vitro* models are the predominant methods through which data is obtained to understand xenobiotic toxicity, permeability and metabolism within the respiratory tract. However, increasingly computer based or *in silico* models are used to contextualise, combine or better understand these data sets. Additionally, with increased study of aerosol properties and the respiratory system, several *in silico* models have emerged that may predict aerosol deposition or xenobiotic toxicokinetics based on *in vitro* data or the chemical structure of the xenobiotic.

##### **1.6.4.1 Aerosol deposition models**

The use of *in silico* models to predict of aerosol deposition is well established (Stahlhofen et al., 1989). Deposition modelling largely relies on the known aerosol properties MMAD and GSD which were described earlier (and may be determined experimentally), however new approaches continue to be developed and validated (Huang et al., 2021). Initial *in vitro* data is commonly collected using either the Anderson Cascade impactor (ACI) originally developed for environmental aerosols or the newer Next-Generation Impactor (NGI) which was developed specifically for inhaled pharmaceuticals (Mohammed et al., 2012, Nichols et al., 1998). Although there are key differences between the two models, both essentially separate particles into separate compartments based on aerodynamic particle size (Guo et al., 2008). This data may be used along with known or standard default settings for the lung (e.g. lung volume, airway branching, airway diameter, inhaled flow rate) to then predict regional deposition.

Computational approaches for deposition prediction may be divided into two categories, those which rely on algebraic whole-lung models and those which use computational fluid dynamics (CFD) instead (Koullapis et al., 2021). The older algebraic approaches in rely on equations that relate to the previously described deposition mechanisms based on particle size, whilst computational fluid-particle dynamics (CFPD) incorporates 3D considerations for airflow, particle transport and turbulence (Huang et al., 2021, Koullapis et al., 2018). The airway geometry itself is most often based on standardised models, such as the Weibel lung model or the ICRP or NCRP models (Bailey, 1994, Kuempel, 1997, Weibel et al., 1963). CFPD models for

deposition prediction are becoming more widely used, as they better account for the complex effects of breathing patterns and geometric variability, however their complexity and high computational expense often limits the number of airway generations/regions that can be modelled (Koullapis et al., 2021). Whilst CFPD models have great potential and are actively being researched, the majority of commercially available deposition models rely on the algebraic 1D or reduced models, such as the “Multi-Path Particle Dosimetry Model” (MMPD) from Applied Research Associates Inc, “Mimetikos Preludium” from Emmace Consulting and adaptations of “GastroPlus” from Simulation Plus Inc (Hofmann, 2011, Koullapis et al., 2021). Regional deposition modelling is useful as it provides insight into the specific site within the respiratory tract that the xenobiotic may deposit, without the need for *in vivo* imaging or quantitative whole-body autoradiography (QWBA), and may highlight the site of local toxicity for an inhaled aerosol. Additionally, as non-absorptive clearance mechanisms such as mucociliary clearance or metabolism vary regionally in the respiratory tract, as does epithelial permeability and perfusion, regional deposition data is useful for understanding the toxicokinetic fate of the inhaled xenobiotic (Himstedt et al., 2021). For these reasons, regional deposition data is often used as a starting point for physiologically-based pharmacokinetic (PBPK) models, especially for the prediction of respiratory bioavailability.

#### **1.6.4.2 Physiologically-based pharmacokinetic (PBPK) models**

Whilst it may be possible to explore pharmacokinetics through the use of *in vivo* models, for the acquisition of human-relevant data early in the drug discovery process or for the purpose of environmental/occupational risk assessments, the use of *ex vivo* or *in vitro* models is required. PBPK *in silico* models can combine *in vitro* data mechanistically to make predictions of pharmacokinetics. The physicochemical properties of the xenobiotic determine in part how it will interact with the physiological system, and absorption, distribution, metabolism and elimination (ADME) processes within the body will determine the kinetic fate of the xenobiotic. Aspects of this process, may be estimated *in vitro*, or through *in vivo* animal data, to provide inputs for a PBPK model (Kuepfer et al., 2016). The model combines this data with internal algorithms that aim to mathematically describe physiologically-relevant processes in order to predict various pharmacokinetic outputs, e.g. % bioavailability, maximum xenobiotic concentration in plasma ( $C_{max}$ ), clearance rate. Well validated PBPK models are capable of producing *in silico* predictions that may reduce the need for *in vivo* studies, or help inform *in vivo* or *in vitro* studies in terms of dose used or time-points for sampling (Zhuang and Lu, 2016, Tan et al., 2020). Although PBPK models are often associated with pre-clinical drug

development, PBPK models are actively being explored for their chemical risk assessment applications and as part of an alternative approach to *in vivo* acute inhalation toxicity testing (Clippinger et al., 2018b, Tan et al., 2020).

A variety of inhalation pharmacokinetic models have been described for assessing absorption/bioavailability, including the AstraZeneca “LungSim” model (Tehler et al., 2018) and the Pfizer “PulmoSim” model (Borghardt et al., 2015). Commercially available models include “GastroPlus” from Simulation Plus Inc and Emmace Consulting’s “Mimetikos Preludium” (Eriksson et al., 2020, Olsson and Bäckman, 2018). PBPK models typically rely on empirical and mechanistic pharmacometric approaches, usually a mixture of the two. Empirical modelling, uses available pharmacokinetic data or standard compartmental parameters, such as an experimentally determined plasma-concentration profile, plasma protein binding coefficients or gastrointestinal absorption, from which other pharmacokinetic parameters may be estimated, such as distribution of the drug, or clearance rates. In contrast, mechanistic modelling simulates certain physiologically relevant bodily processes e.g. rate of mucociliary clearance, perfusion rates, permeation across an epithelium in relation to tissue depth. Subsequently, most PK models are semi-mechanistic, and compartmentalise different organs or tissues, which are characterised by variable factors such as perfusion rates, tissue volumes and depths (Himstedt et al., 2021). An example of this is that the Mimetikos Preludium model, which is semi-mechanistic, mechanistically simulates mucociliary clearance or epithelial absorption based on experimentally determined values (either default values or set by the user), but systemic distribution and elimination are simulated from standard compartmental parameters (Olsson and Bäckman, 2018).

In addition to stand alone PBPK models, several software packages exist to predict *in silico* various pharmacokinetic parameters that would otherwise be determined *in vitro*. Whilst *in vitro* measurements are still optimal, as not every pharmacokinetic property may be accurately predicted *in silico* based on limited “training set” data, *in silico* models may provide rapid estimates that may aid experimental design of *in vitro* experiments or allow for *in silico* pharmacokinetics to be predicted initially in the absence of *in vitro* data. An example of this is that the pCEL-X software (In-ADME Research), allows for the prediction of blood brain barrier (BBB), Caco-2 and PAMPA permeability, based on the 2D molecular structure of the compound, which may help inform the selection of optimal assay conditions for *in vitro* experiments such as timepoints for sampling (Avdeef and Tam, 2010, Yusof et al., 2014). The model can also be used to assess what mode of transport is likely e.g. passive, paracellular,

carrier-mediated, active uptake or efflux (Avdeef et al., 2008). Plasma protein binding predictions may give an early indicator of whether plasma should be diluted for the *in vitro* experiment if binding is predicted to be especially high. Equally, the properties of molecules that have not yet been synthesised can be explored. Additionally, computational approaches to predict not only xenobiotic transport but also distribution at a cellular and subcellular level have been developed, based on mechanistic cellular pharmacokinetic models (Min et al., 2014). These models which focus on microscopic xenobiotic kinetics, may have macroscopic implications, examples include methods for predicting or analysing intracellular binding, lysosomal trapping and P-glycoprotein efflux (Jang et al., 2003, Trapp et al., 2008, Bourdet et al., 2006).

Other *in silico* models may be useful for the prediction of xenobiotic metabolism. A vast variety of computational methods have been described for the prediction of xenobiotic metabolism, mainly as a complementary or preliminary method, before confirmation *in vitro* or *in vivo* (Kirchmair et al., 2015). Most have focused on major CYP isoforms and UGT-mediated metabolism, with relevance to orally administered drugs and hepatic metabolism, however the prediction of pesticide/agrochemical metabolism has also been explored (Clark, 2018). Most of these approaches rely on computational chemistry approaches along with the training sets from known experimental data, to create a “knowledge-based system” for commercially available metabolite predicting software like “MetabolExpert”, “Meteor Nexus”, “MetaDrug” and “TIMES”, all of which predict both Phase I & II metabolism (Kirchmair et al., 2015). Additionally, with the use of toxicity prediction software based either on knowledge-based systems such as “DEREK Nexus” and “HazardExpert” or quantitative structure-activity relationships (QSARs) such as for “TIMES”, “SYMMETRY” or “CASE Ultra”, there is the ability to also predict toxicity *in silico* for both the parent or the metabolite compound (Madden, 2010, Patlewicz and Fitzpatrick, 2016, Dearden, 2003, Kirchmair et al., 2015). With the advent of HTS *in vitro* toxicity assays, training sets for *in silico* toxicity prediction will continue to expand and improve, in addition to increased research into machine learning approaches (Singh et al., 2020, Idakwo et al., 2018, Zhang et al., 2018).

Overall, the use of *in silico* approaches in the form of PBPK models or through other software, present useful opportunities in terms of predicting respiratory toxicokinetics. Quantitative data from these approaches may also aid the refinement of *in vitro* studies and help contextualise the generated data. These applications are partially explored in **Chapter 3** and **4**.

## 1.7 Aims and scope of thesis

The aim of this thesis was to develop experimental methods suitable for exploring pesticide-induced local toxicity in the respiratory tract and the fate of the inhaled pesticides in terms of respiratory bioavailability and toxicokinetics. Based on the literature reviewed above, considerations for this including the aerosol properties of pesticide sprays and site of deposition in the respiratory tract, the influence of non-absorptive clearance mechanisms, the physicochemical properties of the pesticide and the sensitivity of the biological model to pesticide induced toxicity. The research questions below, reflect these considerations.

## 1.8 Research questions and objectives

### **Chapter 2: Which *in vitro* lung models are most suitable for the study of local toxicity, transepithelial permeability and *in situ* metabolism of unintentionally inhaled xenobiotics?**

- Evaluation of differences in sensitivity of respiratory epithelial cell lines to the toxic effects of various pesticides.
- Optimise and evaluate the suitability of different *in vitro* Transwell-based cell layers to present respiratory epithelial-like permeability barriers.
- Identify and develop suitable *in vitro* models for the assaying of xenobiotic metabolism within the respiratory tract.

### **Chapter 3: Can *in vitro* data provide an evidence-based approach for the prediction of respiratory and systemic bioavailability of pesticides inhaled during occupational exposure?**

- Combine *in vitro* data and *in silico* computational methods to estimate lung concentrations and the risk of systemic exposure following pesticide inhalation in an occupational setting based on pesticide physicochemical properties, aerosol deposition, *in vitro* permeability and mechanistic pharmacokinetic modelling.
- Apply this approach to predicting respiratory bioavailability for occupational exposures and evaluate the strengths and weaknesses.

### **Chapter 4: Can NMR metabolomics measure changes to lung cell phenotype following pesticide exposure at subtoxic concentrations?**

- Measure metabolic changes in alveolar and bronchial cells in response to different fungicides.
- Compare the sensitivity and responses of normal “immortalised” and cancer derived alveolar/bronchial epithelial cells to fungicides.



- Elucidate potential modes of action for pesticide respiratory toxicity based on changes to the metabolome,
- Evaluate the benefits and limitations of NMR metabolomics to studying respiratory toxicity

Collectively, these research questions highlight possible methods or strategic approaches for determining local toxicity and respiratory and systemic bioavailability of unintentionally inhaled xenobiotics, by adapting techniques commonly used in pharmaceutical sciences. Occupational exposure to pesticides is used as an example scenario and NMR metabolomics is used as a contemporary approach to studying changes to cell phenotype. It is anticipated that the findings will provide novel *in vitro* toxicology methods which relate to a realistic evaluation of inhaled exposure. Future new approach methodologies (NAMs) developed with improved guidance and clear requirements from regulatory bodies, are key to gaining regulatory acceptance of *in vitro* models for respiratory toxicity and bioavailability. For NAMs to be included in future OECD guidelines for testing of chemicals, along with the existing integrated approaches to testing and assessment (IATA), improved transparency and a clearer roadmap to acceptance are needed from regulatory bodies.

# Chapter 2

## Evaluation of *in vitro* respiratory permeability and toxicity models.

### 2.1 Introduction

Several respiratory models have been studied for their suitability to predict the local toxicity, permeability, and metabolism of inhaled xenobiotics. These models include *in vitro*, *in vivo* and *ex vivo* models that attempt to replicate and understand the human *in vivo* situation. Whilst studies in animal models are currently a requirement for the testing the inhalation safety of pesticide before they are registered by regulatory bodies such as EFSA or the EPA, interspecies differences may limit their ability to accurately predict pesticide safety in humans. This consideration, along with ethical concerns and cost, reinforce the goal to reduce, replace and refine animal models where possible. Human *in vitro* models may overcome several of the issues highlighted above, in addition to being more amenable to high-throughput screening. Although acute respiratory toxicity is most often determined through the use of rodent inhalation studies, and there is no *in vitro* stand-alone replacement that is accepted by regulatory bodies, there remains a need for informative, mechanistic human based *in vitro* models (Movia et al., 2020). It remains a key goal within the field of respiratory toxicology to reduce, refine and replace the use current animal models, by moving towards improved *in vitro* and *in silico* models which eliminate considerations of interspecies differences and better represent the human risk.

The use of *in vitro* respiratory models for toxicity studies is extensive and varied, ranging from simple 2D monocultures of lung cell lines such as A549, to coculture of mixed cell types, complex 3D organotypic models such as the commercially available MucilAir or EpiAirway and also advanced “lung-on-a-chip” models. Whilst none of the models fully replicate the complexity of the respiratory tract, they are useful in elucidating mechanism of action and potential severity of toxicity with inhaled xenobiotics. Whilst the more complex models may more accurately incorporate important features of the respiratory epithelium, the simpler models are often more amenable to high throughput assays both due to ease of use, reduced cost and in the case of cell lines avoid issues with donor availability or genetic variation. The variety of existing respiratory toxicity models, highlights the need for medium to high

throughput toxicity models, that provide reproduceable results which may inform potential adverse outcome pathways following inhaled exposure to various xenobiotics.

This requirement is a key aspect of an integrated toxicity risk assessment approach, that investigates not just toxicity but also toxicokinetics, which focuses also on the fate of the xenobiotic within the body, with respiratory epithelial permeability contributing to absorption and distribution of both the parent compound and possible metabolites formed by lung cells (Coecke et al., 2013).

The use and suitability of different lung epithelial permeability models was recently described by Enlo-Scott et al. (2021b). Whilst many of these models are commonly used, and continue to be improved, there remains the necessity to validate and optimise the experimental conditions and the type of model used. This is exemplified through the “gold-standard” *in vitro* intestinal permeability model using the Caco-2 cell line, for which there is often high lab-to-lab variability, limiting the reproducibility and reliability of predicted xenobiotic permeability and intestinal absorption (Lee et al., 2017). The sources of this variability relate not just to the final experimental conditions of the permeability assay, such as the transport medium used and stirring/shaking speed (the latter of particular importance to lipophilic compounds), key sources of variability also related to factors affecting the cell culturing conditions prior to the experiment, with these influencing the properties of the monolayer/permeability barrier formed. Determinants relating to Transwells include the material and pore size of the Transwell membrane, in addition to whether it was pre-coated with an extracellular matrix such as collagen or fibrinogen. Determinants related to cells include; seeding density which may impact the ease of which a uniform monolayer is formed and cell line passage number due in part to the influence/change in cell phenotype over time. The time taken for the monolayer to form, and the final monolayer thickness are also important, in addition to the TEER achieved prior to the permeability experiment. Finally, the monolayer properties may be altered based on the cell culture medium (including supplements) used and the volume of medium in both the apical and basolateral chambers which may affect the hydrostatic pressure applied to the membrane. Additionally, in the case of respiratory epithelial cell lines, the polarisation and differentiation of the membrane may also benefit from culturing at Air-Liquid Interface (ALI), with this potentially influencing the functional expression of important proteins related to xenobiotic absorption, such as the tight junction proteins ZO-1, E-cadherin, Claudin-1, Claudin-3, Claudin-5 (Grainger et al., 2006, Togami et al., 2017, Ehrhardt et al.,

2002) and drug transporters including P-glycoprotein, MRPs, BCRP, OCTs and OATs (Bosquillon, 2010, Endter et al., 2009).

In contrast to the use of intestinal cell line Caco-2 to predict the absorption of orally administered xenobiotics, the use of respiratory epithelial cell lines to predict the absorption of inhaled xenobiotics is much less standardised and not currently accepted by regulatory bodies, highlighting the need for more extensive characterisation and validation.

Finally, in addition to local toxicity and permeability of inhaled xenobiotics, it is of importance to consider non-absorptive clearance mechanisms. To fully understand the fate of inhaled xenobiotics, the extent to which they may be cleared either by mucociliary clearance (primarily within the conducting airways), or metabolism by respiratory epithelial cells. Only a few *in vitro* models that incorporate mucociliary clearance, such as the commercially available MucilAir™ for which there are functional cilia where the movement of solid particles may be visualised microscopically. However, whilst the MucilAir™ model is composed of reconstituted human primary cells which include functional ciliated cells, mucus producing goblet cells and basal cells, the use of this model is limited by both expense and limited throughput in addition to the potential genetic variability between donors. In contrast, of the respiratory cell lines available only Calu-3 is well-established to produce mucus (Cingolani et al., 2019, Grainger et al., 2006, Haghi et al., 2010), but there is limited evidence for the presence of functional cilia (regardless of the culture conditions).

Another key non-absorptive clearance mechanism is *in situ* metabolism by respiratory epithelial cells. The extent of xenobiotic metabolism in the lungs and the potential implications has recently been reviewed by Enlo-Scott et al. (2021a) highlighting; (i) the expression of xenobiotic metabolising enzymes in the lung, factors affecting metabolic activity, (ii) current models for measuring and predicting xenobiotic metabolism in the lung, and (iii) the implications for inhalation toxicology. Whilst there is an abundance of mRNA transcript data for both human primary cells and cell lines, there is less evidence of functional enzyme activity within the different respiratory epithelial cell lines and due to the existence of several functionally inactive enzyme polymorphisms, mRNA or protein analysis data alone cannot accurately predict enzyme activity within *in vitro* models. A large proportion of functional activity assays have focused on primary cell models or *ex vivo* models such as precision-cut lung slices, those that include human cell lines typically use A549 or BEAS-2B, whilst there is an absence of data for a multitude of other cell lines which may prove to be more representative of the varied enzyme expression within the lung.

Although human lung enzymes are readily available from commercial sources, these are obtained from lung homogenate which means that the xenobiotic metabolising enzymes (XMEs) within the highly metabolically competent epithelial cells are “diluted” by mixing with mesenchymal, blood and vascular cells. Additionally, as this relies on primary human tissue, donor-to-donor genetic variability may also be a concern. Currently, where the xenobiotic metabolising enzyme-rich hepatic cell line HepaRG is now commonly used in similar functional assays, and Caco-2 may be used to model intestinal metabolism, there is currently not a human lung cell line with a club or ciliated cell phenotype that expresses all of the key xenobiotic metabolising enzymes in the lung. Additionally, RPMI-2650 is one of the few commercially available human nasal cell lines, but functional xenobiotic metabolising enzyme activity has not been extensively characterised, despite the presence of xenobiotic metabolism enzymes in normal human nasal epithelium (Oliveira et al., 2016).

## **2.2 Aims and Objectives**

The overall aim of this series of experiments was to develop and evaluate *in vitro* lung models for their suitability to study the local toxicity, transepithelial permeability and *in situ* metabolism of unintentionally inhaled xenobiotics.

Specific objectives included:

- 1.** Evaluate differences between respiratory epithelial cell lines with regard to their sensitivity to the toxic effects of various pesticides.
- 2.** Optimise the culture of respiratory cell lines in Transwells to form permeability barriers.
- 3.** Gauge the suitability of *in vitro* models for assaying xenobiotic metabolism within the respiratory tract.

## 2.3 Methods

### 2.3.1 Evaluating common *in vitro* toxicity models

#### 2.3.1.1 MTT Assay

The MTT assay is a colorimetric cell viability assay used to assess the metabolic activity and reflect the number of viable cells present. It relies on the reducing capability of intracellular enzymes (predominantly mitochondrial dehydrogenases, such as succinate dehydrogenase) to convert the soluble yellow dye 3-(4,5-dimethylthiazol-2-yl)-2,5-diphenyltetrazolium bromide (MTT) to insoluble purple formazan crystals by cleaving the heterocyclic tetrazolium ring in the MTT molecule **Figure 2.1**.

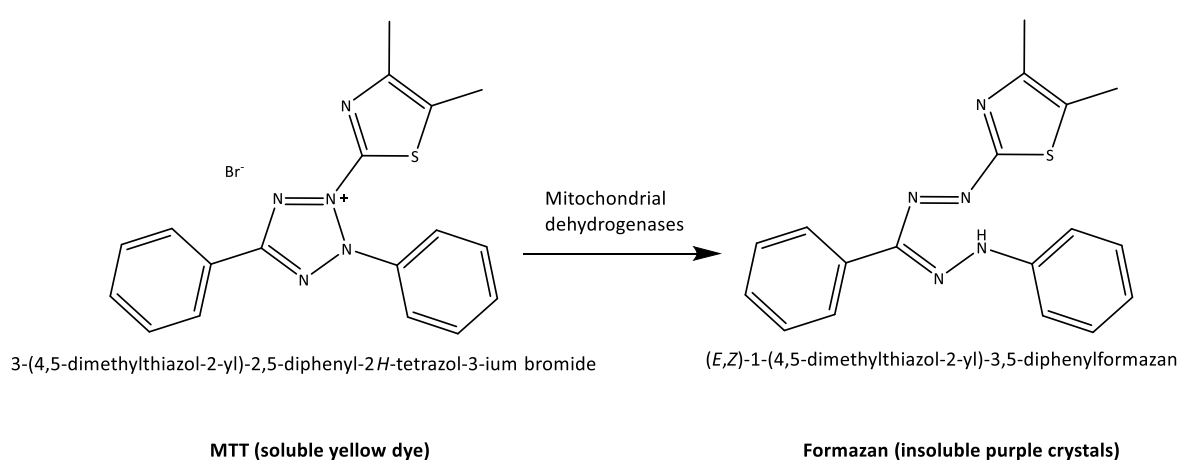


**Figure 2.1. Chemical reduction of MTT to formazan by mitochondrial dehydrogenases in viable cells.**

#### 2.3.1.2 MTT assay calibration

In order to use the MTT assay, the optimum cell seeding density needs to be determined as it will vary depending on assay conditions and cell type. To determine the optimum seeding density, that would allow for the linear quantification of MTT UV absorbance, each cell line was seeded in 96-well plates (Greiner CELLSTAR®) and a calibration curve was made using a serial dilution method. The cell seeding densities varied from 195-100,000 cells per well (growth surface area of 0.34 cm<sup>2</sup>/well), the outer wells were filled with medium only to eliminate edge evaporation effects that may reduce evenly distributed cell binding to the well. The cells were incubated for 48 hours under standard conditions, i.e. using the appropriate cell medium for the particular cell line. Following this, cell culture medium was aspirated and replaced with 100 µL per well of MTT solution (MTT 5 mg/mL in PBS, diluted 1:5 in fresh cell culture medium). After 4 hours the MTT containing medium was gently aspirated and any formazan crystals formed were solubilised with 100 µL of SDS solution (10% SDS in a 1:1

mixture of dimethylformamide: deionised water). After 16-24 hours, the absorbance of each well was measured by spectrophotometry at 570 nm, subtracting the background absorbance at 650 nm. The final absorbance values were calculated as absorbance of cell containing wells was calculated as absorbance subtracted from blanks. The assay was performed with six replicate wells for each seeding density, with the experiment being repeated in triplicate. The optimal seeding density for subsequent toxicity tests was selected based on the highest seeding density within a linear range established for UV absorbance values vs number of cells.

### 2.3.1.3 MTT assay

For the MTT assay, the seeding densities were used for each cell line, as shown in **Table 2.1**.

*Table 2.1. Cell seeding densities and cell medium composition for the MTT assay.*

Cell line	Cell medium	Cell seeding density (cells/well)
A549	DMEM + 10% FBS, 1% NEAA, 1% P/S, 1% SP	4000
BEAS-2B	LHC-8 + 1% P/S	20,000
Calu-3	DMEM + 10% FBS, 1% NEAA, 1% P/S, 1% SP	40,000
RPMI-2650	DMEM + 10% FBS, 1% NEAA, 1% P/S, 1% SP	40,000
TT1	DCCM-1 + 10% FBS, 1% NEAA, 1% P/S	4000
16HBE14o-	DMEM + 10% FBS, 1% NEAA, 1% P/S, 1% SP	4000
Caco-2	DMEM + 10% FBS, 1% NEAA, 1% P/S, 1% SP	40,000

Depending on the cell line, DMEM, LHC-8 and DCCM-1 medium was used, this was based upon what is commonly used in the literature. Supplements such as foetal bovine serum (FBS), non-essential amino acids (NEAA), penicillin-streptomycin (P/S) and sodium pyruvate (SP), were used where necessary.

Regardless of cell seeding density, all cells were seeded in 100  $\mu$ L of the same medium used for their culture in cell culture flasks (**Table 2.1**) and were grown for 24 hours before exposure to the test compounds.

Average cell viability and cell number was quantified prior to cell seeding, using the Trypan Blue dye exclusion method with an automated cell counter (Countess™ II FL Automated Cell Counter, Invitrogen). The compounds tested included; abamectin, acibenzolar-S-methyl, chlorothalonil, diquat, isopyrazam, pinoxaden, propiconazole and prosulfocarb.

With the exception of BEAS-2B (which was cultured in serum free LHC-8 medium), pesticide stock solutions were prepared in phenol red-free minimum essential medium with reduced serum concentration, (2% FBS) to give starting concentrations of 300 µM, this was serially diluted to give the final concentrations of 300, 150, 75, 40, 20, 10, 5 and 2.5 µM in 100µL medium ( $\leq$  0.75% DMSO). Medium containing 0.75% DMSO or 1% Triton X-100 were respectively used as negative and positive controls. Cells were exposed to the test compounds for 24 hours, before the pesticide containing medium was aspirated and replaced with 100µL phenol red free minimum essential medium and 25 µL MTT solution (5 mg/mL in PBS). After 4 hours, the MTT containing medium was aspirated and any formazan crystals formed were solubilised with 100 µL of SDS solution (10% SDS in a 1:1 mixture of dimethylformamide: deionised water). After 16-24 hours, the absorbance of each well was measured by spectrophotometry at 570 nm, subtracting the background absorbance at 650 nm. Relative cell viability was calculated using the equation:

**Equation 2.1. % Cell viability**

$$\% \text{ Cell viability} = \frac{T - B}{C - B} \times 100$$

Where T is the UV absorbance value of the test well, B is the UV absorbance of the blank well (containing no cells) and C is the absorbance of the negative control (0.75% DMSO) representing 100% cell viability.

The assay was performed with six replicate wells for each test concentration, with the experiment being repeated in triplicate.

**2.3.1.4 Mechanistic toxicity assay**

A protocol was adapted from Joshi et al. (2019), the original assay having been designed for high-throughput assessment of mechanistic toxicity using confocal microscopy.

16HBE14o- were seeded (4000 cells/well) in a black walled µClear Greiner 96-well plates (#655090) and cultured in 200 µL fresh medium for 48 hours, to reach 100% confluency.

Following the same protocol described earlier for the MTT assay, cells were exposed for 24 hours to either abamectin, acibenzolar-S-methyl, azoxystrobin, chlorothalonil, diquat, isopyrazam, pinoxaden, propiconazole or prosulfocarb at a final concentration of 10 µM in 100 µL medium (0.025% DMSO). Following this exposure, the pesticide containing medium was aspirated and the cells were rinsed once with warm HBSS before incubating in 50 µL HBSS containing 3 fluorescent dyes; calcein-AM to assess cell viability/membrane integrity,



tetramethyl rhodamine methyl ester (TMRM) to assess changes to mitochondrial membrane potential/mitochondrial impairment and monochlorobimane (MClB) to identify changes intracellular glutathione level. Unlike the original assay, Hoechst 33342 was not included due to overlap with the fluorescence from MClB, additionally DNA damage could not be assessed by this method as images were not obtained. Hoechst 33342 could instead be used to assess cell proliferation, if MClB was not included.

The incubation was performed in the dark for 40 minutes at 37°C, with HBSS containing a mixture of calcein-AM 0.25 µM, TMRM 0.5 µM and MClB) 100 µM for approximately 40 minutes. Following the incubation period, the incubation medium was aspirated and rinsed twice with 100 µL of PBS, and replaced with 50 µL PBS before immediately measuring the fluorescence of MClB (ex/em = 360/465 nm), calcein-AM (ex/em = 485/535 nm) and TMRM (ex/em = 535/595 nm). Relative changes were calculated using the same equation described previously for the MTT assay, where values were subtracted from blank well and normalised against the DMSO control. The assay was performed with four replicate wells for each test concentration, with the experiment being repeated in triplicate. Based on the preliminary results this experiment was then repeated to obtain 0-300 µM dose response curves for 4 pesticides with different mechanisms of cytotoxicity; abamectin (apoptosis and potential mitochondrial inhibition), azoxystrobin (quinone outside/mitochondrial inhibition), chlorothalonil (apoptosis and glutathione depletion) and isopyrazam (mitochondrial/succinate dehydrogenase inhibition).

### **2.3.2 Evaluating common *in vitro* permeability models**

#### **2.3.2.1 Transwell model using epithelial cells**

The Transwell model, is a commonly used *in vitro* permeability model formed by seeding epithelial cells on a semi-permeable membrane and culturing the cells under conditions that allow for the formation of a functional and polarised epithelial permeability barrier, that may then be used to study xenobiotic transport across the barrier. A basic representation of the model is shown in **Figure 2.2**. Additional variations with a focus on lung epithelial cells are described further and illustrated by diagrams in a recent review by Enlo-Scott et al. (2021b).

### 2.3.2.2 Initial culturing conditions

For all Transwell experiments unless stated otherwise, sterile 6.5 mm Transwell® inserts (Corning, C3470) with 0.4 µm pore polyester membranes were used. Prior to cell seeding, Transwells were incubated with 100 µL medium and 500 µL medium on the apical and basolateral side respectively, for at least 30 minutes to pre-wet the membrane. In experiments where cells were cultured on collagen coated Transwells, the membrane was not pre-wet with medium beforehand, instead 100 µL per well of rat tail collagen solution was added to the apical side of the membrane and incubated for 2 hours at 37°C before gently rinsing twice with PBS.

The same cell seeding densities was used for all the cell lines (A549, BEAS-2B, Calu-3, Caco-2, RPMI-2650, TT1 and 16HBE14o-), 100,000 cells/well in 200 µL per well in the apical chamber and with 500 µL of medium in the basolateral chamber. With the exception of the intestinal epithelial cell line Caco-2, all cells were taken to air-liquid interface after 48 hours, by carefully aspirating the medium from the apical layer. A549, Calu-3 and TT1 cells were cultured for 11-14 days, whilst RPMI-2650, Caco-2, 16HBE14o- and BEAS-2B cells were cultured for 20-22 days.

### 2.3.2.3 Trans-Epithelial Electrical Resistance (TEER)

For all the cell lines, the TEER was measured, and the medium was changed every 2 days. TEER readings were performed using an EVOM™ epithelial voltohmmeter with silver chloride “chopstick” electrodes, the electrodes were sterilised in 100% ethanol and then rinsed in PBS prior to inserting into the Transwell inserts. To measure TEER in the inserts, 200 µL of medium and 500 µL medium was pipetted on the apical and basolateral side respectively, the cell layers had been allowed to equilibrate for approximately 20 minutes before inserting the electrodes. After TEER measurements were completed, medium from the apical chamber of the Transwell was immediately aspirated, to return the cells to air-liquid interface conditions (with the exception of Caco-2). TEER values were calculated using **Equation 2.2**. All experiments were performed with 3 replicate wells and repeated in triplicate.

#### ***Equation 2.2. Transepithelial electrical resistance (TEER)***

$$\text{TEER}(\Omega \times \text{cm}^2) = (\text{Test Transwell } \Omega - \text{blank Transwell } \Omega) \times 0.33\text{cm}^2$$

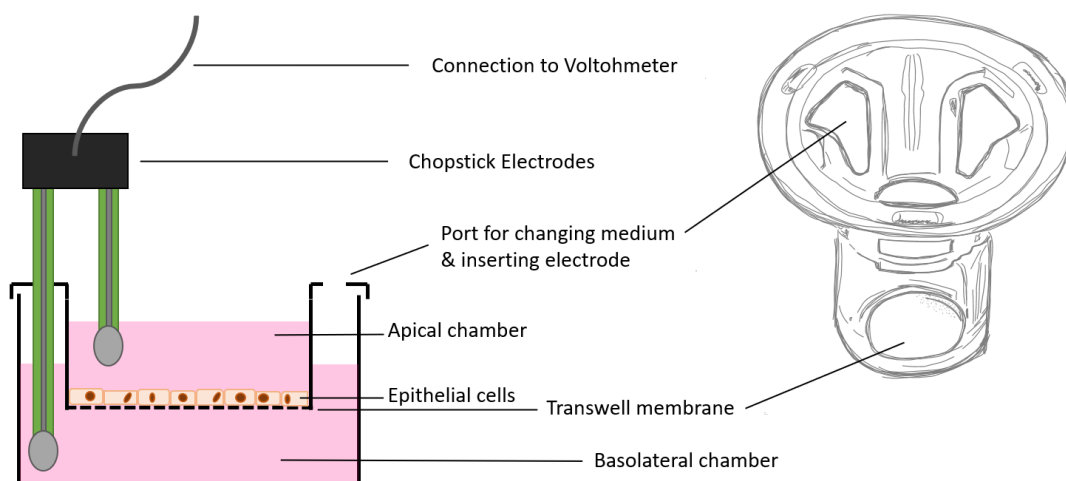


**Figure 2.2.** An illustration showing the structure of a Transwell insert along with a representation of electrodes used to take TEER measurements after growing cells to confluency on the apical side of the membrane.

#### 2.3.2.4 Evaluating different culturing conditions for TT1, BEAS-2B and 16HBE14o-

In order to try to increase the TEER values for the BEAS-2B and 16HBE14o- to be more representative of those described for primary bronchial cells, different culturing conditions were tested. A similar approach was taken to try to increase TEER values for TT1 to be more representative of those described for primary alveolar cells.

Rather than taking the cells to air-liquid interface after 2 days of culturing on Transwells, the cells were kept under submerged liquid culture conditions, replacing the medium every 2 days over the course of 14-16 days for BEAS-2B and TT1 or 20-22 days for 16HBE14o-.

For TT1 three other potential conditions were also tested. Simulated lung fluid (SLF) as has previously been described by Kumar et al. (2017) and shown to be biocompatible with the alveolar cell line A549 for short exposures. SLF was used on the apical surface of TT1 cells, with a total volume of 30  $\mu\text{L}$  on the apical surface and was replaced every two days.

Additionally, rather than pre-coating the Transwell with collagen, basement membrane extract was also tested, as a more representative model of the complex extracellular matrix. This coating has been reported in the literature to be useful in altering the permeability properties of similar *in vitro* models (Mantaj et al., 2018).

Finally, a coculture model was explored using TT1 cells on the apical Transwell surface and the 3T3 mouse fibroblast cell line on the basolateral side of the Transwell. To create this coculture, Transwell membranes were pre-wet with medium as previously described. Cell culture medium was gently aspirated and with sterile tweezers the Transwell insert was removed from the 24 well plate, inverted and placed into the well of a 6 well plate so that the basolateral chamber faced upwards. A 50  $\mu\text{L}$  droplet containing 100,000 3T3 cells in medium, was placed

on the surface of the basolateral chamber, the plate was covered making sure that the lid did not touch the Transwell containing the cell droplet and the plate was placed in the incubator for 2 hours to allow the cells to attach. After cell attachment, the Transwell was placed the correct way up in a 24 well plate, with medium being carefully pipetted into the basolateral chamber, 100,000 TT1 cells/well were pipetted onto the apical side of the Transwell. Following this the coculture was grown as described previously for the TT1 monoculture, with the cells taken to air-liquid interface after 2 days.

For all test conditions TEER values were measured every two days, as previously described.

### **2.3.2.5 Zonula Occludens-1 (Tight Junction Protein 1) confocal imaging**

After the TEER values for each cell line had been measured, the cell layers were stained to visualise expression of the tight junction protein/zonula occludens-1 (ZO-1), and DAPI (4',6-diamidino-2-phenylindole) was used to stain the cell nuclei.

The entire cell staining protocol was performed on ice. The cell layers were incubated for 2 minutes, with a solution containing; 0.2% Triton X-100 in 100 mM KCl, 3 mM MgCl<sub>2</sub>, 1 mM CaCl<sub>2</sub>, 200 mM sucrose and 100 mM HEPES. Cell layers were then rinsed twice with PBS, and permeabilised with 0.05% Triton X-100 in PBS for 5 minutes, rinsed twice with PBS and once with 5% powdered milk in PBS, then incubated with AlexaFluor 488 chicken anti-rabbit IgG 10 µg/mL for 60 minutes at room temperature, before rinsing 4 times with PBS, staining with Prolog Gold antifade reagent with DAPI. Slides were mounted, and refrigerated until imaging within 1 week using an A1 inverted confocal microscope with spectral detector. Fluorescent emissions from DAPI (ex/em= 205/430-480 nm) and AlexaFluor 488 (ex/em = 488/510-570 nm) were collected using separate channels at a magnification of x40 and then the images obtained were overlapped to give a multicoloured composite image. Results shown depict a representative image from a sample size of at least an n = 2 for each cell line.

### **2.3.2.6 Permeability assays with fluorescent permeability markers**

Permeability studies were performed on cell layers after a defined period in culture (14-22 days depending on the cell line), at which point the TEER values had increased to a plateau. The permeability studies made use of three different fluorescent dyes as standard permeability markers. The three permeability probe compounds selected were; sodium fluorescein as a hydrophilic low molecular weight (MW) marker, rhodamine-123 as a low MW lipophilic marker and FITC-dextran-4000 as a hydrophilic high MW marker of permeability.

NaF 8 mg/mL stocks were made in HBSS and Rh-123 10  $\mu$ M stocks in DMSO were frozen at -20°C, FD-4 was made as a 1 mg/mL stock in HBSS on the day of the experiment. Cell medium was aspirated from the apical and basolateral chambers, and replaced with 200  $\mu$ L and 500  $\mu$ L of warm HBSS in the respective compartments, before incubating at 37°C for 30 minutes. HBSS was then aspirated from both chambers, 600  $\mu$ L was placed in the basolateral chamber. 250  $\mu$ L of either 0.2 mg/mL NaF, 50  $\mu$ M Rh-123 or 1 mg/mL FD-4 in HBSS were pipetted into the apical chamber. Immediately 50  $\mu$ L of sample from the apical chamber was transferred to a black walled 96-well plate, and 100  $\mu$ L of sample from the basolateral chamber, the Transwell plate was then incubated at 37°C in the dark until the next timepoint where samples were taken at 5, 15, 30, 60, 120 and 240 minutes, each time replacing with 100  $\mu$ L of fresh HBSS to maintain sink conditions. Immediately after the last time point, the remaining solution in the Transwell was aspirated and replaced with warm HBSS before the TEER value was measured again to ensure that the monolayer integrity had not been significantly reduced during the experiment. HBSS was aspirated and in the basolateral chamber replaced with cell culture medium, the TEER was measured 24 h after the permeability experiment.

The fluorescence of the samples collected in black walled 96 well plates was measured at ex/em = 485/535 nm, using a Tecan Spark 10M plate reader. Apparent permeability coefficients ( $P_{app}$ ) were calculated using the following equation:

**Equation 2.3. Apparent permeability coefficient**

$$P_{app} \text{ (cm/s)} = \left( \frac{dq}{dt} \right) \times \left( \frac{1}{AC_0} \right)$$

Where  $dq/dt$  = transport rate,  $A = 0.33\text{cm}^2$  (the surface area of the Transwell insert),  $C_0$  = the initial concentration of the permeability marker in the donor chamber.

**2.3.2.7 Lipid based permeability models using Transwells**

Non-cell based models were also tested for their suitability as *in vitro* lung permeability models, TEER measurements and permeability assays (NaF and Rh-123) were also repeated for these models. In both cases 10  $\mu$ L of the lipid solution was pipetted onto a blank Transwell and allowed to equilibrate and saturate the membrane for 1 h at room temperature before either measuring the TEER value or starting the transport experiment. For permeability experiments, 10  $\mu$ L of dodecane only was used as a negative control.

### **2.3.2.8 Parallel Artificial Membrane Permeability Assay (PAMPA)**

There are many varying PAMPA formulations using different lipids and organic solvents, the formulation used for these experiments was based on one previously established within the Forbes research group (Akhuemokhan et al., 2019). PAMPA lipid solution was prepared by dissolving 1-palmitoyl-2-oleoyl-sn-glycero-3-phosphocholine (POPC) and cholesterol in dodecane, to give 2% w/w POPC and 1% w/w cholesterol in dodecane.

### **2.3.2.9 Lung tissue sources and lung lipid extraction protocol**

All experiments conducted with animal tissue were obtained from sacrificed animals for different experimental purposes under the project licences of the UK Home Office in accordance with the United Kingdom Animal Scientific Procedures Act, 1986).

Unneeded lungs were obtained freshly from different researchers at King's College London performing *in vivo* studies, immediately snap frozen in liquid nitrogen and stored at -80°C. For all lung lipid experiments adult male Sprague-Dawley rats (250-350 g) were used. Rats were chosen as the model species, primarily due the ubiquity of this species for *in vivo* and *ex vivo* lung permeability studies where human tissue is not available.

Lungs were excised at the trachea and removed from the thoracic cavity intact, the exterior was rinsed in ice cold PBS, weighed and stored in 25 mL plastic tubes, before being snap frozen in liquid nitrogen, after which the lungs were stored at -80°C or processed further.

For the extraction of lipids from tissue samples two of the most commonly used methods are the "Folch" and "Bligh and Dyer" method, for the extraction of lung lipids an adapted version of the Folch method was used (Axelsson and Gentili, 2014, Folch et al., 1957).

Lung tissue was lyophilised overnight, and then the weight was again recorded. The dried tissue was dissected further and then ground with a mortar and pestle to a fine powder and weighed. The powder was resuspended in a 2:1 mixture of chloroform: methanol (v : v) to make a solution of 20 mg/mL. The solution was vortexed vigorously until evenly dispersed and a 0.73% NaCl water solution was added, so that the overall solvent mixture was 2:1:0.8 chloroform: methanol: water. The mixture was then filtered through Whatman paper, allowed to separate into two phases, and the lower phase was collected. The solvent mixture was evaporated using nitrogen gas. The dried lipid content was then resuspended in dodecane, with the final weight equal to the weight of the original lung weight. Finally, the lung lipid extract solution was aliquoted into glass vials and stored at -20°C. For lipid extraction a minimum of one pair of lungs were used in each batch. Three batches of lung lipid were

prepared and for permeability experiments, n=3 represents data from 3 different batches of lung lipid extract.

### 2.3.2.10 Drug transporter validation (P-glycoprotein)

P-glycoprotein is one of the main drug transporters, particularly for xenobiotics and has been described previously both in human lung primary tissue and cell lines such as Calu-3, 16HBE14o- and A549 (Ehrhardt et al., 2003, Hamilton et al., 2001), but not TT1. To identify P-glycoprotein activity in TT1, bidirectional transport assays were performed using the P-glycoprotein substrate Rh-123, A549 cells were included for comparison and as positive control.

TT1 and A549 cell layers were used for drug transporter experiments, 14-16 days after seeding on Transwells, after which stable maximum TEER values had been reached. Cell medium was aspirated and all cell layers were preincubated at 37°C in HBSS (200 µL apical, 500 µL basolateral), with or without 5 µM CsA. Bidirectional transport of 50 µM Rh-123 in HBSS was investigated with or without 5 µM CsA to inhibit P-glycoprotein. Apical to basolateral transport was measured by adding 200 µL of Rh-123 to the apical chamber and 600 µL of HBSS to the basolateral chamber, whilst basolateral to apical transport was measured by adding 200 µL of HBSS to the apical chamber and 500 µL of Rh-123 to the basolateral chamber. The cell layers were incubated at 37°C and 100 µL of the receiver chamber was sampled and replaced with 100 µL of fresh HBSS at; 0, 5, 15, 30, 60, 120, 240 minutes. A549 and TT1 cells were assayed in duplicate for each condition (apical to basolateral transport ± CsA, basolateral to apical ± CsA) in each experiment, with the experiments repeated to give n=3.

To calculate the  $P_{app}$  values, the fluorescence of the samples collected in black walled 96-well plates was measured at ex/em = 485/535 nm, using a Tecan Spark 10M plate reader. Apparent permeability coefficients ( $P_{app}$ ) were calculated using **Equation 2.3**, followed by **Equation 2.4** for the calculation of efflux ratios.

#### **Equation 2.4. Efflux ratio**

$$\text{Efflux ratio} = \frac{P_{app}(B > A)}{P_{app}(A > B)}$$

Where B>A = basolateral to apical, and A>B = apical to basolateral.

P-glycoprotein activity was considered to present if the efflux ratio was  $\geq 2$  based on FDA recommendations on P-gp efflux (Sudsakorn et al., 2020) and could be inhibited using 5 µM CsA.

### 2.3.3 Evaluation of commonly used *in vitro* xenobiotic metabolism models

#### 2.3.3.1 Optimisation of resorufin-based metabolism assay

For rapid and semi-high-throughput measurement of the activity of xenobiotic metabolising enzymes, several fluorescent or colorimetric assays were investigated as reporters of enzyme activity, for either CYP, esterase or GST function.

Many of the assays relied on resorufin based reactions (see **Figure 2.3**), which were selected due to the specificity and sensitivity for detecting the activity of particular enzymes.

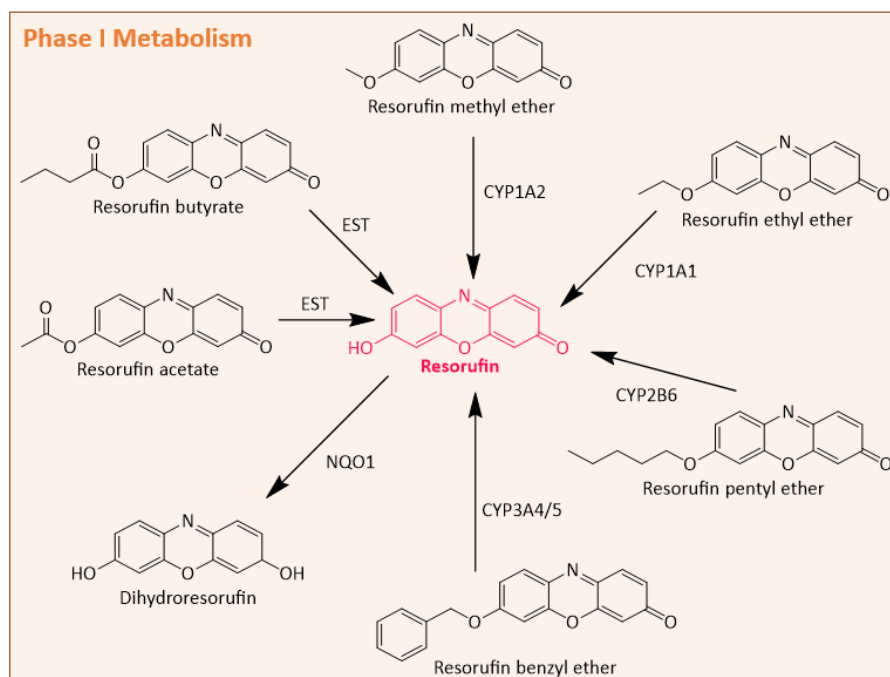


**Figure 2.3.** Resorufin based substrates that may be used to measure the activity of xenobiotic metabolism for CYP, esterase or NQO1 activity.

To ensure the specificity of the method to detect the fluorescence of resorufin rather than resorufin-conjugates (substrates), several preliminary validations were performed. All fluorescence measurements were made using either 100  $\mu\text{L}$  of sample or 200  $\mu\text{L}$  of sample diluted 1:1 in 100% acetonitrile (ACN), in a black walled 96 well  $\mu\text{Clear}$  Greiner plate. All compounds (both substrate and metabolite standards) were assayed over a range of fluorescence settings (ex = 360-635 nm, em = 360-635 nm) in order to calculate the maximum relative fluorescence for resorufin 0.2  $\mu\text{M}$  with the lowest background fluorescence from the substrate 2  $\mu\text{M}$ .

This optimisation step was particularly crucial, as Radenac et al. (2004) previously highlighted the importance of determining the measurement wavelengths experimentally. The importance of this was confirmed as the commonly reported "optimal fluorescence" (ex/em = 535/590



nm) was shown to be significantly less sensitive or accurate under the experimental conditions used in these studies. Once the optimum fluorescence was determined to be ex/em = 580/635 nm, this was used for all further experiments including calibration curves comparing the sensitivity of detection for either resorufin (0.78-1000 nM) or the resorufin conjugate (1.56-2000 nM).

### 2.3.3.2 Confirmation of enzyme-substrate specificity

CYP, NQO1, esterases, carboxylesterase-1 and GST enzymes were selected for assessment based on their importance to xenobiotic metabolism within the lung (Enlo-Scott et al., 2021a, Oesch et al., 2019). UGT activity was not explored as this has been reported to have negligible expression within the lung. Preliminary experiments using either 16HBE14o-, Caco-2 or HepG2 as positive controls were performed to confirm that the selected substrates were specific for particular enzymes. The reaction conditions are shown in **Table 2.2**.

**Table 2.2.. The substrate and inhibitor combinations and concentrations used for enzyme activity assays for CYP, esterase and GST enzymes in vitro.**

Enzyme	Substrate	Inhibitor
CYP1A1	Resorufin ethyl ether 2 µM	α-Naphthoflavone 20 µM
CYP1A2	Resorufin methyl ether 2 µM	α-Naphthoflavone 20 µM
CYP2B6	Resorufin pentyl ether 5 µM	Sertraline 10 µM
CYP3A4	Resorufin benzyl ether 4 µM	CYP3cide 1 µM
CYP3A5	Resorufin benzyl ether 4 µM	Ketoconazole 10 µM
NQO1	Resorufin 500 nM	Dicumarol 10 µM
Esterase	Resorufin acetate 10 µM	Benzil 100 µM
Esterase	Resorufin butyrate 10 µM	Benzil 100 µM
CES1	4-nitrophenol acetate 80 µM	Benzil 100 µM
GST	1-Chloro-2,4-dinitrobenzene 100 µM, Glutathione 200 µM	Ethacrynic acid 20 µM

Under these conditions, preliminary experiments showed that whilst significant metabolism of esterase/CES1 substrates did occur, it was not inhibited by the benzil 100 µM. Further experiments showed that the reaction was non-specific and esterase function was not assayed in further experiments.

The CDNB assay (see **Figure 2.4**) was used to measure GST activity, as this is the most commonly used and well-established *in vitro* assay for GST function. Whilst, a disadvantage of this assay is it is not specific for the different GST isozymes, it is appropriate for assessing total GST function.

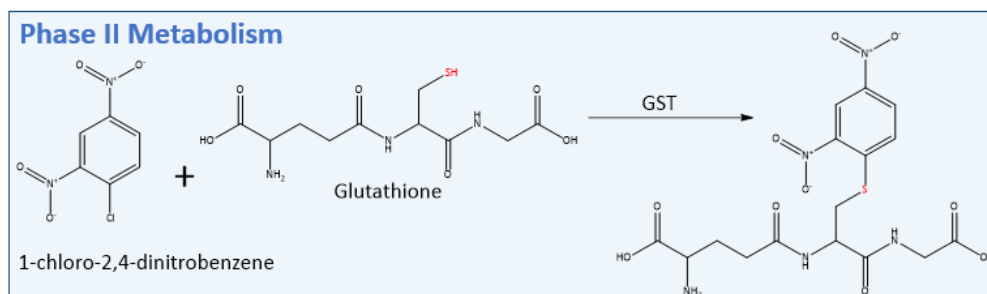


**Figure 2.4.** GST mediated reaction, using CDNB as a substrate that forms a colorimetric glutathione conjugate.

#### 2.3.3.3 EROD assay as a measure of CYP1A1 induction following pesticide exposure

16HBE14o- cells were seeded (4000 cells/well) into black walled 96-well  $\mu$ Clear Greiner plate, after 24 hours, medium was replaced with phenol-red free DMEM containing 2% FBS and cells were grown to confluency. Once confluency was reached, cells were exposed for 24 hours to 100  $\mu$ L/well phenol red free DMEM containing 2% FBS and 10  $\mu$ M of the pesticides or 0.75% DMSO as a negative control. Following the exposure, the cells were rinsed twice with 50  $\mu$ L PBS and to initiate the EROD assay, the cells were incubated in the dark for 40 minutes with 100  $\mu$ L/well HBSS containing resorufin ethyl ether 2  $\mu$ M. The reaction was terminated by pipetting 100  $\mu$ L acetonitrile into each well, and the fluorescence was measured using a Tecan Spark 10M microplate reader (ex/em = 595/630 nm). CYP1A1 activity was calculated by subtracting the relative fluorescence from blank wells (containing no cells) and normalising against the DMSO control. An increase of  $\geq 2$  fold, was taken as confirmatory of CYP1A1 induction.

Subsequent experiments were performed with propiconazole (1.25-10  $\mu$ M) and  $\beta$ -naphthoflavone (2.5-20  $\mu$ M), the latter was included as a potent agonist of the aryl hydrocarbon receptor and a positive control of CYP1A1 induction. The EROD assay was performed following a 48 hour exposure.

The assay was performed with six replicate wells for each test concentration, with the experiment being repeated in triplicate.

#### 2.3.3.4 GST induction/inhibition in snap frozen cells

Following the EROD assay, the EROD buffer was aspirated and cells were carefully rinsed twice with PBS. The GST substrate CDNB does not readily permeate across the cell membrane, and

therefore experiments are usually performed by either solubilising the cell using Triton X-100 or by using cell homogenates. Preliminary experiments were performed using both methods and freezing the cells was determined to be the most suitable method based on maintaining enzyme activity, concentrating the sample and ease of use.

The 96-well plate was snap-frozen, in order to lyse the cells. The plate was allowed to thaw at room temperature before the GST substrate mixture was added to produce a total volume of 100  $\mu$ L, the final concentration was CDNB 100  $\mu$ M, glutathione 200  $\mu$ M in 100 mM  $\text{KH}_2\text{PO}_4$  buffer. The absorbance at 345 nm of each well was measured every 2 minutes (for 60 minutes) by taking kinetic measurements using the Tecan Spark microplate reader, incubated at 37°C. GST activity was calculated by subtracting the relative absorbance from blank wells (containing no cells) and normalising against the DMSO control.

The assay was performed with six replicate wells for each test concentration, with the experiment being repeated in triplicate.

### 2.3.3.5 S9 fraction preparation

To assess the functional activity of the different xenobiotic metabolising enzymes in the different *in vitro* models, S9 fraction was prepared. Whilst commonly, the S9 fraction is taken from liver homogenate, it represents the supernatant fraction obtained from a tissue homogenate centrifuged at 9000 g and containing both the cytosolic and microsomal enzymes, and therefore can be prepared from many different tissue types. In order to compare the functional enzyme activity of the different *in vitro* respiratory models, S9 fraction was prepared for A549, TT1, BEAS-2B, 16HBE14o- Calu-3 and RPMI-2650. Caco-2 S9 fraction was also prepared as a positive control which has been studied more commonly and contains many of the relevant xenobiotic metabolising enzymes. Additionally, to confirm that the enzymatic reactions were relevant to those in the human lung, human lung S9 (obtained from primary tissue) was also tested, with this being purchased from XenoTech, the donor information is listed in **Table 2.3** and additional information may be found in the appendix.

**Table 2.3. Details for human lung S9 fraction donor information**

Sample	Gender	Age	Race	Cause of Death	Smoked within past 10 years?
3	Male	75	Caucasian	Cerebrovascular accident	No
17	Female	37	Caucasian	Cerebrovascular accident	No
22	Female	49	African American	Head Trauma	No
30	Male	22	Hispanic	Head Trauma	No

To prepare the S9 fractions from the cell lines, all cells were cultured in their respective medium (DMEM for all cell lines, with the exception of LHC-8 medium for BEAS-2B and DCCM-1 medium for TT1). Cells were subcultured at a ratio of 1:5 in 175 cm<sup>2</sup> Greiner cell culture flasks and grown until reaching confluency, after which xenobiotic metabolism was induced by replacing cell culture medium with 25 mL fresh medium containing with 25 µM of (CYP1A1/A2 inducer), with a final DMSO concentration of 0.125%. These exposure concentrations were determined to be non-toxic based on earlier preliminary experiments, both inducers are commonly used *in vitro*, often with the aim of inducing CYP expression (Graham et al., 2002, Hewitt et al., 2007). After a 24 hour exposure, cells were harvested from the flask by trypsinising and centrifuging at 1500 g for 5 minutes to obtain the cell pellet. The cell pellet was resuspended in PBS and centrifuged again to remove any residual trypsin or cell culture medium, this was repeated twice before resuspending the pellet in 1 mL cold S9 fraction freezing buffer (50 mM Tris-HCl, 150 mM KCl and 2 mM EDTA in dH<sub>2</sub>O), the same freezing buffer used for the human lung S9 fraction. After incubating the harvested cells on ice for 30 minutes, the samples were snap frozen in liquid nitrogen and stored at -80°C until the next step. In order to fully lyse the cells, the sample was allowed to thaw on ice and was then passed through a 30-gauge needle 5 times, before sonicating on ice 3 times (20 seconds on, 20 seconds off). The homogenate was then centrifuged at 10,000 g for 20 minutes at 4°C, the supernatant was collected, and the protein content was determined using the bicinchonic acid assay (BCA assay) according to the supplier's instructions. Finally, the protein content was normalised to 5 mg/mL and the prepared S9 fraction was stored at -80°C until use.

#### **2.3.3.6 Comparative xenobiotic metabolism studies (CYP, NQO1 and GST)**

All experiments were performed by diluting the 5 mg/mL S9 fraction to 1 mg/mL in 100 mM KH<sub>2</sub>PO<sub>4</sub> pH 7.4 buffer. Fifty microlitres of each S9 fraction sample was pipetted into the well of a black walled 96-well plate which was set up for the experiment according to **Figure 2.5**. DMSO or the appropriate inhibitor were added and the plate was incubated at room temperature for 30 minutes before adding 50 µL of the substrate mixture, to give a final concentration of 0.5 mg/mL S9 fraction in 100 µL. For CYP or NQO1 mediated reactions, the substrate concentration was as specified in **Table 2.2**, however for S9 fraction experiments the cofactor NADPH is required and was added immediately before starting the reaction to give a final concentration of NADPH 500 µM. Total DMSO concentration did not exceed 0.8%. The reactions were performed at 37°C, ranging from 20-60 minutes depending on the activity of the enzyme of interest. With

the exception of the GST assay (which was a kinetic assay, rather than a single timepoint), all reactions were stopped by adding 100  $\mu$ L of ACN.

Resorufin formation/depletion was quantified using calibration curves and CYP or NQO1 activity was calculated as nmol resorufin/min/mg protein.

$$\text{CYP or NQO1 activity} = \text{nmol resorufin/min}/0.5 \text{ mg protein}$$

All experiments were performed with 4 replicate wells for each condition and experiments were repeated in triplicate.

	1	2	3	4	5	6	7	8	9	10	11	12
A												
B												
C	Blank/ buffer only											
D		A549	TT1	BEAS-2B	16HBE14o-	Calu-3	RPMI-2650	Caco-2	Human Lung S9	Blank/ buffer only	Calibration curve	Calibration curve
E												
F												
G												
H												

DMSO (negative control)
Inhibitor (positive control)

**Figure 2.5.** The 96-well plate map and position of each of the S9 fraction samples, for all xenobiotic metabolism reactions

### 2.3.3.7 Statistical Analysis

Where appropriate, data were analysed using GraphPad Prism version 8, (GraphPad Software, San Diego, USA). MTT data was normalised against the negative control (0.75% DMSO), as was enzyme induction data. One-way ANOVA analysis was performed to compare all data sets with categorical groups, results with “ $p \leq 0.05$ ” were considered to be significant. Statistically significant differences are represented on graphs as; \* =  $p < 0.05$ , \*\* =  $p < 0.005$ , \*\*\* =  $p < 0.0005$ , \*\*\*\* =  $p < 0.0001$ .

## 2.4 Results

### 2.4.1 MTT cytotoxicity assay

The MTT calibration curves (data in the appendix), showed a linear relationship between UV absorbance and cell seeding density within the range used for the MTT toxicity assays with the different cell lines (4000-40,000 cells/well) ( $R^2 \geq 0.96$ ).

For all the cell lines, the profile of relative cytotoxicity for the different pesticides was similar (**Figure 2.6**), based on calculated  $LC_{50}$  values, chlorothalonil was consistently the most cytotoxic ( $LC_{50} = 0.3-9.7 \mu M$ ), followed by abamectin, isopyrazam, diquat, prosulfocarb, acibenzolar-S-methyl, propiconazole and pinoxaden, with the latter 4 pesticides having comparatively low toxicity ( $LC_{50} > 150 \mu M$ ).

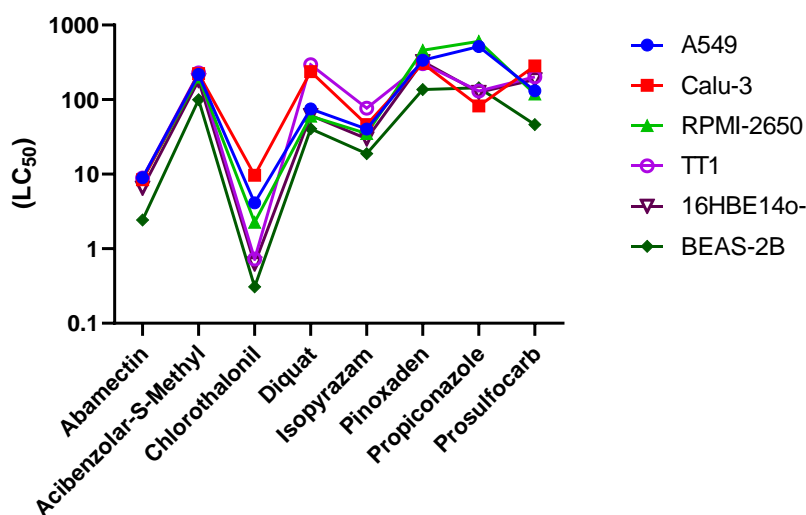


**Figure 2.6.** Comparison of pesticide  $LC_{50}$  values between the different respiratory epithelial cell lines A549, Calu-3, RPMI-2650, TT1, 16HBE14o- and BEAS-2B.

Despite the general trend, there were differences between the cell lines for particular pesticides, for example the non-cancer derived bronchial cell line BEAS-2B was generally the most sensitive to cytotoxicity, with this evident for 7 of the 8 tested compounds. For chlorothalonil, the most evident differences between the cell lines were observed with the non-cancer derived cell lines BEAS-2B, 16HBE14o- and TT1 being more sensitive to the fungicide, than the cancer derived cell lines RPMI-2650, A549 and Calu-3 (**Figure 2.7**).

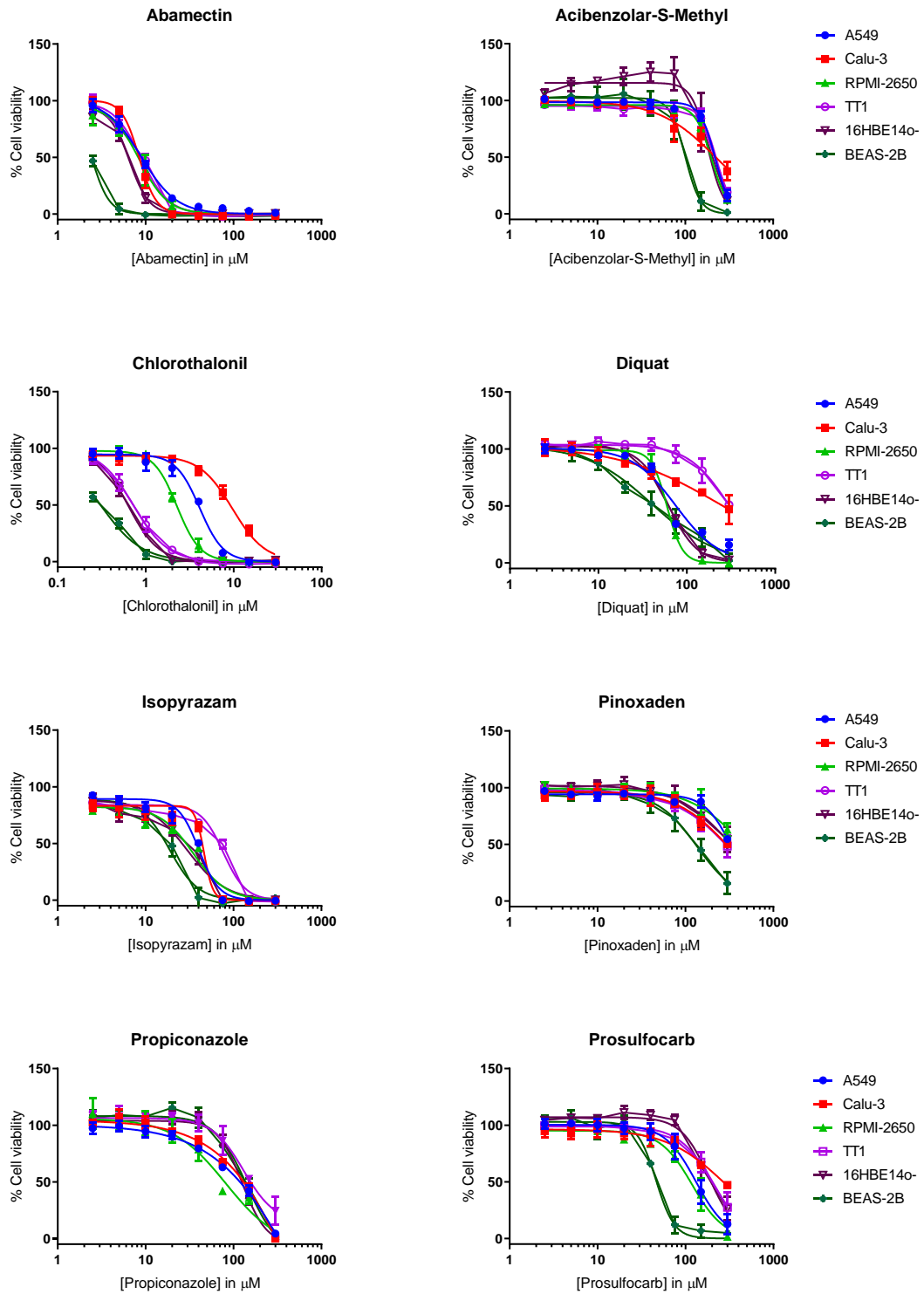


**Figure 2.7. Pesticide cytotoxicity as assessed by the MTT assay , following a 24 hour exposure to either abamectin, acibenzolar-S-methyl, chlorothalonil, diquat, isopyrazam, pinoxaden, propiconazole or prosulfocarb (0-300 μM). Data represented as mean ± SD (n=3).**

### 2.4.2 Mechanistic toxicity assay

Using confluent 16HBE14o- cells and 10  $\mu$ M pesticide exposures as a non-cytotoxic concentration, there was no significant change in cell membrane integrity as assessed by calcein-AM fluorescence (**Figure 2.8**). However, for several of the pesticides there were significant changes in mitochondrial membrane potential as assessed by TMRM, indicating potential mitochondrial toxicity following exposure. Similarly, significant changes in intracellular glutathione concentration (assessed using monochlorobimane), were observed for abamectin, azoxystrobin and chlorothalonil.

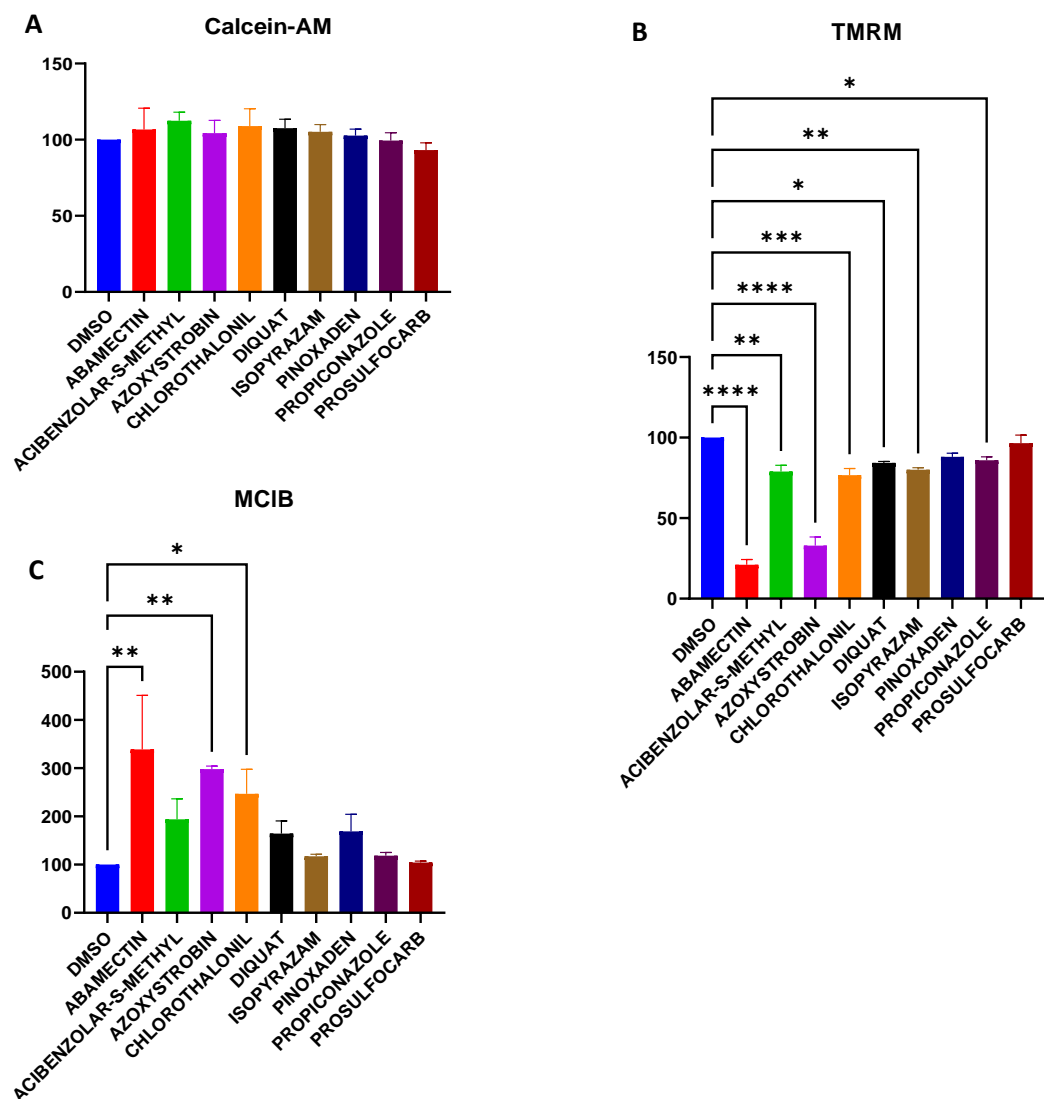


**Figure 2.8.** Mechanistic toxicity assay in the bronchial cell line 16HBE14o- , assessing (A) membrane integrity with calcein-AM, (B) mitochondrial membrane potential with TMRM and (C) glutathione level with MCIB following a 24 hour exposure to 10  $\mu$ M of the different pesticides. Data represented as mean  $\pm$  SD (n=3)



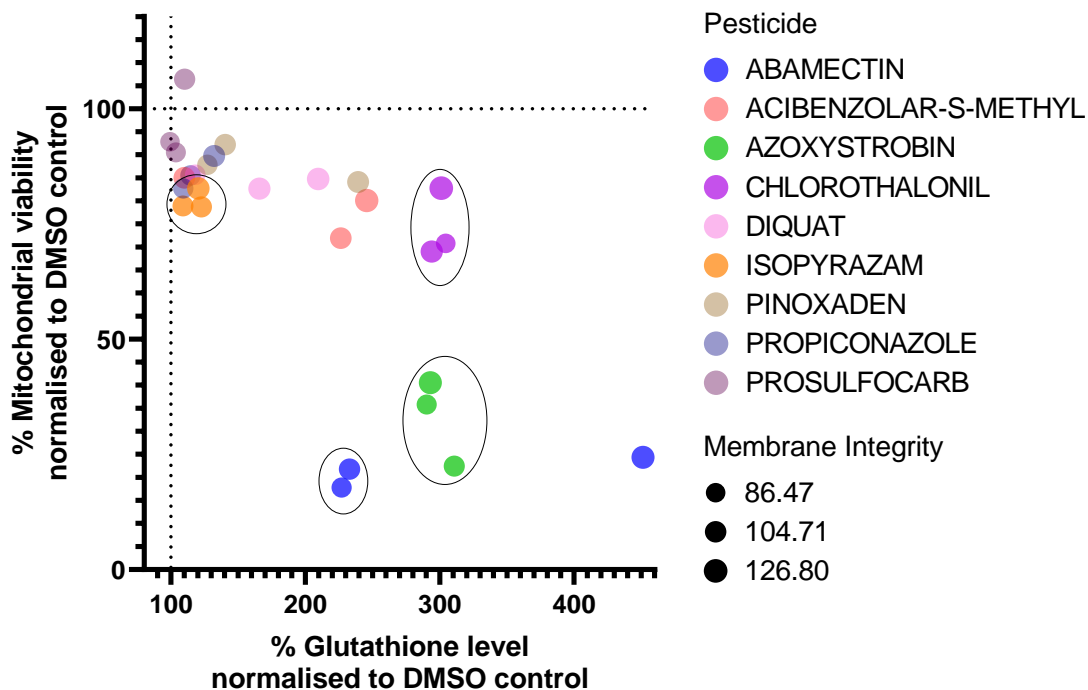


**Figure 2.9.** Bubble plot showing mechanistic toxicity assay in the bronchial cell line 16HBE14o-, assessing membrane integrity with calcein-AM, glutathione level with MCIB and mitochondrial membrane potential with TMRM, following a 24 hour exposure to 10  $\mu$ M of the different pesticides. Highlighted data represents abamectin, azoxystrobin, chlorothalonil and isopyrazam which were selected for further assessment. Each point represents the mean average from a single experiment. The intersecting dotted lines represent equivalence to the DMSO control, deviation from this highlights changes in mitochondrial viability or glutathione level. Each point represents a single replicate (n=3).

Whilst there were no significant changes observed with calcein-AM as a measure of membrane integrity (Figure 2.8A), all three toxicity markers were plotted (Figure 2.9), distinct differences between the different pesticides are evident, likely relating to their different mechanisms of action and potential molecular initiating events following exposure. Whilst membrane integrity was largely unchanged, significant changes did occur to mitochondrial viability and glutathione level following pesticide exposure. Based on this data, abamectin, azoxystrobin, chlorothalonil and isopyrazam were selected for further assessment and dose response curves were obtained (Figure 2.10). The trend observed with calcein-AM between the pesticides is similar to previously shown with the MTT assay, with chlorothalonil the most cytotoxic, followed by abamectin, despite the latter assay being more sensitive in part due to the use of cells prior to reaching confluency. However, the additional toxicity markers highlight that even at the lowest concentration of 2.5  $\mu$ M, intracellular glutathione level was significantly increased following a

24 h exposure to chlorothalonil, whilst mitochondrial toxicity is observed at 2.5  $\mu\text{M}$  of azoxystrobin.

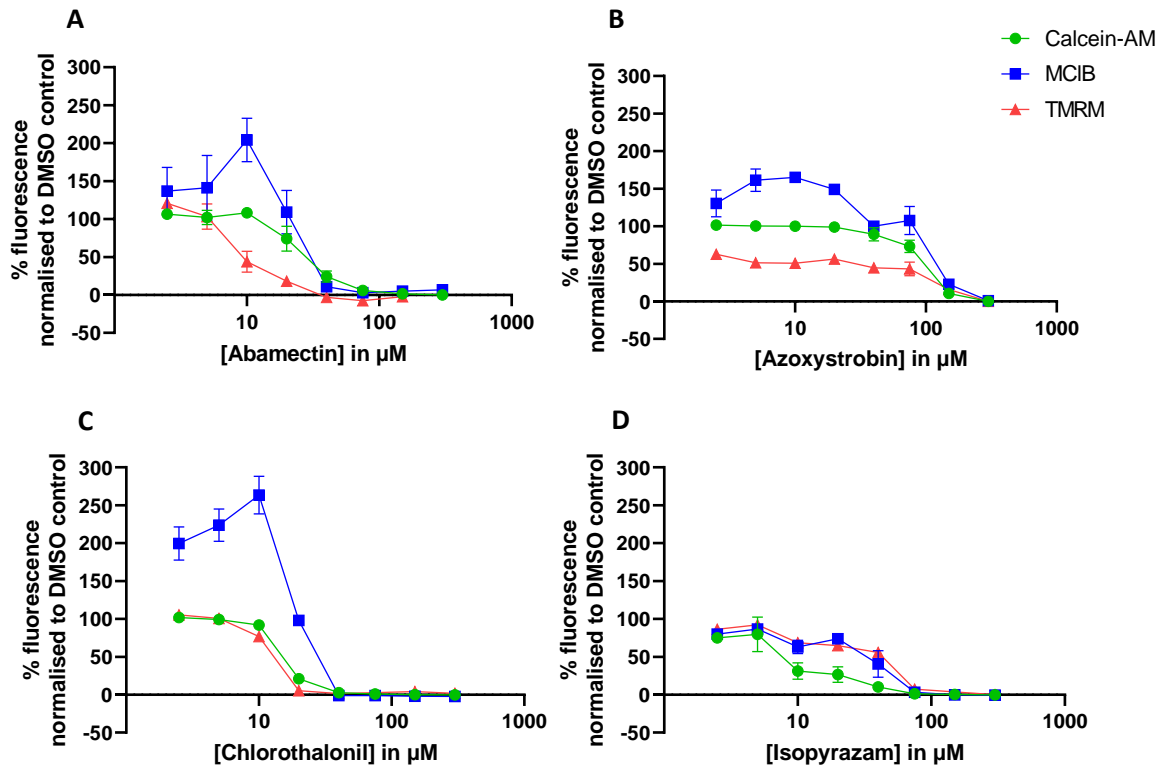


Figure 2.10. Dose response curve using the mechanistic toxicity assay with 16HBE14o- cells for (A) abamectin, (B) azoxystrobin, (C) chlorothalonil and (D) isopyrazam, following a 24 hour exposure. Data represented as mean  $\pm$ SD (n=3).

### 2.4.3 Transepithelial Electrical resistance (TEER)

Calu-3 and Caco-2 rapidly obtained TEER values of  $\geq 300 \Omega \cdot \text{cm}^2$  within 3-4 days of seeding and continued to increase until the optimum TEER was achieved at 14 and 22 days, respectively (Figure 2.11). TEER values for the type-II like alveolar cell line A549, did not increase over the 14 days tested, whilst the type-I like alveolar cell line TT1 showed a gradual increase in TEER (to  $\geq 130 \Omega \cdot \text{cm}^2$ ) until day 16. The nasal cell line RPMI-2650 showed a very modest increase in TEER over the 22 days, reaching  $45 \Omega \cdot \text{cm}^2$ .

Culturing TT1 with SLF had a negative effect on TEER values, whilst no significant difference was observed when Transwells were precoated with basement membrane extract as an extracellular matrices or when TT1 was cocultured with 3T3 cells (TT1 on the apical side and 3T3 on the basolateral side of the membrane).

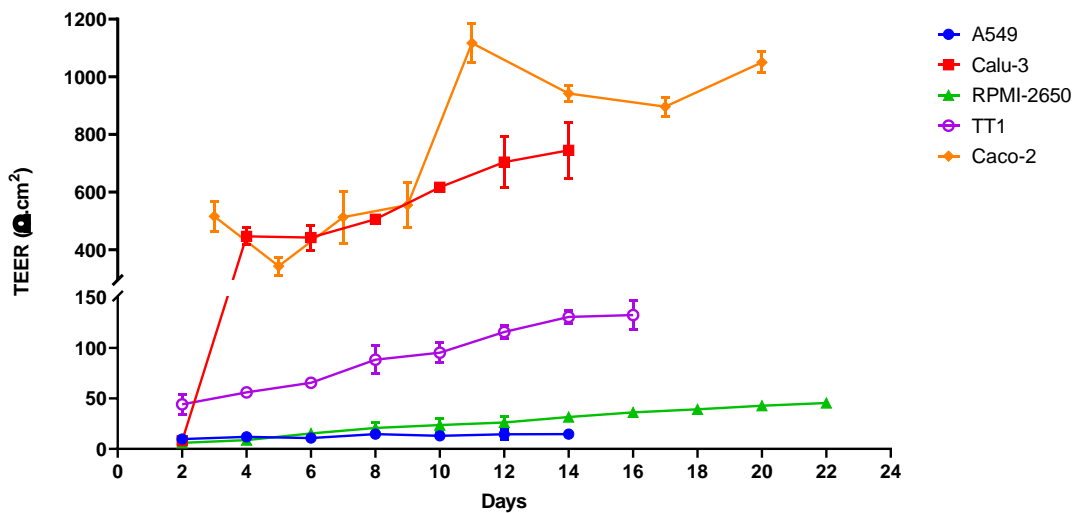


Figure 2.11. Transepithelial electrical resistance over 0-22 days for A549, Calu-3, Caco-2, TT1 and RPMI-2650, cultured on Transwells precoated with rat tail collagen. Data represented as mean  $\pm$ SD ( $n=3$ ), with a total of 9 replicate wells per cell line.

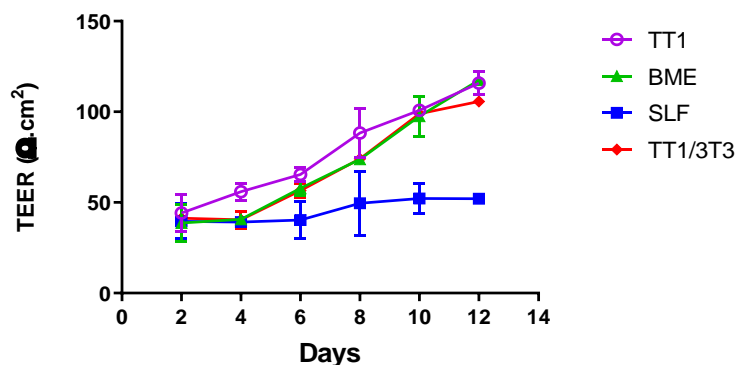
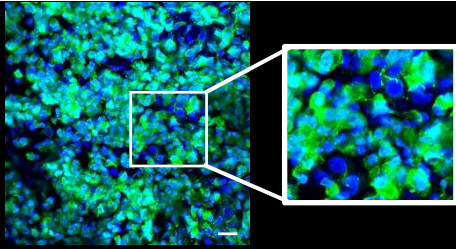
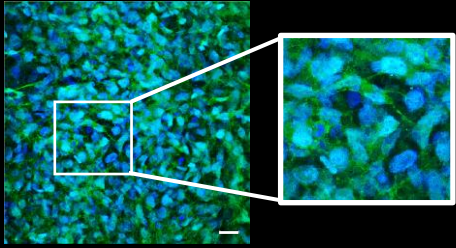
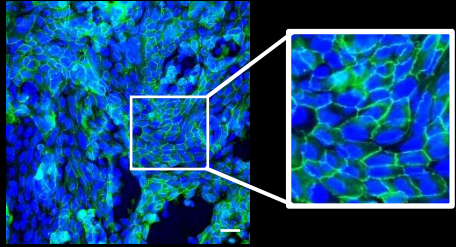
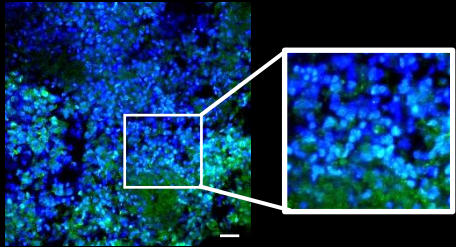


Figure 2.12. Transepithelial electrical resistance over 12 days, for TT1 cultured on Transwells precoated with basement membrane extract (BME), co-cultured with 3T3 cells (basolateral side of membrane) or supplemented with synthetic lung fluid (SLF). Data represented as mean  $\pm$ SD ( $n=3$ ), with a total of 9 replicate wells per cell line.

#### 2.4.4 Zonula Occludens-1 imaging

The relatively high TEER values observed using Calu-3 correspond to the presence of functionally expression of tight junction protein Zonula Occludens-1 as shown in **Table 2.4**. In comparison, the other cell lines did not express ZO-1 under the tested culturing conditions.

**Table 2.4. Representative confocal images of ZO-1 fluorescently stained with AlexaFluor 488 (green) and cell nuclei stained with DAPI (blue), using A549, TT1, Calu-3 and RPMI-2650 cells cultured for 14-22 days on Transwell inserts at air-liquid interface (n=2). Scale bars 25  $\mu\text{m}$ .**

Cell line	ZO-1 staining	Optimum achieved TEER $\Omega.\text{cm}^2$ <i>(Previously reported TEER based on literature)</i>	Time cultured
A549		~14 $\Omega.\text{cm}^2$  40-384 $\Omega.\text{cm}^2$ (Sakagami, 2006, Togami et al., 2017)	14 days
TT1		~130 $\Omega.\text{cm}^2$  41-60 $\Omega.\text{cm}^2$ , (van den Bogaard et al., 2009)	14 days
Calu-3		~605 $\Omega.\text{cm}^2$  300-1200 $\Omega.\text{cm}^2$ (Sakagami, 2006)	14 days
RPMI-2650		~45 $\Omega.\text{cm}^2$  40-120 $\Omega.\text{cm}^2$ , (Kreft et al., 2015b)	22 days

### 2.4.5 Permeability assays with fluorescent permeability markers

The interdependence between TEER values and sodium fluorescein and FD-4  $P_{app}$  values is evident in **Figure 2.13**, for Rh-123 this trend is less pronounced as due to this compounds lipophilicity it is transported predominantly through transcellular rather than paracellular transport.

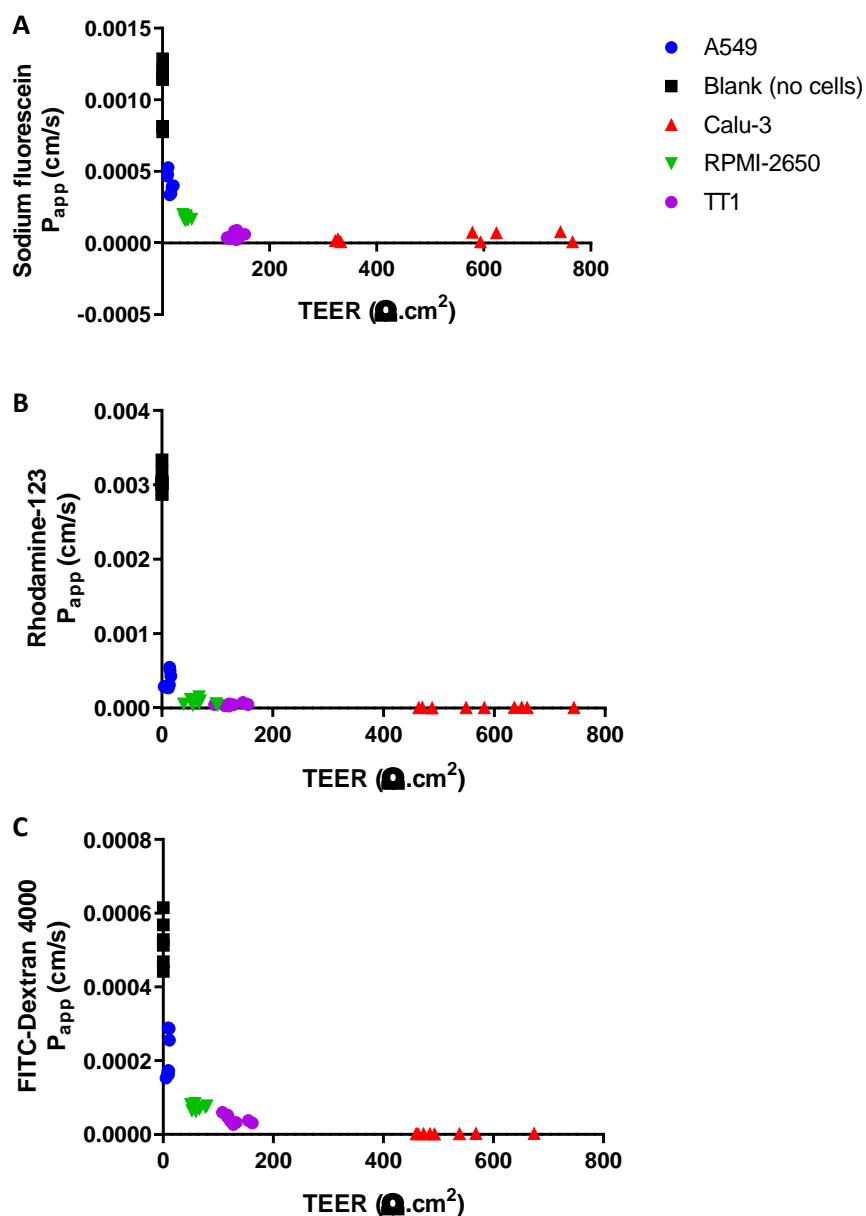


**Figure 2.13.** Interdependence between TEER values for each cell line and  $P_{app}$  values for (A) sodium fluorescein, (B) rhodamine-123 and (C) FITC-Dextran 4000. Each point represents the result from a single well, with a total of 9 wells per cell line.

#### 2.4.6 Lipid based permeability models

Both lipid-based models created a permeability barrier which significantly reduced the transport of the permeability markers in comparison to the dodecane control, confirming that a permeability barrier was created, which can be attributed to cholesterol and POPC in PAMPA or the complex mixture of lipids present in the rat lung lipid extract, rather than the dodecane solvent (**Figure 2.14**). With Rh-123 the rat lung lipid barrier was slightly more permeable than the PAMPA solution, but this difference was not found to be statistically significant. TEER data for both lipid-based models was low ( $\leq 15 \Omega \cdot \text{cm}^2$ ), highlighting the physicochemical nature of the barrier.

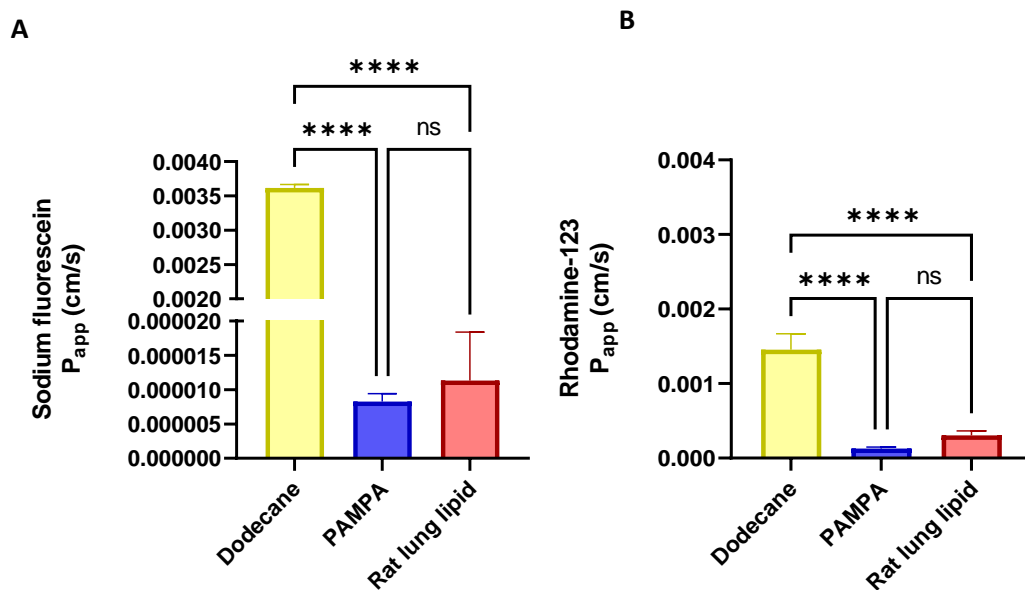


**Figure 2.14.**  $P_{app}$  values corresponding to (A) sodium fluorescein and (B) rhodamine-123 transport across Transwells coated with either dodecane (negative control), PAMPA or rat lung lipid extract. Data represented as mean  $\pm$  SD (n=3)

### 2.4.7 Permeability comparison with all models

$P_{app}$  values for sodium fluorescein, rhodamine-123 and FITC-Dextran 4000 were compared by one-way ANOVA for all permeability barriers, using Calu-3 as the positive control (**Figure 2.15**). Generally, the permeability markers were excluded most by Calu-3 and PAMPA, which particularly for hydrophilic permeability markers NaF and FD-4 had similar  $P_{app}$  values, in contrast to the barriers formed by A549 and RPMI-2650 were the most permeable. Whilst TT1 was significantly less permeable to all permeability markers in comparison to A549, the permeability of FITC dextran 4000 was significantly more in TT1 than for either Calu-3 or PAMPA suggesting that the permeability barrier presented by this model is low compared to other models of the respiratory epithelium. This is consistent with the lack of functional expression of ZO-1 in the TT1 model (**Table 2.4**).

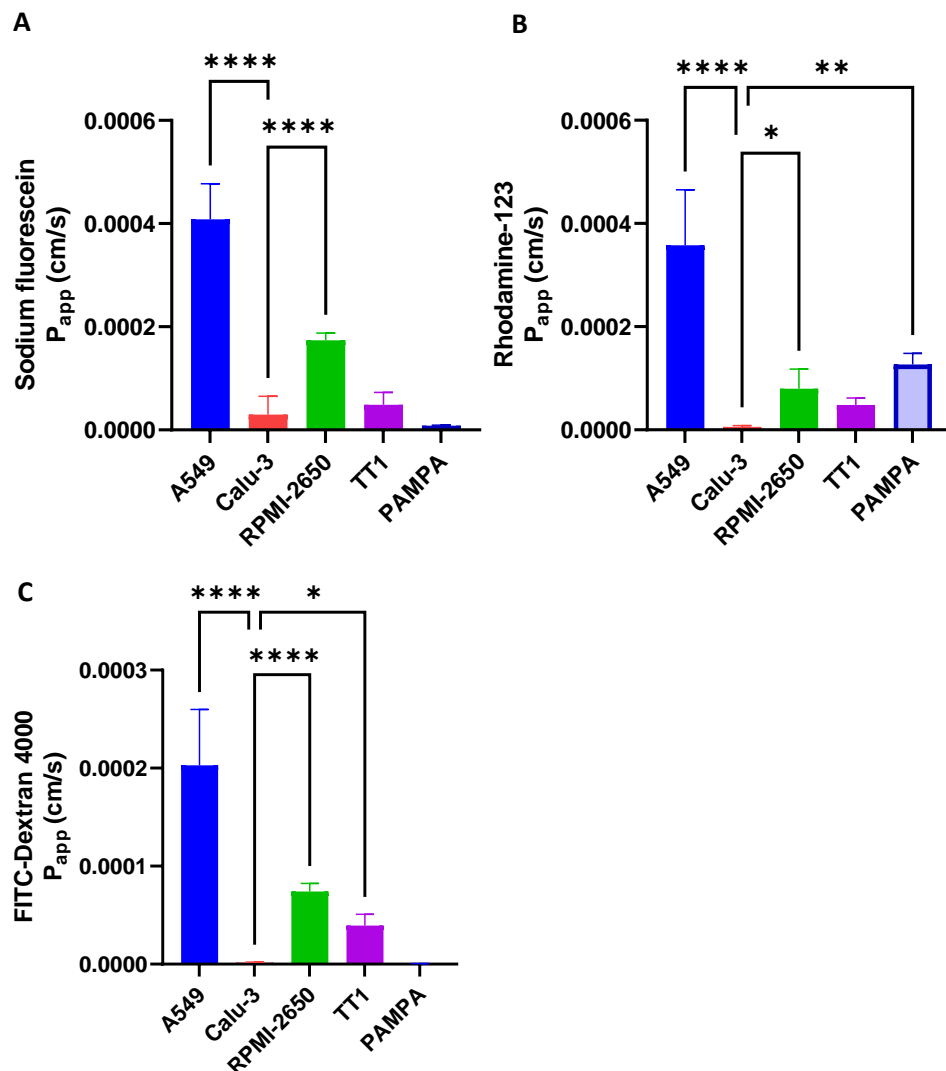


**Figure 2.15.** Comparative  $P_{app}$  values for (A) sodium fluorescein, (B) rhodamine-123 and (C) FITC-Dextran 4000, using the permeability barriers created by A549, Calu-3, RPMI-2650, TT1, PAMPA and rat lung lipid extract models. Data represented as mean  $\pm$  SD ( $n=3$ )

### 2.4.8 P-glycoprotein activity

Bidirectional rhodamine-123 transport assays showed modest efflux with both TT1 and A549, respective efflux ratios were 1.502 and 1.25, these values were halved in the presence of the P-glycoprotein inhibitor cyclosporin A (**Figure 2.16**). As the efflux ratios were less than 2 for both cell lines, based on FDA guidelines this data does not confirm P-glycoprotein activity (Sudsakorn et al., 2020), but does suggest the presence of active transport. The differences in  $P_{app}$  values between the two cell lines, confirm the reduced permeability with TT1 in comparison to A549.

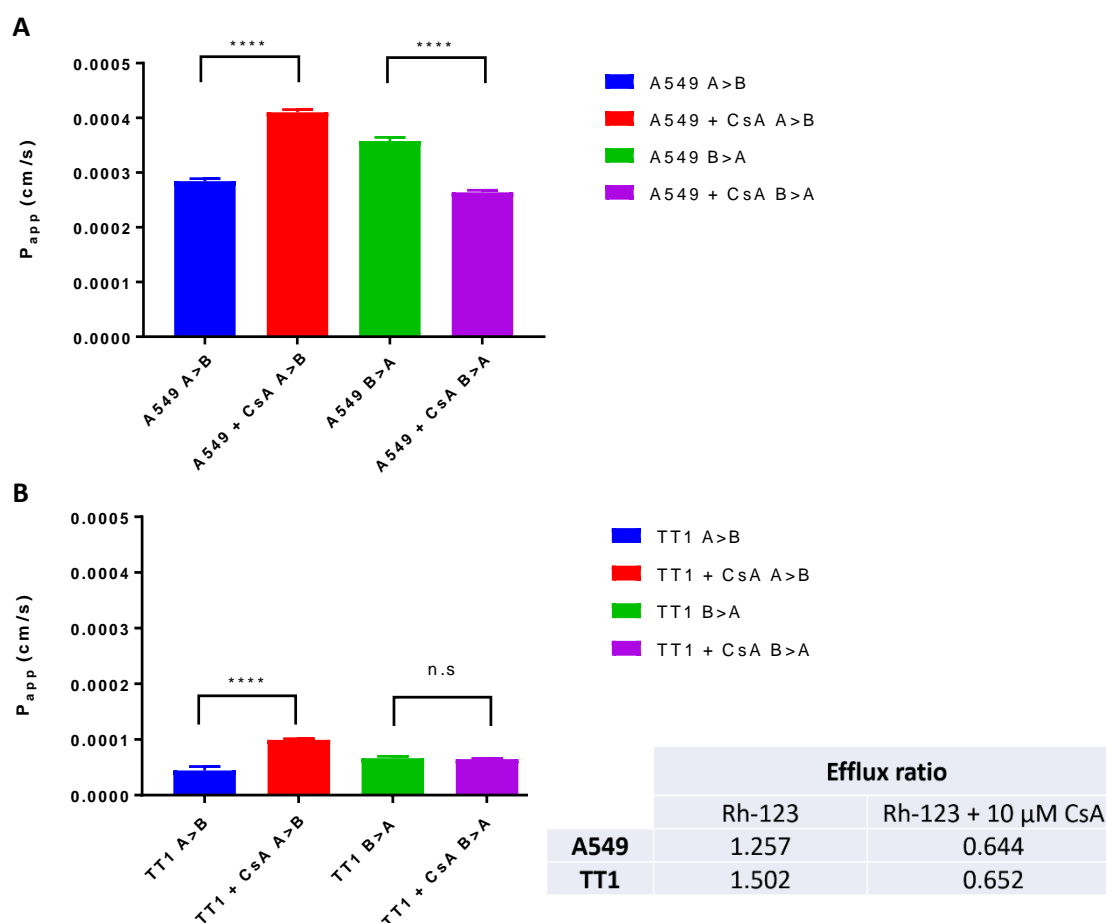


**Figure 2.16.** Rhodamine-123 bidirectional transport across (A) A549 or (B) TT1 cell layers, cultured at air-liquid interface on Transwells. 10  $\mu$ M cyclosporin A was used to inhibit P-glycoprotein transport of rhodamine-123. Data represented as mean  $\pm$ SD (n=3)



### 2.4.9 Optimisation of resorufin-based metabolism assay

A range of excitation wavelengths for resorufin and ethoxyresorufin were evaluated for the fluorescence emission at either 595 or 635 nm. The concentration of resorufin was 1000 times less than that of the metabolite, highlighting the sensitivity of the method and the suitability of the method to exclude background fluorescence of ethoxyresorufin whilst detecting nanomolar concentrations of resorufin. As shown in **Figure 2.17**, the optimum fluorescence setting under the tested experimental conditions was found to be ex/em = 580/635 nm, with this being significantly more selective than the commonly reported ex/em = 535/595 nm (One-way ANOVA,  $p < 0.005$ ). Using the experimentally determined optimum fluorescence settings, resorufin concentration was shown to have a linear relationship with relative fluorescence, within the picomolar range.

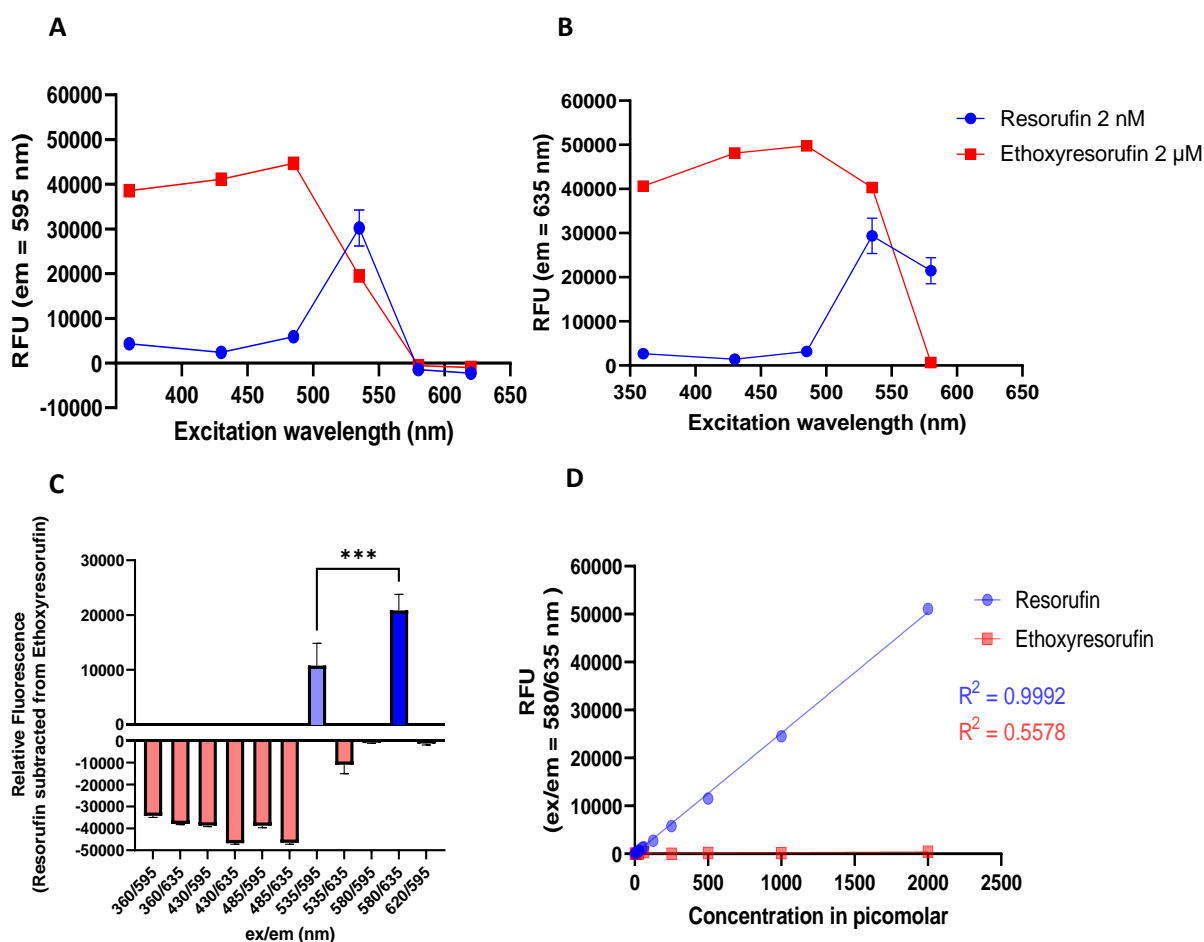


**Figure 2.17.** Comparative emission values at (A) 595 nm and (B) 635 nm are shown, in addition to (C) relative fluorescence of resorufin subtracted from background fluorescence from ethoxyresorufin. The experimentally determined optimum fluorescence (ex/em = 580/635 nm), is sensitive to resorufin concentration within the picomolar range. Data represented as mean  $\pm$  SD ( $n=3$ ).

Calibration curves were obtained for resorufin under the various experimental conditions used for the different assays, under all tested conditions relative fluorescence units correlated to resorufin concentration ( $R^2 \geq 0.998$ ) (Figure 2.18).

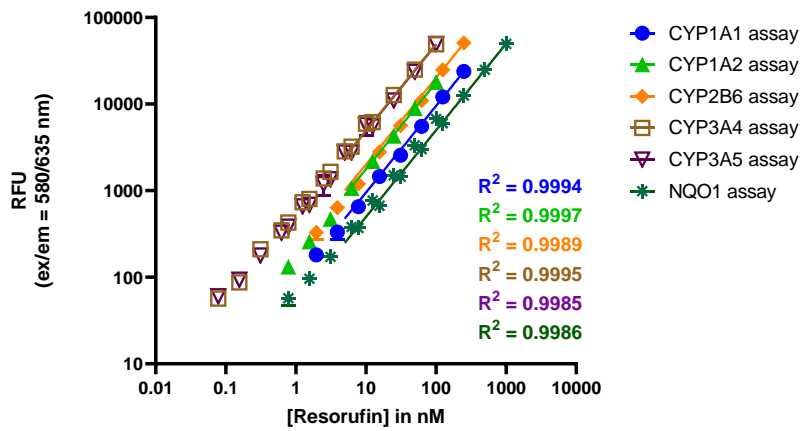


Figure 2.18. Resorufin calibration curves quantified by fluorescence for the different enzyme assays used to assess functional enzyme expression. Data represented as mean  $\pm$ SD (n=3).

#### 2.4.10 EROD assay as a measure of CYP1A1 induction in live 16HBE14o- cells

EROD activity was used as a direct measure of CYP1A1 functional activity and an indirect measure of CYP1A1 induction. In confluent 16HBE14o- cells, CYP1A1 was induced over 4-fold following exposure to propiconazole 10  $\mu$ M, isopyrazam and prosulfocarb caused a modest increase < 1.4 fold. In contrast, EROD activity was significantly reduced by both abamectin and chlorothalonil (Figure 2.19).

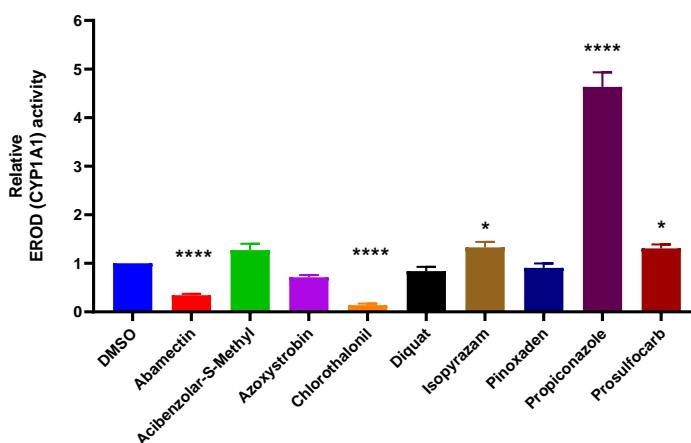
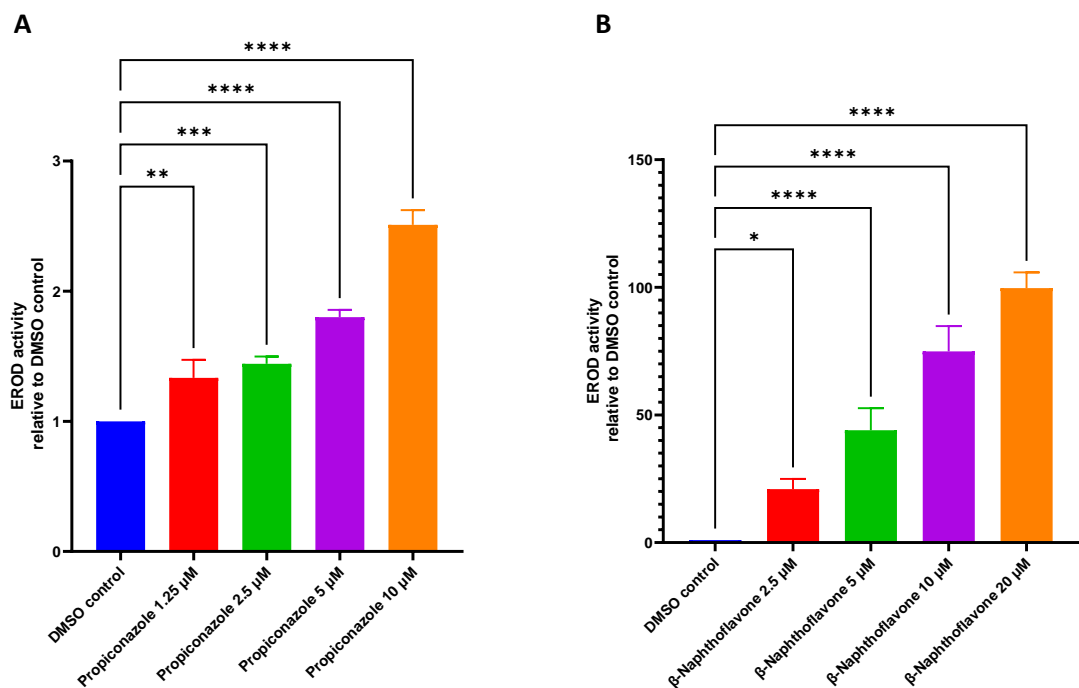


Figure 2.19. EROD activity as a measure of CYP1A1 induction in the bronchial epithelial cell line 16HBE14o-, following a 24 h exposure to 10  $\mu$ M of a range of pesticides. Data represented as mean  $\pm$  SD (n=3), \*  $p < 0.05$ , \*\*\*\*  $p < 0.0001$ .

Following the 24 hour exposure with the range of pesticides, propiconazole was selected for further assessment. 16HBE14o- cells were exposed for 48 hours to either propiconazole (1.25-10  $\mu$ M) or  $\beta$ -Naphthoflavone (2.5-20  $\mu$ M), the latter a known potent inducer of CYP1A1 by acting as an agonist of AhR (**Figure 2.20**). CYP1A1 induction by propiconazole was marginally lower following a 48 hour exposure in comparison to the previous 24 hour exposure and was modest in comparison to the potency of  $\beta$ -naphthoflavone which caused approximately a 100-fold induction at the highest tested concentration. Both compounds showed a dose response, with CYP1A1 induction corresponding with increasing exposure concentrations.



**Figure 2.20.** EROD activity as a measure of CYP1A1 induction in the bronchial epithelial cell line 16HBE14o-, following a 48 h exposure to (A) propiconazole (1.25-10  $\mu$ M) or (B)  $\beta$ -naphthoflavone (2.5-20  $\mu$ M). Data represented as mean  $\pm$  SD (n=3), \* =  $p < 0.05$ , \*\* =  $p < 0.005$ , \*\*\* =  $p < 0.0005$ , \*\*\*\* =  $p < 0.0001$ .

#### 2.4.11 GST induction/inhibition in snap frozen 16HBE14o- cells

The GST activity assay highlighted inhibition of GST activity by over 5-fold following a 24 h exposure to chlorothalonil, whilst abamectin and azoxystrobin caused a slight decrease in GST activity this was not statistically significant (**Figure 2.21**). A modest but not statistically significant increase in GST activity was found following exposure to acibenzolar-S-methyl, however this is likely to be due to increased cell proliferation as previously determined from earlier experiments (**Figure 2.7-8**), rather than a specific induction of GST.

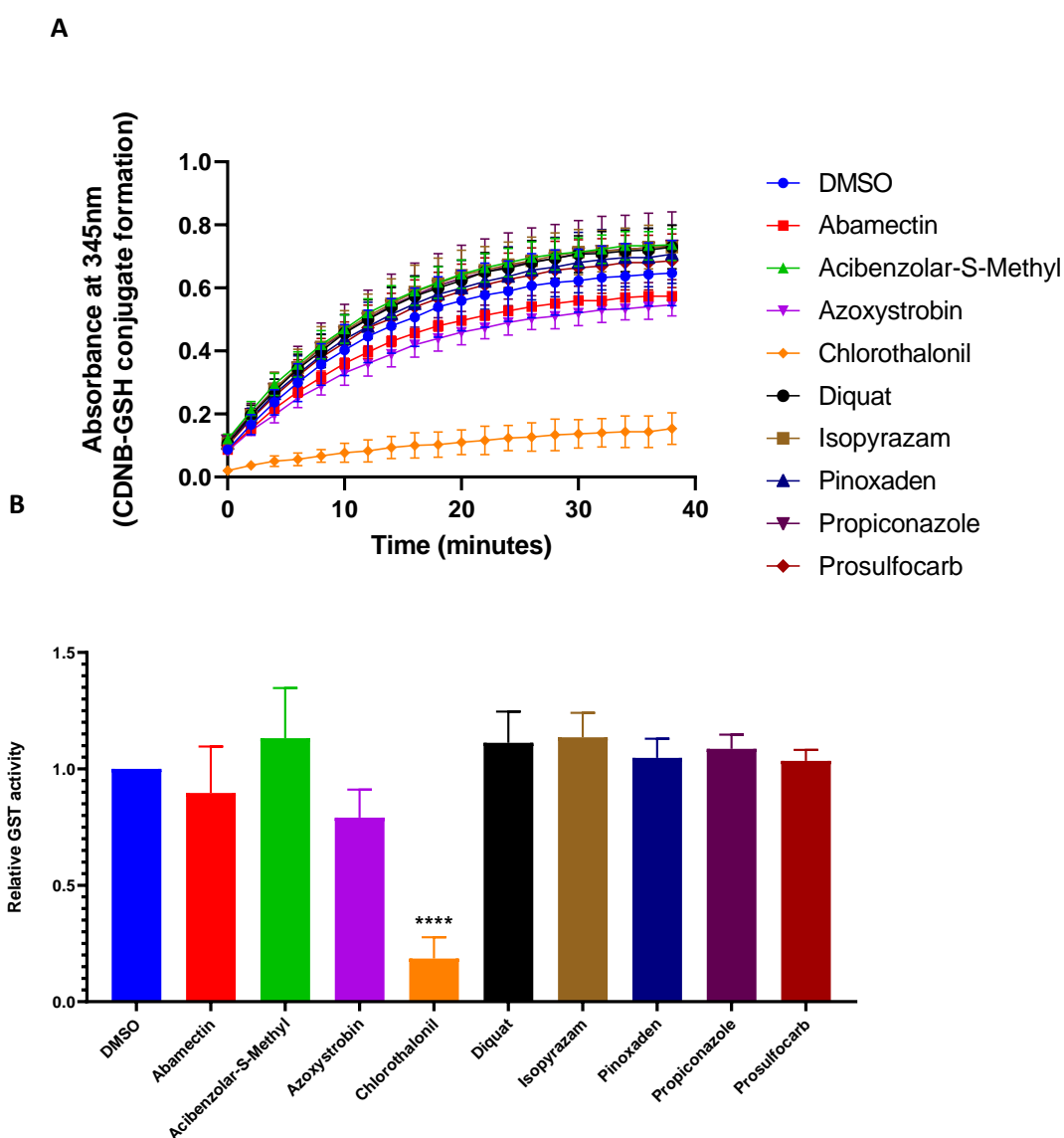


**Figure 2.21.** CDNB-GSH conjugation as a measure of GST activity in the bronchial epithelial cell line 16HBE14o-, following a 24 h exposure to 10  $\mu$ M of a range of pesticides. Results are shown as (A) kinetic activity and (B) activity relative to DMSO control at 30 minutes. Data represented as mean  $\pm$  SD (n=3), \*\*\*\* =  $p < 0.0001$

#### 2.4.12 Comparative xenobiotic metabolism studies

The GST-CDNB and resorufin based assays were used to provide information on comparative functional enzyme expression within the different epithelial models (**Figure 2.22**). By calculating the rate of metabolite production with and without selective enzyme inhibitors, the specific enzyme contribution to the reaction was obtained. The data for the individual enzyme assays can be found in the appendix.

The Caco-2 intestinal cell line was used as a positive control due to its functional expression of most of the xenobiotic metabolising enzymes of interest in this study (Borlak and Zwadlo, 2003, Tran et al., 2020). Calu-3 had the highest enzyme expression of the respiratory epithelial cell lines, with CYP1A1, CYP1A2, CYP2B6, CYP3A5, NQO1 and GST specific reactions all being catalysed by this cell line.

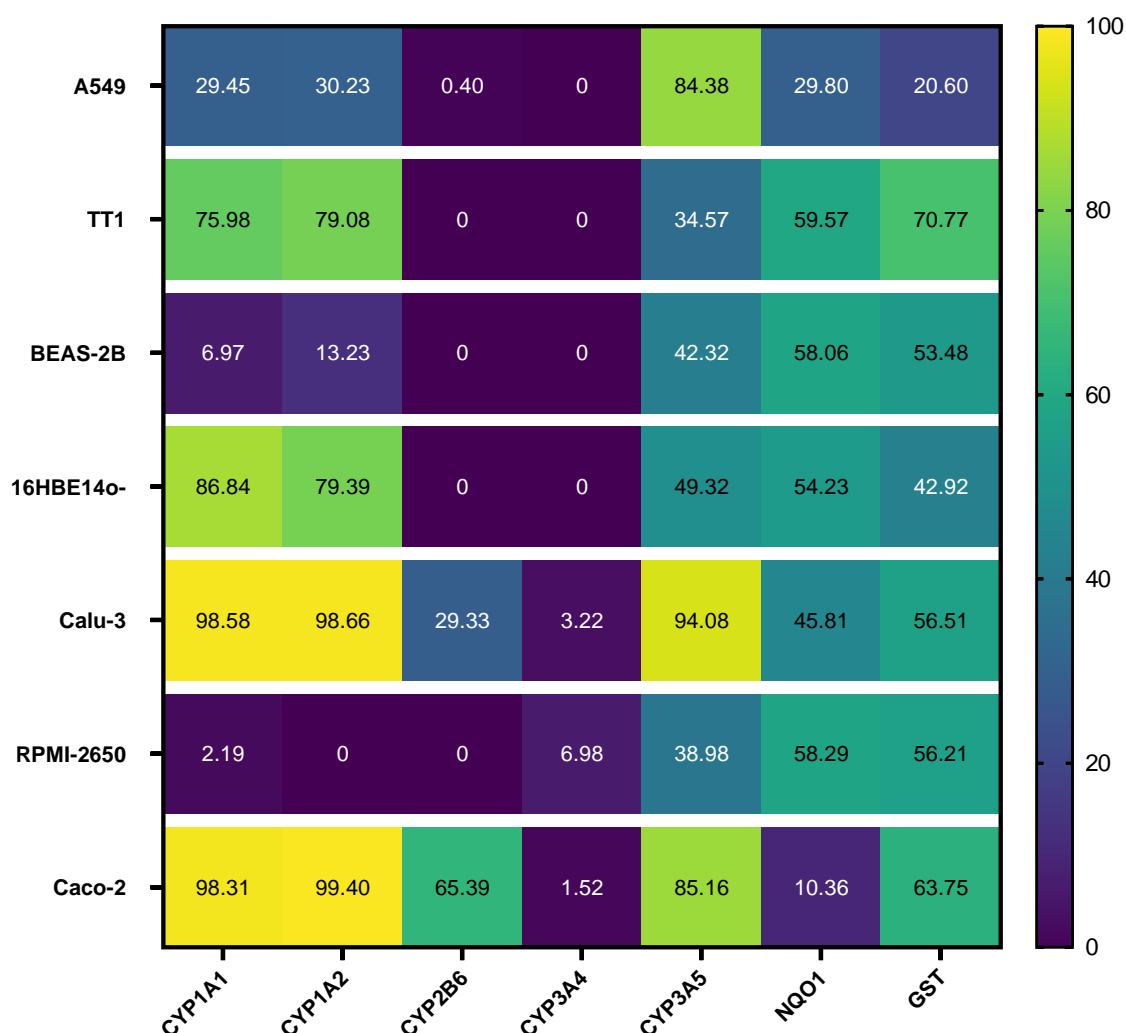


**Figure 2.22.** Heatmap showing differences between cell lines for % inhibition of NQO1, GST and the CYP isozymes; CYP1A1, CYP1A2, CYP2B6, CYP3A4, CYP3A5. All inhibitor concentrations were  $\geq$   $IC_{50}$  values reported in the literature.

In contrast to Calu-3, enzyme activity in A549 and BEAS-2B was generally lower and less specific based on the inhibitors used, with the exception of CYP3A5 which whilst significantly less active than in Calu-3 was selectively inhibited by 84% in A549 cells using ketoconazole. Specific activity illustrated in **Figure 2.23** highlights that whilst under these experimental conditions Calu-3 had the greatest enzyme expression and activity of the bronchial cell lines (and of the respiratory epithelial cell lines generally). Of the alveolar cell lines tested, TT1 possessed higher activity for CYP1A1, CYP1A2, NQO1 and GST in comparison to A549.



**Figure 2.23. Radar graphs illustrating the xenobiotic metabolism profile of each of the cell lines. Data expressed as Log units of specific activity nmol/mg/mL (total activity minus activity with inhibitor).**

## 2.5 Discussion

The different cell lines cultured in this study were tested for their suitability as representative models of the respiratory epithelium (nasal, bronchial and alveolar), with regards to their use to assess toxicity, permeability and metabolism. A range of pesticides with different physicochemical properties and mechanisms of action were tested for toxicity, whilst permeability and metabolism experiments generally relied on the use of standard probes/reporter molecules rather than particular pesticides of interest. Combined these methods were used to analyse the suitability of the different models for their use in future toxicokinetic and metabolomic experiments and to inform concentration and exposures to be used in those experiments.

### 2.5.1 MTT and mechanistic toxicity assays

The MTT assays demonstrated that regardless of the cell line used, there was a ranking trend for pesticide cytotoxicity, with chlorothalonil always being the most cytotoxic followed by abamectin (**Figure 2.6**). Chlorothalonil is a commercial fungicide, that works via glutathione and thiol depletion, this known mechanism of action is likely the cause of its cytotoxicity *in vitro*, with decreased cell viability being reported following the depletion of GSH and the inhibition of respiratory enzymes (Gallagher et al., 1992, Tillman et al., 1973). In addition, to being a known respiratory irritant in humans, has been shown to induce both apoptosis and necroptosis *in vitro* (Li et al., 2020). The mechanism of action for chlorothalonil is consistent with the data shown in **Figure 2.8** as at non-cytotoxic concentrations intracellular GSH was increased by over 2-fold, and further reduction in GSH at higher concentrations corresponded with a decline in cell viability (**Figure 2.10C**). An initial increase in intracellular GSH was observed in 16HBE14o-, even at the lowest tested concentration of 2.5  $\mu$ M, and similar increases in GSH concentration have been shown in catfish *in vivo*, with this being suggested as a protective mechanism observed following sublethal exposure to chlorothalonil (Gallagher et al., 1992). Furthermore, whilst chlorothalonil was the most cytotoxic of the pesticides tested, the significant differences between the tested cell lines, highlight that BEAS-2B may be the most sensitive cell line in part due to its reduced ability to upregulate GSH production in comparison to the more resistant cancer derived cell lines tested **Figure 2.7**. With regards to this, it is notable that of the 6 cell lines tested the 3 “normal immortalised” or non-cancer derived cell lines were significantly more sensitive to chlorothalonil toxicity than the cancer derived cell lines, with this potentially being related either to intrinsic differences in GSH concentration/upregulation or potentially due to the differences in GST-mediated metabolism.

There is evidence of an association between xenobiotic resistance and elevated intracellular glutathione within lung cancers (Balendiran et al., 2004), however this has not been extensively explored by comparing the differences between “normal” immortalised vs cancer-derived bronchial/alveolar cells.

The insecticide abamectin, was the second most cytotoxic pesticide based on the MTT cytotoxicity assay, and with the exception of BEAS-2B there was no significant difference in toxicity with the range of cell lines used (**Figure 2.7**). However as shown in **Figure 2.8-10**, abamectin was capable of inducing mitochondrial toxicity in 16HBE14o-, similar to that which has previously been reported in several *in vitro* models (Zanoli et al., 2012, Maioli et al., 2013, Liang et al., 2019). Interestingly, of the two fungicides whose mechanisms of action are mitochondrial inhibition, only azoxystrobin caused a marked decrease in mitochondrial viability, whilst isopyrazam caused only a modest decline, azoxystrobin acting as a Qo inhibitor which blocks the electron transport chain in contrast to isopyrazam which inhibits succinate dehydrogenase. Combined, the two different assays successfully highlighted pesticides with low cytotoxicity, such as propiconazole and propiconazole. Cell proliferation was observed in both assays following acibenzolar-s-methyl exposure, this effect may relate to either hormesis or the potential of this compound to cause respiratory irritation (APVMA, 2007, EFSA, 2014a).

Overall, the data presented reinforces the value of selecting the most appropriate cell line for toxicity assays, with non-cancer derived cell lines potentially being both more sensitive to toxicity and representative of normal primary cells. The use of 16HBE14o- may be of particular benefit due to its sensitivity, but also has potential for cell proliferation and phenotypic changes in response to sublethal pesticide concentrations. Similarly, the alveolar cell line TT1 may be more suitable for toxicity studies than A549 cells, both due to its increased sensitivity to toxicity and better representing alveolar type I cells which make up ~95% of the alveolar surface area and are therefore of more importance in an exposure scenario in comparison to type II alveolar cells. The dose-response curves also highlight which pesticides may be a toxicity concern based on low concentrations which might occur during occupational exposure, for example chlorothalonil and abamectin are of the most concern, whilst although the LC<sub>50</sub> value for acibenzolar-s-methyl is > 150 µM, cell proliferation and phenotypic changes are observed at ≤ 10 µM in 16HBE14o-. This *in vitro* toxicity data may be paired with predicted aerosol deposition data used to predict realistic respiratory epithelial cell exposure concentrations which may then be used to assess the likelihood of adverse effects following



inhalation of the tested pesticides, with this application being explored further in **Chapter 3** and **4**.

### **2.5.2 Permeability**

Most *in vitro* permeability studies for inhaled xenobiotics have focused on drug delivery rather than for the risk assessment of environmental or occupational exposure (Meindl et al., 2015, Lin et al., 2007, Chandiramohan et al., 2021, Fröhlich and Salar-Behzadi, 2014, Foster et al., 2000). However, the models used for permeability assessments are the same, and may also be explored by employing commonly-used molecules as permeability probes. There is extensive literature highlighting the suitability of Calu-3 cell layers as a permeability model for the bronchial epithelium and more recently even as a surrogate for the nasal epithelium (Grainger et al., 2006, Inoue et al., 2020a, Kreft et al., 2015b, Sibinovska et al., 2020). Despite this, the potential for intra-lab variation with the Calu-3 permeability model has been identified with time- and passage-dependent variability being a consideration (Haghi et al., 2010). Other bronchial epithelial cell lines have also been explored, highlighting the use of 16HBE14o- when cultured under submerged conditions, and the unsuitability of BEAS-2B due to its inability to form functional tight junctions. Similarly to BEAS-2B, numerous researchers have also shown the alveolar cell line A549 has also been shown to be unsuitable (Sakagami, 2006, Forbes, 2000). There is relatively sparse data on the use of TT1 as an alveolar model, however it has been reported to produce TEER values below  $60 \Omega \cdot \text{cm}^2$  (van den Bogaard et al., 2009). More recently, the hAELVi cell line has been shown to be a suitable alveolar model, producing TEER values  $> 1500 \Omega \cdot \text{cm}^2$  with functional occludin and ZO-1 (Kuehn et al., 2016). However, the use of the hAELVi model is new and may be limited by cost, in addition to reports of it containing a heterogeneous cell population (Lehr, 2021), which may cause variability in results ranging from  $1000\text{-}7000 \Omega \cdot \text{cm}^2$  between labs or under modified culturing conditions (Metz et al., 2020, Joelsson et al., 2020). RPMI-2650 as a nasal permeability model has also been described previously to produce relatively low TEER values, but within a similar range to excised human and animal nasal mucosa ( $40\text{-}120 \Omega \cdot \text{cm}^2$ ) (Kreft et al., 2015b).

In contrast to the cell-based models, lipid-based models such as PAMPA have also been explored using various formulations and offers potential advantages over cell-based models which are associated with higher cost, culturing time, risk of contamination, the need for specialist equipment, animal-based products such as growth factors or foetal bovine serum. Furthermore, the use of well characterised proportions of specific lipids may avoid the

biological variability associated with cell models, especially between different labs. However, the PAMPA model is unable to replicate active transport, or unique characteristics of biological membranes such as the mucosal secretions, airway surfactant, or the rich variety of proteins to which a xenobiotic may selectively bind. Some of these limitations may be overcome through the use of a lung specific PAMPA, one with a wider variety of lipids than just POPC and cholesterol. This might be achieved through the novel lung lipid extract approach described earlier, especially if the lipids of interest are characterised by lipodomics to then allow for an easily reproducible and animal-free synthetic version to be formulated.

The outcomes of this study provide a clear and direct comparison between the different permeability models; A549, TT1, Calu-3, RPMI-2650, Caco-2 and PAMPA. Additionally, this represents the first study using rat lung lipid extract as a permeability model.

Generally, the results for the different cell-based models are similar to those previously reported by other researchers, and the interdependence between TEER and xenobiotic permeability is evident in **Figure 2.13**. This trend between TEER and permeability is less obvious in the case of Rh-123 which is lipophilic and transported via a transcellular mechanism, in contrast to the hydrophilic permeability markers NaF and FD-4 which permeate across the epithelial barrier by paracellular transport.

Calu-3 was confirmed to be a suitable model of the bronchial epithelial barrier, with an average TEER of  $605 \Omega \cdot \text{cm}^2$  in addition to the expression of functional ZO-1 and low paracellular transport of FD-4 (**Figure 2.11-15**). TEER values achieved in this study for TT1, were moderately higher than those previously reported in the literature, possibly due to culturing TT1 on Transwells using a modified protocol e.g. collagen-coated Transwells and high seeding density and medium supplemented with non-essential amino acids. Additionally, for the transport of NaF no significant difference was found between Calu-3 and TT1 permeability barriers. Despite this, ZO-1 expression was not visualised by confocal microscopy, FD-4 and Rh-123 permeability was significantly higher than Calu-3 and TEER values greater than  $150 \Omega \cdot \text{cm}^2$ , suggesting a poor alveolar permeability model as TEER of  $1000-2500 \Omega \cdot \text{cm}^2$  is commonly reported using primary alveolar cells (Elbert et al., 1999, Fuchs et al., 2003, Srinivasan et al., 2015). Attempts to increase the TEER values by altering the culturing conditions through using basement membrane extract or co-culturing with the fibroblast cell line 3T3 did not influence TEER, whilst the addition of SLF had a negative effect on TEER potentially due to having a cytostatic effect. As expected based on the literature, A549 formed the lowest TEER values and the poorest permeability barrier, whilst the nasal cell line RPMI-2650 was moderately less permeable and although the TEER values were low, it was within the range of data reported

for excised nasal mucosa  $> 40 \Omega \cdot \text{cm}^2$ . Despite the predictable findings for A549 and RPMI-2650, the models were included to provide a direct comparison with the other *in vitro* models and allow for a holistic presentation of the data.

The lipid-based models, successfully excluded the hydrophilic NaF, to a similar extent to Calu-3 (**Figure 2.15**), but were significantly more permeable to the lipophilic compound Rh-123. Furthermore, the data presented in **Figure 2.14**, clearly highlights it is the lipid content in both the lung extract and the PAMPA formulation responsible for the permeability barrier, rather than the dodecane solvent, with this result being particularly important for the validation of the novel lung lipid extract model whilst also showing it to be comparable to the defined PAMPA formulation.

These results using the lipid-based models, highlight their potential suitability for the prediction of xenobiotic permeability in the lung, particularly as a complementary model to Calu-3 cells whereby the effects of active transport or protein binding may be eliminated. The lipid-based models may also be valuable to estimate permeability where poor biocompatibility precludes the use of cell models (i.e. in the case of toxicity induced by the active ingredient or formulation excipients). With regards to active transport mechanisms, several drug transporters have been reported within the respiratory tract and in the cell lines A549, Calu-3, RPMI-2650, 16HBE14o- and BEAS-2B, with the most common example being P-glycoprotein (Bosquillon, 2010, Brillault et al., 2009, Hamilton et al., 2001, Dolberg and Reichl, 2016). P-glycoprotein is an important drug efflux transporter due to its high substrate promiscuity, ranging from chemotherapeutic drugs such as doxorubicin to potentially inhaled pesticides such as abamectin (Didier and Loor, 1996, Didziapetris et al., 2003). This drug transporter may potentially reduce the xenobiotic bioavailability by reducing the absorption rate in favour of non-absorptive clearance. Furthermore, P-glycoprotein activity has been implicated in reducing the toxicity of orally ingested abamectin in multiple species including humans (Lankas et al., 1997, Macdonald and Gledhill, 2007). It has also been shown to interact with several other pesticides, which may act as substrates such as the insecticide abamectin or inhibitors such as the fungicide propiconazole (Bain and Leblanc, 1996, Abu-Qare et al., 2003). Whilst functional activity of this important drug transporter has previously been reported for the other cell lines included in this study, P-glycoprotein activity in the alveolar cell line TT1 has not been explored to date. As TT1 expresses several markers of an AT1-like phenotype and is morphologically distinct to A549, its characterisation with regards to potential drug transporter activity is of interest. Rh-123 bidirectional transport highlighted marginally higher

efflux by TT1 than A549, with efflux in both models being halved by the addition of the P-glycoprotein inhibitor cyclosporin A. However, the uninhibited efflux ratio was less than 2, which likely related to the assay conditions for this experiment, in which Rh-123 50  $\mu$ M may have oversaturated the active transport pathway. To identify whether the low efflux ratios relate to the relatively high concentration of Rh-123 used, future assays may benefit from a 10-fold reduction in Rh-123 to 5  $\mu$ M so as not to saturate active transport. Additionally, further bidirectional transport experiments would be useful to investigate other drug efflux transporters such as MRP2 and BCRP, in addition to potentially supplementing the data with 2D accumulation/efflux assays.

Overall, the permeability studies listed highlight the value particularly of Calu-3 and the lipid-based models to determine the permeability of different xenobiotics that may potentially be inhaled. In addition to the intrinsic permeability of different biological barriers, the role of drug transporters and the design of experimental methods to estimate xenobiotic efflux in the lung are of great relevance to the toxicokinetics of inhaled xenobiotics. The lung lipid extract model, provides a promising opportunity to develop a lung specific PAMPA model in the future, which contains physiologically relevant and diverse lipids and for which a synthetic formulation would allow reduced biological variability and increased throughput.

### **2.5.3 Metabolism**

Drug transporters often act in concert with intracellular enzymes (Nigam, 2015, Urquhart et al., 2007), which metabolise parent compounds to a more hydrophilic and easily excreted metabolite, either by Phase I metabolism such as the addition of hydroxy-groups or by Phase II metabolism by which conjugative reactions may add GSH, sulphate, glycine or glucuronic acid groups to the parent compound. Xenobiotic metabolism may aid clearance of inhaled xenobiotics and simultaneously detoxify the compound by deactivating reactive groups, a classic example of this is performed by GST enzymes. GST enzymes, may conjugate glutathione to the reactive electrophilic groups of several different substrates, thereby reducing their inherent toxicity and producing polar metabolites less likely to diffuse across cell membranes but which are recognised as substrates of unidirectional efflux transporters such as MRP1, which may thereby aid the clearance of the metabolised compound. Although a similar mechanism exists for UGT-mediated metabolism, generally UGT expression and functional activity is low and therefore less likely to be of relevance to detoxification pathways following xenobiotic inhalation. Based on the reported expression of key xenobiotic metabolising enzymes in the lung, which has been extensively reviewed (Enlo-Scott et al., 2021a, Oesch et

al., 2019), CYP, NQO1 and GST activity in the different epithelial models was investigated. Whilst esterase metabolism is a key important biotransformation pathways within the lung, with relatively high activity, preliminary experiments showed the tested colorimetric and fluorometric reactions to be relatively non-specific and not inhibited by known inhibitors for the respective enzymes (**Table 2.2**) and were not included in subsequent experiments. With regards to the resorufin based CYP-mediated experiments specific inhibitors were identified, and as shown in **Figure 2.17-18**, the assays were both specific and sensitive. Of the tested pesticides, propiconazole was confirmed to induce CYP1A1 at realistic exposure concentrations (**Figure 2.19-20**), and although this has not previously been explored with regard to human lung cells, the result is consonant with previous reports of propiconazole-mediated CYP1A1 induction within rat, mouse and trout liver tissue (Levine et al., 1999, Sun et al., 2005). This is also in accordance with propiconazole being a suggested AhR ligand (Knebel et al., 2018a), additionally there is recent evidence that it may also interact with CAR/PXR (Knebel et al., 2018b, Lake, 2018), potentially inducing CYP2B and CYP3A enzymes. CYP2B6 induction with propiconazole and rifampicin was also tested in 16HBE14o- (data not shown), no result was shown with either compound, however based on later experiments this is likely due to 16HBE14o- not expressing functional CYP2B6 with Calu-3 shown to be a more suitable model (**Figure 2.22**).

The potential induction of CYP3A by propiconazole is of interest as this enzyme has been shown to metabolise the pesticide to several hydrophilic metabolites with reduced cytotoxicity, and is therefore relevant due to both implications on lung detoxification pathways, implications for respiratory bioavailability and also due to potential changes to cell phenotype.

With regards to the other pesticides tested; neither CYP1A1 or GST were induced, however, abamectin did significantly inhibit CYP1A1 and chlorothalonil caused inhibition of both enzymes. Abamectin has been reported to reduce CYP activity at sublethal concentrations in a time dependent manner (Zhu et al., 2014), and there is limited human data to suggest it may be metabolised by CYP3A4 (Abass et al., 2009, Zeng et al., 1998), however, enzyme expression of CYP3A4 in the lung is negligible, which may have implications for abamectin local toxicity if inhaled.

There is limited evidence in the literature to suggest that chlorothalonil is either a substrate or inhibitor of CYP1A1, and the inhibitory effect shown in **Figure 2.19** may instead relate to a general reduction in metabolic activity as a result of chlorothalonil toxicity. In contrast, the inhibition of GST activity by chlorothalonil is well described in the literature, with

chlorothalonil being both a substrate of GST and having the potential to inhibit GST-CDNB activity at concentrations as low as 100 nM (dos Santos et al., 2021, Kim et al., 2004). For the experiments in this study the inhibitory effect likely relates to irreversible inhibition of GST and the need for *de novo* enzyme synthesis, as prior to the experiment chlorothalonil had been removed, and rinsed before snap-freezing the cells, highlighting that the effect is not due to chlorothalonil mediated glutathione depletion (this substrate was in excess for the enzyme reaction). The nature of this chlorothalonil-mediated GST inhibition, has several implications for respiratory exposure due to reducing the likelihood of detoxification especially with regards to sub-chronic exposure in an occupational setting, in addition to the context that chlorothalonil is a known respiratory irritant.

Supplementing the initial 16HBE14o- metabolism data, the enzyme extracts/S9 fractions of all the different cell lines were tested, with the extraction protocol enzyme amount to be normalised against protein concentration, and eliminating inherent differences between cell number, growth rate and surface area coverage between the different cell lines. The differences in functional activity for several XMEs were investigated, the results highlight that of the enzymes tested, with the exception of CYP3A4 all were shown to be active in human lung primary tissue (data from commercially obtained human lung S9 is shown in the appendix), with this result being in accordance with what has previously been reported by other researchers. For the tested enzyme activities, of the respiratory epithelial cell lines, only Calu-3 catalysed the CYP2B6 dependent PROD assay (**Figure 2.22**). The presence of functional CYP2B6 activity in Calu-3 is of note, as this enzyme contributes to the human metabolism of a multitude of environmental chemicals such as PAHs and PCBs but also a range of pesticides such as; alachlor, butachlor, metalochlor, chlorpyrifos, carbaryl, phorate, several organophosphorus insecticides, imidacloprid and atrazine (Hodgson and Rose, 2007). Additionally, Calu-3 had the higher activity for all of the CYP-mediated reactions than all of the other tested respiratory epithelial cell lines, highlighting the suitability of Calu-3 a model of xenobiotic metabolism within the lung. This may be in part due to the responsiveness of Calu-3 to CYP induction following exposure to  $\beta$ -naphthoflavone and rifampicin. Other cell lines may respond better to a different combination of enzyme inducers, for example whilst both the literature and the data obtained from this study highlight the functional activity of CYP3A5 in A549, it has been reported that in this cell line it may not be induced by the CAR/PXR pathway and instead dexamethasone is more effective as it induces CYP3A5 via the glucocorticoid receptor (Hukkanen et al., 2000). Whilst the comparison of the effectiveness of different enzyme inducers in the different respiratory epithelial cell lines, was beyond the scope of this

study, future experiments may make use of a “cocktail” containing the commonly used XME inducers. This cocktail may include rifampicin,  $\beta$ -naphthoflavone and phenobarbital, combined with the less commonly used dexamethasone (with the latter 3 also being shown to induce both CYP and GST enzymes) (Hayes and Pulford, 1995, G Zhang et al., 2010).

Based on the experimental conditions used in this study, whilst Calu-3 had the widest expression profile of the respiratory epithelial models, other differences were noted (**Figure 2.23**). TT1 had higher activity than A549 for NQO1, GST, CYP1A1 and CYP1A2, suggesting that this may be a useful model of alveolar cell metabolism in the future. CYP1A1 and NQO1 expression in TT1 was first highlighted by Jarvis et al. (2018) using western blotting and PCR to show induction of these enzymes in response to PAH exposure, the data presented in **Figure 2.22-23** reinforces the evidence of expression of these enzymes in TT1 and confirms their functional activity.

The data obtained from these metabolism studies may aid the selection of appropriate lung cell lines for the rapid screening of xenobiotic metabolites either using the described microplate-based assays, or for metabolite identification via LC-MS, along with several other commonly performed DMPK studies. Overall, metabolism data contributes to the metabolic fate and toxicity implications of inhaled xenobiotics including pesticides and air pollutants. Although this is not currently included in many PBPK inhalation models, considerations around lung metabolism when combined with toxicity and permeability data may help inform toxicokinetic and data-driven risk assessments for environmental and occupational exposure.

Overall, the results provide novel information about the toxicological activity (cytotoxicity, mitochondrial inhibition and glutathione depletion) of several pesticides in human respiratory epithelial cell lines, as well as interesting new data on the suitability of these models for permeability and metabolism studies. The importance and implications of these findings are partially explored in **Chapter 3 & 4**.

## 2.6 Conclusion

The investigations of the above studies, highlight particular *in vitro* models are most suitable depending on whether toxicity, permeability or metabolism is the research focus, but in all cases the use of human cells over animal tissue is preferable where possible. Generally, Calu-3 may be used for all the above assays, due the generation of a polarised epithelium with

functional tight junction proteins for permeability studies and the potential to induce several of the key XMEs, however for cytotoxicity it may be more appropriate to use a more sensitive model such as the non-cancer derived cell lines TT1, BEAS-2B and 16HBE14o-. Additionally, whilst PAMPA and rat lung lipid models are complementary permeability models to Calu-3, the latter is the most appropriate model for respiratory epithelial permeability.

Generally, the initially outlined research aims for this chapter were achieved. The differences between the respiratory epithelial cell lines with regard to their sensitivity to pesticide toxicity, were effectively evaluated and highlighted that the use of “normal” immortalised cell lines over cancer-derived ones may be preferable. Suitable *in vitro* models for xenobiotic permeability and metabolism within the respiratory tract were also successfully evaluated, with Calu-3 being best suited. Further work is required to better characterise these models in comparison to human primary respiratory epithelial tissue, in addition to the assessment of a wider range of pesticides. Overall this chapter provides a suitable foundation for the use of respiratory *in vitro* models that may be applied to toxicokinetic prediction of inhaled xenobiotics.



# Chapter 3

## **Toxicokinetic prediction of pesticides inhaled during occupational exposure.**

### **3.1 Introduction**

Pesticides are highly regulated to ensure there is no adverse effect on human health by reducing the likelihood and length of exposure, this considers both those working in the agricultural industry who may be occupationally exposed and also the general population (either through bystander exposure or through dietary exposure to pesticide residues). With regards to occupational exposure (OPEX), guidance is given by regulatory bodies such as the US Environmental Protection Agency (EPA) and the European Food Safety Authority (EFSA). EFSA regulation seeks to enforce precautionary principles in risk assessing application of pesticides with regard to “realistic conditions of use, shall not have any harmful effects on human health” (EFSA, 2014b). For risk assessment purposes, one potential scenario is inhalation exposure of agricultural workers, which is estimated using default values for factors such as breathing rates, average air concentrations, hectares treated per day, exposure duration and fraction absorption. With regards to absorption values, oral absorption is specified as a particular value if less than 80% is observed in ADME studies, or considered to be 100% if greater than 80%. Conversion of external exposure to compare systemic hazard (typically derived from oral toxicology studies), requires dermal absorption to be measured through experimentation using the pesticide formulation (EFSA et al., 2017b). However, a less scientific approach is applied to inhalation absorption where values are assumed to be 100% of the inhaled dose/exposure.

The assumption of 100% respiratory bioavailability is likely to be conservative, and is anomalous compared to the use of evidenced-based oral and dermal bioavailability values for occupational exposure assessments. The assumption of 100% respiratory bioavailability is contrary to the learning from the well-established field of inhaled drug delivery and medicines development in which improvements in delivery to the lungs or increase in respiratory bioavailability of pharmaceuticals is sought.

Whilst extensive research has focused on the inhaled pharmacokinetics of several drugs (Winkler et al., 2004, Borghardt et al., 2015, Eriksson et al., 2018), there is comparatively little data on the inhaled toxicokinetics of commonly used pesticides, despite the inherent similarity

in the clearance mechanisms and fate of xenobiotics once inhaled. Whilst the “exposure” or “dosing” scenario is different, the comparison of these two applications can be facilitated by existing regional deposition models based on aerosol properties such as median mass aerodynamic diameter (MMAD). Following deposition considerations are either identical for pesticides and inhaled medicines, for example those processes inherent to the respiratory system, or may be specific for example physicochemical parameters related to the xenobiotic of interest.

In addition to the potential refinement of inhaled absorption values to be comparable to evidence-based oral and dermal values, toxicokinetic prediction of inhaled pesticides may also offer other advantages to current risk assessments. For example, rather than solely focusing on bioavailability or absorption values, realistic pesticide aerosol deposition data for the human respiratory tract and prediction of pesticide concentrations in epithelial lining fluid can inform *in vitro* toxicity assays to estimate the hazard of the inhaled pesticide more accurately. This is of value both to the high-throughput assay approaches highlighted in **Chapter 2** and more advanced but lower throughput models such as MucilAir or EpiAirway, which are limited by cost, or emerging toxicity assays that rely on “omics” methods, such as metabolomics and transcriptomics, for which sample number and subsequently the range of tested concentrations is often limited.

A toxicokinetic approach has the potential to not only improve accuracy in estimations for the inhaled route of exposure in current OPEX risk assessments, but also aid the refinement and replacement of existing *in vivo* toxicity models with *in vitro* models which have increased relevance to human exposure.

The methods for prediction of respiratory permeability have been described in detail (Enlo-Scott et al., 2021b), including considerations for absorptive clearance, epithelial drug transport, lung retention and experimental models for lung permeability. With regards to experimental models, a combined approach using *in vitro* data as inputs for physiologically-based pharmacokinetic (PBPK) *in silico* models has been shown to be capable of predicting the pharmacokinetics of inhaled medicines (Bäckman et al., 2018, Eriksson et al., 2018).

Subsequently, there is scope that this may be applied to the toxicokinetic prediction of pesticides inhaled during OPEX exposure.

## 3.2 Aims and Objectives

The overall aim of this series of experiments was to illustrate an evidence-based approach to predict respiratory bioavailability of pesticides inhaled in occupational exposure scenarios. This was performed by using data obtained from *in vitro* assays as input parameters to a mechanistic computer model to predict the toxicokinetics and respiratory bioavailability of inhaled pesticides, and evaluate the potential of this approach for future risk assessments.

Specific objectives included:

1. Combine *in vitro* data and *in silico* computational methods to estimate the risk of systemic exposure following pesticide inhalation in an occupational setting based on pesticide physicochemical properties, aerosol deposition, *in vitro* permeability, and mechanistic pharmacokinetic modelling.
2. Evaluate this approach to predicting respiratory bioavailability for occupational exposures and evaluate the strengths and weaknesses.

## 3.3 Methods

### 3.3.1 Pesticide selection

The EU Pesticides database was used to explore the list of registered pesticides (Active Ingredients), which are authorised for use and have complete GHS Hazard Classifications. Of the pesticides investigated in **Chapter 2**, three fungicides were chosen for further study, azoxystrobin, chlorothalonil and propiconazole, which not only represent some of the most widely sprayed fungicides globally but also fall into separate GHS hazard classifications. Whilst all three fungicides are organic, low molecular weight and non-volatile compounds, their other physicochemical properties vary as do their mechanisms of action.

### 3.3.2 Exposure scenario

The occupational exposure scenarios used in this study were based on current EFSA guidelines for the risk assessment of exposure for operators/workers using plant protection products (EFSA, 2014b), supplemented by data obtained from chlorothalonil risk assessments submitted to EFSA and the US EPA (Arena et al., 2018, Flack et al., 2018). Briefly, the default duration of exposure is 8 hours to replicate a professional working day and predict potential exposure for non-volatile and moderately volatile pesticides (i.e. the three fungicides used in this study). For typical vehicle mounted spraying using modern machinery “mixing and loading” exposure the duration is relatively short, although there may be multiple mixing/loading steps for smaller/older tanks which in effect mean a greater exposure time. In comparison, “spraying”

typically represents a comparably longer exposure. The median mass aerodynamic diameter (MMAD) values were modelled as 13.5 µm (for “mixing & loading”) and 35 µm (for “spraying”) to examine the impact of different spray properties. Geometric standard deviation was ± 1.5 µm for both aerosol exposure scenarios. Although exposure scenarios vary according to application method, crop/site use, max application rate and area treated, exposure application scenario were selected to represent the highest inhalation exposure concentrations. As shown in **Table 3.1** this was developed for airblast application of pistachios.

**Table 3.1. Chlorothalonil representative spray application scenarios and inhalation exposures, reproduced from (Flack et al., 2018)**

Exposure Scenario	Crop/Use site	Maximum application rate on label (lb AI/A)	Area treated (Acres)	Inhalation Unit Exposure (µg AI/lb handled)	Inhalation Exposure (ng/L)
Aerial application	Soybean	1.8	1200	0.0049	2.68
Aerial application	Cranberries	5.0	350	0.0049	2.13
<u>Airblast application</u>	<u>Pistachio</u>	<u>4.5</u>	<u>40</u>	<u>4.7</u>	<u>213</u>
Airblast application	Stone fruit	3.1	40	4.7	146
Groundboom application	Golf course	11.3	40	0.34	38.6
Groundboom application	Sod farm	11.3	80	0.34	77.1

### 3.3.3 Respiratory tract model & aerosol deposition prediction

The commercially available software Mimetikos Preludium™ (Version 1.1.7, Emmace Consulting AB) was used to estimate regional deposition of the pesticide aerosol in the human respiratory tract. The Weibel lung model (Weibel et al., 1963, Yu and Diu, 1982), was used and lung volume at forced residual capacity (FRC) was set to 3000 mL and extrathoracic volume of 50 mL (Hall et al., 2021). The National Council on Radiation Protection (NCRP) deposition model was used via the nasal inhalation route, with aerosol “inhalability” set to model the

natural inhalation of ambient aerosols, rather than the forced deliberate inhalation of pharmaceutical aerosols. Tidal breathing was selected, as this was most appropriate for estimating an 8 hour exposure. Tidal volume (3000 mL), inspiratory flow rate (1000 mL/s) and expiratory flow rate (1000 mL/s) were the default settings based on a 70 kg male (the default value for a US agricultural worker).

Following respiratory model specification, the aerosol deposition was predicted for aerosols with a MMAD of either 13.5 or 35  $\mu\text{m}$  and GSD of  $\pm 1.5 \mu\text{m}$ . Other aerosol properties were assigned according to the default settings; density ( $1.00 \text{ g/cm}^3$ ) to replicate the density of a predominantly water-based pesticide aerosol, shape factor (1.00) to model a normal spherical aerosol droplet/particle. Aerosol deposition was estimated using the above settings and data was graphically displayed using GraphPad Prism.

### **3.3.4 Preliminary *in vitro* assays**

To ensure that there were no fungicide-induced changes to cell layer permeability, preliminary *in vitro* assays were performed in order to choose an appropriate apical chamber concentration for permeability experiments.

Calu-3 cells were cultured on Transwells using the method described previously in **Chapter 2**. After the maximum TEER was reached at 14 days, experiments were performed. Cell medium was aspirated and the cell layers were rinsed once with warm HBSS. To the apical chamber, 250  $\mu\text{L}$  of warm HBSS was added, containing either a 0.025% DMSO control or azoxystrobin, chlorothalonil or propiconazole 10  $\mu\text{M}$ . HBSS (500  $\mu\text{L}$ ) was added to the basolateral chamber, and TEER measurements were recorded at 0, 0.5, 1, 2, 3, 4 and 6 hours after exposure to the fungicides, taking care to rinse the electrode to avoid transfer of fungicide residue between samples. Each pesticide was assayed in triplicate wells in each experiment. Experiments were repeated to give  $n=3$ .

Additionally, the dose dependent effect of the fungicides on Calu-3 permeability was explored using a high-throughput assay. Calu-3 cells were seeded onto HTS Transwell® 96-well permeable supports (Corning) at a seeding density of 40,000 cells per well with 100  $\mu\text{L}$  medium in the apical chamber. After 2 days, the cells were transferred to air-liquid interface and medium was changed every 2 days until 14 days from seeding the cells. The cell layers were gently rinsed once with PBS, before exposing to either the negative control (DMSO 0.2%), the positive controls (EDTA 2 mM to produce transient changes to tight junctions or SDS 400  $\mu\text{L}$  to irreversibly increase permeability) or varying concentrations of the three fungicides at 0-80  $\mu\text{M}$ . All exposures were 6 hours in duration and used phenol-red free cell culture medium as

the diluent. After the 6 hour exposure, cells were gently rinsed with PBS once, before being incubated with 100  $\mu$ L FD-4 (1 mg/mL) in HBSS in the apical chamber and 400  $\mu$ L HBSS in the basolateral chamber. After a 1 h incubation at 37°C and 200 RPM, 100  $\mu$ L of the basolateral medium was collected for each sample into a black-walled 96-well plate and fluorescence measured as previously described. Data was normalised against the DMSO control and represents duplicate wells for each experiment (n=4).

### 3.3.5 Radiochemicals and fungicide method quantification

For all experiments, quantification of pesticides was performed using a Tri-Carb 2900TR liquid scintillation analyser to analyse  $^{14}$ C-labelled azoxystrobin, chlorothalonil and propiconazole. The details for the certificate of analysis of each radiochemical are listed in the appendix, including  $^{14}$ C- position, activity, radiochemical purity, chemical purity and supplier.

All experiments used radiochemicals which were spiked into the sample at 1.35-5.5 KBq and a DMSO concentration of  $\geq$  1%. For analysis, 50-100  $\mu$ L of the sample was pipetted into a Kartell™ scintillation vial (Thermofisher), to which 4 mL of Ultima Gold™ liquid scintillation cocktail (PerkinElmer) was added. All samples were capped and inverted repeatedly to mix, before placing in the pre-calibrated Tri-Carb 2900TR liquid scintillation analyser. For each sample matrix, calibration curves were prepared to ensure a linear relationship between fungicide concentration and radioactivity measured as disintegrations per minute (dpm).

### 3.3.6 $P_{app}$ measurement *in vitro*

The protocol used to measure  $P_{app}$  *in vitro* was adapted from (Eriksson et al., 2018) and varied slightly from the permeability experiments performed in the previous chapter, with the changes allowing for the prediction of *intrinsic* permeability suitable for *in silico* modelling and excluding potential active transport mechanisms. Calu-3 and Caco-2 cells were seeded onto 24-well plate Transwells at 100,000 cells per well and were cultured for 14 and 22 days, respectively, with TEER measurements recorded every 2 days. Calu-3 cells were cultured at ALI while Caco-2 cells were cultured under submerged conditions. Permeability experiments were conducted using barriers formed by Calu-3, Caco-2, PAMPA or rat lung lipid. On the day of the permeability experiment, medium was aspirated and replaced with HBSS containing the drug transporter inhibitors quinidine 50  $\mu$ M (P-glycoprotein inhibitor), 30  $\mu$ M benzbrumarone (MRP1 inhibitor) and 20  $\mu$ M sulfasalazine (BCRP inhibitor). The buffer applied to the apical chamber was pH 6.6 whilst the buffer in the basolateral chamber was pH 7.4, with the volumes being 250  $\mu$ L and 500  $\mu$ L, respectively. After a 30 minute incubation with the drug transport

inhibitors, TEER measurements were taken and the permeability experiment was started. To the basolateral chamber of each Transwell, 600  $\mu\text{L}$  warm pH 7.4 HBSS buffer containing the transport inhibitor cocktail was added. To the apical chamber 250  $\mu\text{L}$  of pH 6.6 HBSS buffer containing 5  $\mu\text{M}$  of either radiolabelled azoxystrobin, chlorothalonil or propiconazole was added. 50  $\mu\text{L}$  from the apical chamber and 100  $\mu\text{L}$  from the basolateral chamber were immediately sampled, and then the Transwell plate was incubated at 37°C, with shaking at 480 rpm and sampling and replacing HBSS from the basolateral chamber at 5, 15, 30, 60 and 120 minutes. After 120 minutes, final TEER measurements were taken, the Transwell membrane was gently rinsed with PBS twice, before being cut out to analyse fungicide binding to the membrane. Each experiment contained 3 replicate wells and was repeated to give n=3 experiments.

$P_{\text{app}}$  values were calculated as previously described in **Chapter 2**.

### **3.3.7 $P_{\text{app}}$ prediction *in silico***

For the *in silico* prediction of  $P_{\text{app}}$  values and molecular properties, pCEL-X™ (in-ADME Research) was used. The pCEL-X program was developed to predict transport of drug-like molecules across biological membranes related to the brain or intestinal permeability, rather than specifically for the lung and so predicted  $P_{\text{app}}$  values for Caco-2 and PAMPA were used. Based on the molecular structure of each compound, LogP, MW, Log $P_{\text{app}}$  for Caco-2 and PAMPA were predicted, in addition to prediction of  $f_{\text{up}}$  (fraction unbound to plasma and  $K_{\text{p}}$  (tissue/plasma distribution ratio).

### **3.3.8 Protein binding experiments**

To enable toxicokinetic simulations for the three fungicides, various binding coefficients were determined *in vitro* for protein plasma binding ( $f_{\text{up}}$ ) and airway surface liquid binding ( $f_{\text{ue}}$ ). These experiments were performed using rapid equilibrium dialysis (RED), the gold standard for plasma protein binding (PPB) assays used in drug development. The RED device (Thermofisher, UK) used had a molecular weight cut-off (MWCO) of 8.0 kDa, thereby allowing the permeation of low molecular weight compounds whilst separating the protein sample from the buffer. The protocol was followed according to the supplier instructions, with the exception of the ASL binding assay for which no *in vitro* method could be found and was developed specifically for this purpose, by formulating a protein based synthetic lung fluid. The formulation was adapted based on the synthetic lung fluid described by Kumar et al. (2017) containing; albumin (8.8 mg/mL), IgG (2.6 mg/mL) and transferrin (1.5 mg/mL) in PBS. The

lipids DPPC, DPPG and cholesterol were excluded from this formulation as were the antioxidants ascorbate, urate and glutathione, as the MW of these compounds was below 8000 Da and would have permeated through the dialysis membrane. For the plasma protein binding assay, freshly frozen pooled human plasma was used.

All assays were performed by spiking 5 µM of the radiolabelled fungicide into the protein-based sample, before pipetting into the tissue chamber of the RED device and sampling both chambers of the dialysis insert at 0 minutes and after 240 minutes shaking at 250 rpm at 37°C. Each assay contained duplicate samples and was repeated to give n=3 experiments. Sample analysis was performed as specified by the supplier, with the exception that samples were quantified by liquid scintillation counting rather than LC-MS. Calibration curves and quality controls in the appropriate sample matrices were also obtained to make ensure all samples were above the limit of quantification.

The percentage unbound for F<sub>ue</sub> and F<sub>up</sub> was calculated using **Equation 3.1**;

**Equation 3.1 Rapid equilibrium dialysis, % unbound**

$$\% \text{ unbound} = \left( \frac{\text{Concentration in buffer chamber}}{\text{Concentration in protein chamber}} \right) \times 100$$

To confirm the suitability of the assay percentage recovery was also calculated using **Equation 3.2**;

**Equation 3.2 Rapid equilibrium dialysis, % recovery**

$$\% \text{ Recovery} = \left( \frac{\text{Buffer}_0 + \text{Protein sample}_0}{\text{Buffer}_{240} + \text{Protein sample}_{240}} \right) \times 100$$

Where “Buffer<sub>0</sub>” or “Protein<sub>0</sub>” is the initial fungicide concentration in buffer or plasma concentration, whereas “Buffer<sub>240</sub>” or “Protein<sub>240</sub>” is the final concentration. In theory recovery should be 100%, but all data with recovery ≥ 85% was accepted.

### **3.3.9 Toxicokinetic prediction**

Mimetikos Preludium was used for the toxicokinetic prediction of the three fungicides, using the predicted aerosol deposition data. Firstly, the nasal inhalation route was selected and mucociliary clearance was unchanged from the default value at which 95% of the bronchial deposition is cleared in 24 hours if no absorption takes place (equivalent to a mucus velocity of



0.55 cm/min in the trachea). The potential for drug binding to the epithelium was selected, and the default settings were unchanged for epithelial surface area, scaled perfusion factors, airway surface liquid depth, tissue depth and perfusion for the extrathoracic, tracheobronchial, bronchiolar and alveolar regions.

For the “System” module of the model, default settings were largely left unchanged, however for the volume of the central compartment ( $V_c$ ) was 10 L and both nasal and gastrointestinal absorption were selected. Gastrointestinal (GIT) bioavailability was set based on reported oral bioavailability data from rats, which were 80%, 20% and 91% for azoxystrobin, chlorothalonil and propiconazole respectively (EFSA et al., 2018, EFSA, 2010, EFSA et al., 2017a).

Gastrointestinal absorption time was set to 12 hours, mean transit time to the site of absorption 1 hour and the number of GIT compartments was 8 by default (with this representing a median value of GIT compartments for the purpose of modelling).

The rate of nasal absorption was calculated using the “mechanistic” setting, so the software determined absorption in this region based on a scaling factor for the other regions of the respiratory tract, rather than supplying an empirical or experimentally determined value.

For the compound specific values, molecular weight and LogP values were obtained from ChemDraw and confirmed on PubChem, whilst the remaining data was obtained from *in silico* predictions or *in vitro* measurements. Effective alveolar permeability (cm/s) may be estimated based on the correlation between this and Caco-2  $P_{app}$  values (Eriksson et al., 2018), therefore initially Caco-2  $P_{app}$  values predicted using pCEL-X were used, and then later compared with  $P_{app}$  values obtained *in vitro* using Caco-2, Calu-3, PAMPA and lung lipid extract. ASL binding was determined experimentally, whilst plasma protein binding and the tissue/plasma partition coefficient were predicted *in silico* before being determined experimentally. The blood/plasma partition ratio was assumed to be 1:1. The compound was specified as being dissolved, rather than a suspension or vesicle formulation.

For the exposure, the dose was estimated based on the data highlighted in **Table 3.1** and the previously stated exposure scenario, for which the inhalation exposure was 0.213  $\mu\text{g}/\text{L}$  and the total dosing schedule was calculated using the below equation;

### **Equation 3.3 Aerosol exposure dose per minute**

$$\begin{aligned} \text{Total dose} &= (0.213\mu\text{g}/\text{L}) \times (8.3\text{L breath}/\text{min}) \times 60 \text{ mins} \times 8 \text{ hours} = \mathbf{848.592 \mu\text{g}} \\ \text{Dose}/\text{min over 8 hour OPEX exposure} &= 848.592 \mu\text{g}/(60 \text{ mins} \times 8 \text{ hours}) = \\ &= \mathbf{1.7679 \mu\text{g}/\text{min}} \end{aligned}$$

This dosing schedule was specified as via nasal inhalation of 1.7679 µg/min for the first 8 hours, after which the dose was set to zero, with the overall toxicokinetic profile being modelled over a 96 h time course so as to illustrate clearance following the initial exposure. Finally, the toxicokinetic profile was plotted to show total concentration in the blood and epithelial tissues, rather than free plasma concentration. Based on the input data, AUC, C<sub>max</sub>, T<sub>max</sub>, % mucociliary clearance and % respiratory bioavailability, were predicted for each of the three fungicides, using either only *in silico* data or a combination of *in silico* and *in vitro* data.

### **3.3.10 Predicted *in situ* metabolism and toxicokinetic implications**

The formation of potential metabolites within the human lung was predicted by combining data obtained in **Chapter 2** for XME activity within the bronchial cell line Calu-3 with reported metabolism pathways for the three fungicides. Data in the literature confirming fungicide metabolism either in human or rat via CYP, NQO1 or GST enzymes was used as evidence for the potential formation of metabolites within the lungs (Kim et al., 2004, Laird et al., 2003, Mazur et al., 2015, Abass et al., 2012). Metabolites formed via UDP-glucuronyltransferases, esterases, n-acetyltransferases and sulfotransferases were not explored, despite the latter three contributing to lung metabolism. The physicochemical properties of the metabolites were compared against the parent compounds and changes to P<sub>app</sub> values were predicted *in silico* using pCEL-X, in order to explore potential changes to permeability. The influence of metabolism on bioactivation and detoxification mechanisms was also explored.

### 3.4 Results

#### 3.4.1 Respiratory tract model and aerosol deposition prediction

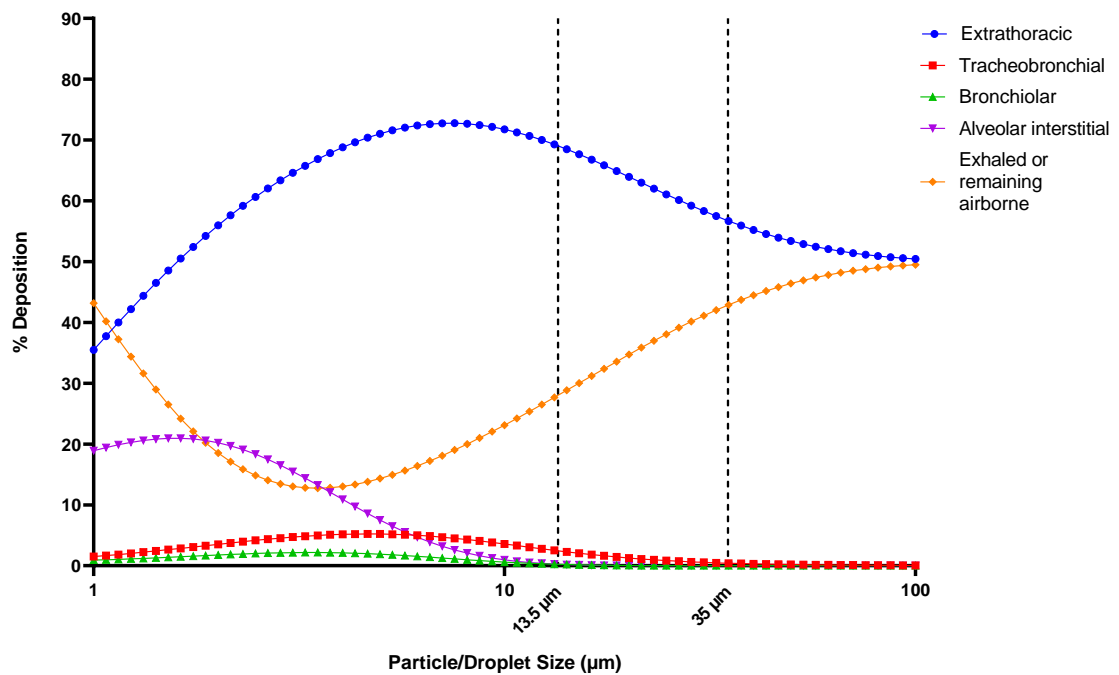


Figure 3.1. Regional lung deposition dependent on median mass aerodynamic diameter. Data generated using Mimetikos Preludium software.

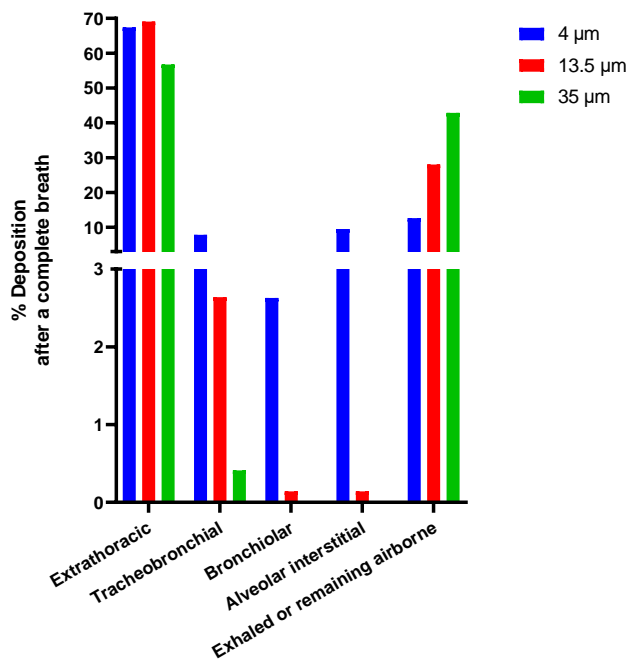
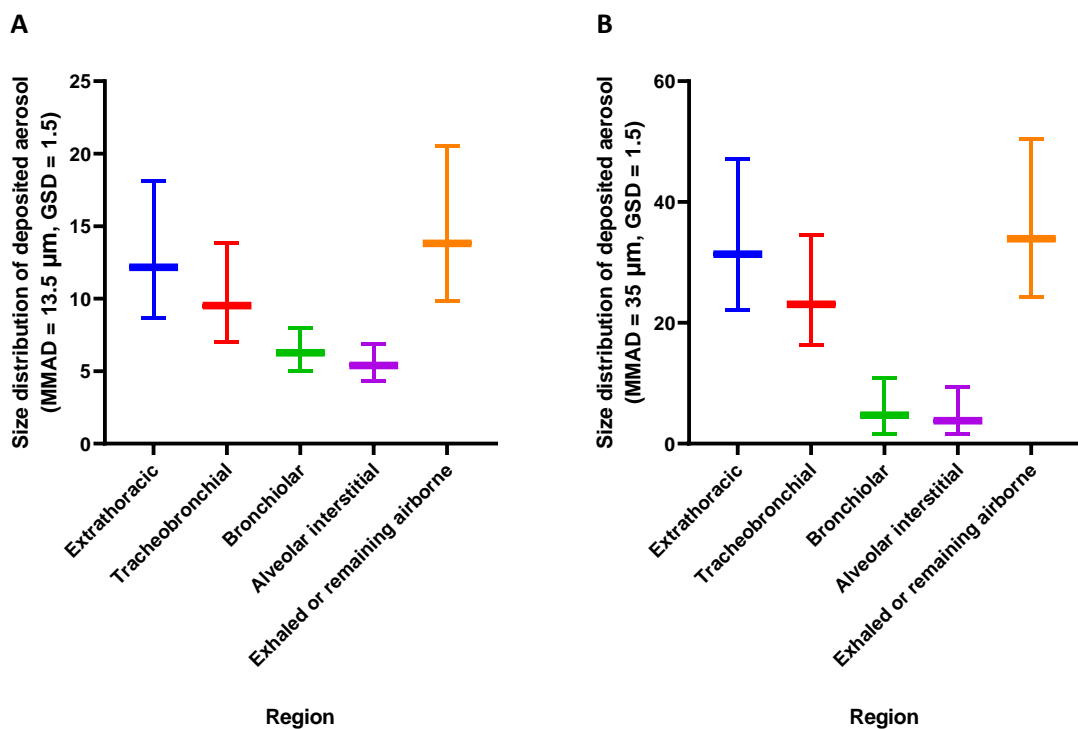


Figure 3.2. Predicted regional deposition for pesticide aerosols inhaled during occupational exposure. 13.5 µm for mixing/loading of pesticide solution and 35 µm for spraying the pesticide aerosol on crops. 4 µm is included for comparison purposes only but represents a “respirable” aerosol with greater lung deposition.

Based on the median mass aerodynamic diameter of a realistic pesticide aerosol during spraying (35  $\mu\text{m}$ ) or mixing and loading (13.5  $\mu\text{m}$ ), deposition is predominantly predicted to occur in the extrathoracic and tracheobronchial region (**Figure 3.2** and **Figure 3.3**). When the MMAD is 35  $\mu\text{m}$  (GSD =  $\pm 1.5$ ), only 57.14% of the aerosol was expected to deposit in the respiratory tract during passive breathing of the ambient aerosol, whilst for an MMAD of 13.5  $\mu\text{m}$  (GSD =  $\pm 1.5$ ), predicted deposition was increased to 71.98%. For a “respirable” aerosol, such as might be used to administer to rodents for *in vivo* inhalation toxicology studies, but does not represent the aerosol properties during occupational exposure, an aerosol with MMAD of 4  $\mu\text{m}$  (GSD =  $\pm 1.5$ ), was predicted to have 87% deposition.



**Figure 3.3.** Size distribution of deposited pesticide aerosol (A) 13.5  $\mu\text{m}$  and (B) 35  $\mu\text{m}$ , in relation to region of deposition. Data shows the median mass aerodynamic diameter, whilst error bars represent the upper and lower quartile. Data generated using *Mimetikos Preludium*.

These predictions for deposition were compared against data obtained from a Syngenta deposition model, and were found to be similar, although generally predicted higher deposition (**Figure 3.4**).

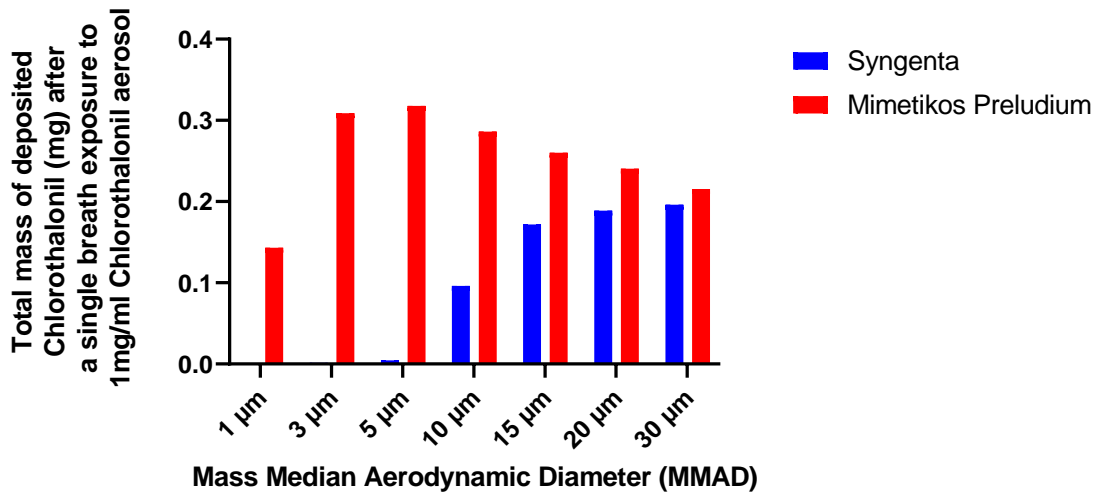


*Figure 3.4. Comparison of Syngenta vs Mimetikos Preludium respiratory tract deposition models. The Syngenta model includes the nasal region and trachea (Corley et al., 2021), whilst the Mimetikos Preludium model includes the entire respiratory tract.*

The Syngenta deposition model only includes the extrathoracic region and tracheobronchial regions of the lungs, which for pesticide aerosols with an MMAD  $\geq 15 \mu\text{m}$  is the main area of interest as the MMAD is predicted to be approximately  $35 \mu\text{m}$  during occupational exposure to pesticide sprays. The Mimetikos Preludium model, includes the entire respiratory tract and so deposition within the bronchiolar and alveolar region is also included, so that deposition of aerosols with an MMAD  $\leq 10 \mu\text{m}$  may also be predicted. Despite these differences, at  $30 \mu\text{m}$  both models predict similar total deposition at the MMAD which is most relevant to occupational exposure. Additional predicted aerosol deposition data is within the appendix, highlighting % deposition within specific regions of the tracheobronchial tree.

### 3.4.2 Preliminary *in vitro* assays

Prior to the experiments used for the collection of *in vitro* data to input into the *in silico* model, preliminary experiments were performed to ensure that a suitable fungicide concentration was used and explore whether the fungicides tested had an effect on epithelial permeability. As shown in **Figure 3.5**, Calu-3 TEER values did not significantly decrease in comparison to the DMSO control, over the course of a 6 hour exposure to any of the three fungicides. This data provides evidence that over the course of the experiments and during a potential occupational exposure, bronchial epithelial permeability is unlikely to be increased following exposure  $\leq 10$   $\mu\text{M}$ .

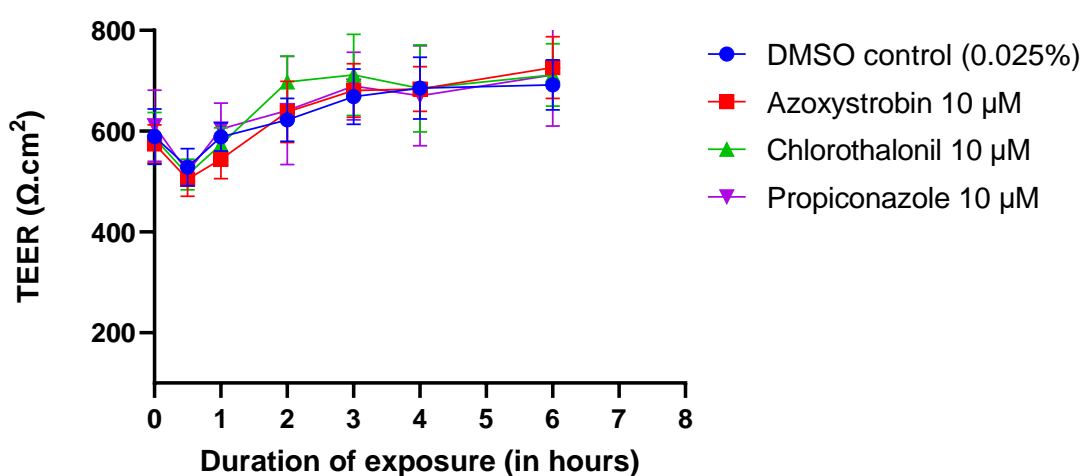


Figure 3.5. TEER values for Calu-3 during a 6 h exposure to azoxystrobin, chlorothalonil, propiconazole 10  $\mu\text{M}$  or DMSO control. Data shown as mean  $\pm$  SD ( $n=3$ ).

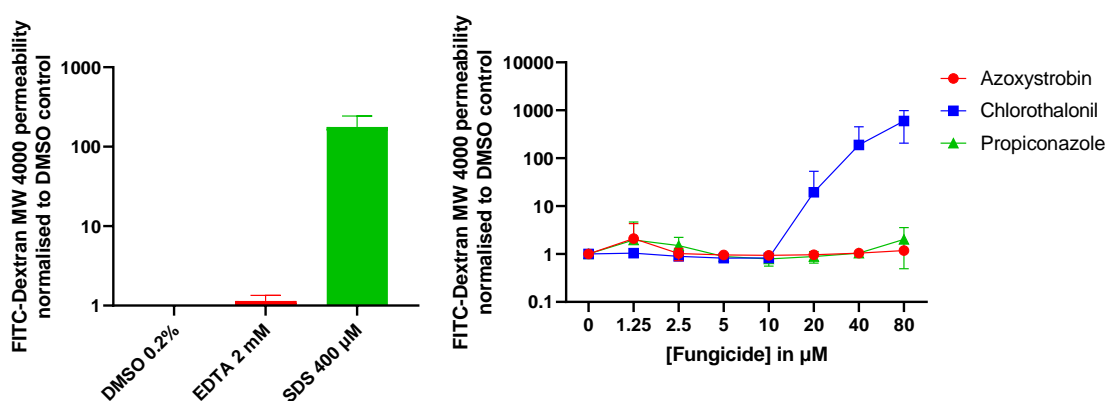


Figure 3.6. FITC-Dextran MW 4000 permeability, across Calu-3 following 6 h apical exposure to (A) the negative control DMSO, positive controls EDTA and SDS or (B) the tested fungicides azoxystrobin, chlorothalonil and propiconazole. Data shown as mean  $\pm$  SD ( $n=3$ ).

FITC-Dextran (FD-4) permeability was not significantly increased by any of the fungicides at concentrations  $\leq 10 \mu\text{M}$ , however at higher concentrations chlorothalonil caused a significant increase in permeability across the Calu-3 epithelial membrane, comparable to the positive control SDS. EDTA did significantly increase permeability, as it was removed prior to the addition of FD-4 and only causes transient disruption of tight junctions. This data suggests that higher concentrations of chlorothalonil caused a permanent change to epithelial permeability, rather than temporary disruption of tight junctions.

The fungicides azoxystrobin and propiconazole, did not increase FD-4 permeability at any of the tested concentrations. Based on this data,  $5 \mu\text{M}$  was selected as the concentration to measure  $P_{\text{app}}$  values in the permeability models, as this was a concentration well below that at which an effect on epithelial permeability was observed.

### 3.4.3 Quantification of radiolabelled fungicides

For the detection and quantification of fungicides during the remaining *in vitro* assays, radiolabelled compounds were used. Calibration curves were generated in the HBSS transport medium **Figure 3.7**, as well as the sample matrices used for protein binding experiments **Figure 3.8**. All assays showed a linear relationship between radioactivity (dpm) and pesticide concentration within the nanomolar range ( $R^2 \geq 0.994$ ) from 5-5000 nM.

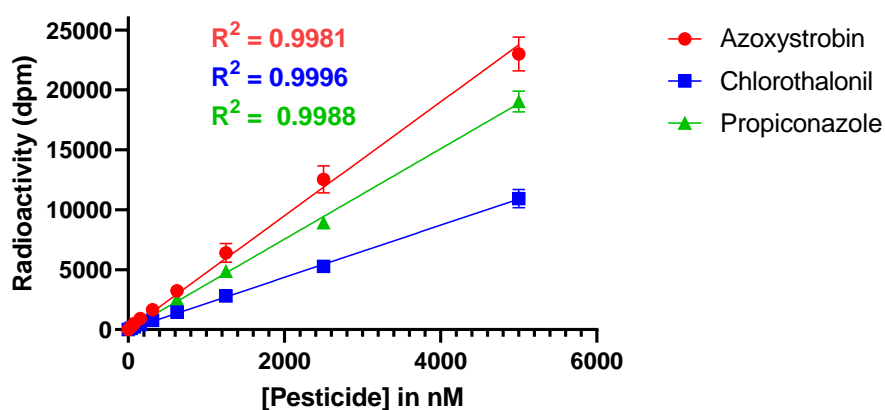


**Figure 3.7.** Calibration curve using  $^{14}\text{C}$ -labelled azoxystrobin, chlorothalonil and propiconazole in HBSS transport medium, 0-5000 nM. Data shown as mean  $\pm$  SD ( $n=3$ )

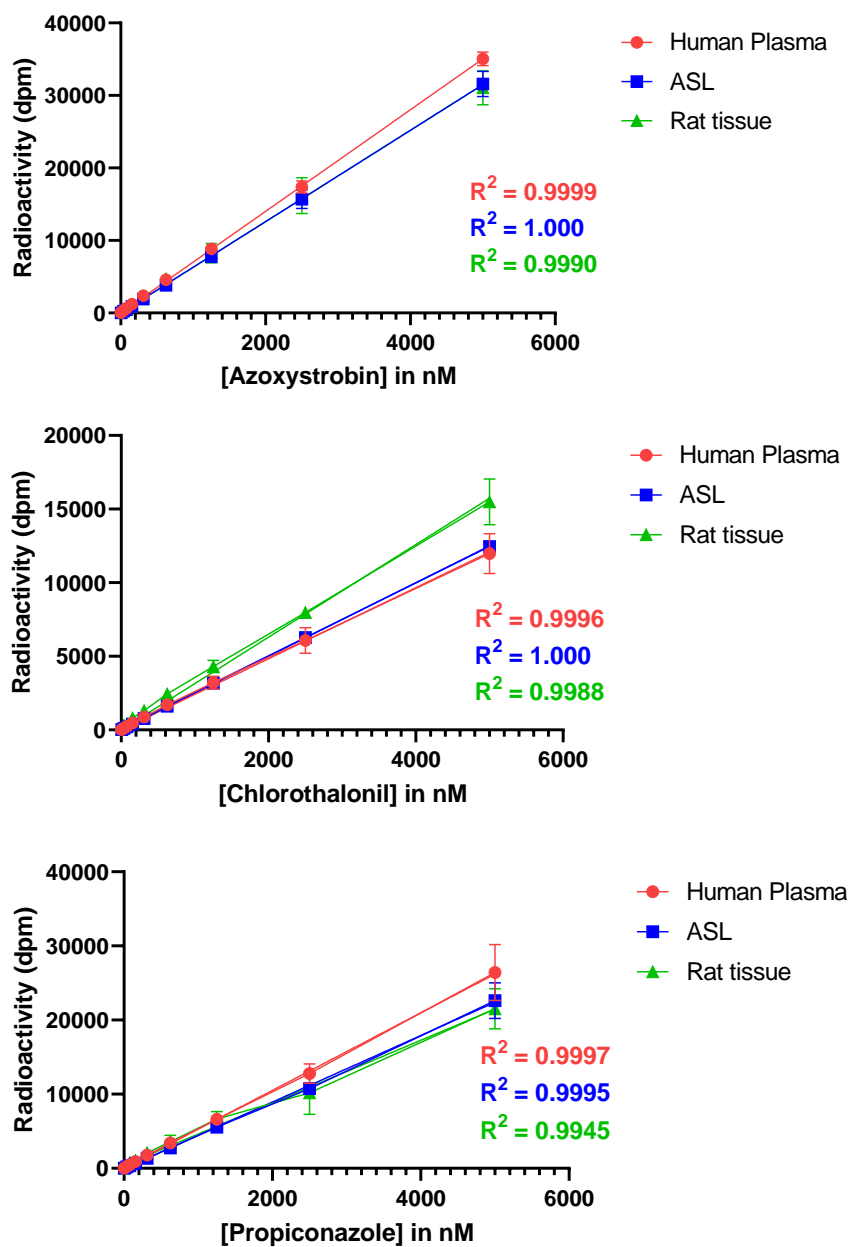


Figure 3.8. Calibration curve using <sup>14</sup>C-labelled (A) azoxystrobin, (B) chlorothalonil and (C) propiconazole in the sample matrices used for protein binding experiments, 0-5000 nM. Data shown as mean ± SD (n=3)



### 3.4.4 P<sub>app</sub> prediction *in vitro* and *in silico*

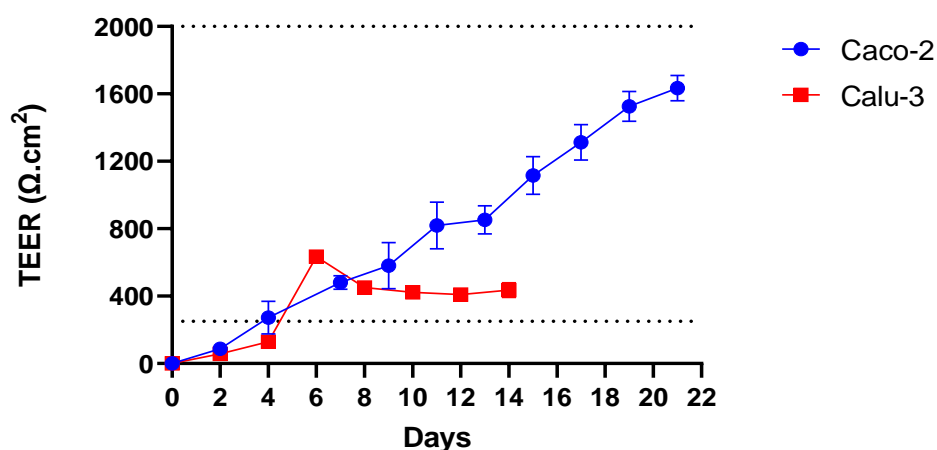


Figure 3.9. Transepithelial electrical resistance over 14 and 21 days, for Calu-3 (Passages 10-12) and Caco-2 (Passages 20-22). Gridlines at 250 and 2000  $\Omega.cm^2$ , highlighting that the permeability barriers formed were within a suitable range. Data represents 36 individual Transwell per cell line, shown as mean  $\pm$  SEM ( $n=3$ ).

As shown in **Figure 3.9** consistent TEER values for the Calu-3 and Caco-2 were achieved within the normal range (inclusion limits), ensuring that epithelial cell monolayer integrity was sufficient to provide a suitable xenobiotic permeability barrier for the fungicide permeability experiments.

For the purposes of *in silico* modelling all P<sub>app</sub> values were converted to LogP<sub>app</sub>, the data for which is shown in **Figure 3.10** and collated in **Table 3.2**.

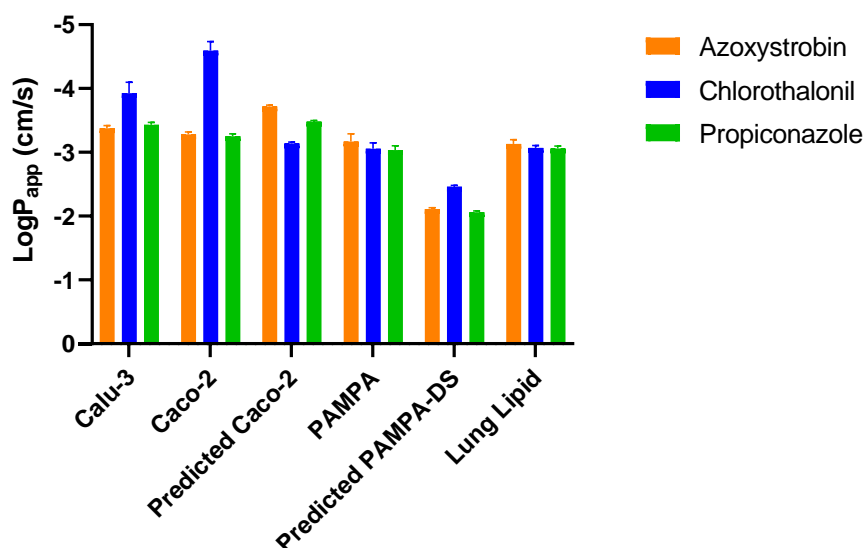
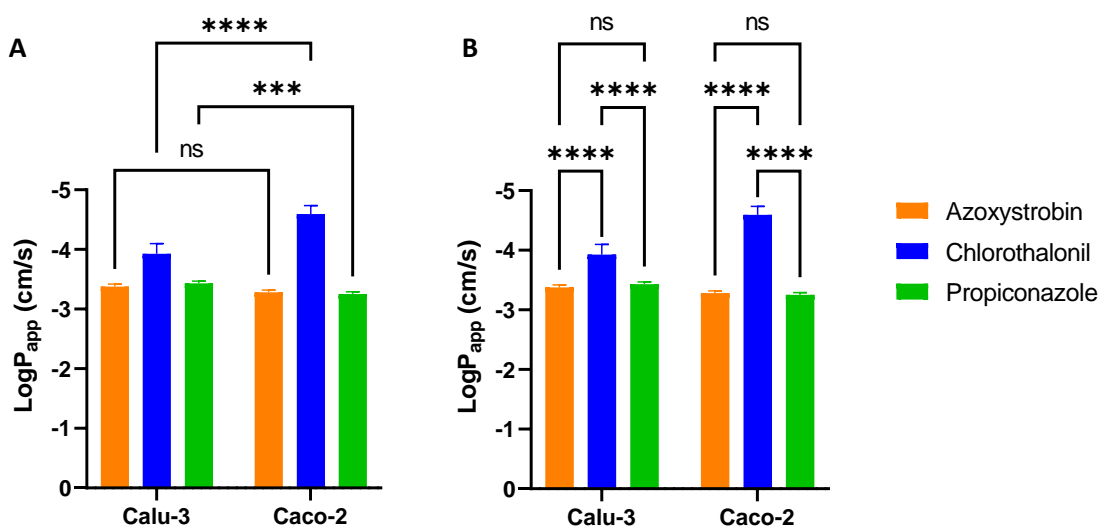


Figure 3.10. LogP<sub>app</sub> data for the three fungicides measured using *in vitro* models (Calu-3, Caco-2, PAMPA, Lung lipid) and *in silico* models (Predicted Caco-2 and Predicted PAMPA-DS). Data represent as mean  $\pm$  SD ( $n=3$ ) for the *in vitro* data and predicted value  $\pm$  5% for the *in silico* data.

The predicted PAMPA-double sink model appears to predict the trend observed in the cell lines but not that observed with PAMPA, furthermore the predicted  $P_{app}$  values are significantly higher than any of the tested PAMPA models. The predicted Caco-2  $P_{app}$  values are of the correct magnitude, but the trend observed with Caco-2 *in vitro* was not reproduced by simulation; this may be as a result of the permeability of chlorothalonil being reduced in the cell models via a mechanism not accounted for *in silico*, such as electrophilic chemical reactivity, protein binding or metabolism.

No statistically significant difference was found between the lipid-based models for any of the pesticides, and neither showed the reduced permeability of chlorothalonil in comparison to azoxystrobin and propiconazole that was observed using the cell-based models. This result suggests that the difference observed for chlorothalonil has a biological/biochemical origin rather than solely due to the physicochemical barrier of a lipid membrane.



**Figure 3.11.** One-Way ANOVA was used to compare (A) inter-model variability and (B) intra-model variability. Data represented as mean  $\pm$  SD (n=3)

Based on the above data (**Figure 3.11**), the cell-based models Calu-3 and Caco-2 were selected as the most suitable for further use, with these  $P_{app}$  values being used as inputs for Mimetikos Preludium, as part of the toxicokinetic prediction. The results showed significant inter-model variability, as fungicide transport experiments in the Calu-3 and Caco-2 models produced significantly different  $P_{app}$  values for chlorothalonil and propiconazole. Regardless of whether Calu-3 or Caco-2 was used, chlorothalonil was consistently less permeable than either azoxystrobin or propiconazole, whilst no significant difference in permeability was found between the latter two fungicides.

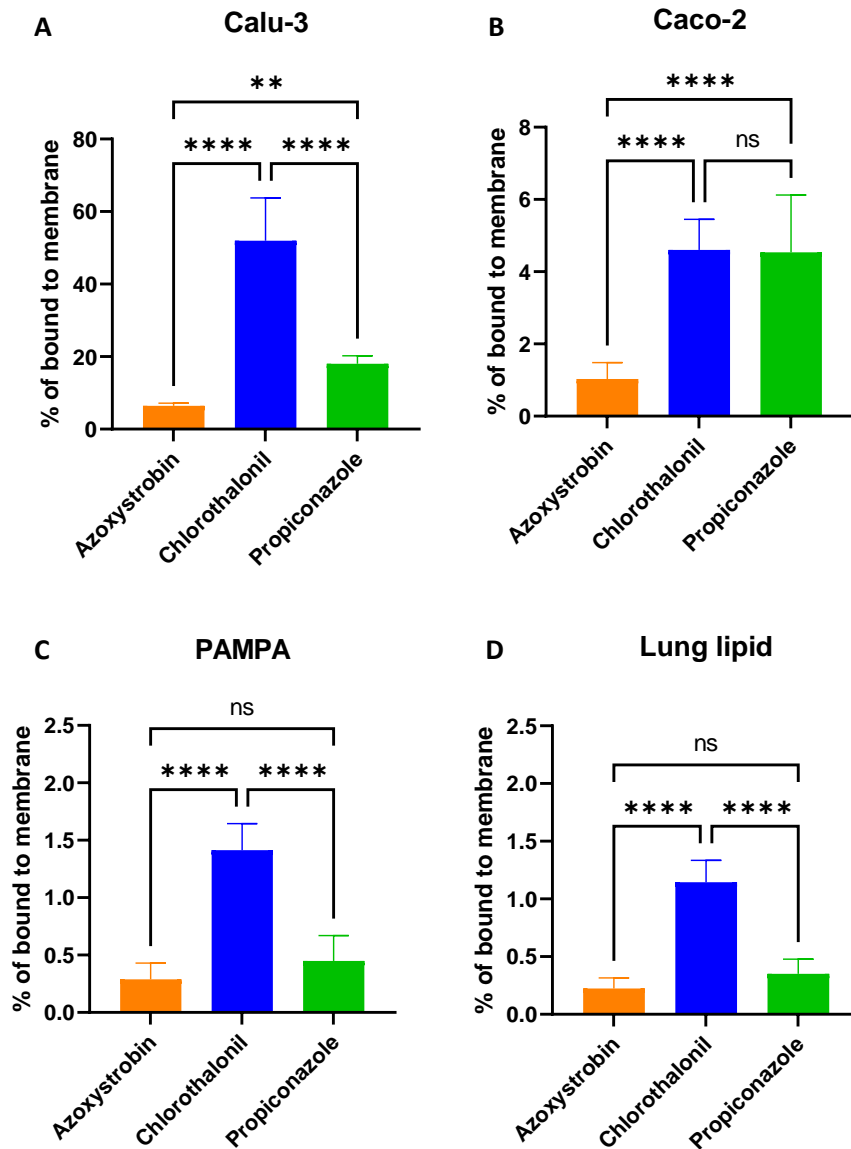


**Figure 3.12.** Fungicide binding to membrane as a percentage of the total mass applied for (A) Calu-3, (B) Caco-2, (C) PAMPA and (D) Lung lipid Transwell membranes. Data represented as mean  $\pm$  SD (n=3), ns = not significant.

The differences in  $P_{app}$  values between the *in vitro* models could not be accounted for purely based on Transwell membrane binding (**Figure 3.12**). As expected based on protein binding, fungicide retention was greatest with the cell based models, and was less than 2% for either of the lipid based models. Membrane binding was most substantial for Calu-3, and generally chlorothalonil bound the most to all models, followed by propiconazole with azoxystrobin binding the least.

### 3.4.5 Protein binding assays

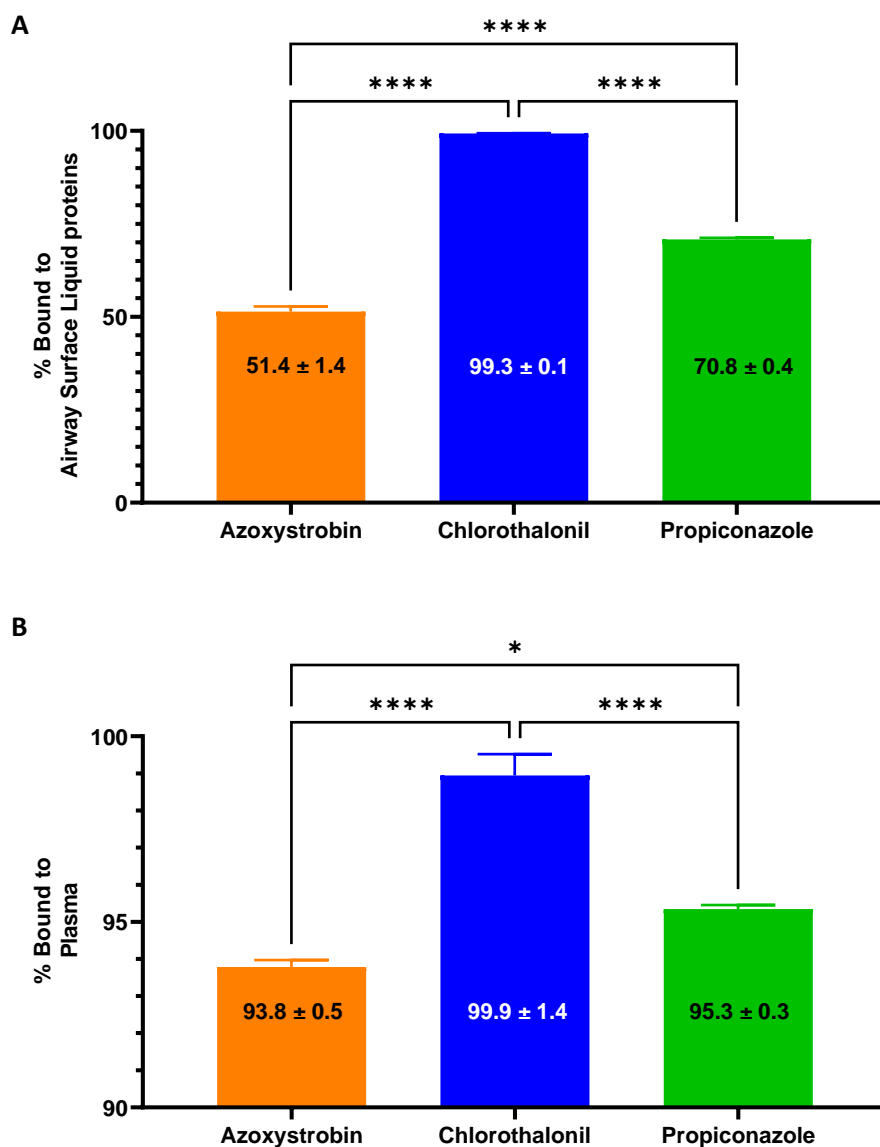


**Figure 3.13.** % Protein binding to (A) Synthetic airway surface liquid or (B) human plasma, following rapid equilibrium dialysis with 5  $\mu$ M of  $^{14}$ C-labelled azoxystrobin, chlorothalonil or propiconazole. Data shown as mean  $\pm$  SD (n=3).

The observed results for assays for binding to ASL and plasma showed chlorothalonil to have the highest % binding, followed by propiconazole and then azoxystrobin. This may be explained in part by the electrophilic chemical reactivity of chlorothalonil, leading to covalent binding at the sites highlighted in **Figure 3.14** with thiol groups of proteins. This high binding was also observed in (**Figure 3.12**), with Calu-3, and may relate to either protein binding, the formation of chlorothalonil-glutathione conjugates or binding to mucus produced by Calu-3. The moderately higher lipophilicity of propiconazole (LogP = 3.72) in comparison to

azoxystrobin (LogP = 2.5), may partially account for the higher binding of propiconazole, this relationship has been described for plasma protein binding and lipophilic drugs (Lázníček et al., 1987, Lázníček and Lázníčková, 1995). For all the tested fungicides, % binding was higher for plasma than for airway surface liquid, likely due to the significantly higher protein concentration in the human plasma. Whilst a statistically significant difference was found between each fungicide for both protein binding assays, the greatest differences were observed for airway surface liquid binding which may influence the toxicokinetics of the fungicides by reducing permeation into tissue because there is less unbound/"free drug" and prolonging airway residence time during which the pesticide is subject to mucociliary clearance.

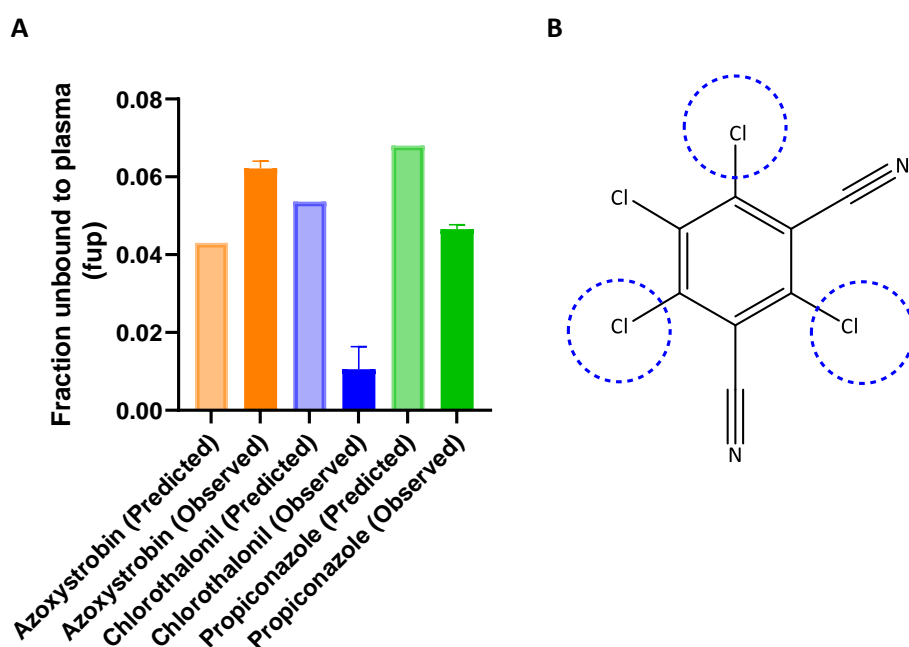


**Figure 3.14.** Fraction unbound to plasma, (A) predicted computationally using pCEL-X versus observed experimentally using rapid equilibrium dialysis. (B) Chlorothalonil which experimentally was <0.02% unbound contains reactive groups highlighted in blue, which may bind to thiol groups within various proteins or glutathione.

Generally, the predicted results were in the same magnitude as the observed values, with binding predicted to be > 90 % for the 3 tested compounds. However, for chlorothalonil there was the fraction unbound was 5 times less for the observed value than the predicted value, this is likely due to the chemical reactivity of chlorothalonil not being accounted for by the *in silico* model, rather than due to physicochemical properties such as lipophilicity, MW and solubility. Chlorothalonil is chemically reactive and binds to the thiol groups within several

proteins, which may include the free thiol from Cys34 in human serum albumin, in addition to any free sulfhydryl groups found in other plasma proteins.

The complete set of compound specific parameters either predicted *in silico* or calculated based on *in vitro* data is listed in **Table 3.2**. Generally, the predicted and observed values were similar, with the most variation being for  $P_{app}$  values and protein binding.

**Table 3.2. Predicted vs calculated inputs for Mimetikos Preludium. LogP values were either calculated computationally with pCEL-X or obtained from experimental PubChem data.  $P_{app}$  values were predicted using pCEL-X or obtained experimentally.  $K_p$  was predicted based on either *in silico* or *in vitro* LogP and  $F_{up}$ .  $F_{ue}$  could not be predicted in silico and was set at 1.00 by default. All *in vitro* data is shown as the mean average of 3 independent experiments (n=3). PAMPA and Lung lipid data were not used as inputs but are listed for comparison with other  $P_{app}$  values.**

Data parameter	Azoxystrobin		Chlorothalonil		Propiconazole	
	<i>In silico only</i>	<i>In vitro (+ in silico)</i>	<i>In silico only</i>	<i>In vitro (+ in silico)</i>	<i>In silico only</i>	<i>In vitro (+ in silico)</i>
<b>MW</b>	403.39		265.91		342.22	
<b>LogP</b>	3.4	2.5	2.99	2.94	3.45	3.72
Log $P_{app}$ PAMPA	-2.11	-3.17	-2.46	-3.06	-2.06	-3.04
<b>Log<math>P_{app}</math> Caco-2</b>	-3.72	-3.28	-3.14	-4.59	-3.48	-3.25
<b>Log<math>P_{app}</math> Calu-3</b>	N/A	-3.38	N/A	-3.93	N/A	-3.43
Log $P_{app}$ Lung lipid	N/A	-3.13	N/A	-3.07	N/A	-3.06
<b>F<sub>up</sub> (fraction unbound to plasma)</b>	0.043	0.0622	0.0536	0.0006	0.068	0.0466
<b>K<sub>p</sub> (tissue/plasma partition ratio)</b>	1.33	0.924	1.19	1.11	1.39	1.41
<b>F<sub>ue</sub> (fraction unbound to ASL)</b>	1.00	0.486	1.00	0.0072	1.00	0.2919
<b>Oral bioavailability (F<sub>oral</sub>) <i>In vivo rat data</i></b>	80%		20%		91%	

### 3.4.6 Toxicokinetic prediction

Theoretically, 100% respiratory bioavailability could be achieved using the toxicokinetic model by eliminating the effect of mucociliary clearance, changing deposition so that 100% of the aerosol deposits in the alveolar region, or imposing 100% bronchial deposition with 0% binding to airway surface liquid. Due to well established correlation between aerodynamic diameter of aerosols and regional deposition, the above scenarios are highly unlikely with non-volatile/semi-volatile organic chemicals, as are those where there is no mucociliary clearance or 0% binding to airway surface liquid. Alternatively, 100% “total bioavailability” could be achieved where oral bioavailability is 100%, or if oral bioavailability was high and the MMAD was altered (so that it was unrepresentative of a pesticide aerosol spray, e.g. < 2.5 µm) so that a greater proportion deposited in the alveolar region.

The data presented below is derived from the use of the experimentally obtained input values in table 2 combined with pre-determined values for human lung physiology/biopharmaceutics in-built into the toxicokinetic software. The toxicokinetic profiles based on realistic aerosol properties and the physicochemical *in vitro* differences between the pesticides are shown as a full dataset (for the 18 different simulations, based on 2 aerosol droplet sizes, 3 permeability models and 3 fungicides tested) in the appendix.

A major determinant of bioavailability following inhalation exposure was oral bioavailability following mucociliary clearance. Therefore, in order to highlight the effects of respiratory bioavailability, oral absorption was excluded from the following graphs unless otherwise stated.

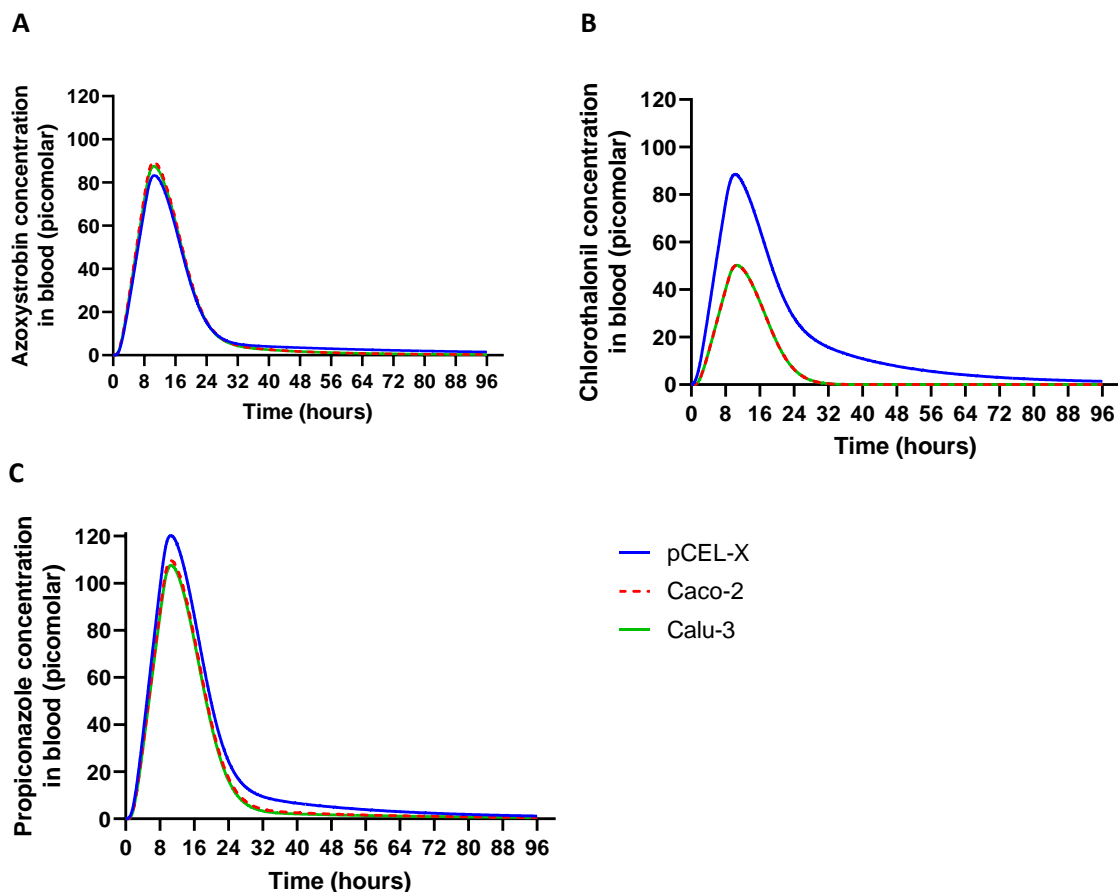


**Figure 3.15.** Comparison of blood toxicokinetic profiles predicted using *Mimetikos Preludium* with *in silico* (pCEL-X) or *in vitro* data (Caco-2 & Calu-3). Toxicokinetic profiles for (A) azoxystrobin, (B) chlorothalonil and (C) propiconazole are shown, based on an 8h occupational exposure during spraying (MMAD = 35  $\mu$ m). Oral absorption has been excluded.

Generally, the predicted toxicokinetic profile in blood was similar regardless of whether only *in silico* data was used or if the model was supplemented with *in vitro* data such as experimentally obtained ASL binding, plasma protein binding and Caco-2/Calu-3  $P_{app}$  values (**Figure 3.15**). The exception to this was for chlorothalonil, which had a significantly different profile dependent on whether experimental *in vitro* data or only *in silico* data was used; this is likely due to the inability of the pCEL-X model to predict the compounds chemical reactivity and high protein binding, in addition to the significantly different  $\text{Log}P_{app}$  values obtained between the *in silico* Caco-2 (-3.14) and the *in vitro* Caco-2 (-4.59).

The toxicokinetic profiles varied between the pesticides (**Figure 3.16**), with bioavailability predicted to be lowest for chlorothalonil and highest for propiconazole when equivalent aerosol exposures were simulated.



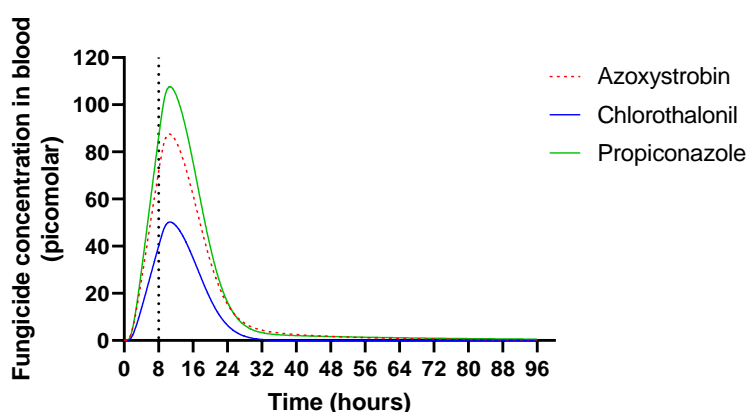


**Figure 3.16.** Azoxystrobin, chlorothalonil and propiconazole blood toxicokinetic profiles following inhalation, predicted using *Mimetikos Preludium*, with *in vitro* data and Calu-3  $P_{app}$  values. Data shown is for an 8 h occupational exposure during crop spraying using an aerosol of mass median aerodynamic diameter of 35  $\mu\text{m}$ . Oral absorption has been excluded from the model to show the extent of exposure from respiratory absorption.

The maximum epithelial fungicide concentration in the respiratory tract was consistently predicted to be within the extrathoracic region (0.1-27.3  $\mu\text{M}$ ), followed by the tracheobronchial region (0.001-1.76  $\mu\text{M}$ ). These concentrations were lower when based on *in vitro* data rather than only *in silico* data, for data obtained from the Calu-3 model epithelial fungicide concentrations did not exceed 10  $\mu\text{M}$  (**Figure 3.17**), likely due to binding to ASL or epithelial tissue (**Table 3.2 & Figure 3.17**). High chlorothalonil binding is a mechanism for increased epithelial concentrations and reduced absorption beyond the epithelial barrier. Maximum cell exposure concentrations, or the fungicide concentration dissolved in the lumen ranged from 2.5-8  $\mu\text{M}$  dependent on the fungicide and the permeability model used, however, due to tissue binding greater concentrations (of up to 27  $\mu\text{M}$ ) were predicted to accumulate in the epithelial tissue (**Table 3.3**).

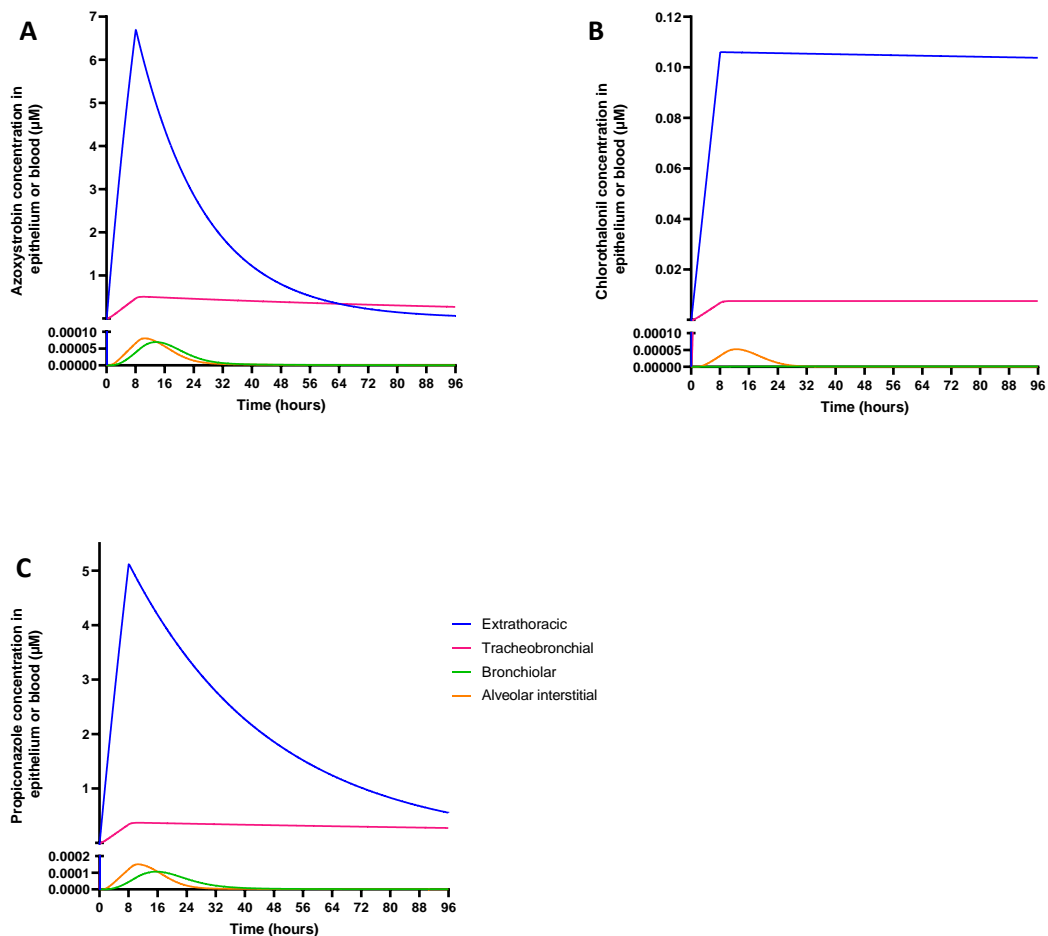


**Figure 3.17. Predicted fungicide toxicokinetics in the respiratory epithelium using *in vitro* Calu-3  $P_{app}$ , ASL and plasma protein binding data. Data is based on an 8 h occupational exposure, to either (A) azoxystrobin, (B) chlorothalonil or (C) propiconazole, during pesticide spraying (MMAD = 35  $\mu\text{m}$ ). Oral absorption has been excluded.**

For all modelled scenarios, fungicide respiratory bioavailability was less than 30%, with bioavailability limited due to 13.5  $\mu\text{m}$  and 35  $\mu\text{m}$  aerosol droplets depositing mainly in the extrathoracic region (**Table 3.3**). Despite this, total bioavailability was significantly higher (20-91%) and was largely determined by oral bioavailability (following mucociliary clearance), with the contribution of pesticide dose absorbed in the respiratory tract often being negligible.

When the effect of oral absorption was included, the differences observed in **Figure 3.15** were masked as respiratory permeability only had a minor contribution to overall absorption, as shown by both **Figure 3.18** and **Table 3.3**. Whilst  $C_{max}$  is on the picomolar scale for respiratory absorbed pesticides, with the inclusion of oral absorption the bioavailability of each pesticide is increased approximately 10-fold. This difference is primarily due to the majority of the

pesticide depositing in the extrathoracic region rather than alveolar region where respiratory absorption would be more rapid.

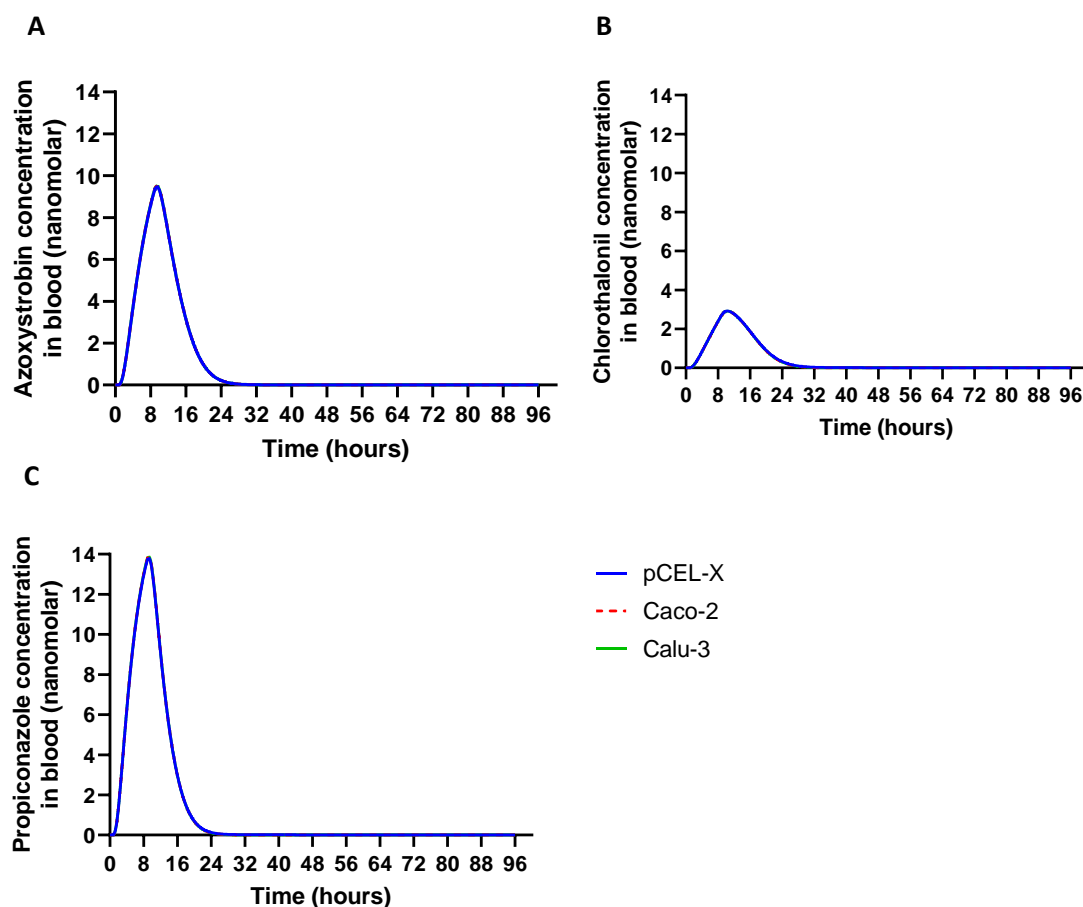


**Figure 3.18.** Oral bioavailability has been included for the comparison of blood toxicokinetic profiles predicted using *Mimetikos Preludium* with *in silico* (pCEL-X) or *in vitro* data (Caco-2 & Calu-3). Toxicokinetic profiles for (A) azoxystrobin, (B) chlorothalonil and (C) Propiconazole are shown, based on an 8h occupational exposure during spraying (MMAD = 35  $\mu$ m).

For the toxicokinetic profiles in **Figure 3.18**, the data overlies regardless of the respiratory permeability data used, as oral bioavailability is the major determinant in this case, with the absorbed fungicide concentration on the nanomolar rather than the picomolar scale as was the case for **Figure 3.15** and **Figure 3.16**, when oral bioavailability was excluded.

Respiratory bioavailability was consistently predicted to be higher when only *in silico* data was used (**Table 3.3**), in comparison to the lower values resulting from inputting *in vitro* data for ASL binding, plasma protein binding and  $P_{app}$  values. As tissue-plasma partition was predicted by the *Mimetikos Preludium* using LogP and plasma protein binding values, the input of *in vitro* plasma protein binding values was important for the prediction of bioavailability, whilst the

inclusion of *in vitro* ASL binding data increased the predicted % mucociliary clearance by up to 0.14%. Mucociliary clearance would be greater if the deposition profile was wider for the pesticides, for example if a lower MMAD was modelled (data shown in the appendix).

**Table 3.3. Summary of key toxicokinetic data predicted using Mimetikos Preludium, for the three fungicides and 3 different models. Data shown is based on for an 8 h exposure during spraying (MMAD = 35 µm), unless otherwise stated. AUct = Area under the Curve during the time modeled, C<sub>max</sub> = maximum blood concentration, MCC% = % of total delivered dose cleared by mucociliary clearance, F<sub>pulm</sub> % = % respiratory bioavailability (% absorbed of the total dose delivered to the lung), F<sub>tot</sub> % = % total bioavailability (% absorbed of the total dose delivered to the body), C<sub>max</sub>LUMEN = maximum concentration dissolved in airway lumen, C<sub>max</sub>EPITHELIAL = maximum concentration in epithelial tissue.**

		Azoxystrobin	Chlorothalonil	Propiconazole
pCEL-X	AUct (nM/h)	96.0	37.4	128.8
	C <sub>max</sub> (nM)	9.5	2.9	13.8
	T <sub>max</sub> (h)	9.45	10.35	9.22
	MCC %	0.62	0.58	0.61
	F <sub>pulm</sub> % (F <sub>pulm</sub> % if MMAD =13.5um)	<b>13.34</b> (21.3)	<b>19.53</b> (26.96)	<b>15.26</b> (23.07)
	F <sub>tot</sub> % (Oral + Respiratory) (F <sub>tot</sub> % if MMAD =13.5um)	<b>80.02</b> (80.17)	<b>20.11</b> (20.87)	<b>91.01</b> (91.08)
	C <sub>max</sub> LUMEN (µM)	4.60814	6.95964	5.42447
	C <sub>max</sub> EPITHELIAL (µM)	11.30	27.74	15.93
Caco-2	AUct (nM/h)	96.2	36.5	128.9
	C <sub>max</sub> (nM)	9.5	2.9	13.9
	T <sub>max</sub> (h)	9.45	10.35	9.217
	MCC %	0.66	0.72	0.67
	F <sub>pulm</sub> % (F <sub>pulm</sub> % if MMAD =13.5um)	<b>8.58</b> (16.95)	<b>0.05</b> (5.31)	<b>6.49</b> (14.98)
	F <sub>tot</sub> % (Oral + Respiratory) (F <sub>tot</sub> % if MMAD =13.5um)	<b>80.01</b> (80.14)	<b>20.00</b> (20.17)	<b>91.00</b> (91.05)
	C <sub>max</sub> LUMEN (µM)	4.62	7.04	5.45
	C <sub>max</sub> EPITHELIAL (µM)	7.21	0.05	6.18
Calu-3	AUct (nM/h)	96.2	36.5	128.9
	C <sub>max</sub> (nM)	9.5	2.9	13.9
	T <sub>max</sub> (h)	9.45	10.35	9.22
	MCC %	0.66	0.72	0.68
	F <sub>pulm</sub> % (F <sub>pulm</sub> % if MMAD =13.5um)	<b>8.02</b> (16.43)	<b>0.1</b> (5.86)	<b>5.47</b> (14)
	F <sub>tot</sub> % (Oral + Respiratory) (F <sub>tot</sub> % if MMAD =13.5um)	<b>80.01</b> (80.13)	<b>20</b> (20.19)	<b>91</b> (91.05)
	C <sub>max</sub> LUMEN (µM)	4.62	7.04	5.46
	C <sub>max</sub> EPITHELIAL (µM)	6.68	0.11	5.12

### 3.4.7 Predicted *in situ* metabolism and toxicokinetic implications

Following a review of the literature and the results obtained in **Chapter 2**, potential metabolism pathways were predicted for azoxystrobin, chlorothalonil and propiconazole. Whilst there is no reported human metabolism data, it was assumed that due to the homology between human and rodent enzymes the fungicides are substrates of the human isoform if they are substrates for the rodent isoform, particularly due to the high substrate promiscuity of the CYP3A and GST.

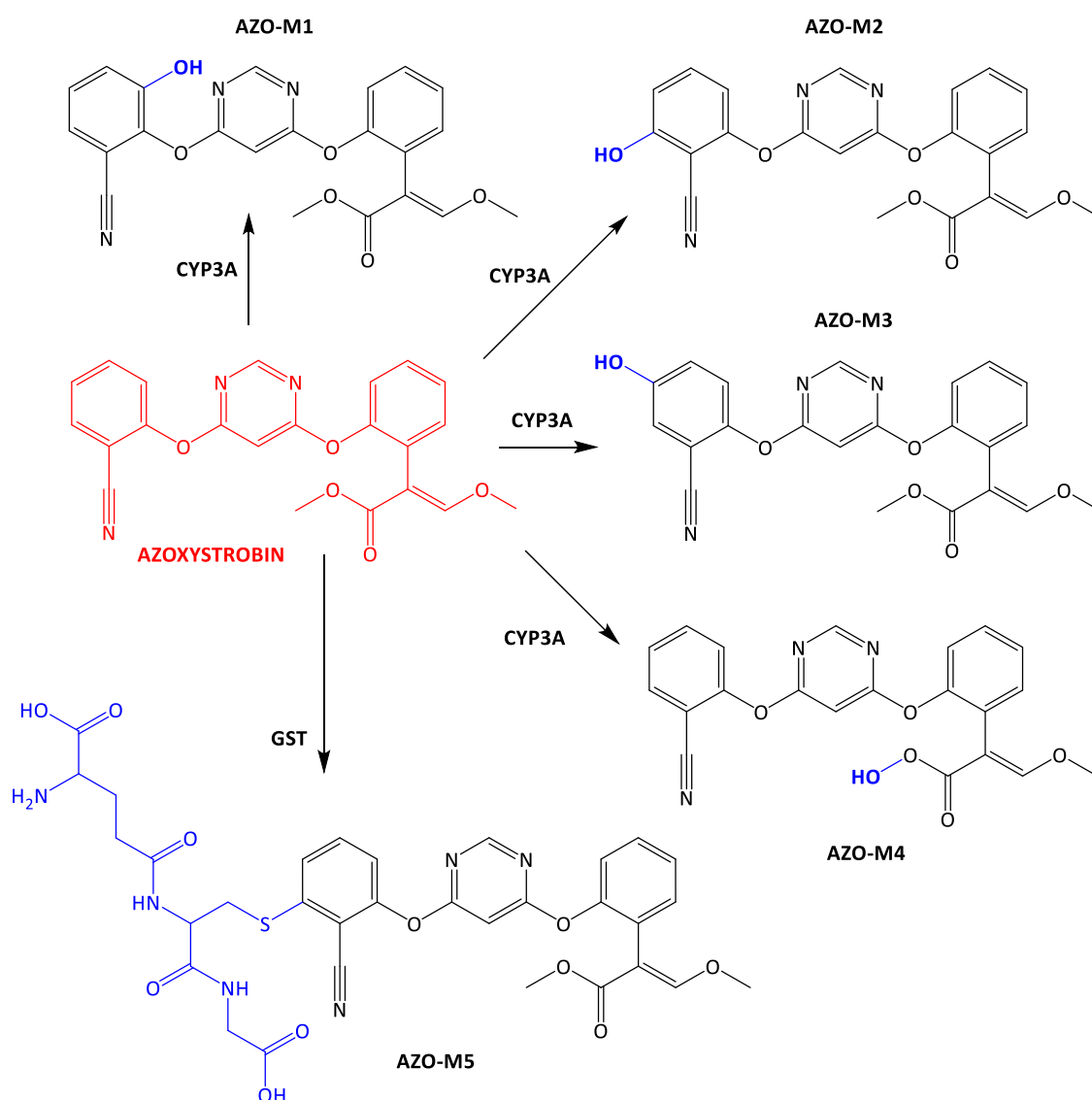


**Figure 3.19.** Metabolic pathway for azoxystrobin metabolites potentially formed within the lung, via GST-mediated glutathione conjugation and CYP3A-mediated hydroxylation. CYP3A and GST activity were found in Calu-3 and human lung homogenate, with these enzymes responsible for the displayed reactions. Figure adapted from Laird et al. (2003).

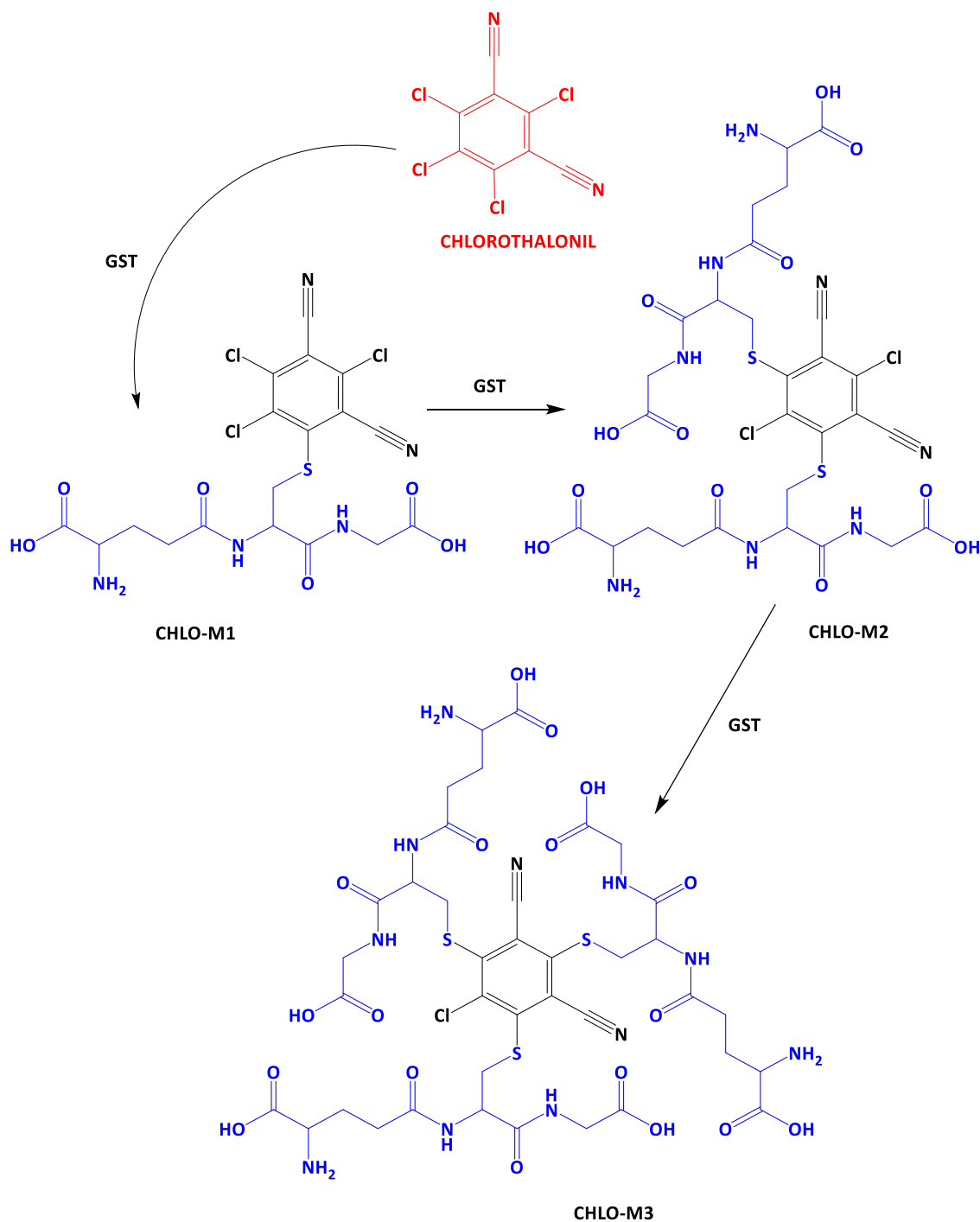


**Figure 3.20.** Metabolic pathway for potential chlorothalonil metabolites formed within the lung, via GST-mediated glutathione conjugation. GST activity was found in all tested respiratory epithelial cell lines and human lung homogenate and this enzyme is responsible for the GSH conjugation of chlorothalonil. Figure adapted from Kim et al. (2004)

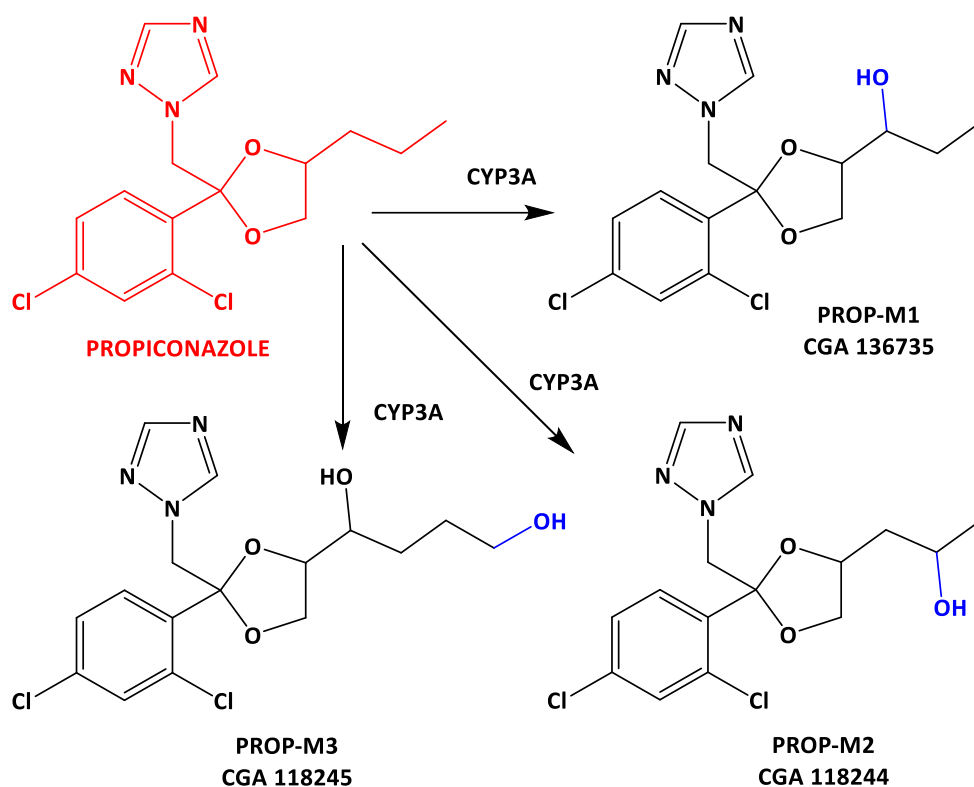


**Figure 3.21.** Metabolic pathway for potential propiconazole metabolites formed within the lung, via CYP3A-mediated hydroxylation. CYP3A activity was found in Calu-3 and human lung homogenate and this enzyme is responsible for the hydroxylation of propiconazole. Figure adapted from Mazur et al. (2015).

At least 15 azoxystrobin metabolites have been identified in rat, with the major metabolic pathways being ester hydrolysis, in addition to glucuronic acid or glutathione conjugation. Of these, CYP3A-mediated hydroxylation and GST-mediated glutathione conjugation were deemed most likely to occur within the human lungs (**Figure 3.19**). Ester hydrolysis is likely, as this is a major mode of metabolism within the lung for inhaled pharmaceuticals such as beclomethasone dipropionate, but was not included due to lack of *in vitro* data for esterases in **Chapter 2**.

For chlorothalonil, although hydroxylation has been identified in several species, the enzyme for this has not been identified, and so this metabolite was not included. The main route of metabolism is glutathione (GSH) conjugation (**Figure 3.20**), with mono-, di- and tri-GSH conjugates being described in the literature (Kim et al., 2004). It is well established in rodents and several other species that the chlorothalonil is conjugated with glutathione by GSTs, additionally as the fungicidal mechanism of action for chlorothalonil is glutathione depletion this reaction may occur spontaneously without GST activity. Based on the potential for GST

mediated and spontaneous glutathione conjugation, the formation of the metabolites shown is highly likely.

With regards to propiconazole, the main metabolite formed within rat is the alpha-hydroxy metabolite “PROP-M1” shown in **Figure 3.21**, which is similar to the other hydroxy metabolites shown to be formed by CYP3A-mediated metabolism, such as the beta-hydroxy and gamma-hydroxy metabolites, “PROP-M2” and “PROP-M3”, respectively (Mazur et al., 2015). Over 20 metabolites, have been identified in rat, and whilst there is limited data to suggest that sulphate and glucuronic acid conjugation may also occur, these were not included due to lack of activity data in **Chapter 2**.

The Caco-2  $P_{app}$  values for parent compounds and metabolites highlighted in the previous figures, were predicted using pCEL-X and are displayed in **Figure 3.22**. Whilst generally, the hydroxylation of the parent compounds caused only a modest decrease in predicted permeability, glutathione conjugation with either azoxystrobin (AZO-M5) or chlorothalonil (CHLO-M1, M2 & M3) significantly reduced the predicted permeability on the logarithmic scale.

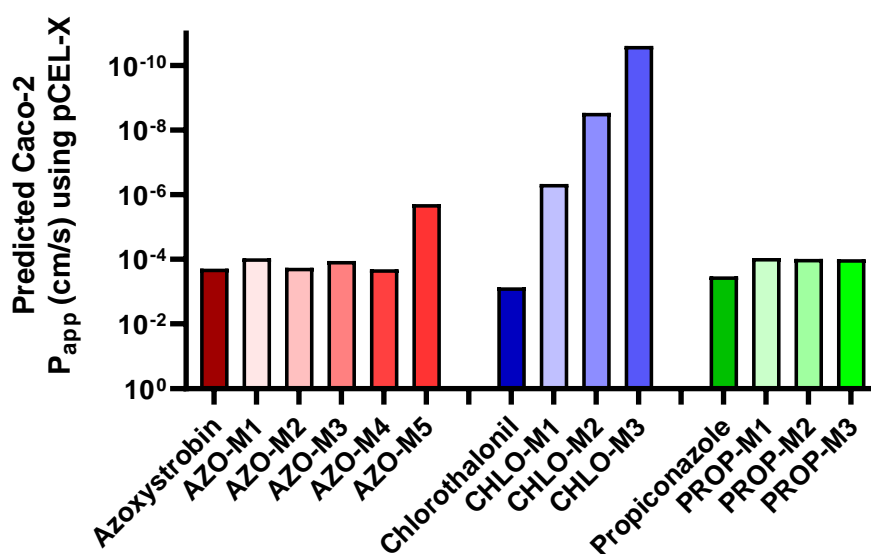


**Figure 3.22.** Caco-2  $P_{app}$  values predicted in silico using pCEL-X, for the parent compounds azoxystrobin, chlorothalonil and propiconazole and their respective metabolites.

The potential effect of metabolism is represented using an adaptation of the Biopharmaceutics Classification System (**Figure 3.23**), for oral immediate release solid oral dosage forms (Reddy and Karunakar, 2011), which is commonly used to differentiate drugs based on solubility and intestinal permeability, due to the implications of these factors on oral bioavailability. Whilst this is common for oral bioavailability (and therefore may relate to Caco-2 permeability), the



concept of an inhaled biopharmaceutical classification system (iBCS), has also been proposed and explored (Terakosolphan et al., 2017, Hastedt et al., 2016), for example inhaled drugs such as indomethacin and salbutamol have been used as an example of class III and class II drugs (Cingolani et al., 2019), respectively. Tronde et al. (2003) also highlighted a correlation between absorption rate of small molecules using the isolated perfused lung model and Caco-2  $P_{app}$  ( $r = 0.87$ ) and LogP ( $r = 0.70$ ).

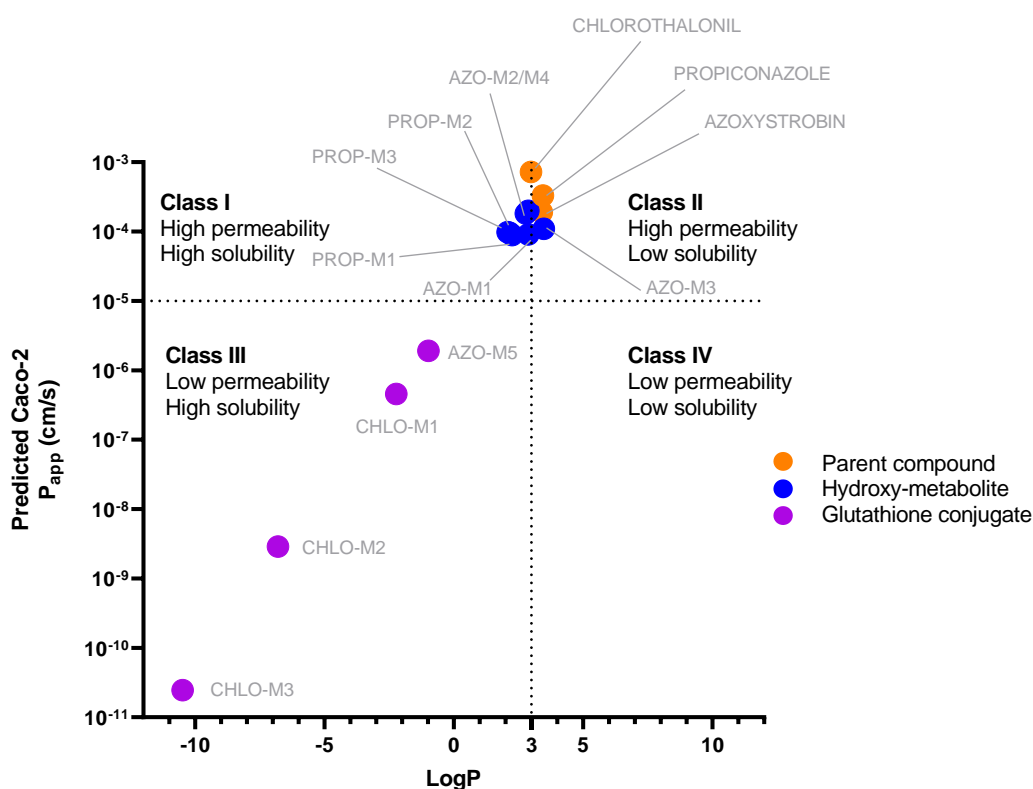


**Figure 3.23.** Predicted Caco-2  $P_{app}$  and LogP values using pCEL-X, illustrating the potential changes to pesticide respiratory bioavailability based on physicochemical properties following metabolism of azoxystrobin, chlorothalonil and propiconazole.

All the predicted metabolites had either equal or reduced permeability when calculated using pCEL-X, with the greatest reduction being caused by glutathione conjugation (**Figure 3.23**). For both propiconazole and chlorothalonil, the predicted metabolites represent detoxification pathways, with hydroxylated propiconazole and chlorothalonil-glutathione conjugates both being described in the literature as less toxic than the respective parent compounds (Chen et al., 2008, Rosner et al., 1996, Yamano and Morita, 1995). In the case of azoxystrobin, the effect of metabolism on toxicity has not been explored in great detail, but limited evidence in the invertebrate *Gammarus pulex* (which produces similar metabolites), suggests that they are also less cytotoxic and represent part of a detoxification mechanism (Rösch et al., 2017).

### 3.5 Discussion

The selected fungicides represent some of the most commonly sold (and sprayed) pesticides globally, with azoxystrobin, chlorothalonil and propiconazole representing the major fungicide classes; strobilurins, chloronitriles and demethylation inhibitors (DMIs), respectively.

Chlorothalonil was the third most used fungicide globally (~120,000 tonnes per year) in part due to its fungicidal mode of action limiting the development of resistance (Maggi et al., 2019).

Chloronitriles (chlorothalonil), demethylation inhibitors (propiconazole) and strobilurins (azoxystrobin) are fungicidal classes that represent 12, 7 and 6% of the total mass of fungicides used in the USA in 2019, their % use in the UK is greater, with DMI fungicides alone accounting for 29% (Zubrod et al., 2019). The global fungicide market was valued at ~13.4 billion USD in 2019, and the economic data indicates the widespread global use of sprayed fungicides to maintain high crop yields (Steinberg and Gurr, 2020).

Whilst there is significant variety in the active ingredients sprayed globally as plant protection products, the aerosol properties during the exposure scenarios are less variable and are likely to be well represented by the median mass aerodynamic diameters 13.5 and 35  $\mu\text{m}$  used in this study. The prediction of regional deposition within the respiratory tract gave similar results to the model used by Syngenta for risk assessment (**Figure 3.4**), with the former being slightly more conservative and predicting greater total deposition.

Preliminary *in vitro* assays revealed the importance of selecting the correct dose for the  $P_{\text{app}}$  studies, chlorothalonil increased Calu-3 epithelial permeability at concentrations greater than 10  $\mu\text{M}$ , this is likely due to toxicity which was observed in **Chapter 2** using sub-confluent Calu-3 in 96-well plates and the MTT assay.

There is evidence both *in vitro* and *in vivo* that pesticides such as imidacloprid, glyphosate, diquat and fipronil disrupting tight junctions and increasing paracellular permeability (Zhao et al., 2021a). A similar effect has been shown with non-cytotoxic concentrations for the pyrethroid insecticides; permethrin, cypermethrin and deltamethrin, fenvalerate and esfenvalerate, using the paracellular permeability marker Lucifer Yellow (Tateno et al., 1993). Based on this, preliminary *in vitro* assays were performed to reveal whether this was likely with azoxystrobin, chlorothalonil or propiconazole. The time dependent TEER measurement with 10  $\mu\text{M}$  of each pesticide, suggest that tight junction disruption was unlikely to occur at or below this concentration and changes to epithelial permeability were not observed with FD-4

at this concentration (**Figure 3.5 & Figure 3.6**). Non-transient increases in permeability observed following 6 h chlorothalonil exposure ( $\geq 20 \mu\text{M}$ ) was comparable to the results shown with the SDS positive control and likely reflect cell toxicity. However, as lumen concentrations of  $\sim 8 \mu\text{M}$  were predicted following occupational exposure, this does suggest a low margin of safety for both toxicity and increased epithelial permeability following either acute or sub-chronic exposure. Based on *in vitro* data shown in Chapter 2 and here in Chapter 3, this is consistent with the GHS classification of chlorothalonil as a respiratory irritant (H335) and potentially fatal if inhaled (H330). In contrast, propiconazole which has no respiratory toxicity concern and azoxystrobin which is classified as toxic if inhaled (H332) did not cause any increase in FD-4 permeability, even at the highest concentrations tested.

With regards to the data obtained as inputs for the *in silico* model, the analytical method was suitably sensitive for the detection of all three fungicides within the required range for both  $P_{\text{app}}$  measurements and protein binding assays. Although the plasma protein binding assay by rapid equilibrium dialysis (RED) is well established and commonly used within the pharmaceutical industry, the adaptation of the RED method to ASL binding is novel. Based on the data shown for its use in toxicokinetic prediction and the high variability observed between compounds, it may be of use for further investigations into xenobiotic binding to ASL. Furthermore, whilst further ASL binding assays were beyond the scope of this immediate study, it would be useful to test a wider range of concentrations to elucidate the concentration at which ASL binding is saturated for a particular compound, particularly as xenobiotics may saturate ASL binding as concentrations realistically exceed the  $5 \mu\text{M}$  concentration tested, at which point greater permeation from the ASL to the underlying epithelium may occur. Generally, the *in silico* only predicted values were similar to the *in vitro* predicted values with the exception of chlorothalonil, hypothesised due to its chemical reactivity and high protein binding to ASL and plasma proteins. Similarly, chlorothalonil permeated across the *in vitro* lipid-based barriers (PAMPA and lung lipid extract) significantly more rapidly than either cell model (**Figure 3.10**), limiting their use for *in silico* modelling. However, this highlights their potential for complementary use with cell models for application when there is an interest in the elimination of biological interactions such as protein binding or adverse effects of formulations.

For the cell-based xenobiotic transport models, predicted respiratory bioavailability followed the same trend as that reported for oral bioavailability in rats, with azoxystrobin being the

most well absorbed, followed by propiconazole, and chlorothalonil being poorly absorbed. Whilst the trend was similar, predicted respiratory bioavailability for all the compounds was only a fraction of those reported for rodent oral bioavailability (80% vs 16.95% for azoxystrobin, 30 vs 5.31 % for chlorothalonil, 91% vs 14.98 for propiconazole), mainly due to the relatively large aerosol droplets failing to deposit in the lower respiratory tract. Therefore, from a risk assessment perspective, unless MMAD is low (i.e. within the respirable range) it may be assumed that respiratory bioavailability is lower than oral bioavailability of the ingested pesticide.

Whilst, the predicted toxicokinetic data highlights that respiratory bioavailability on its own is unlikely to ever be 100%, a more evidence-based approach could be taken by including the effect of oral bioavailability for the pesticide that is ingested following mucociliary clearance. Based on this, where both oral and respiratory bioavailability are low, overall bioavailability is likely to be low. This can be expressed as;

$$\text{Overall bioavailability} = \frac{\text{Dose absorbed by respiratory tract} + \text{dose absorbed by GIT (after MCC)}}{\text{Total deposited dose}}$$

Regardless of the bioavailability, the *in vitro* and *in silico* data do reveal other potential concerns that relate to respiratory toxicokinetics. For example, the prediction of micromolar exposure to inhaled pesticides in lumen and epithelium of the upper airways is of relevance to potential local toxicity. As shown in **Chapter 2**, chlorothalonil is both cytotoxic ( $LC_{50} = 0.6\text{-}9.7 \mu\text{M}$ ) which is within the range of concentration predicted for the ASL ( $7.04 \mu\text{M}$ ), additionally, due to high tissue binding, the epithelial concentration may exceed the ASL concentration (**Table 3.3**). Similarly, azoxystrobin exposure was predicted to be  $4.61\text{-}11.30 \mu\text{M}$  in the airways and even at  $2.5 \mu\text{M}$  this fungicide was found to cause mitochondrial toxicity *in vitro* using the cell line 16HBE14o- (**Figure 2.10**). Propiconazole, which was not *in vitro* cytotoxic at the predicted airway exposure concentrations of  $5.52\text{-}15.93 \mu\text{M}$  (**Figure 2.7**), induced CYP1A1 activity at concentrations between  $2.5\text{-}10 \mu\text{M}$ , with the fungicide potentially acting as a ligand of the aryl hydrocarbon receptor (**Figure 2.20**). This effect has been found *in vivo*, along with other non-cytotoxic phenotypic changes such as cell proliferation, oxidative stress and epithelial-mesenchymal transition (Kwon et al., 2021, Valadas et al., 2019). Additionally, the high protein binding and chemical reactivity of chlorothalonil is also of concern, and whilst well reported in the literature were not predicted with the pCEL-X *in silico* model. These properties not only influence the toxicokinetics of the inhaled pesticide but are

also highly relevant to the compound's local toxicity and likely the ability of chlorothalonil to act as a respiratory irritant and cause localised necrosis in epithelial tissues when inhaled. This is of relevance to other fungicides with a similar mode of action, such as the trichloromethyl sulfenyl fungicides captan and folpet, which also react with glutathione (Tillman et al., 1973, Siegel, 1970) and therefore may be reactive with glutathione in airway surface liquid or with the thiol groups of several endogenous proteins. The extent to which chlorothalonil toxicokinetics were altered based on ASL binding highlights the protective mechanism of ASL *in vivo*, which was likely underestimated due to the exclusion of the antioxidant glutathione within the ASL formulation (for practical reasons as it was below the 8 kDa MWCO of the dialysis membrane).

Conversely, the depletion of GSH and the saturation of protective ASL in the respiratory tract, likely serves to increase the susceptibility of the epithelial cells to pesticide cytotoxicity if there is sub-chronic or chronic occupational exposure. Therefore, it is important that risk assessment is supplemented with classification as to the non-systemic hazard(s), and all precautions are taken to limit local adverse effects from inhalation exposure, i.e. respiratory protective equipment (RPE).

Despite GSH not being included in the ASL simulant, *in vivo* it is likely that chlorothalonil may spontaneously react with GSH within the ASL, which has been reported to be as concentrated as 170  $\mu\text{M}$  within the respiratory tract (Kumar et al., 2017), as well as spontaneous reaction with intracellular GSH within the epithelium expected to be between 0.5-10 mM (Balendiran et al., 2004).

Whilst the interaction between chlorothalonil and GST with regards to toxicity was described in **Chapter 2**, as shown in **Figure 2.21**, the formation of chlorothalonil-GSH conjugates significantly reduces the permeability of the compound, and along with the potential binding of chlorothalonil to ASL and epithelial cell proteins, the respiratory bioavailability of this fungicide is likely to be significantly reduced. Oral bioavailability of chlorothalonil is also significantly limited by these factors, estimated to be only 20% with 5 mg/kg dose in rats and is shown to undergo extensive metabolism, however intravenous administration of chlorothalonil exhibits wide distribution due to a high binding affinity to red blood cells (EFSA et al., 2018).

As it is a common requirement for pesticide registration that pesticide metabolites are identified in rat, there is scope for further exploration of the effects of metabolism on pesticide bioavailability and toxicokinetics both through the oral and inhaled route of

exposure. This may help to further inform risk assessments by including considerations on bioactivation or detoxification mechanisms, and whilst metabolism is considered with regards to genotoxicity studies, it could be further explored with regards to general toxicity. Additionally, the use of a classification system, similar to the BCS system in **Figure 3.22**, may be useful not just for classifying existing pesticides which may have a high oral/inhaled bioavailability but also for identifying and predicting the bioavailability of future pesticides with similar physicochemical properties, for example a new fungicide which shares a chemical class with existing ones. For agrochemicals rather than drugs, the relationship between oral bioavailability and computationally predicted physicochemical properties (such as MW, LogP, LogS<sub>w</sub>, PK<sub>a</sub> and hydrogen-bond donors/acceptors) has been investigated previously (Tice, 2001, Clarke and Delaney, 2003), and a similar approach may in part be applied to respiratory bioavailability.

With regards to the outputs of the toxicokinetic model, other than respiratory bioavailability, the prediction of fungicide concentrations within the lumen and epithelium of different regions of the respiratory tract is of great value. Particularly, as this data may be used to contextualise *in vitro* data or optimise exposure concentrations for future experiments. For example the prediction of extrathoracic lumen concentrations of around 4-7 µM following chlorothalonil exposure (aerosol MMAD = 35 µm), is of interest when related to the chlorothalonil LC<sub>50</sub> value of 2.27 µM for the nasal cell line RPMI-2650 from **Chapter 2**. Additionally, the prediction of low concentrations of chlorothalonil in the lumen and higher epithelial concentrations within the bronchiolar region due to high tissue binding are also of interest due to toxicological implications.

Similarly, at low micromolar concentrations which are shown to be achievable following occupational exposure, phenotypic changes are possible even with pesticides that are non-cytotoxic. For example in **Chapter 2** propiconazole was shown to induce CYP1A1 and other researchers have also reported the potential to induce ROS, dysregulate cholesterol synthesis and increase cell proliferation at similar concentrations (Nesnow et al., 2011).

Despite the value of this approach, there remain limitations and further validation by either *in vivo* permeability experiments such as isolated perfused lung (IPL) or nasal absorption experiments would be useful. Additionally, whilst the three fungicides are not known to be transported by drug transporters which exist in the lungs (Ehrhardt et al., 2017), the potential contribution of active transport mechanisms or confirmation of pesticide metabolism *in vivo* or

*in vitro* has not been explored. However, through the use of drug transport inhibitors, radiolabelled chemicals to eliminate the underprediction of permeability due to metabolism of the parent compound and the measurement of “intrinsic permeability” (by using a stirring speed of 480 rpm to eliminate the effect of the aqueous boundary layer), this current approach seeks to model the “worst-case” scenario and also reduces the potential effect of genetic variability for metabolism/active transport mechanisms.

### 3.6 Conclusion

The outlined approach proved to be useful for estimating pesticide respiratory toxicokinetic and bioavailability, using real world exposure scenarios. For the prediction of deposition, the model was comparable with others such as the Syngenta model (Corley et al., 2021), suggesting a good degree of certainty that this is close to the real result experienced *in situ*. For the toxicokinetic aspect of the prediction, whilst the *in silico* only method was a useful starting point, the Mimetikos Preludium predictive model benefited from *in vitro* data, particularly where chemical reactivity and subsequent binding coefficients could not be accurately projected using pCEL-X. The Mimetikos Preludium model, has several strengths relating to the ability to predict regional % deposition and inhaled pharmacokinetics, including not just bioavailability but also the influence of mucociliary clearance or local pesticide concentrations within the ASL or epithelium. Limitations relate to those that currently exist for other inhalation pharmacokinetic models, such as GastroPlus, which do not allow for the prediction of *in situ* metabolism, and on their own are not capable of predicting epithelial  $P_{app}$  values (although the latter issue may be overcome with other separate models such as pCEL-X). The main limitation is the need for increased validation of this novel approach, particularly for the toxicokinetic aspect of the predictions. Although there is scope for further validation and refinements of both the *in silico* predictive model and the *in vitro* data inputs, as well as a review into a wider range of pesticides, this approach presents significant advantages over a non-evidence based assumption of 100% bioavailability. This is particularly relevant where oral bioavailability is low but ASL binding and mucociliary clearance is substantial. Furthermore, the estimation of pesticide concentration within the lumen and epithelial tissue of the respiratory tract provides useful context and guidance for the exposure concentrations used in *in vitro* toxicity assays.

In summary, this chapter highlights that a combined *in vitro-in silico* approach has the potential to improve predictions of respiratory toxicity and bioavailability and optimise future occupational risk assessments for respiratory exposure to xenobiotics.

# Chapter 4

## A metabolomic investigation into respiratory epithelial cell responses to pesticide exposures.

### 4.1 Introduction

The inherent biological activity of pesticides means that these compounds often exert unintended effects on non-target organisms, which may, or may not, be through the same mechanism of action as the target species. Whilst pesticides are developed specifically with the goal of having a biocidal effect on the target species, many have been shown to have adverse biological effects in humans, both in the context of occupational and dietary exposure. Of the 526 registered pesticides in the EFSA pesticide database with known GHS classification (accessed May 2020), 378 had no respiratory toxicity concern, whilst 158 were classified as either harmful, toxic, or fatal if inhaled. Of the 158 pesticides that were classified as causing respiratory toxicity, 40 were also classified as respiratory irritants. These classifications are predominantly based on rodent *in vivo* inhalation data and are supported in the literature by sparse human data from reported case studies of occupational exposures (Hoppin et al., 2009, Mamane et al., 2015, Ye et al., 2013).

The use of *in vitro* data to assess pesticide toxicity is gaining in significance, and a range of models have been described in the literature. Many of these models employ endpoints, such as the MTT and Alamar Blue assays to infer information on metabolic competence and cytotoxicity respectively, or more prescribed endpoints on established adverse outcome pathways, such as those described by Tox21, such as: agonism of the oestrogen receptor, androgen receptor, aryl hydrocarbon receptor, peroxisome proliferator-activated receptor gamma, Nrf2/antioxidant responsive element, heat shock factor response element, or changes to mitochondrial membrane potential, and p53 (Tice et al., 2013, Huang et al., 2016, Fischer et al., 2017). Whilst these assays are suitable for high throughput analysis and may aid the development of predictive toxicity models, based on structure-activity relationships (and machine learning), multiple different assays are required to assess how these compounds may interfere with biochemical pathways and impact human health. The Tox21 methodology and described bioassays will undoubtedly aid the improvement of human hazard classifications and potentially reduce the reliance on rodent *in vivo* data in future, however these methods do not



fully encapsulate the range of potential biological changes that may occur following pesticide exposure.

A common research question within the field of toxicology/safety pharmacology, is the no-observed-adverse-effect level (NOAEL) or no-observed-effect level (NOEL), after an organism is exposed to a xenobiotic. This is a key aspect of preclinical safety assessments for drug development, but also of importance to pesticide risk assessments. Many assays and experiments seek to determine the NOAEL/NOEL, and of those performed using *in vitro* techniques often only examine a few endpoints, e.g. change in cell morphology, cell viability, growth rate. Single endpoint assays, whilst useful may still fail to identify changes to cell phenotype which may influence the organism on a molecular, cellular or tissue level. In comparison, omic-based techniques such as transcriptomics, proteomics and metabolomics which are data rich, enable the characterisation of a wide range of biological molecules and therefore present a more comprehensive picture of the response phenotype at a cellular level. Following the central dogma of biology from DNA, to RNA and proteins, each step which essentially determines cell phenotype is represented by genomics, transcriptomics and proteomics respectively. Metabolomics provides a method for the final biochemical determination of cell phenotype and may be useful as a method for determining biological changes induced by pesticide exposure both *in vitro* and *in vivo*.

The potential applications of metabolomics with regards to human pesticide exposure have been widely reviewed (Aliferis and Chrysai-Tokousbalides, 2011, Keum et al., 2010), however the number of experimental studies performed using metabolomics to assess the impact of pesticide exposure on humans has been limited (**Figure 4.1**).

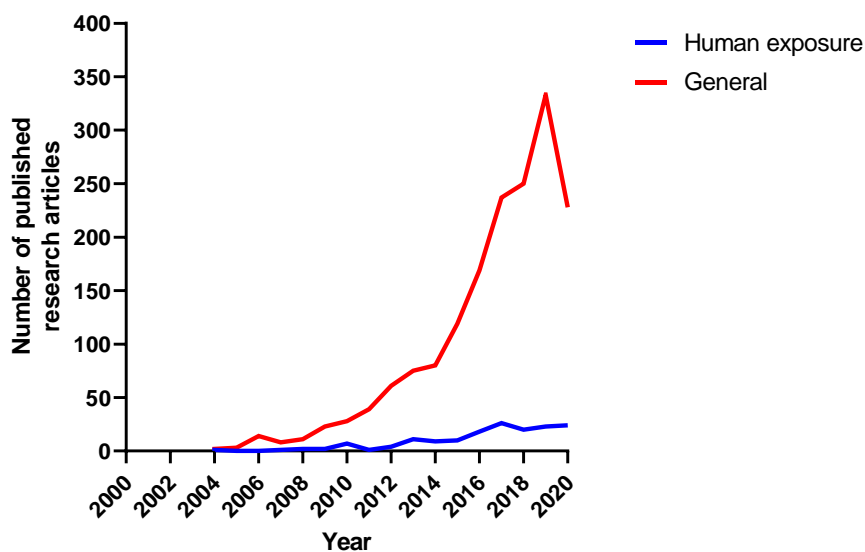


**Figure 4.1.** Diagram indicating the number of original research articles related to metabolomics and pesticide exposure, published between 2000-2020. Data obtained from Web of Science™, using the terms "metabolomics" and "pesticide" and "exposure" with or without "human".

Most of the pesticide related metabolomic studies to date have focused on model organisms for ecological toxicology/environmental risk assessment. Of the few human studies reported, impaired amino acid metabolism and mitochondrial function, as well as increased fatty acid  $\beta$ -oxidation and oxidative stress have been shown through the metabolomic analysis of urine and plasma samples (Yan et al., 2021, Ding and Bao, 2014, Bonvallot et al., 2013), however this typically relies on the "likelihood" of exposure to a complex mixture of pesticides based on participants living near agricultural land, rather than known/specific pesticide exposures. Despite the comparative ease of collecting samples from workers that have been occupationally exposed to known pesticides, there is little in the literature to suggest this has been explored fully. Similarly, although metabolomics has been used extensively for invertebrates, either to study insecticidal effects on target/non-target species following environmental exposure and with rodent tissue samples, the use *in vitro* samples from human cell lines have not been extensively explored for metabolomic analysis following pesticide exposure (Zuluaga et al., 2016, Keum et al., 2010, Gu et al., 2018, Bonvallot et al., 2018).

With regards to metabolomics, there are two predominant methods LC-MS metabolomics and NMR metabolomics, for which the respective advantages and disadvantages of each technique are summarised in **Table 4.1** (Wishart, 2016).

**Table 4.1. A comparison of NMR and LC-MS metabolomic methods, adapted from Wishart (2016).**

<b>NMR</b>	<b>LC-MS</b>
Quantitative, linear response without standard.	Quantitative with isotopic standards.
Non-destructive, sample may be reused.	Destructive.
Low sensitivity, $\mu\text{M}$ to $\text{mM}$	High sensitivity, $\text{pM}$ to $\mu\text{M}$
Lower number of detectable metabolites (50-200).	High number of detectable metabolites (100-1000)
Rapid spectral acquisition (per sample).	Slow spectral acquisition (per sample).
Higher sample volume required (typically $\sim 600 \mu\text{L}$ ).	Low sample volumes (10-100 $\mu\text{L}$ ).
Most spectral features are identifiable, 2D $^1\text{H}$ NMR spectra and structural information may help in cases of spectral peak overlap.	Many spectral features not yet identifiable. Little to no structural information obtained.
Very reproduceable spectra following pH adjustment, reduced matrix effects.	Typically, more variation between samples, introduced due matrix effects or by sample preparation.
Simple sample preparation/extraction.	Sample preparation requires extraction, desalting, filtration and the addition of isotopic standards.

Whilst the techniques are complementary, either may be useful for the identification of response biomarkers to identify changes in cell phenotype, as evidenced through their increased use in the emerging field of exposomics (Vineis et al., 2020, Misra, 2019). LC-MS metabolomics is primarily beneficial due to its increase sensitivity, whereas the reduced sample preparation and increased reproducibility of NMR metabolomics make it particularly well suited where rapid screening is needed to accommodate multiple timepoints/doses with *in vitro* samples. The advantages of NMR metabolomics lend it to biomarker discovery due to the scalability of the technique, with regards to sample number, particularly for the analysis of *in vitro* samples, where the range of metabolites that can be detected by NMR provide sufficient information on biochemical changes related to changes in metabolic state (i.e. amino acid and sugar synthesis/uracilisation, formation of Krebs cycle intermediates etc.).

The core features of cell metabolism may be explored using this technique, either through the assessment of intracellular or extracellular samples, which have been used to study normal vs., tumour cell metabolism, drug-induced toxicity and to determine the influence of xenobiotics at non-toxic concentrations (Čuperlović-Culf et al., 2010b, Kostidis et al., 2017).

NMR metabolomics has been used with the alveolar cell line A549 to explore potential changes indicative of lung toxicity following exposure to fine particulate matter ( $\text{PM}_{2.5}$ ) or

graphene/zinc oxide nanoparticles (Huang et al., 2015, Huang et al., 2018, Wu et al., 2019). Similar methods have been used with Calu-3 to characterise changes to glucose metabolism associated with acute lung injury following mechanical ventilation (Eckle et al., 2013) or *S. aureus*  $\alpha$ -toxin induced cell membrane damage to 16HBE14o- (Gierok et al., 2014).

Based on the above studies, and the data obtained in the previous two experimental chapters, NMR metabolomics was explored to provide further insight into how pesticides may affect lung epithelial cell phenotype.

## 4.2 Aims and Objectives

The overall aim of this series of experiments was to investigate changes to lung cell phenotype following pesticide exposure at subtoxic concentrations using NMR based metabolomics.

Specific objectives included:

3. Measurement of metabolic changes in alveolar and bronchial cells in response to different fungicides.
4. Comparison of the sensitivity and responses of normal “immortalised” or cancer derived alveolar/bronchial epithelial cells to fungicides.
5. Elucidation of potential modes of action for pesticide respiratory toxicity based on changes to the extracellular metabolome.

## 4.3 Methods

### 4.3.1 Experimental design

Respiratory epithelial cell lines were selected based on the experiments previously outlined in **Chapter 2** and **Chapter 3**. Briefly, the experiments were designed to allow the comparison of both alveolar and bronchial cell lines, either immortalised or cancer derived. A549, TT1, BEAS-2B, 16HBE14o- and Calu-3 cells were used for this comparison, as shown in **Figure 4.2**.

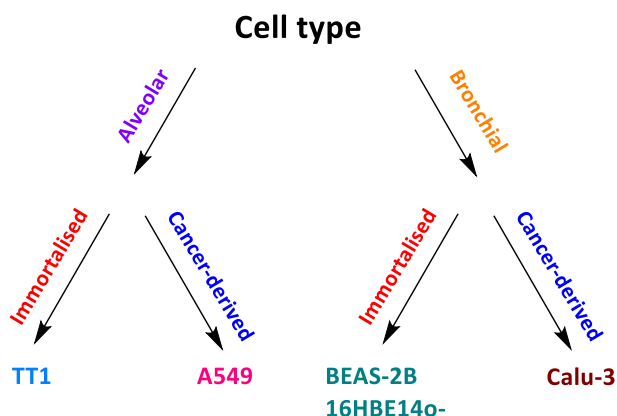


Figure 4.2. Categories for the different respiratory epithelial cell lines selected for inclusion in NMR metabolomics studies.

Of the pesticides previously studied, 5 fungicides were selected, each with a different mode of action and toxicity classification, based on the Globally Harmonised System of Classification and Labelling of Chemicals (GHS) and information obtained from the EU pesticides database and PubChem (accessed May 2020), as summarised in **Figure 4.3**. Acibenzolar-S-Methyl, azoxystrobin, chlorothalonil, isopyrazam and propiconazole were selected with the hypothesis that the outlined differences between these fungicides may cause different but identifiable metabolomic changes with the cell lines used.

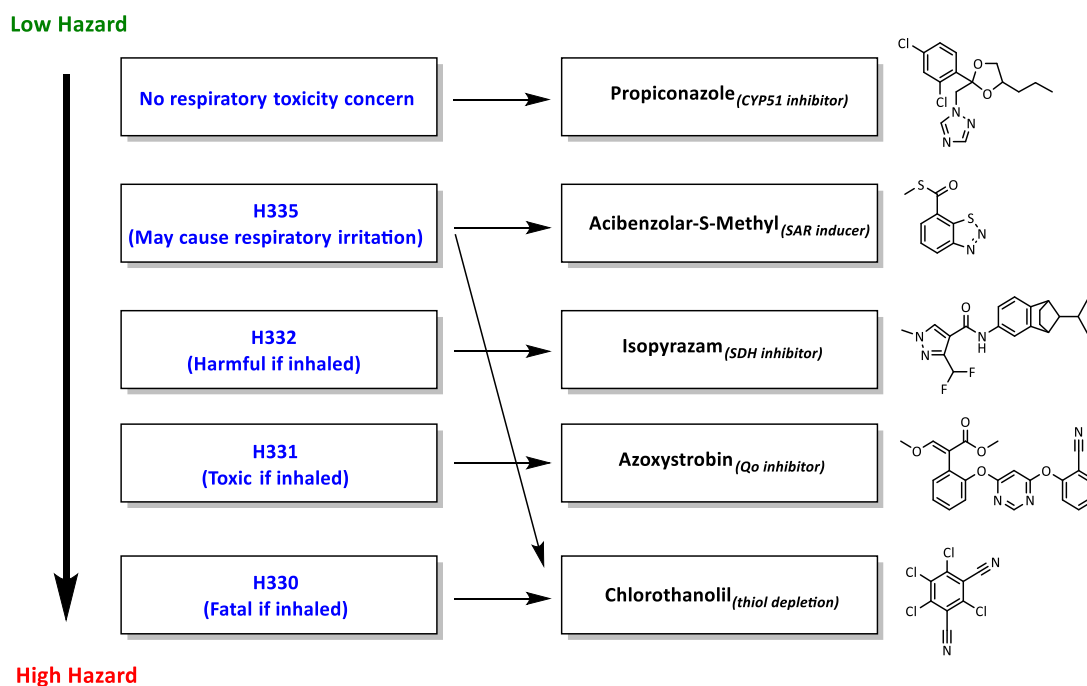


Figure 4.3. Selected fungicides (including mode of action) arranged based on GHS classification.

#### 4.3.2 Cell culture conditions

To allow for the direct comparison of metabolomic results between the different cell lines A549, TT1, BEAS-2B, 16HBE14o- and Calu-3, attempts were made to use the same medium for all the cell lines, both for subculturing and for the experimental samples collected. DMEM:F12 Hams (Sigma, D8062) was selected as a basal medium, due to previous researchers using this medium with several of the above cell lines (A549, BEAS-2B, 16HBE14o- and Calu-3). A formulation without HEPES was selected as HEPES is known to overlap the NMR spectra of key metabolites commonly assessed using NMR metabolomics, the pH was instead buffered with sodium bicarbonate.

Preliminary experiments showed that BEAS-2B underwent morphologic changes when grown in medium supplemented with FBS (1-10% FBS), whilst Calu-3 failed to adhere to the flask in the absence of FBS and could not be adapted to FBS-free conditions even when using specialised "Advanced DMEM/F12", which allows reduced FBS supplementation. Due to the incompatibility of FBS/FBS-free conditions for particular cell lines, the following conditions were used.

- (1) DMEM:F12 Ham medium was supplemented with non-essential amino acids, penicillin-streptomycin and sodium pyruvate, as previously described, and 10% FBS was used for all cell lines other than BEAS-2B.
- (2) BEAS-2B had the additional supplements of hydrocortisone (500 ng/mL), epidermal growth factor (0.5 ng/mL), triiodothyronine (6.5 ng/mL), retinoic acid (0.1 ng/mL) and Gibco™ ITS-X to give final concentration of insulin (10 µg/mL), transferrin (5.5 µg/mL), selenium (6.7 ng/mL) and ethanolamine (2 µg/mL). This formulation was adapted from one previously described for culturing BEAS-2B, in addition to including the key supplements identified for serum-free culture of normal human bronchial epithelial cells (Oh et al., 2011, Lechner and LaVeck, 1985).

This culture method was used so that the basal culturing medium was similar for all cell lines, in comparison to the use of proprietary medium formulations such as DCCM-1 for TT1 and LHC-8 for BEAS-2B, which would have complicated metabolite identification due to the presence of unknown media formulation along with the presence of HEPES in LHC-8. Preliminary experiments were performed to ensure that cell growth rate, morphology

(assessed visually using light microscopy) and cell viability did not significantly differ from the responses obtained using typical medium for the respective cell lines.

### 4.3.3 Sample generation

Following at least 3 passages in the medium described above, cells were trypsinised and seeded into 6 well plates (details shown in **Table 4.2**). Seeding densities were selected based on the different growth rates for the cell lines, so that ~80% confluency was achieved prior to pesticide exposure. The total culture medium volume used was 2 mL per well, cells were cultured for 48 hours after which the medium was aspirated, wells gently rinsed twice with PBS and the replaced with DMEM:F12 Ham's containing no supplements (2 mL/well).

**Table 4.2. Cell line, passage number and seeding density for the metabolomic experiments. Culturing medium supplements are shown, including foetal bovine serum (FBS), non-essential amino acids (NEAA), sodium pyruvate (SP), insulin-transferrin-selenium-ethanolamine (ITS-X), retinoic acid (RA), hydrocortisone (HC), triiodothyronine (T3) and epidermal growth factor (EGF).**

Cell line	Passage no.	Seeding density cells/well	Culturing medium supplements	Exposure medium supplements
<b>A549</b>	P57 – P60	250,000	+ FBS, NEAA, SP, P/S	N/A
<b>TT1</b>	P+7 – P+10	150,000	+ FBS, NEAA, SP	N/A
<b>BEAS-2B</b>	P+7 – P+10	200,000	+ ITS-X, RA, HC, T3, EGF, SP, P/S	N/A
<b>16HBE14o-</b>	P27 – P30	150,000	+ FBS, NEAA, SP, P/S	N/A
<b>Calu-3</b>	P7 – P10	500,000	+ FBS, NEAA, SP, P/S	N/A

Following a 24 h incubation with blank medium, cells were exposed to the fungicides by replacing with 2.8 mL per well of either; acibenzolar-s-methyl (10 or 100 µM), azoxystrobin (1 or 10 µM), chlorothalonil (1 or 10 µM), isopyrazam (1 or 10 µM), propiconazole (10 or 100 µM) or a 0.25% DMSO control. Wells containing medium only (with no cells) were also included as a fresh medium control. This method generated a total of 56 different conditions, for which 8 replicate samples were collected (representing experimental duplicate samples, n=4).

The samples were incubated for 24 h before the spent medium was collected for metabolomic analysis. After 24 h, 2 mL of spent medium was collected from each sample into a deep well plate, placed on ice and centrifuged at 4000 g for 10 minutes, aliquots of the supernatant were collected and frozen at -70°C prior to subsequent preparation for NMR. Cell layers were rinsed with PBS and used to measure cell viability with the Alamar blue cytotoxicity assay.

#### 4.3.4 Alamar Blue cytotoxicity assay

After the cell layers were rinsed twice with PBS, 2 mL of a 10% Alamar blue solution in phenol red free DMEM was added to each well, incubated for 1-2 hours dependent on the cell line, and an aliquot of 50  $\mu$ L was transferred to a black walled 96 well plate and diluted with 200  $\mu$ L PBS, before measuring the fluorescence (ex/em = 535/595 nm) using a Tecan Spark 10M microplate reader. Relative cell viability was calculated using the equation below:

##### *Equation 4.1. % Cell viability (Alamar Blue)*

$$\% \text{ Cell viability} = \frac{T - B}{N - B} \times 100$$

Where T is the UV fluorescence value of the test well, B is the UV fluorescence of the blank well (containing no cells) and N is the fluorescence of the negative control (0.25% DMSO) representing 100% cell viability.

#### 4.3.5 NMR metabolomics sample preparation

The preparation and subsequent analysis of metabolomic samples was adapted from the method described by Kostidis et al. (2017). Briefly, 1.3 mL of spent medium was lyophilised overnight and pH corrected so that all samples were pH  $7.4 \pm 0.2$ , before being reconstituted to a final volume of 650  $\mu$ L in 0.15 M  $\text{KH}_2\text{PO}_4$ , 0.2 mM  $\text{NaN}_3$ , and 0.4 mM TSP- $d_4$ ) in 10%  $\text{D}_2\text{O}$ . From each sample, 7  $\mu$ L was collected and then pooled for 2D  $^1\text{H}$  NMR analysis required for metabolite assignments. The samples were then transferred to NMR tubes ( $\sim$ 640  $\mu$ L/tube) and kept on ice until analysis. Sample preparation was performed in 5 batches to limit potential metabolite degradation and ensure NMR analysis within 24 h of sample thawing.

#### 4.3.6 NMR data acquisition

NMR data acquisition settings were adapted from (Kostidis et al., 2017). 1H NMR spectra were recorded on a Bruker 600 MHz Bruker Avance III NMR spectrometer (Bruker BioSpin, Coventry, United Kingdom) equipped with a 5-mm  $^1\text{H}$ ,  $^{13}\text{C}$ ,  $^{15}\text{N}$  TCI Prodigy Probe and a cooled SamplePro sample changer for automation with 8 sample replicates tested per condition and all kept at 277 K before acquisition. 1D spectra were recorded under automation at 298 K using a Carr-Purcell-Meiboom-Gill (CPMG) pre-saturation (cpmgpr1d) pulse sequence. Spectra were acquired with 32 transients, a spectrum width of 20.83 ppm, an acquisition time of 2.62 s and a relaxation time of 4 s. After acquisition, the FID were processed with an exponential window of 0.3 Hz, phase corrected, and baseline corrected using a polynomial function of order 2. For metabolite identification, 2D spectra were acquired on a couple of samples, consisting of J-



resolved spectroscopy (J-RES), with 8 scans, 32 t1 increments, an acquisition time of 1.63 s and a relaxation time of 2s, total correlation spectroscopy (TOCSY), with 16 scans, 256 t1 increments, a TOCSY mixing time of 0.08 s, an acquisition time of 0.25 s and a relaxation time of 2 s, and <sup>1</sup>H-<sup>13</sup>C Heteronuclear Single Quantum Correlation (HSQC) spectra with 16 scans, 256 t1 increments, an acquisition time of 0.08 s and a relaxation time of 1.75 s. All peak positions were measured relative to the methyl peak of TSP-d4 set to 0.0 ppm.

#### **4.3.7 Metabolomic data processing and analysis**

Much of the data processing made use of either commercial NMR metabolomics software or custom software and Python scripts from the Mason group at King's College London (Institute of Pharmaceutical Sciences). Metabolite profiles were generated using <sup>1</sup>H NMR spectra acquisition and Orthogonal Projections to Latent Structures Discriminant Analysis (OPLS-DA) as described by Man et al. (2018). The use of OPLS-DA allowed for the visualisation of inter- and intra-group variation, to determine if there was a significant difference between DMSO and fungicide exposed cells, additionally it was used to identify and remove samples which were outliers or had anomalous data. Of the 480 samples tested using <sup>1</sup>H NMR, 1 sample (Chlorothalonil 10 µM using TT1) was an outlier and was removed from the remainder of data processing, the other 7 replicates for this sample type were used. Spectral regions ≤ 0.5 and ≥ 8.5 ppm were excluded due to noise, as were water peaks and the TSP-*d*<sub>4</sub> reference signal. A total of 34 metabolites were identified using the Chenomx NMR software (Chenomx, Edmonton Canada) in addition to confirmation of metabolite assignments by comparing 2D <sup>1</sup>H NMR data using Bruker TopSpin 4.0 (Bruker Biospin, Coventry, UK) against that in the Human Metabolome Database.

The remainder of the data processing made use of custom python scripts from the Mason group to calculate metabolite fold change (comparing each cell line against either fresh medium or a particular pesticide treatment against the DMSO control for a specific cell line). Normalised intensity for each metabolite and significant differences following pesticide exposure were visualised using boxplots and statistically determined using a one way-ANOVA. Cluster maps (heatmaps clustered by similarity) were also generated to visualise any potential patterns or associations in metabolic changes between fungicides.

Unless otherwise stated, all data represents 8 replicate samples and for NMR metabolomics boxplots, normalisation refers to probabilistic quotient normalisation (PQN) for sample intensities rather than normalisation against either fresh medium or DMSO control. PQN is a

data pre-processing method which is applied to  $^1\text{H}$  NMR metabolomics to account for the effect of dilution on the entire spectra rather than only individual analytes/metabolites (Dieterle et al., 2006). This is particularly useful in examples such as the analysis of cell culture medium where glucose concentration may be very high, or if there is low metabolic variation between samples. To determine statistical significance in the fold change of a particular metabolite compared against the control, a one-way ANOVA was used with Tukey's multiple comparison test.

## 4.4 Results

### 4.4.1 Alamar Blue cytotoxicity assay

Generally, when cultured under the conditions used in this study, no significant change in cell viability was observed, allowing for the subsequent metabolomic analysis of phenotypic changes following subtoxic exposures to the tested fungicides. The exceptions to this were with the highest tested chlorothalonil concentration (10  $\mu$ M) in the “normal” immortalised cell lines BEAS-2B and TT1 which caused a near complete loss of cell viability, and the highest tested concentration of isopyrazam and propiconazole (10 & 100  $\mu$ M, respectively) which likely caused an increase in cell proliferation in the cancer-derived Calu-3 bronchial cell line (**Figure 4.4**). For the purpose of metabolomics, significant changes in cell viability were assessed as being  $\pm$  25% in comparison to the DMSO control.

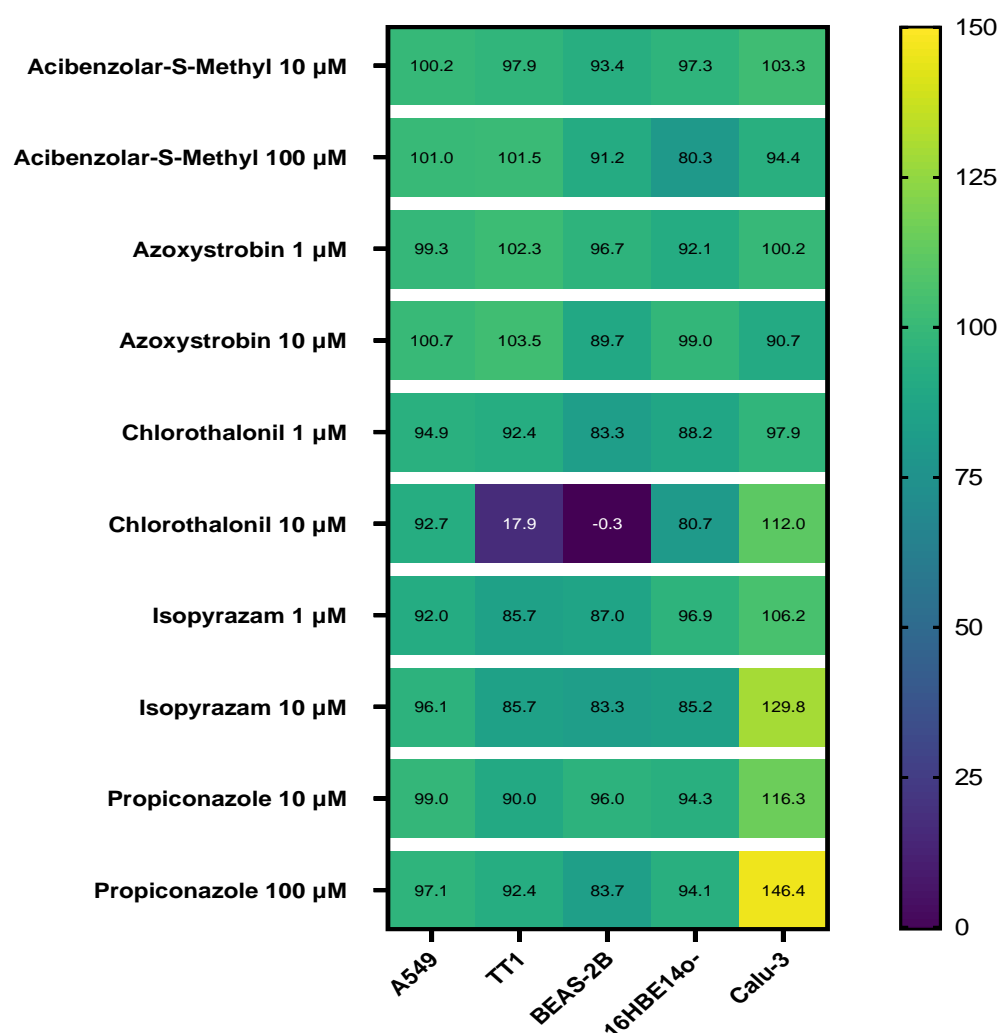


**Figure 4.4.** Heatmap showing Alamar Blue cytotoxicity data for A549, TT1, BEAS-2B, 16HBE14o- and Calu-3, following exposure to various fungicides. Data represented as mean average of % viability (n=4).

The cell viability data shown in **Figure 4.5** corresponds well with the data from **Chapter 2 and 3**, for which confluent 16HBE14o- was resistant to cytotoxicity with all the fungicides at 10  $\mu\text{M}$ , whereas BEAS-2B and TT1 were found to be the most sensitive cell lines to chlorothalonil toxicity. Additionally, both propiconazole and isopyrazam have been reported to potentially cause both ROS and cell proliferation *in vitro* which may explain the increased values observed in Calu-3. However, no cell proliferation was observed in 16HBE14o- following exposure to 10 or 100  $\mu\text{M}$  of acibenzolar-S-methyl, despite this effect being observed at concentrations between 5 and 75  $\mu\text{M}$  in the MTT assay in **Chapter 2**. This is likely due to the different experimental conditions, e.g. seeding density, confluency at exposure, and the subculturing or experimental medium used. Significant changes to cell viability, were deemed likely to influence the metabolomic profile and therefore, the culturing conditions and cell exposures were developed in part to avoid large changes in cell viability. Generally, this goal was achieved and cell viability data was maintained at  $\sim 100\%$ , with the dotted lines shown in **Figure 4.5** highlighting where changes to cell viability were outside the desired range ( $\pm 25\%$ ).

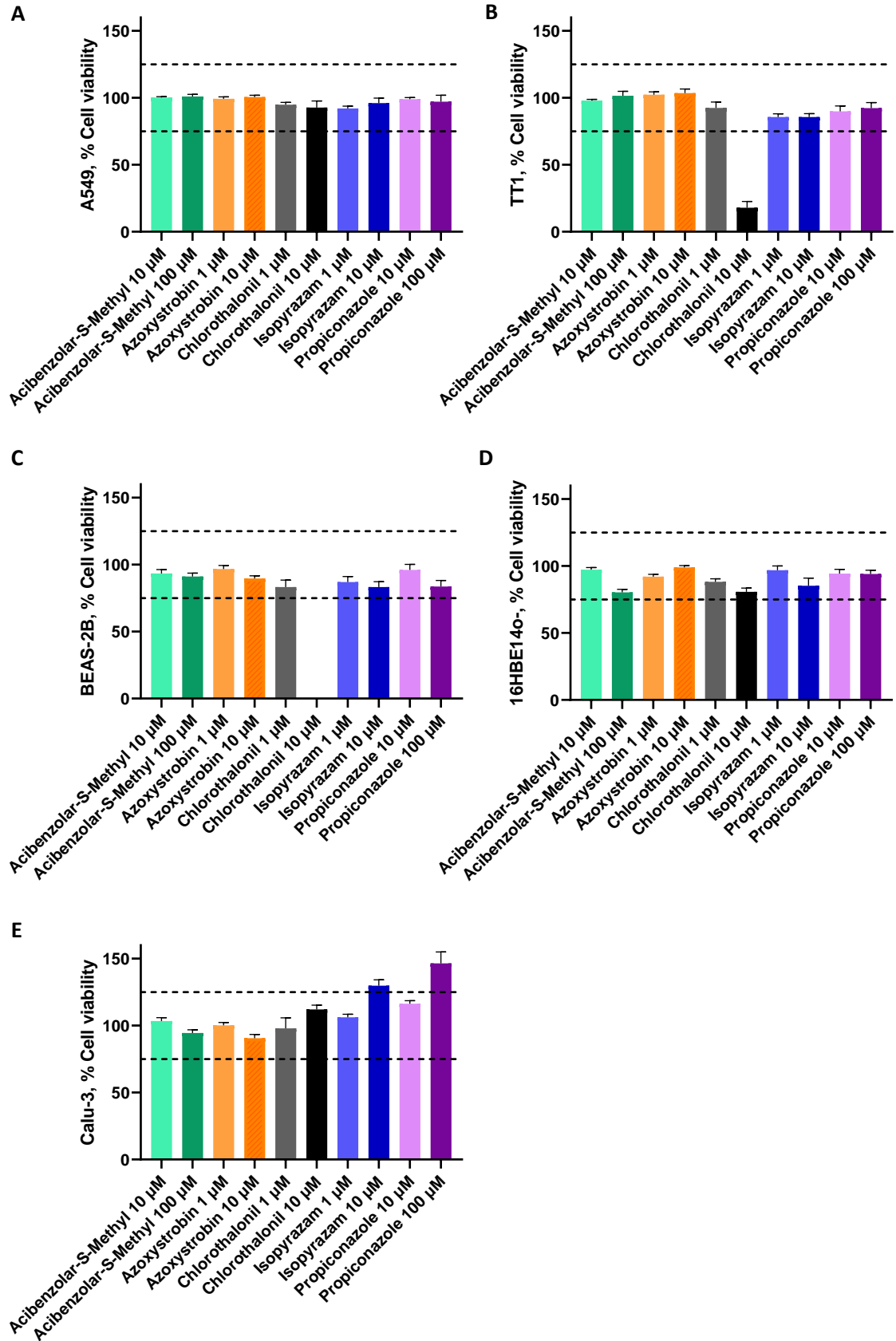


**Figure 4.5.** Individual graphs for (A) A549, (B) TT1, (C) BEAS-2B, (D) 16HBE14o- and (E) Calu-3, showing % cell viability as assessed by the Alamar Blue assay following 24 h fungicide exposure. Data represented as mean average  $\pm$ SD (n=4).

#### 4.4.2 NMR metabolomics

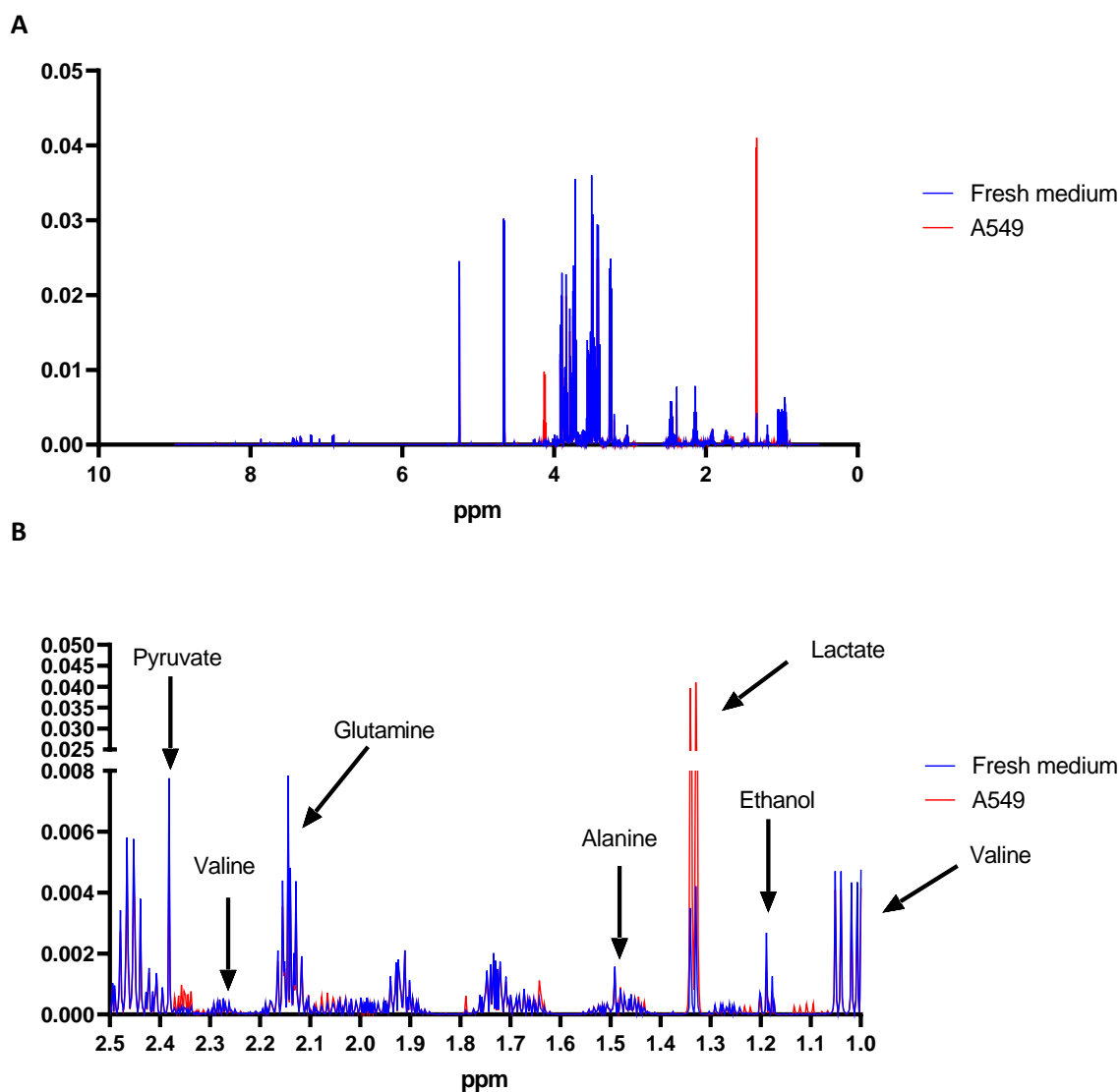


*Figure 4.6. Example NMR spectra, comparing fresh medium with spent A549 medium. (A) Entire spectra shown following removal of noise, water and TSP reference peaks, (B) example of metabolite assignments for a particular spectral region.*

As shown in **Figure 4.6B** the method used achieved a suitable spectral resolution, with an optimal signal-to-noise ratio to allow for the identification of several metabolites within the samples. The total number of identified metabolites are shown below (**Table 4.2**).

**Table 4.3. Assignments of extracellular metabolites identified by NMR, using Chenomyx & the Human Metabolome Database, arranged in ascending order of ppm. Metabolites shown in red are those not found within the DMEM:F12 Ham's media formulation, whilst metabolites shown in blue are known to be within the medium formulation but could not be identified by NMR. Concentration ( $\mu\text{M}$ ) represents the known concentration in the fresh media formulation.**

Metabolite	ppm	Concentration ( $\mu\text{M}$ )	Metabolite	ppm	Concentration ( $\mu\text{M}$ )
Pantothenate	0.897	9.362	Threonine	3.598	448.71
Isoleucine	0.942	415.247	Serine	3.969	247.81
Leucine	0.965	450.162	Myo-inositol	4.079	69.94
Valine	1.040	476.235	Cystine	4.096	99.90
Ethanol	1.188	N/A	Pyroglutamate	4.172	N/A
Lactate	1.339	N/A	Glucose	5.242	17484.85
Alanine	1.479	49.947	Histidine	7.092	150.17
Acetate	1.923	N/A	Tryptophan	7.546	44.17
Succinate	2.047	N/A	Hypoxanthine	8.206	17.93
Methionine	2.143	115.543	Niacinamide	8.255	16.54
Choline	2.208	64.316	Formate	8.459	N/A
Glutamate	2.338	49.956	Cysteine	N/A	82.797
Pyruvate	2.381	493.194	D-Biotin	N/A	0.014
Glutamine	2.453	2497.502	Folic acid	N/A	6.026
Aspartate	2.803	49.961	Pyridoxal	N/A	9.822
Asparagine	2.943	49.955	Pyridoxine	N/A	9.877
Lysine	3.036	499.595	Riboflavin	N/A	0.582
Tyrosine	3.079	211.97	Thiamine	N/A	6.434
Phenylalanine	3.139	214.78	Vitamin B12	N/A	0.502
Arginine	3.251	700.17	Linoleic Acid	N/A	0.150
Betaine	3.262	N/A	Putrescine	N/A	0.503
Proline	3.357	149.83	DL-Thioctic Acid	N/A	0.509
Glycine	3.571	249.78	Thymidine	N/A	1.507

As shown in **Table 4.3**, a number of metabolites produced by the cells and released into the extra-cellular media were identified, in addition to those which were expected to be present in the medium formulation. Generally, the expected compounds, which were identified had a concentration  $\geq 10 \mu\text{M}$  in the medium formulation and so were within the range of quantification generally reported for NMR metabolomics studies. Compounds  $\leq 10 \mu\text{M}$  but known to be within the medium formulation included, could generally not be detected, or identified with the exception of pantothenate ( $9.362 \mu\text{M}$ ). Cysteine which was theoretically at a concentration of  $82.797 \mu\text{M}$  was not identified, this may potentially be due to either degradation over the 24 h incubation, as cysteine was not identified even when the “fresh”

medium sample was incubated in 6-well plates at 37°C in order to have a directly comparable sample to the spent cell medium. Whilst in the reductive environment of the cell cysteine is predominant, under oxidative conditions such as in the extracellular environment cysteine may dimerise to cystine (**Figure 4.7**), this may have occurred during the 24 h incubation or afterwards during the sample preparation e.g. pH correction, lyophilisation and reconstitution.

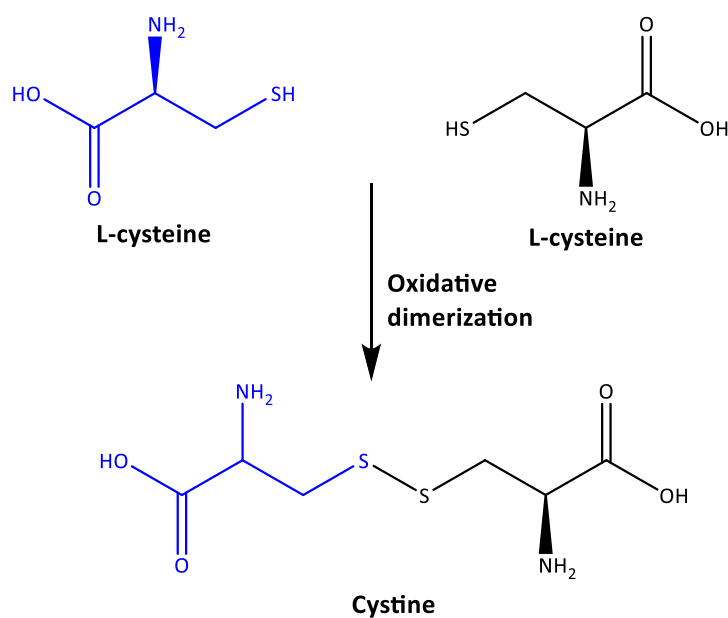


**Figure 4.7.** Oxidative dimerisation of L-cysteine to cystine, as a potential reason for the absence of cysteine in the NMR metabolomics samples.

Despite the absence of cysteine within the samples, most expected metabolites were identified in the medium, with most being above the limit of detection via NMR metabolomics. The absence of cysteine and the presence of the additional metabolites found to be produced by the cells in this study were also reported by Kostidis et al. (2017) using the same medium, but with the thyroid carcinoma cell line BHP2-7.

PCA and OPLS-DA plots highlighted metabolomic differences prior to the assignment of individual metabolites. As shown in **Figure 4.8** there were significant differences between some of the cell lines, for example BEAS-2B with the other cell lines, as well as similarities between TT1 and A549.



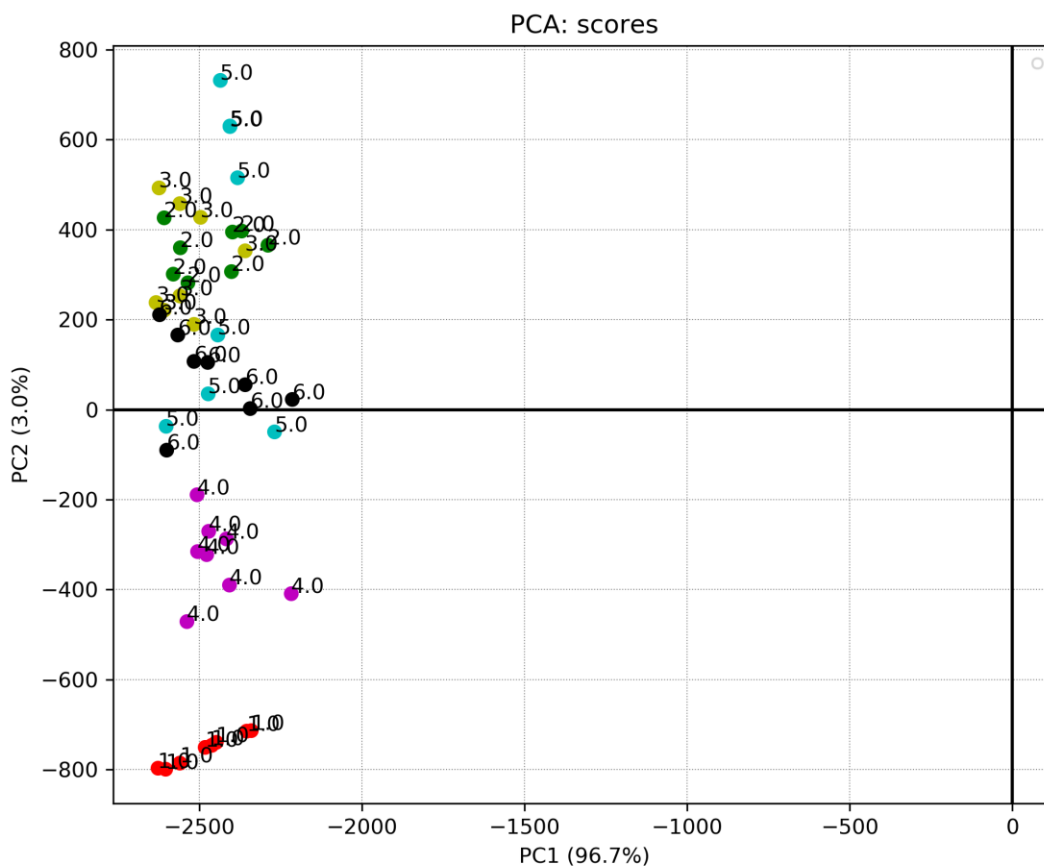


**Figure 4.8.** PCA plot comparing NMR metabolomic spectra for (1) Fresh medium, (2) A549, (3) TT1, (4) BEAS-2B, (5) 16HBE14o- and (6) Calu-3. Data based on 8 replicates for each sample type ( $n=4$ ).

Individual PCA and OPLS-DA plots are included in the appendix, however a summary is provided in **Table 4.4**. Generally, all cell lines were significantly different following exposure to the high pesticide concentration. TT1 and 16HBE14o- were overall the most responsive to the range of pesticides. TT1 was the only cell line to respond to 1  $\mu$ M chlorothalonil and 16HBE14o- was the only one to respond to 1  $\mu$ M azoxystrobin, with the latter likely relating to its high growth rate and greater sensitivity to mitochondrial inhibition.

**Table 4.4. Summary of OPLS-DA analysis of NMR metabolomics data, where a significant difference between DMSO vs fungicide treatment was if  $Q^2 \leq -0.5$  or  $\geq 0.5$ .**

Exposure ( $\mu\text{M}$ )		A549	TT1	BEAS-2B	16HBE14o-	Calu-3
Acibenzolar-S-Methyl	10	NO	NO	NO	NO	NO
	100	YES	YES	YES	YES	YES
Azoxystrobin	1	NO	NO	NO	YES	NO
	10	YES	YES	YES	YES	YES
Chlorothalonil	1	NO	YES	NO	NO	NO
	10	YES	YES	YES	YES	YES
Isopyrazam	1	NO	YES	NO	YES	NO
	10	YES	YES	YES	YES	YES
Propiconazole	10	NO	NO	NO	NO	NO
	100	YES	YES	YES	YES	YES
<b>Total no. of OPLS-DA significant differences detected</b>		<b>5/10</b>	<b>7/10</b>	<b>5/10</b>	<b>7/10</b>	<b>5/10</b>

The sensitivity of the selected cell lines to particular pesticides was not reflected in the Alamar Blue cytotoxicity assays, where for example following exposure to chlorothalonil 1  $\mu\text{M}$ , TT1 viability was only 2.5% lower than A549 cell viability, however with the same samples significant metabolomic changes ( $Q^2 \geq 0.5$ ) in comparison to the DMSO control occurred in TT1 but not A549 (Figure 4.9).

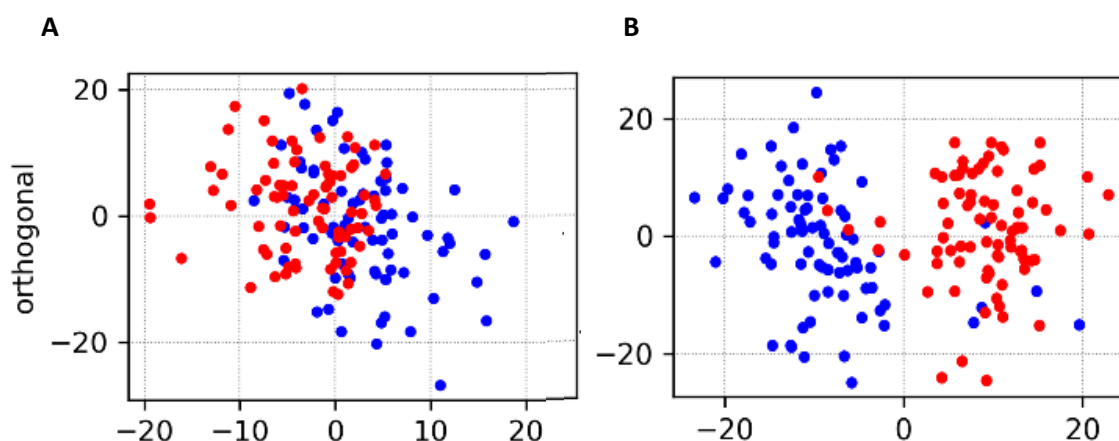


**Figure 4.9. OPLS-DA plots illustrating discrimination of NMR metabolomics spectra for DMSO control in blue vs chlorothalonil 1  $\mu\text{M}$  groups, with either (A) A549 or (B) TT1 in red ( $n=4$ ).**

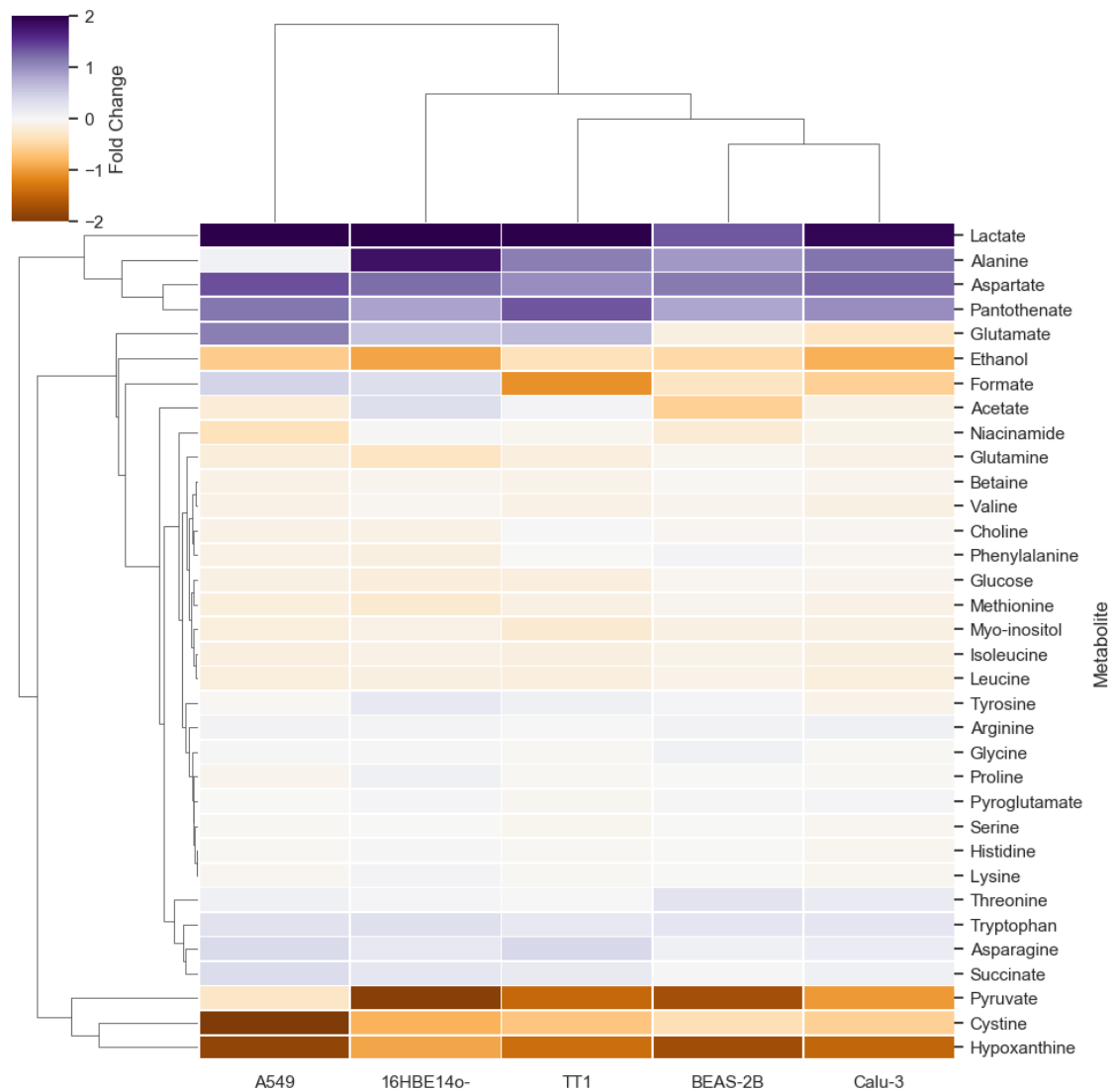


**Figure 4.10.** Differences in basal metabolism for the different cell lines, normalised against a fresh medium control. The cluster map shows the fold change of metabolites in comparison to fresh medium control. Changes either represent consumption (orange) or production (blue). Clusters show where there is a similarity in the changes between metabolites ( $n=4$ ).

Generally, the extracellular metabolomic profiles of the 5 different cell lines were similar (**Figure 4.10**), but unique enough that each cell line was significantly different to the other (data shown in the appendix). 16HBE14o- which was the cell line that divided most rapidly, was also the cell line that consumed the most pyruvate, whilst A549 consumed the least despite having a significantly faster growth rate than Calu-3 (**Figure 4.11**). BEAS-2B which is significantly different to Calu-3 in terms of phenotype, growth rate and sensitivity to fungicidal toxicity was most similar to Calu-3 for its extracellular metabolomic profile. Whilst intracellular metabolomics would likely reveal more significant differences between the two bronchial cell lines, this was an unexpected result.

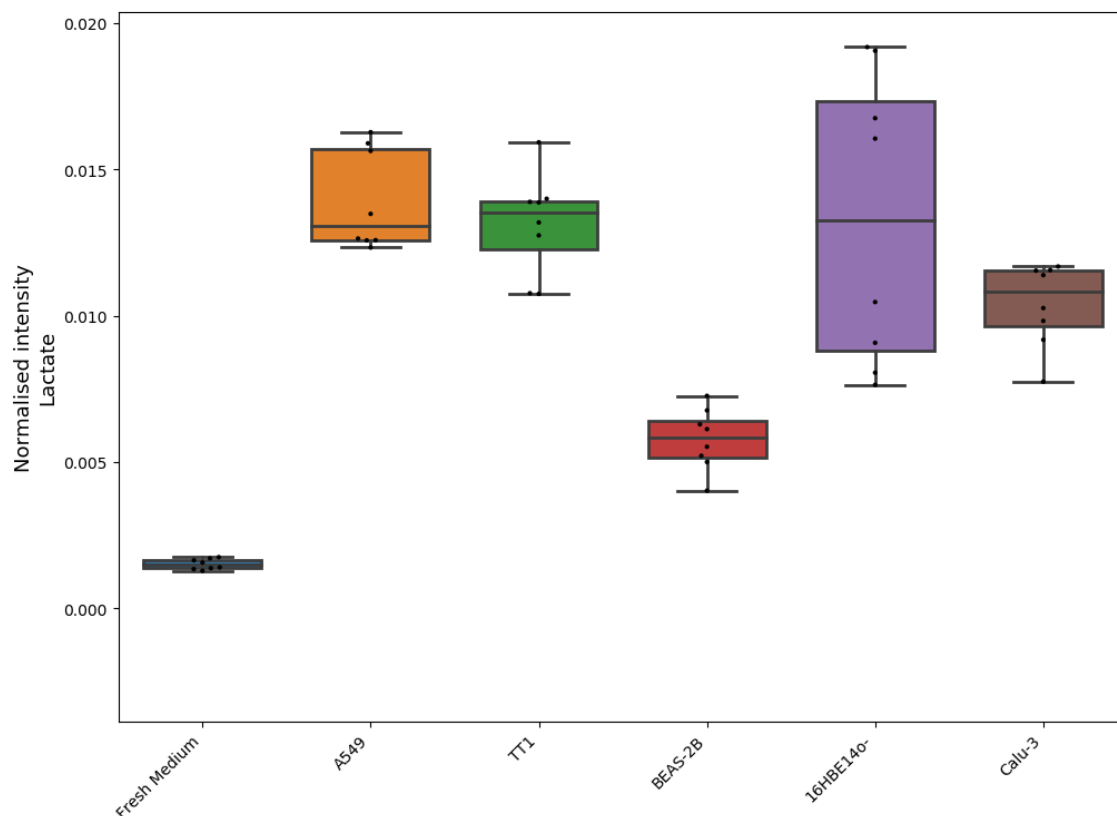


**Figure 4.11.** Boxplots showing differences in normalised extracellular lactate concentration (n=4).

With A549, many of the identified metabolites did not significantly change following exposure to the tested fungicides. Despite this, the overall metabolomic changes that occurred were enough to form two major clusters based on whether the profile was significantly different to the DMSO control. The low concentrations of all tested fungicides and the high 100  $\mu\text{M}$  acibenzolar-S-Methyl exposure formed a cluster which likely represents a negligible change in cell phenotype, whilst the other exposures (propiconazole 100  $\mu\text{M}$  and azoxystrobin, chlorothalonil and isopyrazam 10  $\mu\text{M}$ ) formed a separate cluster indicating a more pronounced change in metabolomic profile (**Figure 4.12**). Generally, this second cluster was associated with increased consumption of pyruvate and the amino acids asparagine, phenylalanine, aspartate, and tyrosine, along with increased production of lactate and availability of hypoxanthine. The most significant changes in the overall metabolomic profile were elicited following exposure to 10  $\mu\text{M}$  of azoxystrobin, followed by propiconazole, chlorothalonil and isopyrazam 10  $\mu\text{M}$ . No significant changes in A549 cell viability were detected for any fungicide exposure ( $\geq 92\%$ ), highlighting the sensitivity of NMR metabolomics to detect phenotypic changes at subtoxic concentrations.

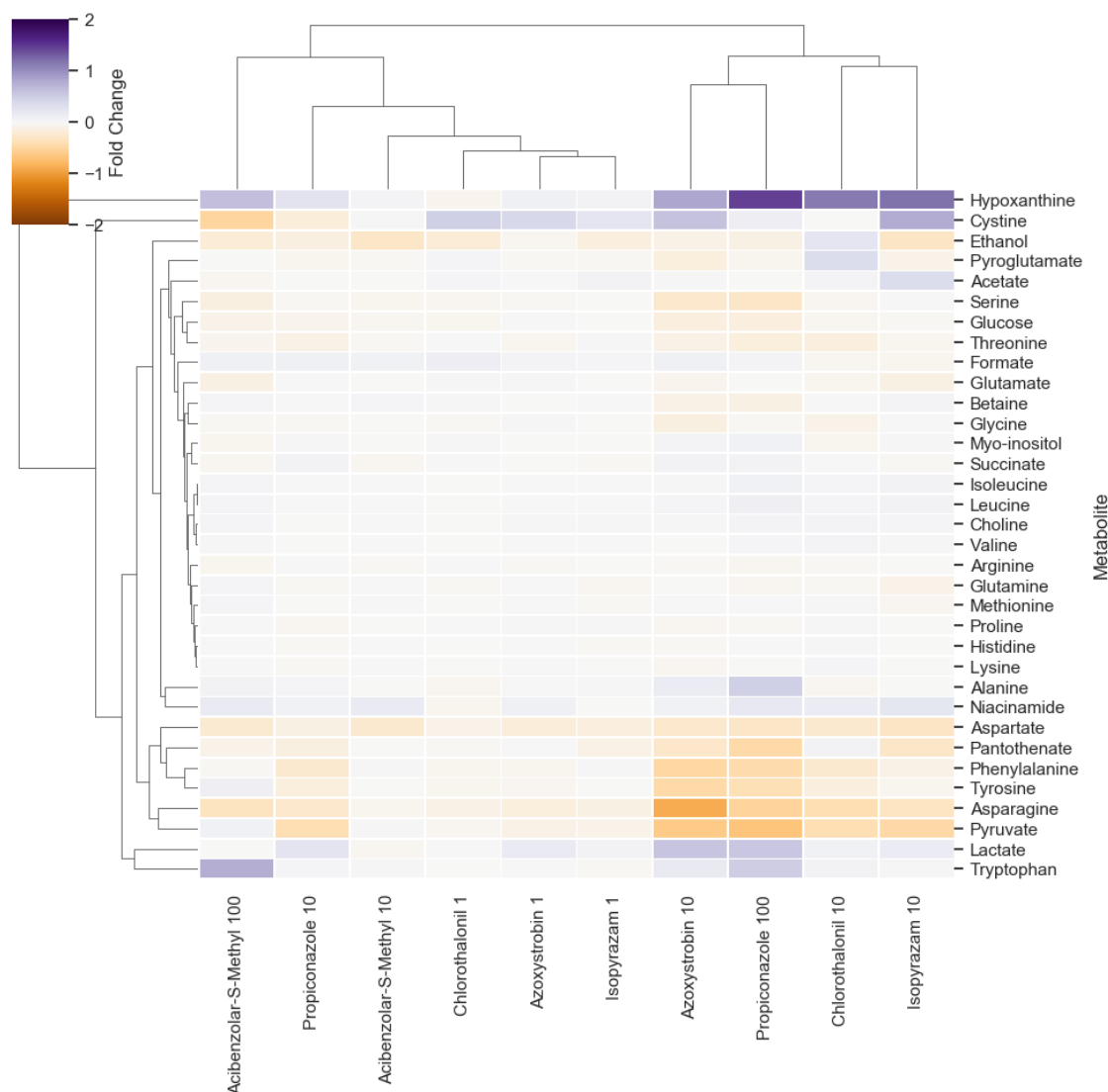


**Figure 4.12.** Differences in A549 metabolism following 24 h exposure to the different fungicides, normalised against the A549 DMSO control. Data shown as fold changes either represent consumption (orange) or production (n=4).

The increase in lactate production shown in **(Figure 4.13)** likely reflects the impact of mitochondrial inhibition by azoxystrobin 10 μM, which is known to block electron transport, this is also consistent with the increased consumption of glucose and pyruvate. Exposure to 100 μM propiconazole caused a similar effect however this may relate to inhibition/dysregulation of lipid metabolism.

The increased extracellular concentration of hypoxanthine is observed in comparison to the DMSO control was observed with most exposures, and was most evident for the high exposure concentrations for azoxystrobin, chlorothalonil, isopyrazam and propiconazole, which caused the greatest metabolomic changes. There are a number of potential reasons the observed differences in change, which are explored further in the discussion.

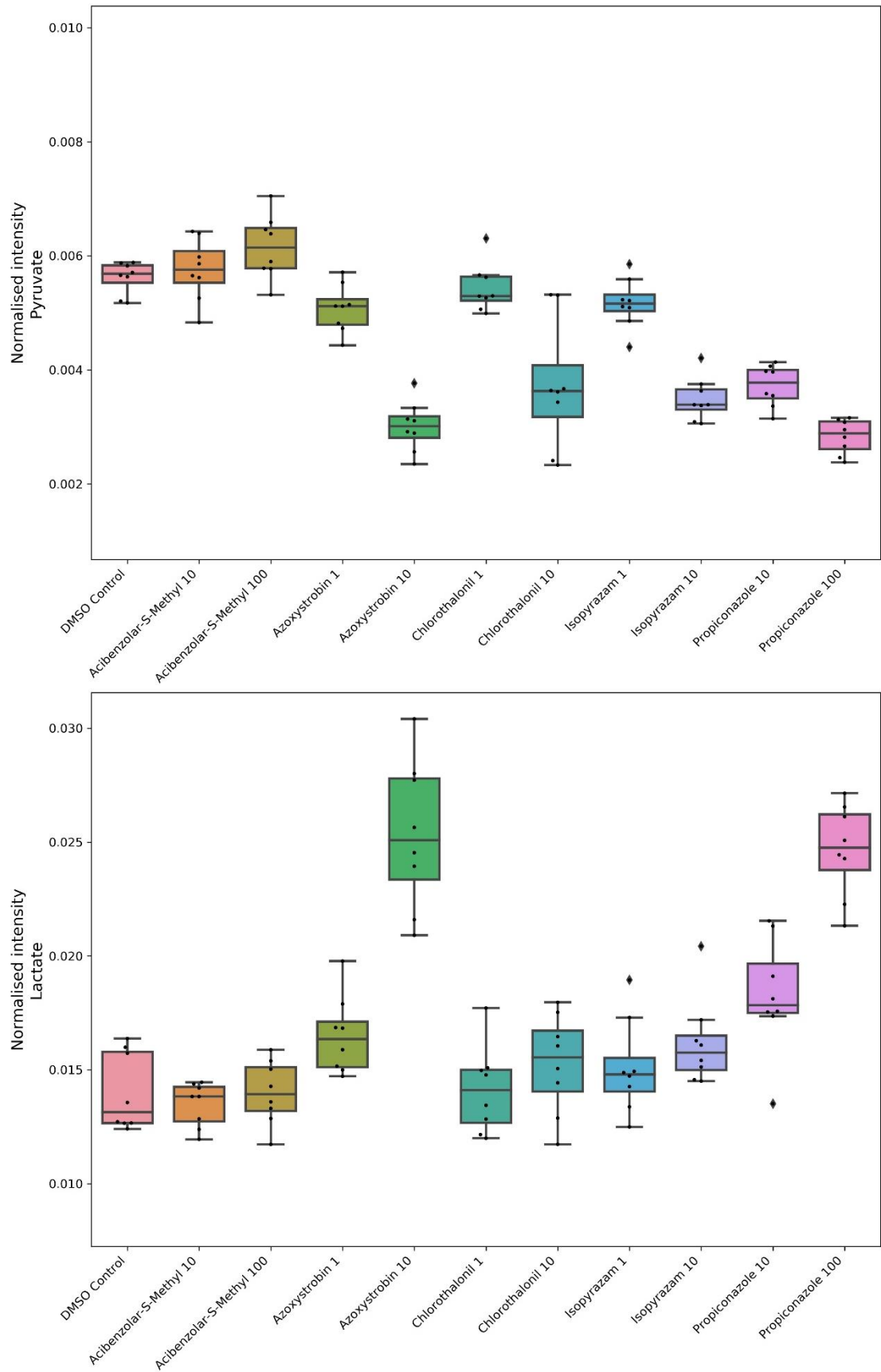


**Figure 4.13. Boxplots showing differences in A549 extracellular pyruvate and lactate concentration, following 24 h exposure to DMSO, acibenzolar-s-methyl, azoxystrobin, chlorothalonil, isopyrazam or propiconazole. (n=4).**

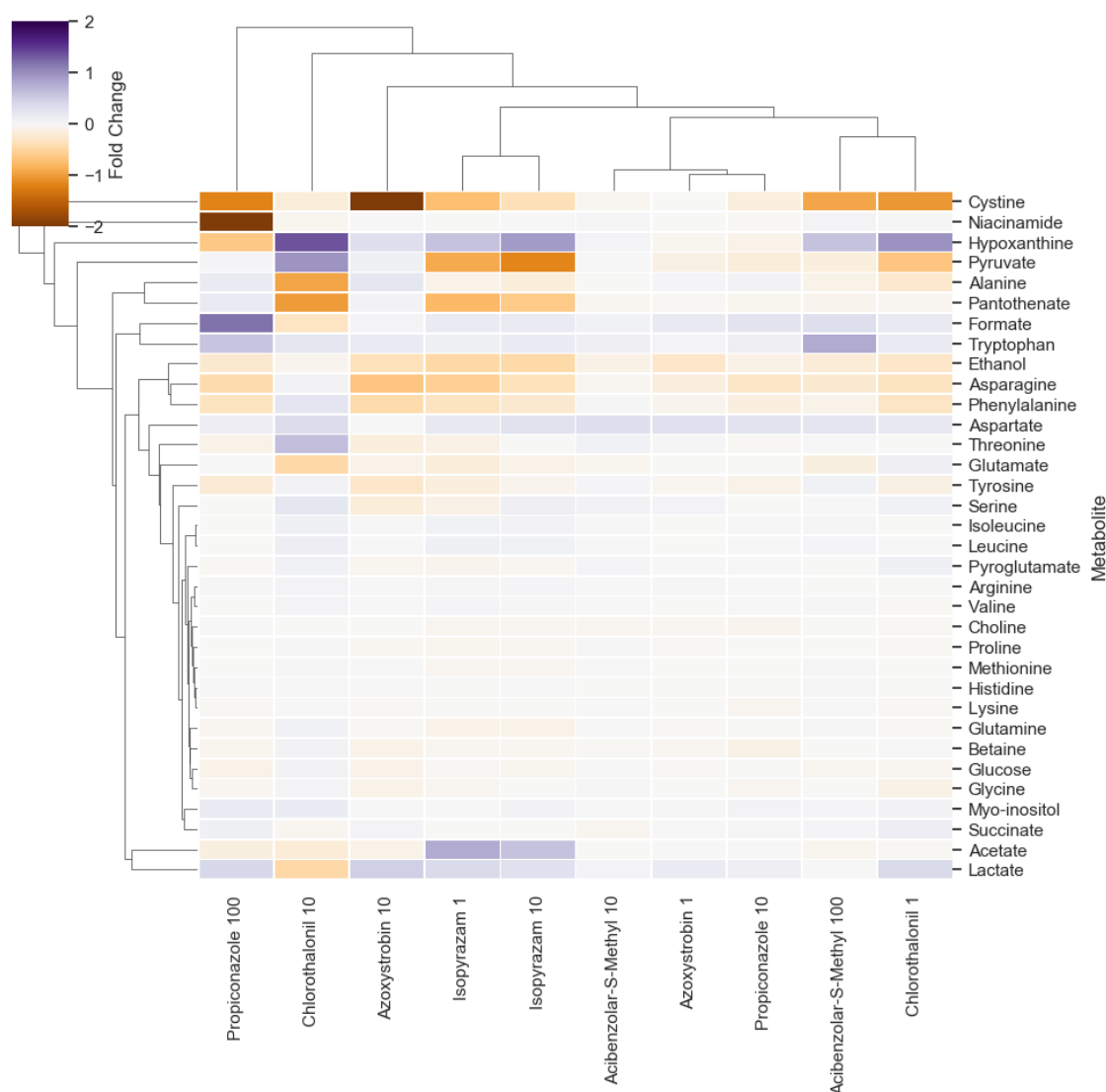


**Figure 4.14.** Differences in TT1 metabolism following 24 h exposure to the different fungicides, normalised against the TT1 DMSO control. Data shown as fold changes either represent consumption (orange) or production (n=4).

In comparison to A549, for which two independent clusters were formed, fungicide exposures with the alveolar type-I like cell line TT1, formed several subdivisions. As shown previously in **Table 4.4**, exposures to acibenzolar-s-methyl 10  $\mu$ M, azoxystrobin 1  $\mu$ M and propiconazole 10  $\mu$ M were not significantly different to the DMSO control, and these 3 exposures are clustered together in **Figure 4.14**, representing no significant metabolomic change. Of the remaining exposures, the overall clustering is more complex and perhaps more informative than those shown previously with A549. Again, the most significant changes were caused by the highest concentrations of pesticides, however, both isopyrazam exposures (1 & 10  $\mu$ M) were grouped together. Isopyrazam was unique in its ability to increase acetate production (**Figure 4.15**), this effect was also observed in A549 but only at 10  $\mu$ M, in comparison to TT1.

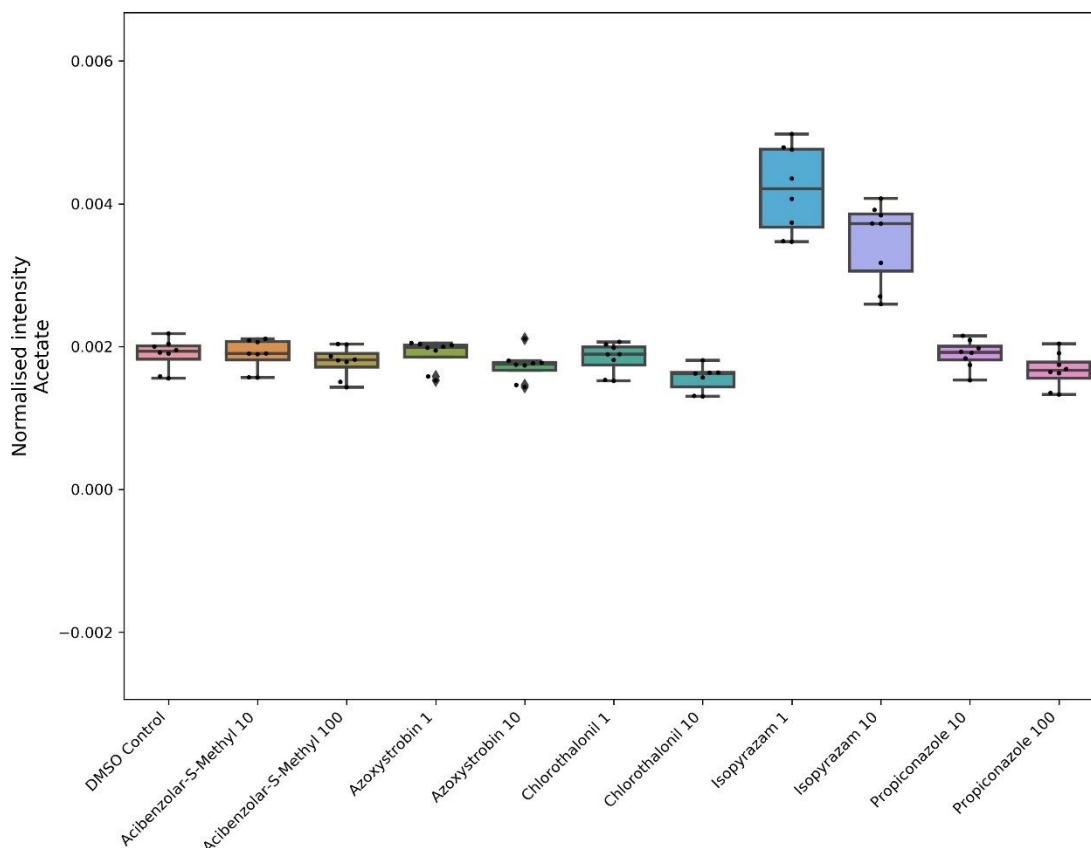


**Figure 4.15.** Boxplot showing increased acetate production by TT1 following 24 h to isopyrazam, in comparison to exposure to DMSO, acibenzolar-s-methyl, azoxystrobin, chlorothalonil or propiconazole. (n=4).

In addition to the unique effects of isopyrazam on TT1, the metabolomic profile of the acibenzolar-s-methyl 100  $\mu$ M and the chlorothalonil 1  $\mu$ M exposure were similar, potentially representing irritative effects at these concentrations. In contrast, the high concentration of chlorothalonil, which significantly reduced TT1 cell viability as assessed by the Alamar Blue assay (~17.9%), gave a unique metabolomic profile. This is likely due to many of the metabolites not being consumed or produced as due to cell death, for example lactate production was significantly lower in these samples compared to the DMSO control (**Figure 4.16**), whilst pyruvate consumption was also greatly reduced, as was amino acid consumption, albeit to a lesser extent.



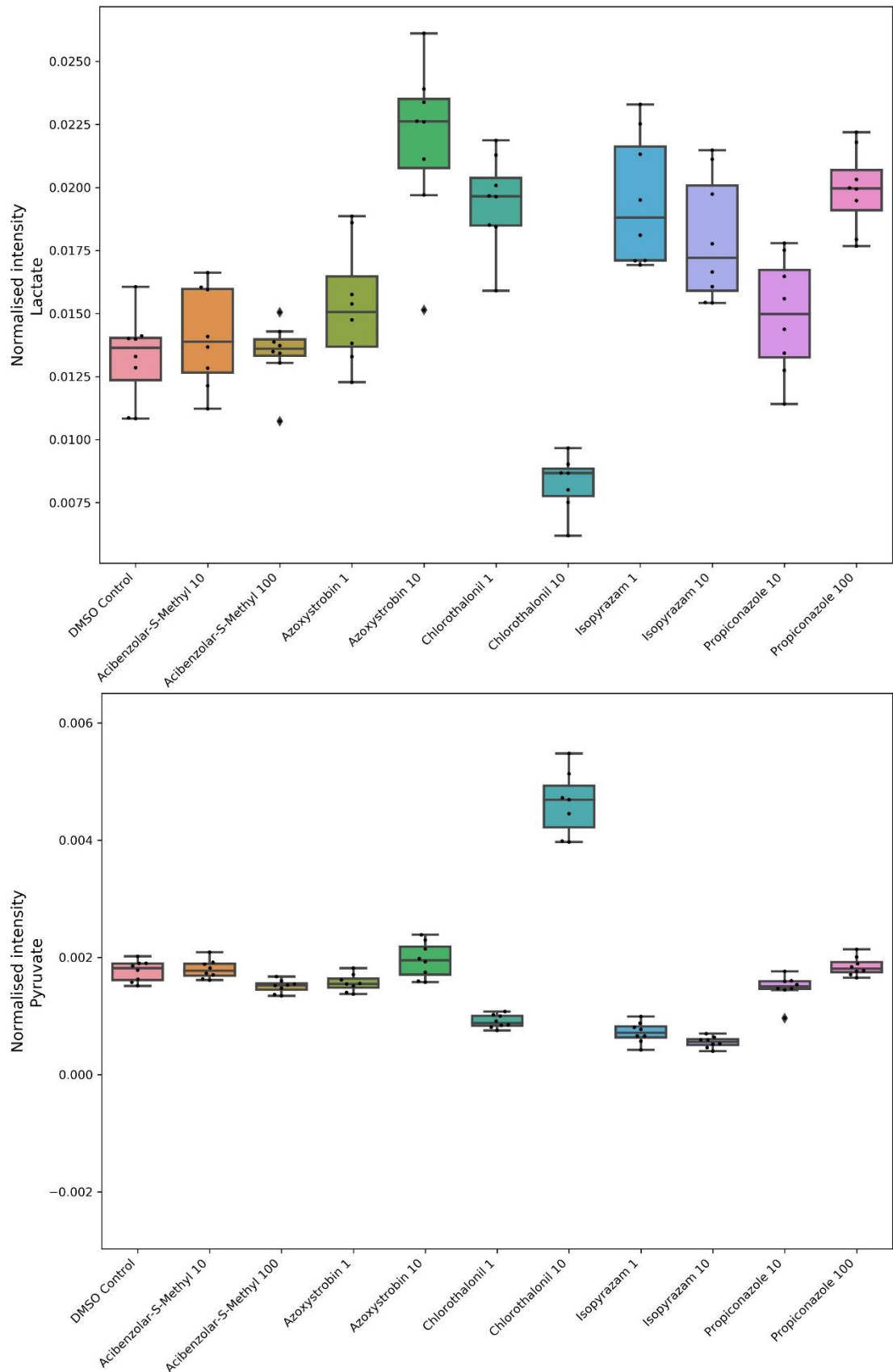


**Figure 4.16.** Boxplot showing differences in TT1 extracellular pyruvate and lactate concentration, following 24 h exposure to DMSO, acibenzolar-s-methyl, azoxystrobin, chlorothalonil, isopyrazam or propiconazole. (n=4).

The overall metabolomic profile of the azoxystrobin 10  $\mu\text{M}$ , was most similar to the isopyrazam exposures, with both these fungicides working via mitochondrial inhibition, the reason for increased cystine consumption could not be determined. Spearman's rank data showed that the increased consumption of cystine did not have a strong relationship with increased consumption of other amino acids, and therefore this result is not expected to reflect increased GSH production or protein synthesis. Similarly, increased consumption of alanine following exposure to chlorothalonil 1 & 10  $\mu\text{M}$ , could not be explained (**Figure 4.17**), however this result was observed in both TT1, BEAS-2B and Calu-3, suggesting a specific mechanism. Within the cell medium formulation, alanine was at a low concentration ( $\leq 50 \mu\text{M}$ ) and nearly 10-fold lower than some of the other amino acids, so it may be that whilst this is a non-essential amino acid, exposure to chlorothalonil reduces the cell's ability to synthesise more, resulting in greater consumption of extracellular alanine. Reduced consumption of extracellular alanine in the case of azoxystrobin may related to reduced metabolic activity due to mitochondrial inhibition.

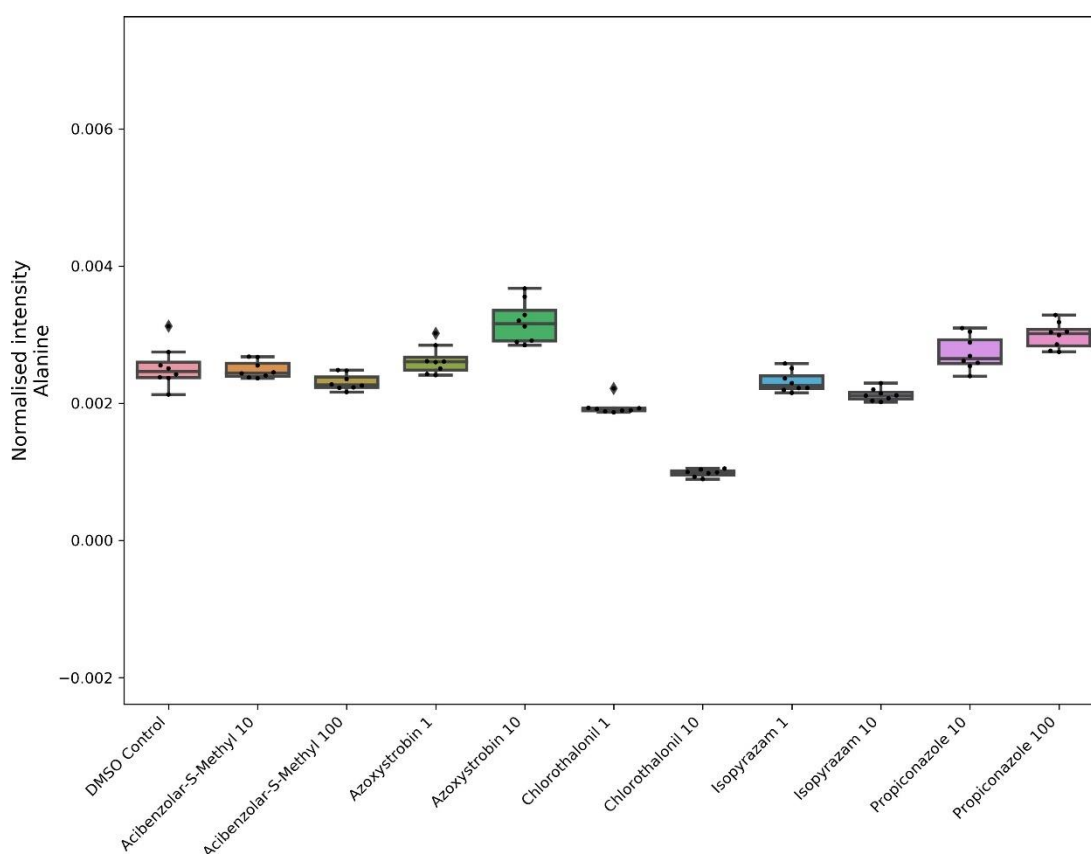


**Figure 4.17.** Boxplot showing reduced alanine consumption in TT1 following 24 h to chlorothalonil, in comparison to exposure to DMSO, acibenzolar-s-methyl, azoxystrobin, chlorothalonil or propiconazole (n=4).

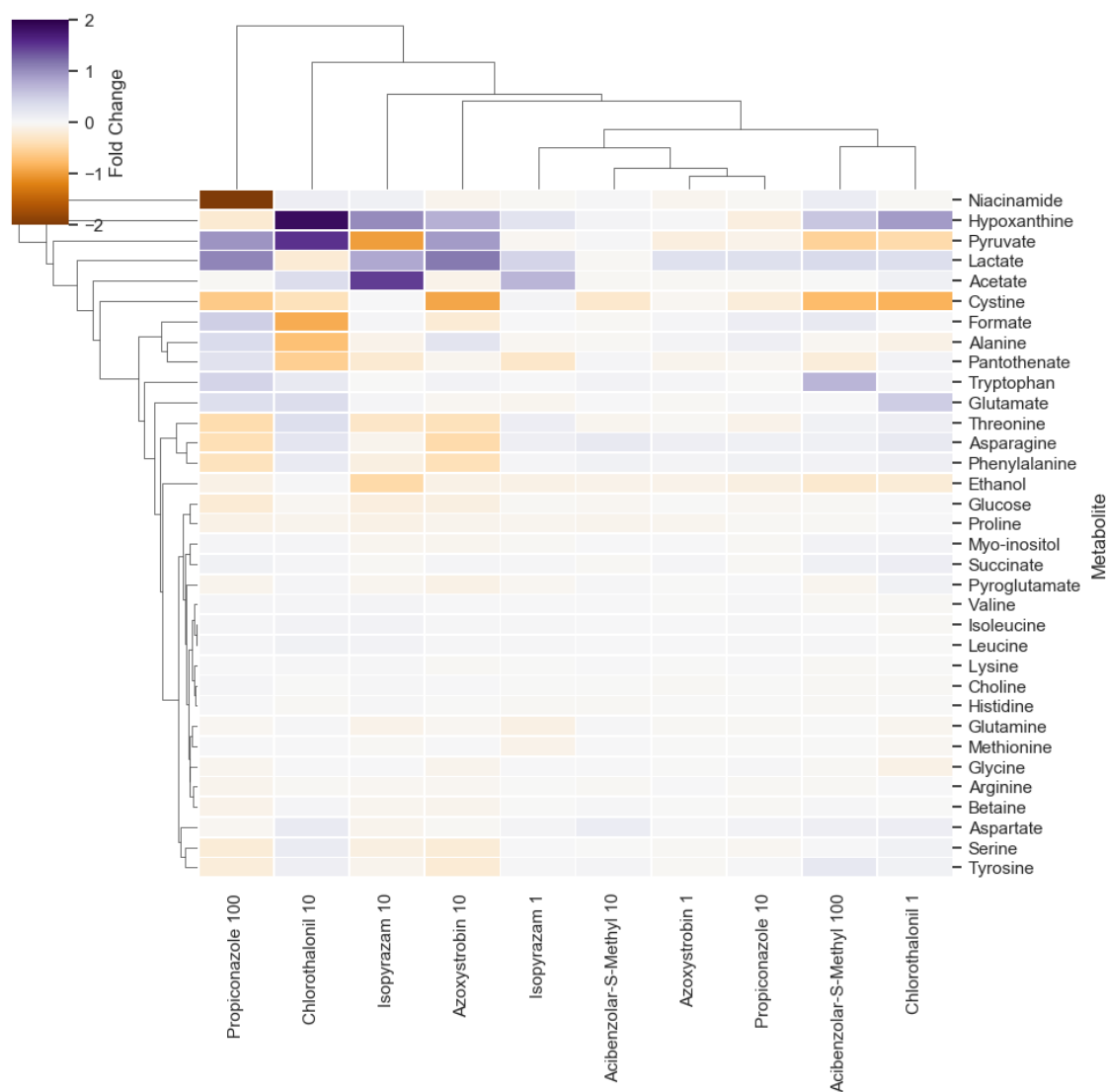


**Figure 4.18.** Differences in BEAS-2B metabolism following 24 h exposure to the different fungicides, normalised against the BEAS-2B DMSO control. Data shown as fold changes either represent consumption (orange) or production (n=4).

Once again, similar to the previously described cell lines, the cluster map grouped the fungicides according to metabolomic changes, however with BEAS-2B the pattern varied slightly (**Figure 4.18**). Exposure to isopyrazam 1  $\mu$ M, acibenzolar-s-methyl 10  $\mu$ M, azoxystrobin 1  $\mu$ M and propiconazole 10  $\mu$ M did not significantly change the BEAS-2B metabolomic profile in comparison to the DMSO control. A second cluster formed based on moderate extracellular metabolomic changes produced following exposure to chlorothalonil 1  $\mu$ M and acibenzolar-s-methyl 100  $\mu$ M, this grouping also occurred with the TT1 cell line, based on reduced extracellular cystine and increased extracellular hypoxanthine concentrations. Extracellular hypoxanthine concentration was 6-fold higher than the DMSO control in BEAS-2B cells following exposure to chlorothalonil 10  $\mu$ M, however, in this case it likely relates to 0% cell

viability following this exposure and therefore the negligible consumption of hypoxanthine within the medium. This result also corresponds with the high extracellular pyruvate concentration and reduced production of lactate. The other exposures caused unique metabolomic profiles, however the effect of isopyrazam exposure on acetate production was replicated in BEAS-2B. The near complete consumption of extracellular niacinamide was observed following exposure to propiconazole 100  $\mu$ M, with this result occurring with both TT1 and BEAS-2B but not the other cell lines.

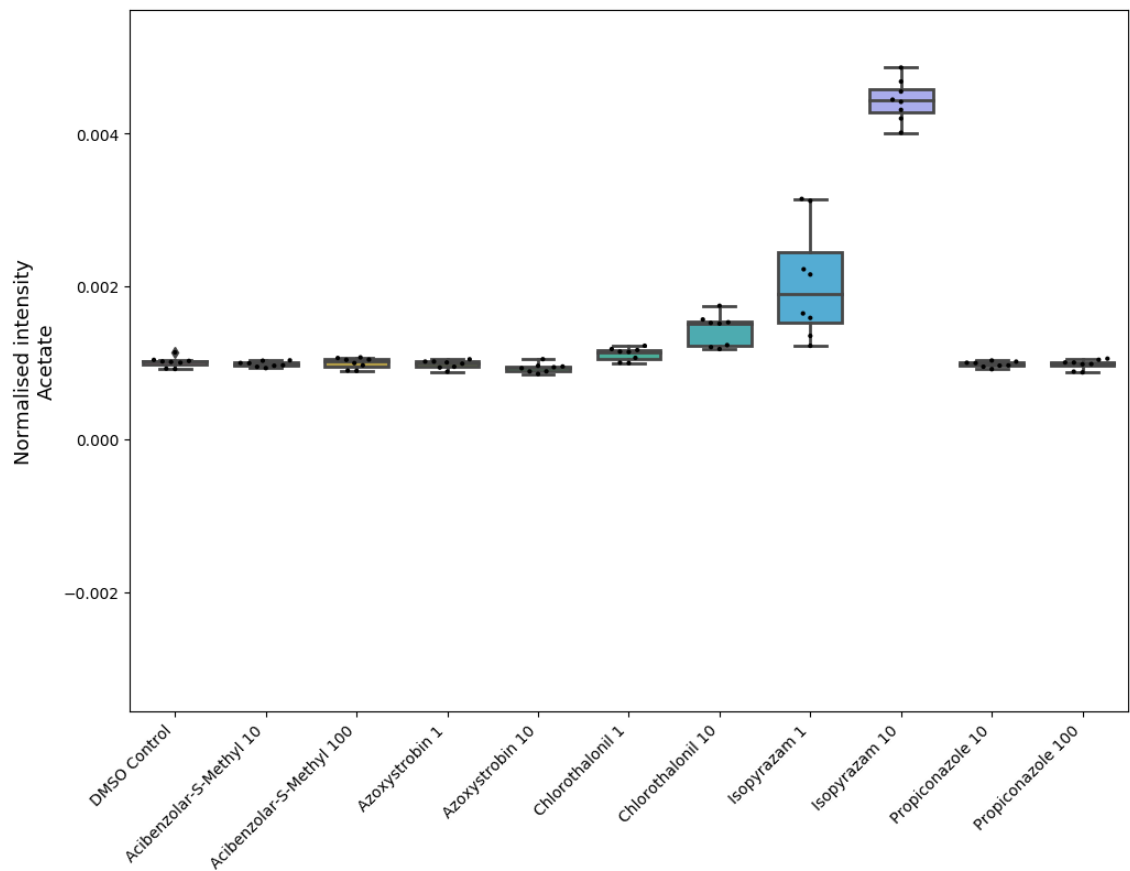


**Figure 4.19. Boxplot showing increased acetate production by BEAS-2B following 24 h to isopyrazam, in comparison to exposure to DMSO, acibenzolar-s-methyl, azoxystrobin, chlorothalonil or propiconazole (n=4).**

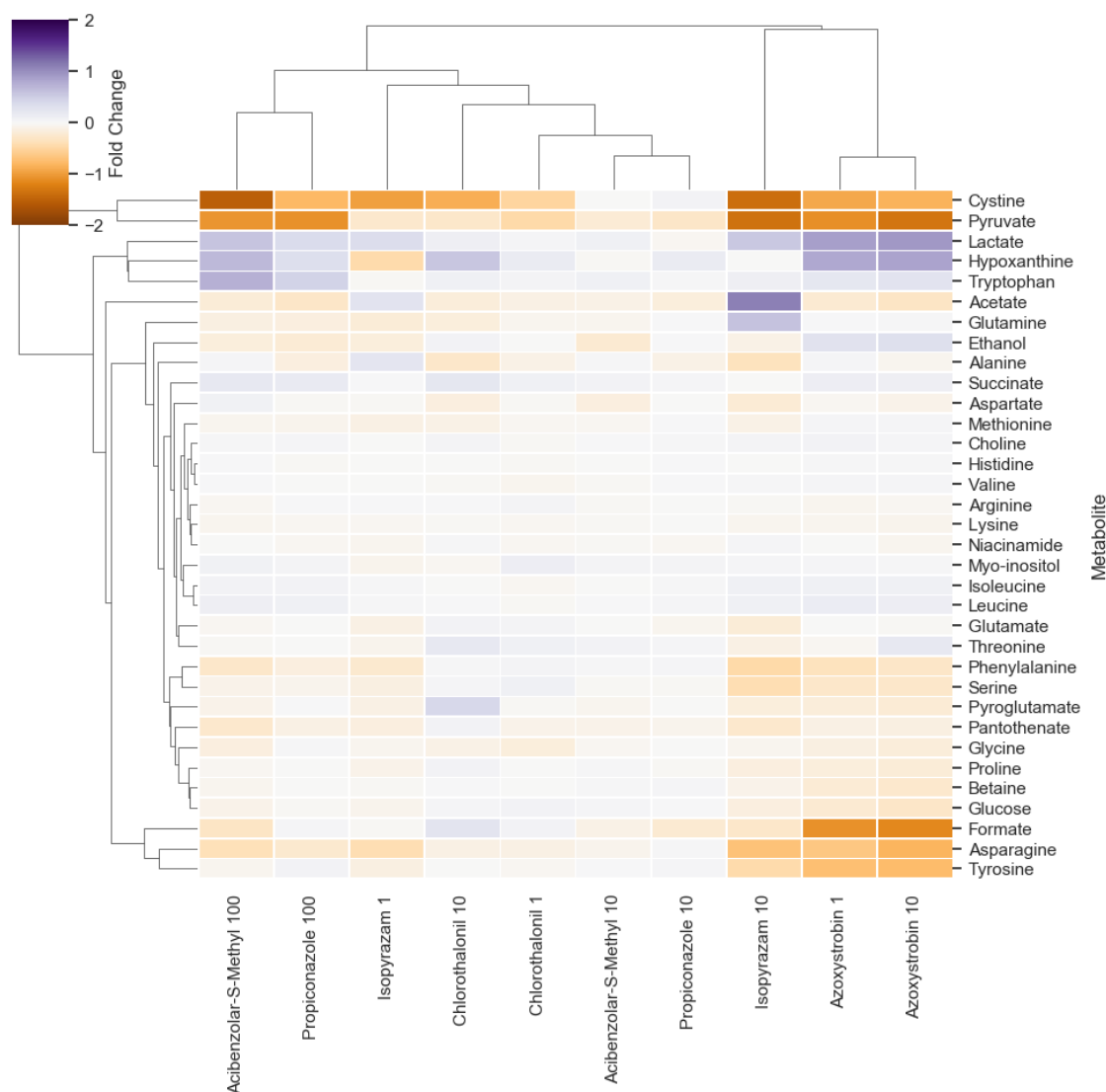


**Figure 4.20.** Differences in 16HBE14o- metabolism following 24 h exposure to the different fungicides, normalised against the 16HBE14o- DMSO control. Data shown as fold changes either represent consumption (orange) or production (n=4).

The metabolomic data for 16HBE14o- was divided into multiple clusters, representing defined changes in cell phenotype following fungicide exposure (**Figure 4.20**). Most notably, the mitochondrial inhibitors azoxystrobin and isopyrazam were group together, both concentrations of the former fungicide gave nearly identical responses, whilst isopyrazam 10  $\mu\text{M}$  was unique in causing increased acetate production, this effect was also observed with isopyrazam 1  $\mu\text{M}$ , despite this exposure being grouped in a separate cluster (**Figure 4.21**). The direct grouping of acibenzolar-s-methyl and propiconazole 100  $\mu\text{M}$  is unique to this cell line, and likely relates to its distinct phenotypic response to these two fungicides. Whilst not observed in the Alamar Blue data as the cells were grown near confluency, acibenzolar-s-methyl is able to increase cell proliferation (data highlighted and discussed in **Chapter 2**),

similarly propiconazole also causes significant but non-toxic changes to cell phenotype. Whilst acibenzolar-s-methyl and propiconazole are classified as the safest based on GHS classification in comparison to the other fungicides tested in this study, they are still capable of significant changes to cell phenotype. The acibenzolar-s-methyl and propiconazole 10  $\mu$ M exposures, were similar in that these were the only two exposures that did not result in a significant decrease in extracellular cystine in comparison to the DMSO control.

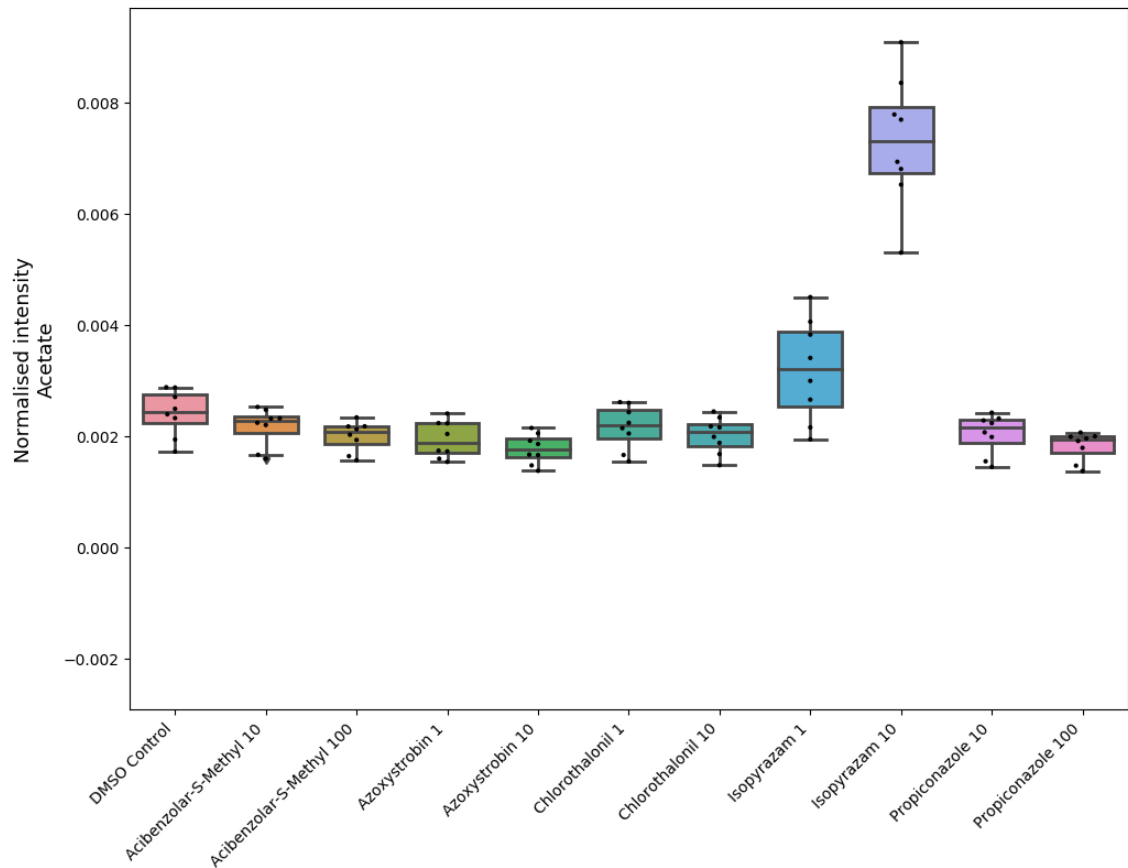


**Figure 4.21.** Boxplot showing increased acetate production by 16HBE14o- following 24 h to isopyrazam, in comparison to exposure to DMSO, acibenzolar-s-methyl, azoxystrobin, chlorothalonil or propiconazole (n=4).

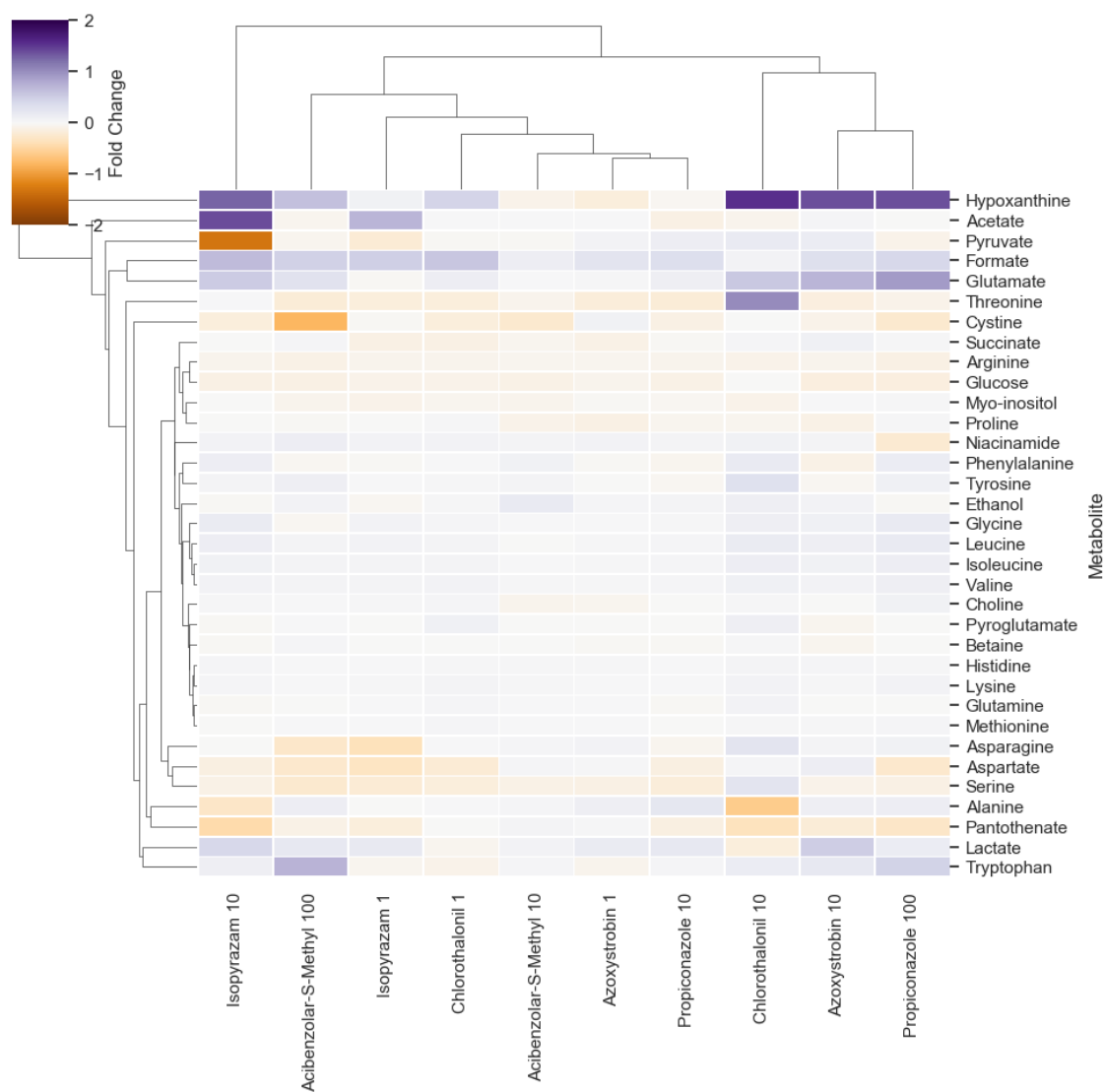


**Figure 4.22.** Differences in Calu-3 metabolism following 24 h exposure to the different fungicides, normalised against the Calu-3 DMSO control. Data shown as fold changes either represent consumption (orange) or production (n=4).

Generally, the cluster map obtained from Calu-3 data was the least informative in comparison to the other cell lines used, with the fewest recorded fold changes following different fungicide exposures. This result is consonant with previous data, showing Calu-3 to have both the slowest growth rate in addition to being the most resistant to the tested compounds based on the dose response curves obtained in **Chapter 2**. Additionally, the implications of the clustering for metabolomic data was less obvious, for example the mitochondrial inhibitors were not grouped together, lactate production only significantly increased in response to the highest tested concentrations of azoxystrobin and isopyrazam and pyruvate consumption only

significantly increased with the latter fungicide. Despite this, the previously shown effects of isopyrazam on acetate production in TT1, BEAS-2B and 16HBE14o- were replicated using the Calu-3 cell line (**Figure 4.23**). Similarly, the increased consumption of alanine following exposure to chlorothalonil 10  $\mu$ M, which was observed in all cell lines except A549, was also shown to occur in Calu-3 (**Figure 4.24**).

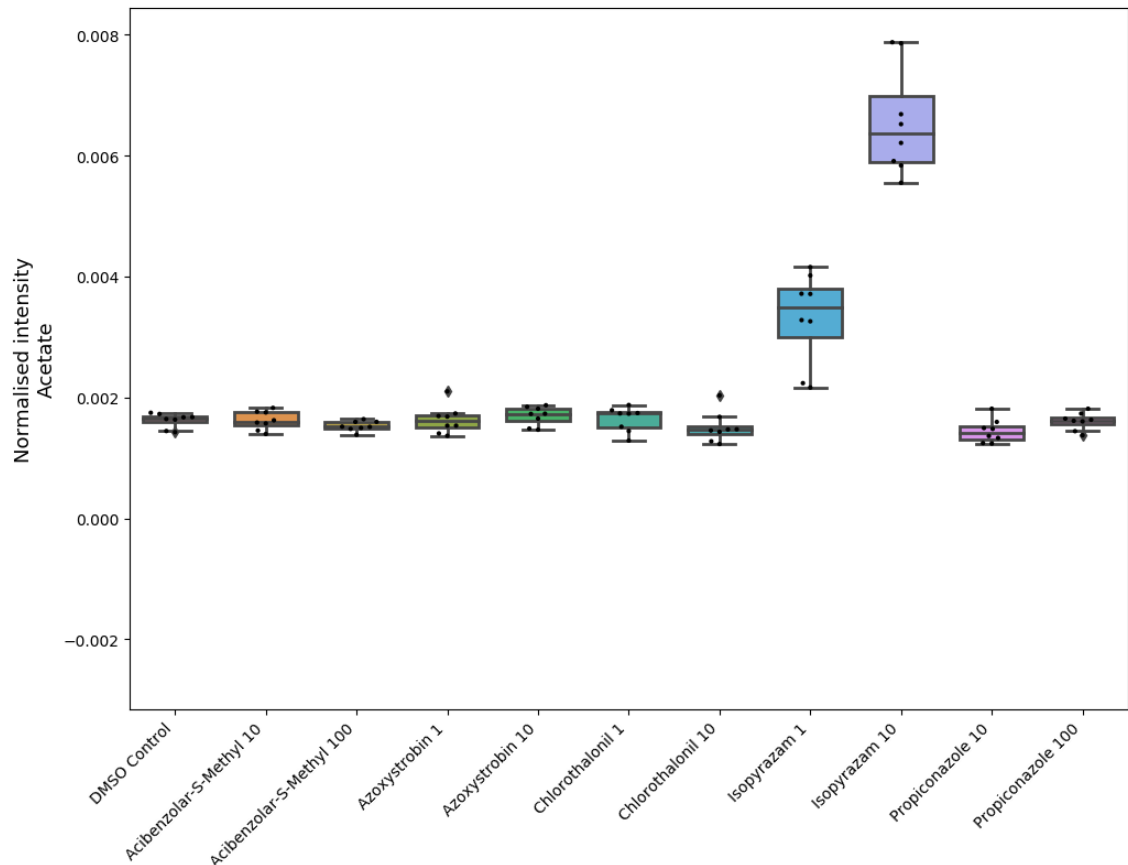


**Figure 4.23.** Boxplot showing increased acetate production by Calu-3 following 24 h to isopyrazam, in comparison to exposure to DMSO, acibenzolar-s-methyl, azoxystrobin, chlorothalonil or propiconazole (n=4).



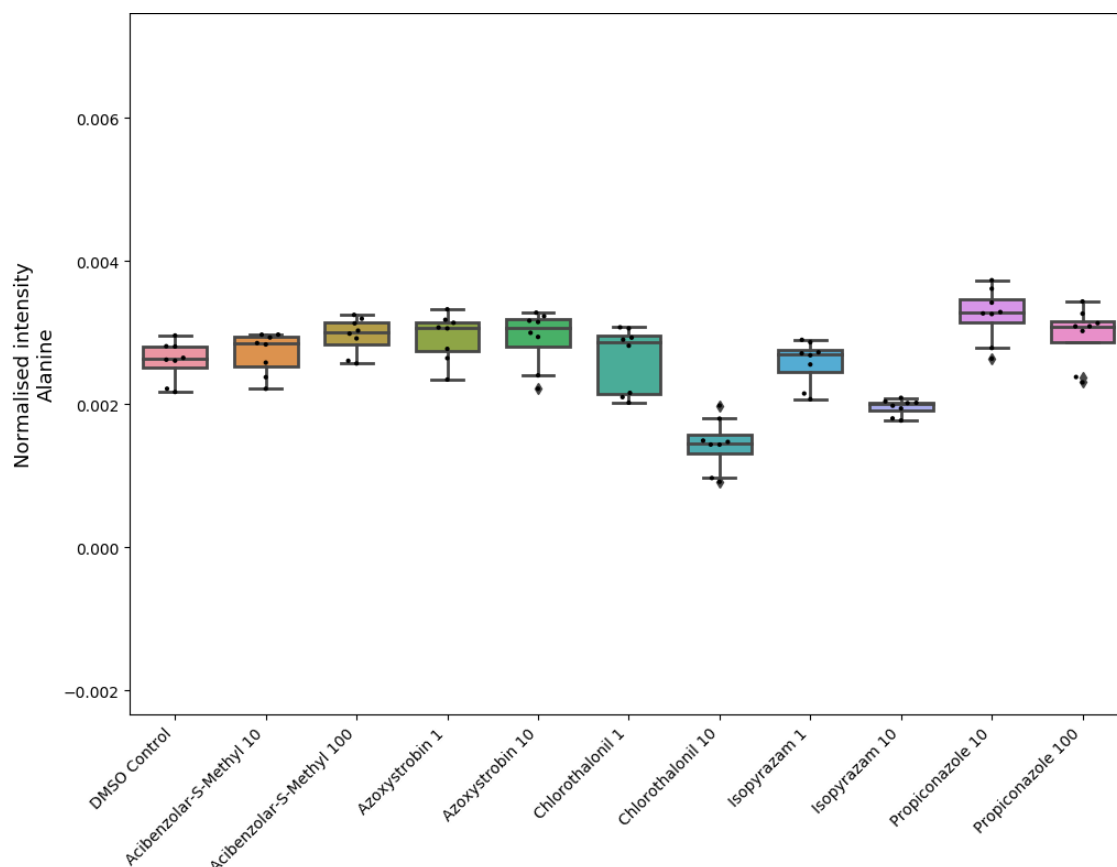


**Figure 4.24.** Boxplot showing increased alanine consumption by Calu-3 following 24 h to chlorothalonil 10  $\mu$ M, in comparison to exposure to DMSO, acibenzolar-s-methyl, azoxystrobin, chlorothalonil or propiconazole (n=4).

Additionally, hypoxanthine consumption was significantly decreased by over 3.5 fold in Calu-3 following exposure to azoxystrobin 10  $\mu$ M, chlorothalonil 10  $\mu$ M, isopyrazam 10  $\mu$ M and propiconazole 100  $\mu$ M, with this effect observed in the other cell lines also.

## 4.5 Discussion

The different cell lines cultured in this study were chosen to allow the comparison between alveolar vs bronchial, as well as “normal” immortalised vs cancer derived. Additionally, they contribute to some of the most used cell lines to model the lung epithelium (Selo et al., 2021, Forbes and Ehrhardt, 2005, Abraham et al., 2004). The inclusion of a variety of cell lines was valuable, as each of the cell lines have different phenotypes and may respond differently to xenobiotic toxicity, for example BEAS-2B has been suggested as more sensitive and specific to pulmonary toxicants and so is more predictive of respiratory toxicity than A549 (Lee et al., 2018). Similar results have been observed with 16HBE14o- being more sensitive to toxicity than A549 (Guadagnini et al., 2015), in **Chapter 2** the both BEAS-2B and 16HBE14o- were

shown to be more sensitive to pesticide toxicity than A549 or Calu-3. Therefore, if NMR metabolomics is to be used to assess pesticide-induced changes in cell phenotype, it is prudent to be aware of potential intrinsic differences in the cell line used and the subsequent implications on sensitivity and selectivity.

The combination of the different cell lines with a range of fungicides with different cytotoxicity and mechanisms of action, generated 56 test conditions. This allowed for the evaluation of whether NMR metabolomics data may be indicative of pesticide respiratory toxicity, highlight potential modes of action related to the perturbation of biochemical pathways, and also if it may indicate which cell lines give the most sensitive/identifiable responses.

#### **4.5.1 Comparison of general metabolomic responses between cell lines**

Generally, basal cell metabolism between the cell lines was similar, which is to be expected. A549 was unique in that it consumed significantly less alanine or pyruvate than the other cell lines (**Figure 4.10**), which may partially explain why the results for some of the fungicide exposures were less pronounced than in the other cell lines (**Figure 4.12**). The cell lines could at least partially be differentiated by their basal metabolism as shown in **Figure 4.8**, lending support for the sensitivity of the model to detect differences in cell phenotype based on the extracellular metabolome. Similar applications have previously been explored with regards to NMR metabolomics for the identification of cancerous cells or metabolism-associated disease biomarkers (Beger, 2013, Bamji-Stocke et al., 2018).

Prior to the identification of specific metabolite changes based on the NMR spectra, significant differences between samples were identified using OPLS-DA, with this data summarised in **Table 4.4**. Interestingly, despite the similarities between the cell lines, significant metabolomic changes were detected in all following exposure to the highest concentration of each pesticide, the normal “immortalised” cell lines 16HBE14o- and TT1 were also responsive to low concentrations of fungicides. Both of these cell lines had significant changes to their extracellular metabolome following exposure to isopyrazam 1  $\mu\text{M}$ , whilst 16HBE14o- responded to azoxystrobin 1  $\mu\text{M}$  and TT1 responded to chlorothalonil 1  $\mu\text{M}$ . These changes were at subtoxic concentrations which were not detected by the Alamar Blue cytotoxicity assay, or previously in **Chapter 2** with the MTT assay. Importantly, these 3 additional fungicide exposures which were detected by TT1 and 16HBE14o- represent the most toxic of the 5 tested fungicides based on their GHS classification. The lowest tested concentrations (10  $\mu\text{M}$ )

of the fungicides propiconazole and acibenzolar-s-methyl, which have a lower hazard classification (no respiratory concern and may cause respiratory irritation, respectively), did not induce significant changes to the extracellular metabolome of any of the cell lines as detected by OPLS-DA. Whilst further validation of this approach is needed with a wider range of compounds, these results do suggest that NMR metabolomics may be valuable in determining the potential hazard of inhaled fungicides, particularly with realistic exposure concentrations ( $\leq 10 \mu\text{M}$ ).

Even with the least sensitive cell line Calu-3, for which metabolomic changes were less obvious, significant changes were detected at concentrations lower than observed with previous assays in **Chapter 2 & 3**. However, the results presented in this study, do highlight that 16HBE14o- and TT1 may be preferable cell models in comparison to the other bronchial and alveolar cell lines used, due to their increased sensitivity.

#### **4.5.2 Metabolites of interest & potential modes of action for toxicity**

The use of extracellular rather than intracellular metabolomics allowed for a higher throughput, due to reduced sample preparation time (based on requirements of cell number, sample extraction, etc). Countering this, it is slightly less informative than assessment of the intracellular metabolome due to the reduced number of metabolites detected. For example using a similar protocol Kostidis et al. (2017) detected 45 extracellular metabolites and 65 intracellular metabolites. Whilst only 34 extracellular metabolites were detected in this present study, this is likely due to the exclusion of foetal bovine serum (FBS) from the medium (justification included in the methods section), with FBS being identified as the source of at least 6 metabolites identified in the other study. The use of intracellular metabolomics would have allowed the quantification glutathione and a range of phospholipids, which may be of particular value particularly for pesticides that stimulate ROS generation, are detoxified by glutathione conjugation (i.e. azoxystrobin & chlorothalonil) or directly affect lipid metabolism (such as 14 $\alpha$ -demethylation inhibitors like propiconazole). However, the use of extracellular metabolomics was found to be suitable for the outlined experimental aims, feasible in terms of throughput and allowed the cell samples to be stored for further analysis if necessary (i.e. mRNA analysis or intracellular metabolomics by LC-MS/NMR).

Based on the data provided in this study several metabolites of interest were identified. The effects of either mitochondrial inhibition by isopyrazam and azoxystrobin or induction of cell

proliferation by acibenzolar-s-methyl and propiconazole, were most obvious in 16HBE14o-, followed by TT1. Whilst both effects corresponded to increased consumption of pyruvate and increased production of lactate, the distinction of these phenotypic changes was clear when contextualised with previous MTT cell viability data and the greater reliance on glucose consumption in the case of mitochondrial inhibition in 16HBE14o-. Additionally, the production of acetate was significantly increased in all cell lines other than A549, following exposure to the succinate dehydrogenase inhibitor isopyrazam. This likely related to the interruption of the Krebs cycle, with excess acetate eventually being released extracellularly. Although the exact mechanism is unknown, it may be that as the Krebs cycle is inhibited, acetyl-CoA is hydrolysed to acetate which is then released extracellularly, this mechanism has been proposed *in vivo* for the release of acetate into the circulatory system (Knowles et al., 1974). More recently, increased extracellular acetate has been linked to reactions coupled with mitochondrial function (Liu et al., 2018), whereby pyruvate is converted to acetate which is used to synthesise acetyl-CoA for use in lipogenesis or acetylation (with excess acetate secreted extracellularly). As isopyrazam-induced acetate production was associated with increase pyruvate consumption, and the pesticide is a known mitochondrial inhibitor this may be a more likely mechanism. Additionally, this mechanism was shown to occur during mitochondrial dysfunction, and the conversion of pyruvate to acetate was shown to occur via coupling with ROS, this may be the case following isopyrazam exposure, as this fungicide has been shown to cause oxidative stress *in vivo* (Yao et al., 2018). However, this does not fully explain why acetate production was not increased following exposure to the mitochondrial inhibitor azoxystrobin.

Whilst increased acetate production was unique to exposure to isopyrazam, chlorothalonil specifically caused an increase in alanine consumption, with this effect most evident in TT1 (**Figure 4.17**), partially explaining the significant changes to the metabolome of this cell line following exposure to both chlorothalonil 1 and 10  $\mu$ M. As basal consumption of alanine by A549 was shown to be significantly lower than in TT1, this may be one reason that metabolomic changes in A549 are less obvious following exposure to chlorothalonil 1  $\mu$ M (**Figure 4.9**). Whilst chlorothalonil 10  $\mu$ M exposure significantly reduced TT1 viability (17.9% based on Alamar Blue data), the depletion of alanine, likely took place before cell death both as it is not released back into the cell medium and also as Calu-3 which experienced no decline in cell viability with this exposure, also had significantly lower extracellular alanine in comparison to the DMSO control. Whilst the reason for increased alanine consumption could not be determined, most of the other amino acids were in excess whilst alanine was limited,

which may also explain why no relationship could be established between the other amino acids and alanine consumption. It is also possible that chlorothalonil either inhibited enzymes needed for the biosynthesis of alanine or due to non-specific protein binding of chlorothalonil, the cells required alanine to synthesise new proteins.

Another metabolite of interest was niacinamide, which was almost completely consumed following exposure to propiconazole 100  $\mu$ M, but only in TT1 and BEAS-2B. Niacinamide is a precursor to NADP<sup>+</sup> which is used intracellularly in a multitude of redox reactions, therefore the specific cause of this change could not be identified. Finally, two sensitive biomarkers of metabolomic change were cystine and hypoxanthine. The mechanism could not be identified but cystine consumption was significantly increased in all the non-cancer derived immortalised cell lines following exposure to the highest tested concentration of azoxystrobin, acibenzolar-s-methyl, chlorothalonil and propiconazole. This effect may relate to increased ROS or redox reactions, with cystine being converted to cysteine intracellularly (**Figure 4.7**).

The extracellular concentration of hypoxanthine was frequently higher in fungicide exposed samples in comparison to the DMSO control, this effect was observed regardless of the cell line used (**Figure 4.12-Figure 4.22**). There are many possible reasons for this, the first being that healthy and actively dividing cells consumed more of this as part of purine metabolism or an intermediate for DNA synthesis. However, even in samples for which cell proliferation was expected to increase (such as 16HBE14o- exposed to acibenzolar-s-methyl), there was still a higher hypoxanthine concentration than in the DMSO control.

Another potential reason is that xanthine oxidase is a superoxide-producing enzyme which may oxidise hypoxanthine to xanthine and in the process create ROS, and reduced activity of this enzyme may help decrease endogenous ROS formation, with this being protective in cells exposed to various xenobiotics (Park et al., 2009, Kayyali et al., 2003, Saito et al., 2005).

Whilst, further studies would be required to determine the cause of increased extracellular hypoxanthine, it is of interest as this has been explored *in vivo* as a biomarker of acute respiratory distress syndrome, oxidative stress (Quinlan et al., 1997, Zhang et al., 2000).

Additionally two *in vivo* metabolomic studies also identified it as a biomarker of acute lung injury in rats and mice, with the latter study describing a similar increase in extracellular hypoxanthine (Cui et al., 2016, Xiong et al., 2018).

Although the results of metabolite changes were sometimes challenging to interpret or relate to particular biochemical pathways, the data did highlight specific metabolomic changes following fungicide exposure, which were sensitive and reproducible across the different cell lines. From a risk assessment perspective, even prior to metabolite identification, the use of metabolomics in the form of OPLS-DA data is useful in determining potential phenotypic changes, that may be more sensitive for determining the NOAEL than other assays. Furthermore, with the identification of metabolites the mechanism of action for pesticide toxicity may start to be explored further.

## **4.6 Conclusion**

In summary NMR metabolomics represents a promising method for determining changes to cell phenotype following sub-cytotoxic fungicide exposure. Whilst other methods such as LC-MS or even intracellular NMR metabolomics may be more informative due to increased sensitivity and the quantification of a wider range of metabolites, which may be of particular benefit to elucidating potential toxicity mechanisms and adverse outcome pathways, this current method provides the benefit of being sensitive enough to identify changes in metabolomic response between chemical compounds and across cell lines. In addition it also allows greater sample throughput due to reduced sample preparation. Additionally, the data presented in this study provides initial evidence of metabolomic differences between the non-cancer derived and cancer derived cell lines commonly used to model the respiratory epithelium, both in terms of basal metabolism and following fungicide exposure. This may inform future metabolomic experiments with these models and may also highlight NMR metabolomics as a useful method for determining the similarities between these models and their primary cell alternatives. The outlined metabolomic method for the detection of phenotypic changes to the cell lines following exposure to occupationally relevant concentrations, as determined in the previous chapter, may be of use for future risk assessments.

## General Discussion

### 5.1 Original Premise

Chemical risk assessments are a necessary component of regulating xenobiotic exposures within the occupational and environmental setting. The importance of this is highlighted by the number of regulatory bodies responsible, including the US Environmental Protection Agency founded in 1970, the European Food Safety Authority established in 2002 and the European Chemicals Agency formed in 2007 (Herman et al., 2019, Lewis, 1985, Martin and Julian, 2020). Whilst various chemicals are regulated at a national level, the use of a globally harmonised system for the classification and labelling of chemicals (GHS) allows for the classification of chemicals based on toxicological assessments for relative hazard (Winder et al., 2005). As inhalation exposure represents one of the three main chemical exposure routes; acute toxicity data is required and currently this relies on the use of *in vivo* rodent models. This is both expensive and time demanding and so there has been an increased focus on alternative approaches (Clippinger et al., 2018b), including toxicokinetic modelling for chemical risk assessment (Andersen, 2003). Currently, this approach is more established for oral exposures, but they are likely to become relevant to the assessment of inhaled toxicology in the future.

Currently, the European Food Safety Authority (EFSA) state that pesticide respiratory bioavailability must be assumed to be 100% (EFSA, 2014b), and whilst this is a conservative approach, research methods that suggest more appropriate, evidence-based estimates are required. More recently EFSA have shown a greater willingness for the use of mechanistic evidence in regulatory pesticide risk assessment (Pelkonen et al., 2019), and other regulatory bodies such as the EPA and OECD have also shown increased receptiveness to the use of *in vitro* models for chemical risk assessments (Corley et al., 2021, Jackson et al., 2018, Natsch et al., 2021). Based on the available literature, it seems likely that current occupational exposure risk assessments can be improved by utilising an evidence-based approach considering: regional aerosol deposition, the suitability of *in vitro* models to predict respiratory toxicity and transepithelial permeability, the use of *in silico* models to predict respiratory toxicokinetics and the contextualisation of *in vitro* toxicity data based on realistic exposure concentrations. The

work in this thesis aimed to explore these issues, with the aim of improving pesticide exposure risk assessments for occupational inhalation.

The pesticides used in this study, include; acibenzolar-s-methyl, abamectin, azoxystrobin, chlorothalonil, diquat, isopyrazam, pinoxaden, propiconazole and prosulfocarb, which represent some of the most commonly sprayed pesticides globally (Casida and Bryant, 2017, Singh and Merchant, 2012, European Food Safety et al., 2020). Each of the selected pesticides is from a different chemical class and has a unique mode of action. The compounds of interest were selected to give variable toxicity within the different cell line models used. The effect of aerosol deposition, and different physicochemical properties of the inhaled pesticide on respiratory toxicokinetics was explored further using the semi-mechanistic Mimetikos Preludium *in silico* model. Additional insights into the significance of this predicted exposure data were gained through additional toxicity assays and the assessment of changes to cell phenotype using extracellular <sup>1</sup>H-NMR metabolomics.

## **5.2 Local respiratory toxicity and bioavailability of inhaled pesticides**

The aims of this thesis were achieved by exploring the suitability of *in vitro* models to estimate respiratory cytotoxicity, in addition to xenobiotic permeability and metabolism, along with the *in silico* prediction of respiratory toxicokinetics. The key findings are outlined below in relation to the experiments within this thesis.

In **Chapter 2**, the main research question centred around which *in vitro* model was most suitable for the study of local toxicity, transepithelial permeability and *in situ* metabolism. The data clearly highlighted Calu-3 to be the most suitable for transepithelial permeability measurements, based on tight junction function, TEER values and exclusion of paracellular permeability markers (sodium fluorescein and FITC dextran MW-4000). This conclusion is strongly supported by the literature, which highlight it is a representative model of the bronchial epithelial barrier and well suited for xenobiotic permeability assays (Kreft et al., 2015a, Inoue et al., 2020b, Grainger et al., 2006). In contrast, whilst the permeability barrier formed by TT1 excluded sodium fluorescein to a similar extent as Calu-3 and the TT1 TEER values achieved were double those reported by van den Bogaard et al. (2009), confocal microscopy failed to show well defined or functional expression of ZO-1. Furthermore, other efforts to increase TT1 barrier function, including pre-coating with basement membrane extract, coculturing with 3T3 or the addition of synthetic lung fluid apically, did not elicit more positive results. In contrast the acellular permeability barriers formed by PAMPA and the novel



rat lung lipid extract method, showed comparable exclusion of the hydrophilic paracellular permeability markers sodium fluorescein and FITC dextran MW-4000. A549 yielded results comparable to those reported by other researchers and were, therefore, not ideal for xenobiotic permeability. Similarly, RPMI-2650 yielded low TEER values, as has been reported previously, however methods to improve upon this e.g. supplementation with retinoic acid or hydrocortisone, were not attempted (Bai et al., 2008, Kürti et al., 2013). Despite the low TEER values, these were in the range reported for human excised nasal mucosa (40-120  $\Omega\cdot\text{cm}^2$ ), which have also been found to correlate with the primary nasal epithelial MucilAir model (Sibinovska et al., 2019), therefore it may still prove useful for future studies on the nasal epithelium.

In addition to the suitability of Calu-3 for studying xenobiotic permeability, functional enzyme activity studies presented in this thesis also revealed it to be the most suitable for studying xenobiotic metabolism. Crucially, of the respiratory epithelial cell lines it was the only one with combined functional expression of both CYP2B6 and CYP3A5, with these enzymes contributing considerably to pesticide metabolism for a wide range of substrates (Abass et al., 2012, Hodgson and Rose, 2007). Although A549 did have functional CYP3A5 activity, which has also been reported by other researchers (Wu et al., 2017, Hukkanen et al., 2000), this was significantly lower than Calu-3 overall. The overall enzyme activity profile of A549 was also considerably less than the type I like alveolar cell line TT1, particularly for CYP1A2, NQO1 and GST. Providing initial evidence that TT1 might be a more suitable model the assessment of alveolar xenobiotic metabolism.

TT1, was also more sensitive to pesticide cytotoxicity than A549, as assessed by the MTT assay for the 8 different pesticides. This was found to be the case for all the non-cancer derived cell lines, suggesting that as A549, Calu-3 and RPMI-2650 are more resistant to pesticide cytotoxicity than BEAS-2B, TT1 and 16HBE14o- which might therefore represent more sensitive and suitable models for toxicity risk assessments. The results support Calu-3 being used as a permeability and metabolism model of the bronchial epithelium, as has been stated in the literature (Ehrhardt et al., 2008, Enlo-Scott et al., 2021b), however, it also highlights that TT1, BEAS-2B or 16HBE14o- may be better suited for toxicity assays due to their increased sensitivity. Overall, the research objectives in **Chapter 2**, were achieved and the findings were employed in the experimental design of **Chapter 3**.

The key objective of **Chapter 3**, was to illustrate an evidence-based approach for the prediction of the respiratory bioavailability of pesticides inhaled during occupational exposure. This objective built on the preliminary data obtained in the previous chapter, which identified 4 potential permeability barriers (Calu-3, Caco-2, PAMPA and rat lung lipid extract) suitable for providing permeability data which can be integrated with the *in silico* modelling approaches.

Through the use of deposition modelling, along with the input of data obtained experimentally *in vitro*, the predicted respiratory bioavailability was shown to vary significantly dependent on the physicochemical properties of the pesticide. This provides strength to the hypothesis that respiratory bioavailability is unlikely to be 100% for a realistic occupational exposure, and is instead determined by regional aerosol deposition, physicochemical properties of the pesticide and their interaction with physiologically relevant processes such as transepithelial permeability, tissue and plasma protein binding. This was especially evident in the case of chlorothalonil, for which *in vitro* measurements were particularly important, as chemical reactivity and increased protein binding was not predicted by the *in silico* pCEL-X model. Overall, in the absence of *in vitro* data, the pCEL-X model was highlighted as a useful alternative, both for the tested compounds and also for highlighting how potential xenobiotic metabolism may reduce their passive permeability.

The prediction of luminal and epithelial concentrations of the tested fungicides, provided context for the *in vitro* toxicity assays performed in **Chapter 2**, including the potential for epithelial damage illustrated in **Chapter 3**, and also ensured that subsequent experiments performed in **Chapter 4** included relevant test concentrations of 1  $\mu\text{M}$  and 10  $\mu\text{M}$  (100  $\mu\text{M}$  exposures were only used in the cases of acibenzolar-s-methyl and propiconazole, to demonstrate that metabolomic changes do occur, albeit not at relevant exposure concentrations).

Finally, in **Chapter 4** the main research objective was to explore if NMR metabolomics was a sensitive measure of changes to lung cell phenotype following pesticide exposure at subtoxic concentrations. This objective was accomplished, with the caveat that only the extracellular metabolome was tested, and a greater number of metabolites (and potentially greater sensitivity to phenotypic changes) might have been achieved by also including the intracellular metabolome, or LC-MS based approaches had been adopted. Of interest, prior to metabolite identification, PCA and OPLS-DA statistical analysis revealed that each cell line was significantly

different to each other based on their extracellular metabolome (complete set of OPLS-DA data shown in the appendix). This provided initial support for this experimental method being sensitive to differences in cell phenotype, as it was capable of discriminating NMR spectral differences between the different cell lines. Whilst this has been demonstrated for comparisons between normal and cancerous cells (Bernacchioni et al., 2017, Čuperlović-Culf et al., 2010a), the data in the study presents the first data comparing this combination of respiratory epithelial cell lines.

Overall, the data presented in this study highlighted that subtoxic changes in cell phenotype could be identified by NMR metabolomics following fungicide challenge. Furthermore, that the cell lines responded differently depending on the fungicide, for example metabolomic changes in 16HBE14o- were more evident following exposure to 1  $\mu$ M azoxystrobin than for any other cell line, whilst changes in extracellular alanine were most commonly observed in A549 cells. However, an additional research question was whether the “normal” immortalised cell lines would be more sensitive than the cancer-derived cell lines to the fungicides, as had been observed in prior toxicity assays. Whilst the use of “normal” immortalised cell lines TT1 and 16HBE14o- resulted in significant phenotypic changes for 7/10 of the exposures, the other cell lines only detected 5/10, however a wider range of test compounds and exposure concentrations is needed to confirm this result. It is notable however, that no phenotypic changes were detected in any of the cell lines following exposure to 10  $\mu$ M acibenzolar-s-methyl and propiconazole, the fungicides with the lowest toxicity and GHS classification.

### 5.3 Contribution to knowledge

The existing literature has extensively explored the applicability of *in vitro* respiratory models for toxicity and absorption testing, from the perspective of inhaled drug delivery. This thesis, applies many of these techniques for their application to pesticide related occupational risk assessments, for which the methods highlighted in **Chapters 2-4** have typically not been applied previously. Overall, the presented data highlights an evidence-based approach that with further validation, may be used to improve predictions of respiratory toxicity and bioavailability, to inform occupational exposure risk assessments and in the long-term reduce, replace or refine the use of animal models currently used for this purpose.

More specifically, the data included in this thesis makes several new contributions to the field. This thesis presents the first functional activity studies of xenobiotic metabolising enzyme

(XME) activity in the alveolar model TT1, which was shown to have a comparatively wider enzyme expression profile than the more commonly used A549 alveolar model. Similarly, although BEAS-2B is more widely used, it also highlights the suitability of Calu-3 as a bronchial metabolism model, although this has been shown partially based on CYP mRNA data (Ehrhardt et al., 2008, Oesch et al., 2019), this study confirms this based on functional activity, and also includes NQO1 and GST activity. Additionally, whilst XME data has been published in terms of mRNA transcripts and western blotting, functional activity data for this range of respiratory epithelial cell lines is less widely available (Enlo-Scott et al., 2021a, Oesch et al., 2019). Importantly, the method developed in this thesis which involved producing S9 fraction from the harvested epithelial cell lines, resulted in concentrated lung relevant XME samples with significantly higher functional activity over commercially available lung S9 (data shown in the appendix). Lung epithelial S9 is likely an improved method for determining lung epithelial metabolism, compared with commercially available lung S9, which is taken from whole lung homogenate and therefore diluted with non-metabolically competent cells.

With regards to TT1 cells, the data presented in this thesis is one of the few studies to experimentally determine its suitability as a permeability barrier and the first to attempt to look at P-glycoprotein activity in this model (van den Bogaard et al., 2009).

Whilst the approach in **Chapter 3**, is relatively common for drug delivery it is novel for occupational exposure assessments for pesticides, although there is emerging work investigating an evidence-based approach with regards to pesticide aerosol deposition and epithelial exposure concentrations (Corley et al., 2021). Furthermore, the developed procedures for the lung lipid extract model and for the prediction of airway surface liquid binding are novel. Particularly, for the ASL binding assay, the importance of this data to *in silico* modelling and implications for xenobiotic bioavailability and the extent of mucociliary clearance should not be understated.

Finally, the data presented in **Chapter 4** provides one of the few metabolomic comparisons between respiratory epithelial cell lines and provides novel data not just in regards to pesticide-induced phenotypic changes, but also more generally as an approach to assessing differences in lung epithelial cell phenotype (either between different models, or following xenobiotic exposure to a range of chemicals). This lends additional support to research investigating the suitability of metabolomic approaches for regulatory toxicology applications or chemical risk assessment (Hernández-Mesa et al., 2021, Olesti et al., 2021).

Despite some experimental limitations and the need for future work, the above represents several contributions to the existing literature, particularly with regards to *in vitro* respiratory toxicity, absorption, and metabolism models.

## 5.4 Experimental limitations

Ideally many of the results presented in **Chapter 2** would include direct comparisons with primary cells, this was unfortunately limited by resource availability and time constraints (based on the 6 respiratory epithelial cell lines that were tested). However, comparison against literature data was considered sufficient to ensure that the data obtained for the cell lines was comparable to what might be found *in vivo*.

Additionally, for the testing of P-glycoprotein activity in TT1, the study would have benefited from a lower Rh-123 concentration, i.e. 1-5  $\mu\text{M}$  to avoid potentially saturating P-glycoprotein, particularly where expression is likely lower than for other cell lines such as Caco-2. Additional experiments, looking not only at bidirectional transport but also efflux/accumulation would complement this data. Ideally, MRP2 and BRCP activity would have also been studied.

For the metabolism-based experiments, whilst the data presented in **Chapter 2** highlights functional activity of the specific enzymes studied, in **Chapter 3** had the resources been available pesticide metabolite identification by LC-MS following azoxystrobin, chlorothalonil or propiconazole incubation with Calu-3 would have been valuable. The use of radiolabelled pesticides was deemed suitable to exclude the effects of metabolites not being detected in the basolateral samples, and whilst this was ideal from a permeability perspective, data showing pesticide metabolism via a bronchial cell line would have provided a direct example of non-absorptive clearance, rather than using surrogate readouts based on standard markers (resorufin-based CYP substrates).

With regards to **Chapter 3**, the use of an *in vivo* study investigating differences in respiratory bioavailability based on pesticide physicochemical properties, would have proved very valuable as a method for validating the *in vitro-in silico* approach. This will likely represent a major focus for future experiments.

Overall, for **Chapter 4**, the main limitation was that intracellular metabolomics was not studied, as this would have provided a greater range of identified metabolites, including the ability to look at glutathione depletion (the mode of action for chlorothalonil) in addition to changes in intracellular lipids (which may have been affected by low concentrations of

propiconazole). Intracellular metabolomics was not performed due to the requirement to culture a considerably larger volume of cells to obtain a sample, in addition to the extra processing time and equipment required to extract and purify the NMR sample. This would have significantly reduced the number of samples that could have been analysed, and therefore with the time and resources available it was more prudent to focus on the extracellular metabolome, which preliminary experiments had highlighted as being capable of elucidating differences in phenotype, albeit slightly less informative due to the reduced number of metabolites identified. Although the equipment was not accessible at the time the research was performed, the above issue may be circumvented by using LC-MS metabolomics, which is readily available in other labs and for which a smaller volume of sample is required due to the technique's increased sensitivity. Additionally, the study would have benefited from a wider range of test concentrations, to allow for a dose response curve to be obtained. Once again, the use of primary cells would have proved valuable to explore, if the cell lines were comparably sensitive to pesticide-induced changes to the metabolome, and also to explore if the "normal" immortalised cell lines used in this study had a metabolome more similar to primary alveolar/bronchiolar cells than the cancer-derived cell lines. Despite these limitations, the findings presented from the existing experimental work, highlight several interesting research avenues for future experiments.

## 5.5 Future work

With regards to experimental work, the primary focus for future work should centre around the further characterisation of the *in vitro* models used, and the validation of the approaches used, either through replication of the findings in primary epithelial cells or highlighting an *in vitro-in vivo* correlation for the toxicokinetic aspect of the work. The key aspects of the experimental work are summarised in **Table 5.1**. The necessity for this research relates to the need to further explore the suitability of the models used, but also consideration of the precise requirements for future chemical risk assessments and regulatory toxicology, i.e. standardisation and more extensive validation. Central to the decision-making process will be modelling the exposure and toxicokinetics of the inhaled xenobiotic, followed by toxicodynamic considerations such as chemical-induced molecular initiating events or cellular key events, that have implications on an tissue/organ level. The approach highlighted in this thesis includes aspects of this, but may be expanded upon further, as components of a regulatory decision tree for classifying the extent of the hazard posed by the inhaled xenobiotic (Clippinger et al., 2018a).

**Table 5.1. Summary of possible future research considerations, referencing similar work or suggestions from other researchers in the field, with relevance to the techniques used in this thesis and improvements necessary to better predict respiratory toxicity and bioavailability.**

<b>General research</b>	<b>Specific improvements</b>	<b>Reference</b>
<b>Non-absorptive clearance mechanisms</b>	Further characterisation of xenobiotic metabolism and drug transporters by respiratory epithelial cells, focusing on functional activity and relevant exposure concentrations.  Assessment of mucociliary clearance <i>in vitro</i> .	(Ehrhardt et al., 2017, Enlo-Scott et al., 2021a, Oesch et al., 2019)  (Inoue et al., 2018)
<b>Rat lung lipid extract</b>	Lipidomic analysis to identify key lipids in the lung lipid extract to create a defined lung relevant PAMPA formulation. A synthetic formulation will increase throughput and reduce both biological variability and the use of animal tissue.  Evaluate correlation with <i>in vivo</i> data for compounds that are not actively transported.	(Abbott et al., 2013)  (Bicker et al., 2016)
<b><i>In vivo</i> toxicokinetic studies</b>	<i>In vivo</i> studies would be useful for validation of the PBPK model, with regards to differences in pesticide bioavailability. This would also provide inputs for clearance parameters.	(Lin et al., 2017, Ren et al., 2021)
<b><i>In silico</i> prediction of toxicity, metabolism and permeability</b>	Test a wider range of compounds to confirm “predictiveness” between <i>in vitro</i> and <i>in vivo</i> data.	(Enlo-Scott et al., 2021a, Kirchmair et al., 2015, Yusof et al., 2014)
<b>Metabolomics</b>	Combination of extracellular and intracellular metabolomics. To better encompass the full range of metabolomic changes.  Evaluation of a greater range of test concentrations to identify the NOEL/NOAEL.	(Kostidis et al., 2017)  (Keller et al., 2019)

## 5.6 Conclusion

The data presented in this thesis provides evidence that respiratory toxicity and bioavailability in an occupational exposure setting is highly dependent on the exposure scenario and compound of interest. The suite of *in vitro* models used in this thesis, along with the *in silico* modelling approach, demonstrate their suitability for informing occupational risk assessments, and predicting the toxicokinetic fate of inhaled pesticides.

The selection of physiologically relevant *in vitro* models of the respiratory tract are key and the data highlights that whilst Calu-3 may be useful for metabolism and permeability studies, the use of non-cancer derived cell lines for studying toxicity may be beneficial due to increased xenobiotic sensitivity.

Additionally, with regards to the body of evidence presented in this thesis based on *in vitro* and *in silico* data, it is clear that respiratory bioavailability varies significantly based on regional aerosol deposition, and competing ADME interactions, including non-absorptive clearance mechanisms. Where the MMAD of the pesticide aerosol is 35  $\mu\text{m}$  (GSD =1.5), based on the extent of aerosol deposition in the upper respiratory tract, respiratory absorption is unlikely to be 100%, but overall bioavailability may approach this in cases where significant mucociliary clearance followed by high oral bioavailability is the case (for example with propiconazole). Furthermore, toxicokinetic data other than bioavailability predictions are of great relevance to occupational exposure assessments. The *in silico* prediction of relevant pesticide concentrations at the epithelial surface of the respiratory tract, provided valuable information in contextualising the effects observed *in vitro*, including cytotoxicity, XME induction/inhibition, glutathione depletion, mitochondrial inhibition, epithelial damage and metabolomic changes. The cellular effects observed following exposure to azoxystrobin, chlorothalonil and isopyrazam ( $\leq 10 \mu\text{M}$ ) observed by NMR metabolomics, reveal this to be a method that can contribute to inhaled chemical risk assessments and aid in the elucidation of potential mechanisms of toxicity. Despite the need for further studies including a wider range of test concentrations and the use of intracellular metabolomics in combination with other markers of adverse response, this method provides initial support for the identification of extensive biochemical changes to cell phenotype, along with defined effects such as mitochondrial inhibition.

Overall, the work presented in this thesis, provides a solid foundation for future research in this area, and strong arguments for further incorporation of *in vitro* and *in silico* models for respiratory occupational exposure risk assessments and regulatory toxicology.



## References

- ABASS, K., TURPEINEN, M. & PELKONEN, O. 2009. An evaluation of the cytochrome P450 inhibition potential of selected pesticides in human hepatic microsomes. *Journal of Environmental Science and Health, Part B*, 44, 553-563.
- ABASS, K., TURPEINEN, M., RAUTIO, A., HAKKOLA, J. & PELKONEN, O. 2012. Metabolism of pesticides by human cytochrome P450 enzymes in vitro—a survey. *Insecticides—advances in integrated pest management*, 165-194.
- ABBOTT, S. K., JENNER, A. M., MITCHELL, T. W., BROWN, S. H. J., HALLIDAY, G. M. & GARNER, B. 2013. An Improved High-Throughput Lipid Extraction Method for the Analysis of Human Brain Lipids. *Lipids*, 48, 307-318.
- ABRAHAM, G., KNEUER, C., EHRHARDT, C., HONSCHA, W. & UNGEMACH, F. R. 2004. Expression of functional  $\beta$ 2-adrenergic receptors in the lung epithelial cell lines 16HBE14o–, Calu-3 and A549. *Biochimica et Biophysica Acta (BBA) - Molecular Cell Research*, 1691, 169-179.
- ABU-QARE, A., ELMASRY, E. & ABOU-DONIA, M. 2003. A role for P-glycoprotein in environmental toxicology. *Journal of Toxicology Environmental Health*, 6, 279-288.
- AGU, R., MACDONALD, C., COWLEY, E., SHAO, D., RENTON, K., CLARKE, D. B. & MASSOUD, E. 2011. Differential expression of organic cation transporters in normal and polyps human nasal epithelium: Implications for in vitro drug delivery studies. *International Journal of Pharmaceutics*, 406, 49-54.
- AKHUEMOKHAN, P., SWEDROWSKA, M., WILLIAMS, J., HARVEY, R. & FORBES, B. Developing Alternative Models for in vitro Investigation of Excipient Influence on Drug Transport. *JOURNAL OF AEROSOL MEDICINE AND PULMONARY DRUG DELIVERY*, 2019. MARY ANN LIEBERT, INC 140 HUGUENOT STREET, 3RD FL, NEW ROCHELLE, NY 10801 USA, A12-A12.
- AL-GHABEISH, M., SCHEETZ, T., ASSEM, M. & DONOVAN, M. D. 2015. Microarray Determination of the Expression of Drug Transporters in Humans and Animal Species Used for the Investigation of Nasal Absorption. *Molecular Pharmaceutics*, 12, 2742-2754.
- ALI, M. 2010. CHAPTER 9 - Pulmonary Drug Delivery. In: KULKARNI, V. S. (ed.) *Handbook of Non-Invasive Drug Delivery Systems*. Boston: William Andrew Publishing.
- ALIFERIS, K. A. & CHRYSAYI-TOKOUSBALIDES, M. 2011. Metabolomics in pesticide research and development: review and future perspectives. *Metabolomics*, 7, 35-53.
- ANAND, U., PARIKH, A., UGWU, M. C. & AGU, R. U. 2014. Drug transporters in the nasal epithelium: an overview of strategies in targeted drug delivery. *Future Medicinal Chemistry*, 6, 1381-1397.
- ANDERSEN, M. E. 2003. Toxicokinetic modeling and its applications in chemical risk assessment. *Toxicology Letters*, 138, 9-27.
- ANNESI-MAESANO, I. 2017. The air of Europe: where are we going? *European Respiratory Review*, 26, 170024.
- APVMA 2007. Evaluation of the new active acibenzolar-S-methyl in the product Bion plant activator seed treatment. *Australian Pesticides and Veterinary Medicines Authority*.
- ARENA, M., AUTERI, D., BARMAZ, S., BELLISAI, G., BRANCATO, A., BROCCA, D., BURA, L., BYERS, H. & CHIUSOLO, A. 2018. Peer review of the pesticide risk assessment of the active substance chlorothalonil. *European Food Safety Authority*, 16, e05126.
- ARMITAGE, J. M., HUGHES, L., SANGION, A. & ARNOT, J. A. 2021. Development and intercomparison of single and multicompartment physiologically-based toxicokinetic models: Implications for model selection and tiered modeling frameworks. *Environment International*, 154, 106557.

- ARMSTRONG, L. 2018. Pluripotent stem cells for drug discovery and toxicity assessment. *Applied In Vitro Toxicology*, 4, 69-79.
- ARTS, J. H. E., MUIJSER, H., JONKER, D., VAN DE SANDT, J. J. M., BOS, P. M. J. & FERON, V. J. 2008. Inhalation toxicity studies: OECD guidelines in relation to REACH and scientific developments. *Experimental and Toxicologic Pathology*, 60, 125-133.
- ATKINS, W. M. 2020. Mechanisms of promiscuity among drug metabolizing enzymes and drug transporters. *The FEBS Journal*, 287, 1306-1322.
- AVDEEF, A. 2005. The rise of PAMPA. *Expert Opinion on Drug Metabolism & Toxicology*, 1, 325-342.
- AVDEEF, A., KANSY, M., BENDELS, S. & TSINMAN, K. 2008. Absorption-exciipient-pH classification gradient maps: Sparingly soluble drugs and the pH partition hypothesis. *European Journal of Pharmaceutical Sciences*, 33, 29-41.
- AVDEEF, A. & TAM, K. Y. 2010. How Well Can the Caco-2/Madin– Darby Canine Kidney Models Predict Effective Human Jejunal Permeability? *Journal of medicinal chemistry*, 53, 3566-3584.
- AXELSSON, M. & GENTILI, F. 2014. A single-step method for rapid extraction of total lipids from green microalgae. *PLoS one*, 9, e89643.
- BÄCKMAN, P., ARORA, S., COUET, W., FORBES, B., DE KRUIJF, W. & PAUDEL, A. 2018. Advances in experimental and mechanistic computational models to understand pulmonary exposure to inhaled drugs. *European Journal of Pharmaceutical Sciences*, 113, 41-52.
- BAI, S., YANG, T., ABBRUSCATO, T. J. & AHSAN, F. 2008. Evaluation of human nasal RPMI 2650 cells grown at an air–liquid interface as a model for nasal drug transport studies. *Journal of Pharmaceutical Sciences*, 97, 1165-1178.
- BAILEY, K. E., PINO, C., LENNON, M. L., LYONS, A., JACOT, J. G., LAMMERS, S. R., KÖNIGSHOFF, M. & MAGIN, C. M. 2019. Embedding of Precision-Cut Lung Slices in Engineered Hydrogel Biomaterials Supports Extended Ex Vivo Culture. *American Journal of Respiratory Cell and Molecular Biology*, 62, 14-22.
- BAILEY, M. 1994. The new ICRP model for the respiratory tract. *Radiation protection dosimetry*, 53, 107-114.
- BAILLIE, T. A. & RETTIE, A. E. 2010. Role of Biotransformation in Drug-Induced Toxicity: Influence of Intra- and Inter-Species Differences in Drug Metabolism. *Drug Metabolism and Pharmacokinetics*, advpub, 1010210091-1010210091.
- BAIN, L. J. & LEBLANC, G. A. 1996. Interaction of structurally diverse pesticides with the human MDR1 gene product P-glycoprotein. *Toxicology applied pharmacology*, 141, 288-298.
- BAIR, W. J. 1994. The Revised International Commission on Radiological Protection (ICRP) Dosimetric Model for the Human Respiratory Tract—An Overview. *The Annals of Occupational Hygiene*, 38, 251-256.
- BALÁSHÁZY, I., HOFMANN, W., FARKAS, Á. & MADAS, B. G. 2008. Three-Dimensional Model for Aerosol Transport and Deposition in Expanding and Contracting Alveoli. *Inhalation Toxicology*, 20, 611-621.
- BALENDIRAN, G. K., DABUR, R. & FRASER, D. 2004. The role of glutathione in cancer. *Cell Biochemistry & Function*, 22, 343-352.
- BALOGH SIVARS, K., SIVARS, U., HORNBERG, E., ZHANG, H., BRÄNDÉN, L., BONFANTE, R., HUANG, S., CONSTANT, S., ROBINSON, I., BETTS, C. J. & ÅBERG, P. M. 2018. A 3D Human Airway Model Enables Prediction of Respiratory Toxicity of Inhaled Drugs In Vitro. *Toxicological Sciences*, 162, 301-308.
- BAMJI-STOCKE, S., VAN BERKEL, V., MILLER, D. M. & FRIEBOES, H. B. 2018. A review of metabolism-associated biomarkers in lung cancer diagnosis and treatment. *Metabolomics*, 14, 81.
- BARNES, J. L., ZUBAIR, M., JOHN, K., POIRIER, M. C. & MARTIN, F. L. 2018. Carcinogens and DNA damage. *Biochemical Society Transactions*, 46, 1213-1224.

- BEGER, R. D. 2013. A Review of Applications of Metabolomics in Cancer. *Metabolites*, 3.
- BÉMER, D., FISMES, J., SUBRA, I., BLACHÈRE, V. & PROTOIS, J.-C. 2007. Pesticide Aerosol Characteristics in the Vicinity of an Agricultural Vehicle Cab During Application. *Journal of Occupational and Environmental Hygiene*, 4, 476-482.
- BERNACCHIONI, C., GHINI, V., CENCETTI, F., JAPTOK, L., DONATI, C., BRUNI, P. & TURANO, P. 2017. NMR metabolomics highlights sphingosine kinase-1 as a new molecular switch in the orchestration of aberrant metabolic phenotype in cancer cells. *Molecular oncology*, 11, 517-533.
- BÉRUBÉ, K., PRYTHERCH, Z., JOB, C. & HUGHES, T. 2010. Human primary bronchial lung cell constructs: The new respiratory models. *Toxicology*, 278, 311-318.
- BESSEMS, J. G., LOIZOU, G., KRISHNAN, K., CLEWELL, H. J., BERNASCONI, C., BOIS, F., COECKE, S., COLLNOT, E.-M., DIEMBECK, W., FARCAL, L. R., GERAETS, L., GUNDERT-REMY, U., KRAMER, N., KÜSTERS, G., LEITE, S. B., PELKONEN, O. R., SCHRÖDER, K., TESTAI, E., WILK-ZASADNA, I. & ZALDÍVAR-COMENEGES, J.-M. 2014. PBTK modelling platforms and parameter estimation tools to enable animal-free risk assessment: Recommendations from a joint EPAA – EURL ECVAM ADME workshop. *Regulatory Toxicology and Pharmacology*, 68, 119-139.
- BICER, E. M., FORBES, B., SOMERS, G., BLOMBERG, A., BEHNDIG, A. F. & MUDWAY, I. S. 2012. Characterizing The Composition Of Human Respiratory Tract Lining Fluids In Health And Disease. *American Thoracic Society*, A4661-A4661.
- BICKER, J., ALVES, G., FORTUNA, A., SOARES-DA-SILVA, P. & FALCÃO, A. 2016. A new PAMPA model using an in-house brain lipid extract for screening the blood–brain barrier permeability of drug candidates. *International journal of pharmaceutics*, 501, 102-111.
- BIDDISCOMBE, M. F., USMANI, O. S. & BARNES, P. J. 2003. A system for the production and delivery of monodisperse salbutamol aerosols to the lungs. *International Journal of Pharmaceutics*, 254, 243-253.
- BLANCO-MUÑOZ, J. & LACASAÑA, M. 2011. Practices in Pesticide Handling and the Use of Personal Protective Equipment in Mexican Agricultural Workers. *Journal of Agromedicine*, 16, 117-126.
- BLEIER, B. S., NOCERA, A. L., IQBAL, H., HOANG, J. D., FELDMAN, R. E. & HAN, X. 2013. P-glycoprotein functions as an immunomodulator in healthy human primary nasal epithelial cells. *International Forum of Allergy & Rhinology*, 3, 433-438.
- BLOM, R. A., ERNI, S. T., KREMPASKÁ, K., SCHAEERER, O., VAN DIJK, R. M., AMACKER, M., MOSER, C., HALL, S. R., VON GARNIER, C. & BLANK, F. 2016. A triple co-culture model of the human respiratory tract to study immune-modulatory effects of liposomes and virosomes. *PLoS One*, 11, e0163539.
- BOEGH, M., FOGED, C., MÜLLERTZ, A. & MØRCK NIELSEN, H. 2013. Mucosal drug delivery: barriers, in vitro models and formulation strategies. *Journal of Drug Delivery Science and Technology*, 23, 383-391.
- BONVALLOT, N., CANLET, C., BLAS-Y-ESTRADA, F., GAUTIER, R., TREMBLAY-FRANCO, M., CHEVOLLEAU, S., CORDIER, S. & CRAVEDI, J.-P. 2018. Metabolome disruption of pregnant rats and their offspring resulting from repeated exposure to a pesticide mixture representative of environmental contamination in Brittany. *PLOS ONE*, 13, e0198448.
- BONVALLOT, N., TREMBLAY-FRANCO, M., CHEVRIER, C., CANLET, C., WAREMBOURG, C., CRAVEDI, J.-P. & CORDIER, S. 2013. Metabolomics Tools for Describing Complex Pesticide Exposure in Pregnant Women in Brittany (France). *PLOS ONE*, 8, e64433.
- BORGHARDT, J. M., WEBER, B., STAAB, A. & KLOFT, C. 2015. Pharmacometric Models for Characterizing the Pharmacokinetics of Orally Inhaled Drugs. *The AAPS Journal*, 17, 853-870.

- BORLAK, J. & ZWADLO, C. 2003. Expression of drug-metabolizing enzymes, nuclear transcription factors and ABC transporters in Caco-2 cells. *Xenobiotica*, 33, 927-943.
- BOSQUILLON, C. 2010. Drug transporters in the lung—do they play a role in the biopharmaceutics of inhaled drugs? *Journal of Pharmaceutical Sciences*, 99, 2240-2255.
- BOURDET, D. L., POLLACK, G. M. & THAKKER, D. R. 2006. Intestinal Absorptive Transport of the Hydrophilic Cation Ranitidine: A Kinetic Modeling Approach to Elucidate the Role of Uptake and Efflux Transporters and Paracellular vs. Transcellular Transport in Caco-2 Cells. *Pharmaceutical Research*, 23, 1178-1187.
- BOYD, M. R. 1980. Biochemical mechanisms in chemical-induced lung injury: roles of metabolic activation. *Crit Rev Toxicol*, 7, 103-76.
- BRÉCHOT, J.-M., HURBAIN, I., FAJAC, A., DATY, N. & BERNAUDIN, J.-F. 1998. Different Pattern of MRP Localization in Ciliated and Basal Cells from Human Bronchial Epithelium. *Journal of Histochemistry & Cytochemistry*, 46, 513-517.
- BRILLAULT, J., DE CASTRO, W. V., HARNOIS, T., KITZIS, A., OLIVIER, J.-C. & COUET, W. 2009. P-glycoprotein-mediated transport of moxifloxacin in a Calu-3 lung epithelial cell model. *Antimicrobial agents chemotherapy*, 53, 1457-1462.
- BURDEN, N., CHAPMAN, K., SEWELL, F. & ROBINSON, V. 2015. Pioneering Better Science through the 3Rs: An Introduction to the National Centre for the Replacement, Refinement, and Reduction of Animals in Research (NC3Rs). *Journal of the American Association for Laboratory Animal Science*, 54, 198-208.
- BURGSTALLER, G., SENGUPTA, A., VIERKOTTEN, S., PREISLER, G., LINDNER, M., BEHR, J., KÖNIGSHOFF, M. & EICKELBERG, O. 2018. Distinct niches within the extracellular matrix dictate fibroblast function in (cell free) 3D lung tissue cultures. *American Journal of Physiology-Lung Cellular and Molecular Physiology*, 314, L708-L723.
- CANTIN, A. M., NORTH, S. L., HUBBARD, R. C. & CRYSTAL, R. G. 1987. Normal alveolar epithelial lining fluid contains high levels of glutathione. *Journal of Applied Physiology*, 63, 152-157.
- CASIDA, J. E. & BRYANT, R. J. 2017. The ABCs of pesticide toxicology: amounts, biology, and chemistry. *Toxicology research*, 6, 755-763.
- CASTELL, J. V., TERESA DONATO, M. & GÓMEZ-LECHÓN, M. J. 2005. Metabolism and bioactivation of toxicants in the lung. The in vitro cellular approach. *Experimental and Toxicologic Pathology*, 57, 189-204.
- CHANDIRAMOHAN, A., DABAGHI, M., AGUIAR, J. A., TIESSEN, N., STEWART, M., CAO, Q. T., NGUYEN, J. P., MAKHDAMI, N., COX, G., DOXEY, A. C. & HIROTA, J. A. 2021. Development and validation of an open-source, disposable, 3D-printed &lt;em>in vitro</em> environmental exposure system for Transwell culture inserts. *ERJ Open Research*, 7, 00705-2020.
- CHEN, P.-J., MOORE, T. & NESNOW, S. 2008. Cytotoxic effects of propiconazole and its metabolites in mouse and human hepatoma cells and primary mouse hepatocytes. *Toxicology in vitro*, 22, 1476-1483.
- CHEN, W., HRUDEY, S. E. & ROUSSEAU, C. 1995. *Bioavailability in environmental risk assessment*, CRC Press.
- CHENG, Y. S., ZHOU, Y., IRVIN, C. M., PIERCE, R. H., NAAR, J., BACKER, L. C., FLEMING, L. E., KIRKPATRICK, B. & BADEN, D. G. 2005. Characterization of Marine Aerosol for Assessment of Human Exposure to Brevetoxins. *Environmental Health Perspectives*, 113, 638-643.
- CINGOLANI, E., ALQAHTANI, S., SADLER, R. C., PRIME, D., STOLNIK, S. & BOSQUILLON, C. 2019. In vitro investigation on the impact of airway mucus on drug dissolution and absorption at the air-epithelium interface in the lungs. *European Journal of Pharmaceutics and Biopharmaceutics*, 141, 210-220.

- CLARK, R. D. 2018. Predicting mammalian metabolism and toxicity of pesticides in silico. *Pest management science*, 74, 1992-2003.
- CLARKE, E. D. & DELANEY, J. S. 2003. Physical and Molecular Properties of Agrochemicals: An Analysis of Screen Inputs, Hits, Leads, and Products. *CHIMIA International Journal for Chemistry*, 57, 731-734.
- CLIPPINGER, A. J., ALLEN, D., BEHRING, H., BÉRUBÉ, K. A., BOLGER, M. B., CASEY, W., DELORME, M., GAÇA, M., GEHEN, S. C., GLOVER, K., HAYDEN, P., HINDERLITER, P., HOTCHKISS, J. A., ISKANDAR, A., KEYSER, B., LUETTICH, K., MA-HOCK, L., MAIONE, A. G., MAKENA, P., MELBOURNE, J., MILCHAK, L., NG, S. P., PAINI, A., PAGE, K., PATLEWICZ, G., PRIETO, P., RAABE, H., REINKE, E. N., ROPER, C., ROSE, J., SHARMA, M., SPOO, W., THORNE, P. S., WILSON, D. M. & JARABEK, A. M. 2018a. Pathway-based predictive approaches for non-animal assessment of acute inhalation toxicity. *Toxicology in Vitro*, 52, 131-145.
- CLIPPINGER, A. J., ALLEN, D., JARABEK, A. M., CORVARO, M., GAÇA, M., GEHEN, S., HOTCHKISS, J. A., PATLEWICZ, G., MELBOURNE, J., HINDERLITER, P., YOON, M., HUH, D., LOWIT, A., BUCKLEY, B., BARTELS, M., BÉRUBÉ, K., WILSON, D. M., INDANS, I. & VINKEN, M. 2018b. Alternative approaches for acute inhalation toxicity testing to address global regulatory and non-regulatory data requirements: An international workshop report. *Toxicology in Vitro*, 48, 53-70.
- COECKE, S., PELKONEN, O., LEITE, S. B., BERNAUER, U., BESSEMS, J. G., BOIS, F. Y., GUNDERT-REMY, U., LOIZOU, G., TESTAI, E. & ZALDÍVAR, J.-M. 2013. Toxicokinetics as a key to the integrated toxicity risk assessment based primarily on non-animal approaches. *Toxicology in vitro*, 27, 1570-1577.
- COHEN HUBAL, E. A., WETMORE, B. A., WAMBAUGH, J. F., EL-MASRI, H., SOBUS, J. R. & BAHADORI, T. 2019. Advancing internal exposure and physiologically-based toxicokinetic modeling for 21st-century risk assessments. *Journal of Exposure Science & Environmental Epidemiology*, 29, 11-20.
- CORLEY, R. A., KUPRAT, A. P., SUFFIELD, S. R., KABILAN, S., HINDERLITER, P. M., YUGULIS, K. & RAMANARAYANAN, T. S. 2021. New Approach Methodology for Assessing Inhalation Risks of a Contact Respiratory Cytotoxicant: Computational Fluid Dynamics-Based Aerosol Dosimetry Modeling for Cross-Species and in Vitro Comparisons. *Toxicological Sciences*.
- COURCOT, E., LECLERC, J., LAFITTE, J.-J., MENSIER, E., JAILLARD, S., GOSSET, P., SHIRALI, P., POTTIER, N., BROLY, F. & LO-GUIDICE, J.-M. 2012. Xenobiotic metabolism and disposition in human lung cell models: comparison with in vivo expression profiles. *Drug Metabolism and Disposition*, 40, 1953-1965.
- CUI, L., ZHENG, D., LEE, Y. H., CHAN, T. K., KUMAR, Y., HO, W. E., CHEN, J. Z., TANNENBAUM, S. R. & ONG, C. N. 2016. Metabolomics Investigation Reveals Metabolite Mediators Associated with Acute Lung Injury and Repair in a Murine Model of Influenza Pneumonia. *Scientific Reports*, 6, 26076.
- ČUPERLOVIĆ-CULF, M., BARNETT, D. A., CULF, A. S. & CHUTE, I. 2010a. Cell culture metabolomics: applications and future directions. *Drug discovery today*, 15, 610-621.
- ČUPERLOVIĆ-CULF, M., BARNETT, D. A., CULF, A. S. & CHUTE, I. 2010b. Cell culture metabolomics: applications and future directions. *Drug Discovery Today*, 15, 610-621.
- DAHL, A. R. & HADLEY, W. M. 1991. Nasal Cavity Enzymes Involved in Xenobiotic Metabolism: Effects on the Toxicity of Inhalants. *Critical Reviews in Toxicology*, 21, 345-372.
- DANIELSEN, P. H., LOFT, S., KOCBACH, A., SCHWARZE, P. E. & MØLLER, P. 2009. Oxidative damage to DNA and repair induced by Norwegian wood smoke particles in human A549 and THP-1 cell lines. *Mutation Research/Genetic Toxicology and Environmental Mutagenesis*, 674, 116-122.

- DARQUENNE, C. 2020. Deposition Mechanisms. *Journal of Aerosol Medicine and Pulmonary Drug Delivery*, 33, 181-185.
- DEARDEN, J. C. 2003. In silico prediction of drug toxicity. *Journal of computer-aided molecular design*, 17, 119-127.
- DEN BESTE, H. E., FJELDE, A., JACKSON, J. L., ANDRESEN, W. F., KERR, H. A. & EVANS, V. J. 1966. Adaptation, growth, and chromosomal analysis of HEp-2 cells in chemically defined medium. *Journal of the National Cancer Institute*, 36, 1075-1088.
- DETAMPEL, P., GANGULY, A., TEHRANIAN, S., GREEN, F., SINGHA, S., SANTAMARIA, P., JEJE, A. A., CHO, C. S., PETRI, B. & AMREIN, M. W. 2019. In vivo clearance of nanoparticles by transcytosis across alveolar epithelial cells. *PLOS ONE*, 14, e0223339.
- DIDIER, A. & LOOR, F. 1996. The abamectin derivative ivermectin is a potent P-glycoprotein inhibitor. *Anti-cancer drugs*, 7, 745-751.
- DIDZIAPETRIS, R., JAPERTAS, P., AVDEEF, A. & PETRAUSKAS, A. 2003. Classification analysis of P-glycoprotein substrate specificity. *Journal of drug targeting*, 11, 391-406.
- DIETERLE, F., ROSS, A., SCHLOTTERBECK, G. & SENN, H. 2006. Probabilistic Quotient Normalization as Robust Method to Account for Dilution of Complex Biological Mixtures. Application in 1H NMR Metabonomics. *Analytical Chemistry*, 78, 4281-4290.
- DING, G. & BAO, Y. 2014. Revisiting pesticide exposure and children's health: Focus on China. *Science of The Total Environment*, 472, 289-295.
- DING, X. & KAMINSKY, L. S. 2003. Human Extrahepatic Cytochromes P450: Function in Xenobiotic Metabolism and Tissue-Selective Chemical Toxicity in the Respiratory and Gastrointestinal Tracts. *Annual Review of Pharmacology and Toxicology*, 43, 149-173.
- DINIS-OLIVEIRA, R. J., DUARTE, J. A., SÁNCHEZ-NAVARRO, A., REMIÃO, F., BASTOS, M. L. & CARVALHO, F. 2008. Paraquat Poisonings: Mechanisms of Lung Toxicity, Clinical Features, and Treatment. *Critical Reviews in Toxicology*, 38, 13-71.
- DJIDROVSKI, I., GEORGIU, M., HUGHES, G. L., PATTERSON, E. I., CASAS-SANCHEZ, A., PENINGTON, S. H., BIAGINI, G. A., MOYA-MOLINA, M., VAN DEN BOR, J. & SMIT, M. J. 2021. SARS-CoV-2 infects an upper airway model derived from induced pluripotent stem cells. *STEM CELLS*.
- DOLBERG, A. M. & REICHL, S. 2016. Expression of P-glycoprotein in excised human nasal mucosa and optimized models of RPMI 2650 cells. *International Journal of Pharmaceutics*, 508, 22-33.
- DORRIAN, M.-D. & BAILEY, M. R. 1995. Particle Size Distributions of Radioactive Aerosols Measured in Workplaces. *Radiation Protection Dosimetry*, 60, 119-133.
- DORYAB, A., AMOABEDINY, G. & SALEHI-NAJAFABADI, A. 2016. Advances in pulmonary therapy and drug development: Lung tissue engineering to lung-on-a-chip. *Biotechnology Advances*, 34, 588-596.
- DOS SANTOS, R. N., MACHADO, B. R., HEFLER, S. M. & ZANETTE, J. 2021. Glutathione S-transferase activity in aquatic macrophytes and halophytes and biotransformation potential for biocides. *Journal of Plant Research*, 134, 577-584.
- DUFFNEY, P. F., EMBONG, A. K., MCGUIRE, C. C., THATCHER, T. H., PHIPPS, R. P. & SIME, P. J. 2020. Cigarette smoke increases susceptibility to infection in lung epithelial cells by upregulating caveolin-dependent endocytosis. *PLOS ONE*, 15, e0232102.
- ECKLE, T., BRODSKY, K., BONNEY, M., PACKARD, T., HAN, J., BORCHERS, C. H., MARIANI, T. J., KOMINSKY, D. J., MITTELBRONN, M. & ELTZSCHIG, H. K. 2013. HIF1A Reduces Acute Lung Injury by Optimizing Carbohydrate Metabolism in the Alveolar Epithelium. *PLOS Biology*, 11, e1001665.
- EFSA 2010. Conclusion on the peer review of the pesticide risk assessment of the active substance azoxystrobin. *EFSA Journal*, 8, 1542.
- EFSA 2014a. Conclusion on the peer review of the pesticide risk assessment of the active substance acibenzolar-S-methyl. *EFSA Journal*, 12, 3691.

- EFSA 2014b. Guidance on the assessment of exposure of operators, workers, residents and bystanders in risk assessment for plant protection products. *European Food Safety Authority*, 12, 3874.
- EFSA 2021. EU Pesticides database: Active substances, safeners and synergists. European Commission.
- EFSA, ARENA, M., AUTERI, D., BARMAZ, S., BELLISAI, G., BRANCATO, A., BROCCA, D., BURRA, L., BYERS, H., CHIUSOLO, A., COURT MARQUES, D., CRIVELLENTI, F., DE LENTDECKER, C., DE MAGLIE, M., EGSMOSE, M., ERDOS, Z., FAIT, G., FERREIRA, L., GOUMENOU, M., GRECO, L., IPPOLITO, A., ISTACE, F., JARRAH, S., KARDASSI, D., LEUSCHNER, R., LYTHGO, C., MAGRANS, J. O., MEDINA, P., MIRON, I., MOLNAR, T., NOUGADERE, A., PADOVANI, L., PARRA MORTE, J. M., PEDERSEN, R., REICH, H., SACCHI, A., SANTOS, M., SERAFIMOVA, R., SHARP, R., STANEK, A., STREISSL, F., STURMA, J., SZENTES, C., TARAZONA, J., TERRON, A., THEOBALD, A., VAGENENDE, B., VERANI, A. & VILLAMAR-BOUZA, L. 2017a. Peer review of the pesticide risk assessment of the active substance propiconazole. *EFSA Journal*, 15, e04887.
- EFSA, ARENA, M., AUTERI, D., BARMAZ, S., BELLISAI, G., BRANCATO, A., BROCCA, D., BURRA, L., BYERS, H., CHIUSOLO, A., COURT MARQUES, D., CRIVELLENTI, F., DE LENTDECKER, C., EGSMOSE, M., ERDOS, Z., FAIT, G., FERREIRA, L., GOUMENOU, M., GRECO, L., IPPOLITO, A., ISTACE, F., JARRAH, S., KARDASSI, D., LEUSCHNER, R., LYTHGO, C., MAGRANS, J. O., MEDINA, P., MIRON, I., MOLNAR, T., NOUGADERE, A., PADOVANI, L., PARRA MORTE, J. M., PEDERSEN, R., REICH, H., SACCHI, A., SANTOS, M., SERAFIMOVA, R., SHARP, R., STANEK, A., STREISSL, F., STURMA, J., SZENTES, C., TARAZONA, J., TERRON, A., THEOBALD, A., VAGENENDE, B., VERANI, A. & VILLAMAR-BOUZA, L. 2018. Peer review of the pesticide risk assessment of the active substance chlorothalonil. *EFSA Journal*, 16, e05126.
- EFSA, BUIST, H., CRAIG, P., DEWHURST, I., HOUGAARD BENNEKOU, S., KNEUER, C., MACHERA, K., PIEPER, C., COURT MARQUES, D., GUILLOT, G., RUFFO, F. & CHIUSOLO, A. 2017b. Guidance on dermal absorption. *EFSA Journal*, 15, e04873.
- EHRHARDT, C., BÄCKMAN, P., COUET, W., EDWARDS, C., FORBES, B., FRIDÉN, M., GUMBLETON, M., HOSOYA, K.-I., KATO, Y., NAKANISHI, T., TAKANO, M., TERASAKI, T. & YUMOTO, R. 2017. Current Progress Toward a Better Understanding of Drug Disposition Within the Lungs: Summary Proceedings of the First Workshop on Drug Transporters in the Lungs. *Journal of Pharmaceutical Sciences*, 106, 2234-2244.
- EHRHARDT, C., FORBES, B. & KIM, K.-J. 2008. In vitro models of the tracheo-bronchial epithelium. *Drug absorption studies*. Springer.
- EHRHARDT, C., KNEUER, C., FIEGEL, J., HANES, J., SCHAEFER, U., KIM, K.-J. & LEHR, C.-M. 2002. Influence of apical fluid volume on the development of functional intercellular junctions in the human epithelial cell line 16HBE14o-: implications for the use of this cell line as an in vitro model for bronchial drug absorption studies. *Cell and Tissue Research*, 308, 391-400.
- EHRHARDT, C., KNEUER, C., LAUE, M., SCHAEFER, U. F., KIM, K.-J. & LEHR, C.-M. 2003. 16HBE14o- Human Bronchial Epithelial Cell Layers Express P-Glycoprotein, Lung Resistance-Related Protein, and Caveolin-1. *Pharmaceutical Research*, 20, 545-551.
- ELBERT, K. J., SCHÄFER, U. F., SCHÄFERS, H.-J., KIM, K.-J., LEE, V. H. & LEHR, C.-M. 1999. Monolayers of human alveolar epithelial cells in primary culture for pulmonary absorption and transport studies. *Pharmaceutical research*, 16, 601-608.
- ENDTER, S., FRANCOMBE, D., EHRHARDT, C. & GUMBLETON, M. 2009. RT-PCR analysis of ABC, SLC and SLCO drug transporters in human lung epithelial cell models. *Journal of Pharmacy and Pharmacology*, 61, 583-591.

- ENLO-SCOTT, Z., BÄCKSTRÖM, E., MUDWAY, I. & FORBES, B. 2021a. Drug metabolism in the lungs: opportunities for optimising inhaled medicines. *Expert Opinion on Drug Metabolism & Toxicology*, 17, 611-625.
- ENLO-SCOTT, Z., SWEDROWSKA, M. & FORBES, B. 2021b. Chapter 10 - Epithelial permeability and drug absorption in the lungs. *In: KASSINOS, S., BÄCKMAN, P., CONWAY, J. & HICKEY, A. J. (eds.) Inhaled Medicines*. Academic Press.
- ERIKSSON, J., SJÖGREN, E., THÖRN, H., RUBIN, K., BÄCKMAN, P. & LENNERNÄS, H. 2018. Pulmonary absorption – estimation of effective pulmonary permeability and tissue retention of ten drugs using an ex vivo rat model and computational analysis. *European Journal of Pharmaceutics and Biopharmaceutics*, 124, 1-12.
- ERIKSSON, J., THÖRN, H., LENNERNÄS, H. & SJÖGREN, E. 2020. Pulmonary drug absorption and systemic exposure in human: Predictions using physiologically based biopharmaceutics modeling. *European Journal of Pharmaceutics and Biopharmaceutics*, 156, 191-202.
- EUROPEAN FOOD SAFETY, A., MEDINA-PASTOR, P. & TRIACCHINI, G. 2020. The 2018 European Union report on pesticide residues in food. *EFSA journal. European Food Safety Authority*, 18, e06057-e06057.
- EVANS, K. V. & LEE, J.-H. 2020. Alveolar wars: The rise of in vitro models to understand human lung alveolar maintenance, regeneration, and disease. *STEM CELLS Translational Medicine*, 9, 867-881.
- FARDEL, O., KOLASA, E. & LE VEE, M. 2012. Environmental chemicals as substrates, inhibitors or inducers of drug transporters: implication for toxicokinetics, toxicity and pharmacokinetics. *Expert Opinion on Drug Metabolism & Toxicology*, 8, 29-46.
- FIONI, A., SELG, E., CENACCHI, V., ACEVEDO, F., BROGIN, G., GERDE, P. & PUCCINI, P. 2017. Investigation of Lung Pharmacokinetic of the Novel PDE4 Inhibitor CHF6001 in Preclinical Models: Evaluation of the PreciseInhale Technology. *Journal of Aerosol Medicine and Pulmonary Drug Delivery*, 31, 61-70.
- FISCHER, F. C., HENNEBERGER, L., KÖNIG, M., BITTERMANN, K., LINDEN, L., GOSS, K.-U. & ESCHER, B. I. 2017. Modeling Exposure in the Tox21 in Vitro Bioassays. *Chemical Research in Toxicology*, 30, 1197-1208.
- FISCHER, H. & WIDDICOMBE, J. H. 2006. Mechanisms of Acid and Base Secretion by the Airway Epithelium. *The Journal of Membrane Biology*, 211, 139-150.
- FLACK, S., HINDERLITER, P., CHARLTON, A., PARR-DOBRZANSKI, R., RAMANARAYANAN, T., SZARKA, A., WOLF, D. C. & HOFSTRA, A. 2018. Chlorothalonil: A Source to Outcome Approach for Inhalation Risk Assessment Final Report. *Environmental Protection Agency*, 1, 1-43.
- FOLCH, J., LEES, M. & STANLEY, G. S. 1957. A simple method for the isolation and purification of total lipides from animal tissues. *Journal of Biological Chemistry*, 226, 497-509.
- FORBES, B. 2000. Human airway epithelial cell lines for in vitro drug transport and metabolism studies. *Journal of Pharmaceutical science technology today*, 3, 18-27.
- FORBES, B. & EHRHARDT, C. 2005. Human respiratory epithelial cell culture for drug delivery applications. *European Journal of Pharmaceutics and Biopharmaceutics*, 60, 193-205.
- FORBES, B., O'LONE, R., ALLEN, P. P., CAHN, A., CLARKE, C., COLLINGE, M., DAILEY, L. A., DONNELLY, L. E., DYBOWSKI, J., HASSALL, D., HILDEBRAND, D., JONES, R., KILGOUR, J., KLAPWIJK, J., MAIER, C. C., MCGOVERN, T., NIKULA, K., PARRY, J. D., REED, M. D., ROBINSON, I., TOMLINSON, L. & WOLFREYS, A. 2014. Challenges for inhaled drug discovery and development: Induced alveolar macrophage responses. *Advanced Drug Delivery Reviews*, 71, 15-33.
- FORBES, B., RICHER, N. H. & BUTTINI, F. 2015. Dissolution: a critical performance characteristic of inhaled products. *Pulmonary Drug Delivery: Advances and Challenges*, 223-240.



- FOSTER, K. A., AVERY, M. L., YAZDANIAN, M. & AUDUS, K. L. 2000. Characterization of the Calu-3 cell line as a tool to screen pulmonary drug delivery. *International Journal of Pharmaceutics*, 208, 1-11.
- FOTH, H. 1995. Role of the Lung in Accumulation and Metabolism of Xenobiotic Compounds — Implications for Chemically Induced Toxicity. *Critical Reviews in Toxicology*, 25, 165-205.
- FRANKS, T. J., COLBY, T. V., TRAVIS, W. D., TUDER, R. M., REYNOLDS, H. Y., BRODY, A. R., CARDOSO, W. V., CRYSTAL, R. G., DRAKE, C. J., ENGELHARDT, J., FRID, M., HERZOG, E., MASON, R., PHAN, S. H., RANDELL, S. H., ROSE, M. C., STEVENS, T., SERGE, J., SUNDAY, M. E., VOYNOW, J. A., WEINSTEIN, B. M., WHITSETT, J. & WILLIAMS, M. C. 2008. Resident Cellular Components of the Human Lung. *American Thoracic Society*, 5, 763-766.
- FRÖHLICH, E. & SALAR-BEHZADI, S. 2014. Toxicological Assessment of Inhaled Nanoparticles: Role of in Vivo, ex Vivo, in Vitro, and in Silico Studies. *International Journal of Molecular Sciences*, 15.
- FUCHS, S., HOLLINS, A., LAUE, M., SCHAEFER, U., ROEMER, K., GUMBLETON, M. & LEHR, C.-M. 2003. Differentiation of human alveolar epithelial cells in primary culture: morphological characterization and synthesis of caveolin-1 and surfactant protein-C. *Cell and Tissue Research*, 311, 31-45.
- FUJIOKA, K. & CASIDA, J. E. 2007. Glutathione S-transferase conjugation of organophosphorus pesticides yields S-phospho-, S-aryl-, and S-alkylglutathione derivatives. *Chem Res Toxicol*, 20, 1211-7.
- FURUBAYASHI, T., INOUE, D., NISHIYAMA, N., TANAKA, A., YUTANI, R., KIMURA, S., KATSUMI, H., YAMAMOTO, A. & SAKANE, T. 2020. Comparison of Various Cell Lines and Three-Dimensional Mucociliary Tissue Model Systems to Estimate Drug Permeability Using an In Vitro Transport Study to Predict Nasal Drug Absorption in Rats. *Pharmaceutics*, 12, 79.
- G ZHANG, J., HO, T., L CALLENDRELLO, A., L CRESPI, C. & M STRESSER, D. 2010. A multi-endpoint evaluation of cytochrome P450 1A2, 2B6 and 3A4 induction response in human hepatocyte cultures after treatment with  $\beta$ -naphthoflavone, phenobarbital and rifampicin. *Drug metabolism letters*, 4, 185-194.
- GALLAGHER, E. P., CANADA, A. T. & DI GIULIO, R. T. 1992. The protective role of glutathione in chlorothalonil-induced toxicity to channel catfish. *Aquatic Toxicology*, 23, 155-168.
- GERAGHTY, R. J., CAPES-DAVIS, A., DAVIS, J. M., DOWNWARD, J., FRESHNEY, R. I., KNEZEVIC, I., LOVELL-BADGE, R., MASTERS, J. R. W., MEREDITH, J., STACEY, G. N., THRAVES, P. & VIAS, M. 2014. Guidelines for the use of cell lines in biomedical research. *British Journal of Cancer*, 111, 1021-1046.
- GHAEDI, M., MENDEZ, J. J., BOVE, P. F., SIVARAPATNA, A., RAREDON, M. S. B. & NIKLASON, L. E. 2014. Alveolar epithelial differentiation of human induced pluripotent stem cells in a rotating bioreactor. *Biomaterials*, 35, 699-710.
- GIEROK, P., HARMS, M., RICHTER, E., HILDEBRANDT, J.-P., LALK, M., MOSTERTZ, J. & HOCHGRÄFE, F. 2014. Staphylococcus aureus Alpha-Toxin Mediates General and Cell Type-Specific Changes in Metabolite Concentrations of Immortalized Human Airway Epithelial Cells. *PLOS ONE*, 9, e94818.
- GORDON, S., DANESHIAN, M., BOUWSTRA, J., CALONI, F., CONSTANT, S., DAVIES, D. E., DANDEKAR, G., GUZMAN, C. A., FABIAN, E. & HALTNER, E. 2015. Non-animal models of epithelial barriers (skin, intestine and lung) in research, industrial applications and regulatory toxicology. *Altex*, 32, 327-378.
- GRAHAM, R. A., DOWNEY, A., MUDRA, D., KRUEGER, L., CARROLL, K., CHENGELIS, C., MADAN, A. & PARKINSON, A. 2002. In Vivo and in Vitro Induction of Cytochrome P450 Enzymes in Beagle Dogs. *Drug Metabolism and Disposition*, 30, 1206-1213.

- GRAINGER, C. I., GREENWELL, L. L., LOCKLEY, D. J., MARTIN, G. P. & FORBES, B. 2006. Culture of Calu-3 cells at the air interface provides a representative model of the airway epithelial barrier. *Pharmaceutical research*, 23, 1482-1490.
- GU, J., JI, C., YUE, S., SHU, D., SU, F., ZHANG, Y., XIE, Y., ZHANG, Y., LIU, W. & ZHAO, M. 2018. Enantioselective Effects of Metalaxyl Enantiomers in Adolescent Rat Metabolic Profiles Using NMR-Based Metabolomics. *Environmental Science & Technology*, 52, 5438-5447.
- GUADAGNINI, R., MOREAU, K., HUSSAIN, S., MARANO, F. & BOLAND, S. 2015. Toxicity evaluation of engineered nanoparticles for medical applications using pulmonary epithelial cells. *Nanotoxicology*, 9, 25-32.
- GUO, C., GILLESPIE, S. R., KAUFFMAN, J. & DOUB, W. H. 2008. Comparison of delivery characteristics from a combination metered-dose inhaler using the Andersen cascade impactor and the next generation pharmaceutical impactor. *J Pharm Sci*, 97, 3321-34.
- GUSTAVSSON, L., BOSQUILLON, C., GUMBLETON, M., HEGELUND-MYRBÄCK, T., NAKANISHI, T., PRICE, D., TAMAI, I. & ZHOU, X.-H. 2016. Drug transporters in the lung: expression and potential impact on pulmonary drug disposition. *Drug transporters: role and importance in ADME and drug development*, 1, 184-227.
- GUTBIER, S., MAY, P., BERTHELOT, S., KRISHNA, A., TREFZER, T., BEHBEHANI, M., EFREMOVA, L., DELP, J., GSTRAUNTHALER, G., WALDMANN, T. & LEIST, M. 2018. Major changes of cell function and toxicant sensitivity in cultured cells undergoing mild, quasi-natural genetic drift. *Archives of Toxicology*, 92, 3487-3503.
- HAGHI, M., YOUNG, P. M., TRAINI, D., JAISWAL, R., GONG, J. & BEBAWY, M. 2010. Time- and passage-dependent characteristics of a Calu-3 respiratory epithelial cell model. *Drug development industrial pharmacy*, 36, 1207-1214.
- HALL, G. L., FILIPOW, N., RUPPEL, G., OKITIKA, T., THOMPSON, B., KIRKBY, J., STEENBRUGGEN, I., COOPER, B. G., STANOJEVIC, S. & ON BEHALF OF THE CONTRIBUTING, G. L. I. N. M. 2021. Official ERS technical standard: Global Lung Function Initiative reference values for static lung volumes in individuals of European ancestry. *European Respiratory Journal*, 57, 2000289.
- HAMILTON, K. O., BACKSTROM, G., YAZDANIAN, M. A. & AUDUS, K. L. 2001. P-glycoprotein efflux pump expression and activity in Calu-3 cells. *Journal of Pharmaceutical Sciences*, 90, 647-658.
- HAN, B. & HIRAHARA, H. 2016. Effect of gas oscillation-induced irreversible flow in transitional bronchioles of human lung. *Journal of Flow Control, Measurement & Visualization*, 4, 171-193.
- HASSOUN, M., MALMLÖF, M., SCHEIBELHOFER, O., KUMAR, A., BANSAL, S., SELG, E., NOWENWIK, M., GERDE, P., RADIVOJEV, S., PAUDEL, A., ARORA, S. & FORBES, B. 2019. Use of PBPK Modeling To Evaluate the Performance of DissolvIt, a Biorelevant Dissolution Assay for Orally Inhaled Drug Products. *Molecular Pharmaceutics*, 16, 1245-1254.
- HASSOUN, M., ROYALL, P. G., PARRY, M., HARVEY, R. D. & FORBES, B. 2018. Design and development of a biorelevant simulated human lung fluid. *Journal of Drug Delivery Science and Technology*, 47, 485-491.
- HASTEDT, J. E., BÄCKMAN, P., CLARK, A. R., DOUB, W., HICKEY, A., HOCHHAUS, G., KUEHL, P. J., LEHR, C.-M., MAUSER, P. & MCCONVILLE, J. 2016. Scope and relevance of a pulmonary biopharmaceutical classification system AAPS/FDA/USP Workshop March 16-17th, 2015 in Baltimore, MD. Springer.
- HAYDUK, W. & LAUDIE, H. 1974. Prediction of diffusion coefficients for nonelectrolytes in dilute aqueous solutions. *AIChE Journal*, 20, 611-615.
- HAYES, C., ANSBRO, D. & KONTOYIANNI, M. 2014. Elucidating Substrate Promiscuity in the Human Cytochrome 3A4. *Journal of Chemical Information and Modeling*, 54, 857-869.

- HAYES, J. D. & PULFORD, D. J. 1995. The Glutathione S-Transferase Supergene Family: Regulation of GST and the Contribution of the Isoenzymes to Cancer Chemoprotection and Drug Resistance Part I. *Critical Reviews in Biochemistry and Molecular Biology*, 30, 445-520.
- HERMAN, L., CHEMALY, M., COCCONCELLI, P. S., FERNANDEZ, P., KLEIN, G., PEIXE, L., PRIETO, M., QUEROL, A., SUAREZ, J. E. & SUNDH, I. 2019. The qualified presumption of safety assessment and its role in EFSA risk evaluations: 15 years past. *FEMS microbiology letters*, 366, fny260.
- HERMANN, M. I., UNGER, R. E., KEHE, K., PETERS, K. & KIRKPATRICK, C. J. 2004. Lung epithelial cell lines in coculture with human pulmonary microvascular endothelial cells: development of an alveolo-capillary barrier in vitro. *Laboratory investigation*, 84, 736-752.
- HERNÁNDEZ-MESA, M., LE BIZEC, B. & DERVILLY, G. 2021. Metabolomics in chemical risk analysis – A review. *Analytica Chimica Acta*, 1154, 338298.
- HEWITT, N. J., LECLUYSE, E. L. & FERGUSON, S. S. 2007. Induction of hepatic cytochrome P450 enzymes: methods, mechanisms, recommendations, and in vitro–in vivo correlations. *Xenobiotica*, 37, 1196-1224.
- HIMSTEDT, A., BÄCKMAN, P. & BORGHARDT, J. M. 2021. Chapter 12 - Physiologically-based pharmacokinetic modeling after drug inhalation. In: KASSINOS, S., BÄCKMAN, P., CONWAY, J. & HICKEY, A. J. (eds.) *Inhaled Medicines*. Academic Press.
- HODGSON, E. & ROSE, R. L. 2007. The importance of cytochrome P450 2B6 in the human metabolism of environmental chemicals. *Pharmacology & Therapeutics*, 113, 420-428.
- HOFFMANN, W., GRADINARU, J., FARCAL, L., CAUL-FUTY, M., HUANG, S., WISZNIEWSKI, L., PARISSIS, N., MORATH, S., FORTANER, S., COLE, T., REGINATO, E., CARRUPT, P.-A., CONSTANT, S. & COECKE, S. 2018. Establishment of a Human 3D Tissue-Based Assay for Upper Respiratory Tract Absorption. *Applied In Vitro Toxicology*, 4, 139-148.
- HOFMANN, W. 2011. Modelling inhaled particle deposition in the human lung—A review. *Journal of Aerosol Science*, 42, 693-724.
- HOFMANN, W., KOBLINGER, L. & MARTONEN, T. B. 1989. Structural differences between human and rat lungs: implications for Monte Carlo modeling of aerosol deposition. *Health physics*, 57 Suppl 1, 41-6; discussion 46-7.
- HOPPIN, J. A., UMBACH, D. M., LONDON, S. J., HENNEBERGER, P. K., KULLMAN, G. J., COBLE, J., ALAVANJA, M. C. R., BEANE FREEMAN, L. E. & SANDLER, D. P. 2009. Pesticide use and adult-onset asthma among male farmers in the Agricultural Health Study. *European Respiratory Journal*, 34, 1296.
- HORVATH, G., SCHMID, N., FRAGOSO, M. A., SCHMID, A., CONNER, G. E., SALATHE, M. & WANNER, A. 2007. Epithelial Organic Cation Transporters Ensure pH-Dependent Drug Absorption in the Airway. *American Journal of Respiratory Cell and Molecular Biology*, 36, 53-60.
- HU, X., XIA, H., SRIVASTAVA, S. K., HERZOG, C., AWASTHI, Y. C., JI, X., ZIMNIAK, P. & SINGH, S. V. 1997. Activity of four allelic forms of glutathione S-transferase hGSTP1-1 for diol epoxides of polycyclic aromatic hydrocarbons. *Biochemical and biophysical research communications*, 238, 397-402.
- HUANG, D., ZOU, Y., ABBAS, A. & DAI, B. 2018. Nuclear magnetic resonance-based metabolomic investigation reveals metabolic perturbations in PM2.5-treated A549 cells. *Environmental Science and Pollution Research*, 25, 31656-31665.
- HUANG, F., ZHU, Q., ZHOU, X., GOU, D., YU, J., LI, R., TONG, Z. & YANG, R. 2021. Role of CFD based in silico modelling in establishing an in vitro-in vivo correlation of aerosol deposition in the respiratory tract. *Advanced Drug Delivery Reviews*, 170, 369-385.

- HUANG, H., YU, L. & WANG, T. 2014. Expression of the xenobiotic metabolizing enzyme cytochrome P450 1B1 alters anti-inflammatory activity of quercetin, kaempferol and taxifolin in macrophage and monocyte (830.25). *The FASEB Journal*, 28, 830.25.
- HUANG, Q., ZHANG, J., LUO, L., WANG, X., WANG, X., ALAMDAR, A., PENG, S., LIU, L., TIAN, M. & SHEN, H. 2015. Metabolomics reveals disturbed metabolic pathways in human lung epithelial cells exposed to airborne fine particulate matter. *Toxicology Research*, 4, 939-947.
- HUANG, R., XIA, M., SAKAMURU, S., ZHAO, J., SHAHANE, S. A., ATTENE-RAMOS, M., ZHAO, T., AUSTIN, C. P. & SIMEONOV, A. 2016. Modelling the Tox21 10 K chemical profiles for in vivo toxicity prediction and mechanism characterization. *Nature Communications*, 7, 10425.
- HUGHES, P., MARSHALL, D., REID, Y., PARKES, H. & GELBER, C. 2007. The costs of using unauthenticated, over-passaged cell lines: how much more data do we need? *BioTechniques*, 43, 575-586.
- HUKKANEN, J., LASSILA, A., PAIVARINTA, K., VALANNE, S., SARPO, S., HAKKOLA, J., PELKONEN, O. & RAUNIO, H. 2000. Induction and regulation of xenobiotic-metabolizing cytochrome P450s in the human A549 lung adenocarcinoma cell line. *American journal of respiratory cell and molecular biology*, 22, 360-366.
- IDAKWO, G., LUTTRELL, J., CHEN, M., HONG, H., ZHOU, Z., GONG, P. & ZHANG, C. 2018. A review on machine learning methods for in silico toxicity prediction. *Journal of Environmental Science and Health, Part C*, 36, 169-191.
- INOUE, D., FURUBAYASHI, T., TANAKA, A., SAKANE, T. & SUGANO, K. 2020a. Quantitative estimation of drug permeation through nasal mucosa using in vitro membrane permeability across Calu-3 cell layers for predicting in vivo bioavailability after intranasal administration to rats. *J European Journal of Pharmaceutics Biopharmaceutics*, 149, 145-153.
- INOUE, D., FURUBAYASHI, T., TANAKA, A., SAKANE, T. & SUGANO, K. 2020b. Quantitative estimation of drug permeation through nasal mucosa using in vitro membrane permeability across Calu-3 cell layers for predicting in vivo bioavailability after intranasal administration to rats. *European Journal of Pharmaceutics and Biopharmaceutics*, 149, 145-153.
- INOUE, D., TANAKA, A., KIMURA, S., KIRIYAMA, A., KATSUMI, H., YAMAMOTO, A., OGAWARA, K.-I., KIMURA, T., HIGAKI, K. & YUTANI, R. 2018. The relationship between in vivo nasal drug clearance and in vitro nasal mucociliary clearance: Application to the prediction of nasal drug absorption. *European Journal of Pharmaceutical Sciences*, 117, 21-26.
- JACKSON, G. R., MAIONE, A. G., KLAUSNER, M. & HAYDEN, P. J. 2018. Prevalidation of an Acute Inhalation Toxicity Test Using the EpiAirway In Vitro Human Airway Model. *Applied In Vitro Toxicology*, 4, 149-158.
- JAKOB, F., HOMANN, D., SEUFERT, J., SCHNEIDER, D. & KOHRLE, J. 1995. Expression and regulation of aromatase cytochrome P450 in THP 1 human myeloid leukaemia cells. *Molecular and Cellular Endocrinology*, 110, 27-33.
- JANG, S. H., WIENTJES, M. G. & AU, J. L.-S. 2003. Interdependent effect of P-glycoprotein-mediated drug efflux and intracellular drug binding on intracellular paclitaxel pharmacokinetics: application of computational modeling. *Journal of Pharmacology and Experimental Therapeutics*, 304, 773-780.
- JARC, T., NOVAK, M., HEVIR, N., RIŽNER, T. L., KREFT, M. E. & KRISTAN, K. 2019. Demonstrating suitability of the Caco-2 cell model for BCS-based biowaiver according to the recent FDA and ICH harmonised guidelines. *Journal of Pharmacy and Pharmacology*, 71, 1231-1242.
- JARVIS, I. W., ENLO-SCOTT, Z., NAGY, E., MUDWAY, I. S., TETLEY, T. D., ARLT, V. M. & PHILLIPS, D. H. 2018. Genotoxicity of fine and coarse fraction ambient particulate matter in

- immortalised normal (TT1) and cancer-derived (A549) alveolar epithelial cells. *Environmental and molecular mutagenesis*, 59, 290-301.
- JOELSSON, J. P., MYSZOR, I. T., SIGURDSSON, S., LEHMANN, F., PAGE, C. P., GUDMUNDSSON, G. H., GUDJONSSON, T. & KARASON, S. 2020. Azithromycin has lung barrier protective effects in a cell model mimicking ventilator-induced lung injury. *ALTEX*.
- JOSHI, P., KANG, S. Y., DATAR, A. & LEE, M. Y. 2019. High-Throughput Assessment of Mechanistic Toxicity of Chemicals in Miniaturized 3D Cell Culture. *Current protocols in toxicology*, 79, e66.
- JUNQUEIRA, L. C. & MESCHER, A. L. 2013. *Junqueira's basic histology: text & atlas*, New York [etc.]: McGraw-Hill Medical.
- KANSY, M., AVDEEF, A. & FISCHER, H. 2004. Advances in screening for membrane permeability: high-resolution PAMPA for medicinal chemists. *Drug Discovery Today: Technologies*, 1, 349-355.
- KAUR, G. & DUFOUR, J. M. 2012. Cell lines. *Spermatogenesis*, 2, 1-5.
- KAYALI, U. S., BUDHIRAJA, R., PENNELLA, C. M., COORAY, S., LANZILLO, J. J., CHALKLEY, R. & HASSOUN, P. M. 2003. Upregulation of xanthine oxidase by tobacco smoke condensate in pulmonary endothelial cells. *Toxicology and Applied Pharmacology*, 188, 59-68.
- KELLER, J., MELLERT, W., SPERBER, S., KAMP, H., JIANG, X., FABIAN, E., HEROLD, M., WALK, T., STRAUSS, V. & VAN RAVENZWAAY, B. 2019. Added value of plasma metabolomics to describe maternal effects in rat maternal and prenatal toxicity studies. *Toxicology Letters*, 301, 42-52.
- KEUM, Y. S., KIM, J.-H. & LI, Q. X. 2010. Chapter 22 - Metabolomics in Pesticide Toxicology. In: KRIEGER, R. (ed.) *Hayes' Handbook of Pesticide Toxicology (Third Edition)*. New York: Academic Press.
- KILGOUR, J. D., FOSTER, J., SOAMES, A., FARRAR, D. G. & HEXT, P. M. 2002a. Responses in the respiratory tract of rats following exposure to sulphuric acid aerosols for 5 or 28 days. *Journal of Applied Toxicology*, 22, 387-95.
- KILGOUR, J. D., RATTRAY, N. J., FOSTER, J., SOAMES, A. & HEXT, P. M. 2002b. Pulmonary responses and recovery following single and repeated inhalation exposure of rats to polymeric methylene diphenyl diisocyanate aerosols. *Journal of Applied Toxicology*, 22, 371-85.
- KIM, K. C. 2012. Role of epithelial mucins during airway infection. *Pulmonary Pharmacology & Therapeutics*, 25, 415-419.
- KIM, R. B. 2002. Drugs as P-glycoprotein substrates, inhibitors, and inducers. *Drug Metabolism Reviews*, 34, 47-54.
- KIM, Y.-M., PARK, K., JOO, G.-J., JEONG, E.-M., KIM, J.-E. & RHEE, I.-K. 2004. Glutathione-Dependent Biotransformation of the Fungicide Chlorothalonil. *Journal of Agricultural and Food Chemistry*, 52, 4192-4196.
- KIRCHMAIR, J., GÖLLER, A. H., LANG, D., KUNZE, J., TESTA, B., WILSON, I. D., GLEN, R. C. & SCHNEIDER, G. 2015. Predicting drug metabolism: experiment and/or computation? *Nature Reviews Drug Discovery*, 14, 387-404.
- KLETTING, S., BARTHOLD, S., REPNIK, U., GRIFFITHS, G., LORETZ, B., SCHNEIDER-DAUM, N., DE SOUZA CARVALHO-WODARZ, C. & LEHR, C.-M. 2018. Co-culture of human alveolar epithelial (hAELVi) and macrophage (THP-1) cell lines. *ALTEX*.
- KNEBEL, C., KEBBEN, J., EBERINI, I., PALAZZOLO, L., HAMMER, H. S., SÜSSMUTH, R. D., HEISE, T., HESSEL-PRAS, S., LAMPEN, A. & BRAEUNING, A. 2018a. Propiconazole is an activator of AHR and causes concentration additive effects with an established AHR ligand. *Archives of toxicology*, 92, 3471-3486.
- KNEBEL, C., NEEB, J., ZAHN, E., SCHMIDT, F., CARAZO, A., HOLAS, O., PAVEK, P., PÜSCHEL, G. P., ZANGER, U. M. & SÜSSMUTH, R. 2018b. Unexpected effects of propiconazole,

- tebuconazole, and their mixture on the receptors CAR and PXR in human liver cells. *Toxicological Sciences*, 163, 170-181.
- KNOWLES, S. E., JARRETT, I. G., FILSELL, O. H. & BALLARD, F. J. 1974. Production and utilization of acetate in mammals. *Biochemical Journal*, 142, 401-411.
- KOEHLER, K. A., CLARK, P. & VOLCKENS, J. 2009. Development of a Sampler for Total Aerosol Deposition in the Human Respiratory Tract. *The Annals of Occupational Hygiene*, 53, 731-738.
- KOLANJIYIL, A. V., KLEINSTREUER, C., KLEINSTREUER, N. C., PHAM, W. & SADIKOT, R. T. 2019. Mice-to-men comparison of inhaled drug-aerosol deposition and clearance. *Respiratory Physiology & Neurobiology*, 260, 82-94.
- KOLLE, S. N., LANDSIEDEL, R. & NATSCH, A. 2020. Replacing the refinement for skin sensitization testing: Considerations to the implementation of adverse outcome pathway (AOP)-based defined approaches (DA) in OECD guidelines. *Regulatory Toxicology and Pharmacology*, 115, 104713.
- KOLLE, S. N., MATHEA, M., NATSCH, A. & LANDSIEDEL, R. 2021. Assessing Experimental Uncertainty in Defined Approaches: Borderline Ranges for In Chemico and In Vitro Skin Sensitization Methods Determined from Ring Trial Data. *Applied In Vitro Toxicology*.
- KOSTIDIS, S., ADDIE, R. D., MORREAU, H., MAYBORODA, O. A. & GIERA, M. 2017. Quantitative NMR analysis of intra- and extracellular metabolism of mammalian cells: A tutorial. *Analytica Chimica Acta*, 980, 1-24.
- KOULLAPIS, P., KASSINOS, S. C., MUELA, J., PEREZ-SEGARRA, C., RIGOLA, J., LEHMKUHL, O., CUI, Y., SOMMERFELD, M., ELCNER, J., JICHA, M., SAVELJIC, I., FILIPOVIC, N., LIZAL, F. & NICOLAOU, L. 2018. Regional aerosol deposition in the human airways: The SimInhale benchmark case and a critical assessment of in silico methods. *European Journal of Pharmaceutical Sciences*, 113, 77-94.
- KOULLAPIS, P., STYLIANOU, F., LIN, C.-L., KASSINOS, S. & SZNITMAN, J. 2021. Chapter 7 - In silico methods to model dose deposition. In: KASSINOS, S., BÄCKMAN, P., CONWAY, J. & HICKEY, A. J. (eds.) *Inhaled Medicines*. Academic Press.
- KREFT, M. E., JERMAN, U. D., LASIČ, E., HEVIR-KENE, N., RIŽNER, T. L., PETERNEL, L. & KRISTAN, K. 2015a. The characterization of the human cell line Calu-3 under different culture conditions and its use as an optimized in vitro model to investigate bronchial epithelial function. *European Journal of Pharmaceutical Sciences*, 69, 1-9.
- KREFT, M. E., JERMAN, U. D., LASIČ, E., LANIŠNIK RIŽNER, T., HEVIR-KENE, N., PETERNEL, L. & KRISTAN, K. 2015b. The Characterization of the Human Nasal Epithelial Cell Line RPMI 2650 Under Different Culture Conditions and Their Optimization for an Appropriate in vitro Nasal Model. *Pharmaceutical Research*, 32, 665-679.
- KUEHN, A., KLETTING, S., DE SOUZA CARVALHO-WODARZ, C., REPNIK, U., GRIFFITHS, G., FISCHER, U., MEESE, E., HUWER, H., WIRTH, D. & MAY, T. 2016. Human alveolar epithelial cells expressing tight junctions to model the air-blood barrier. *ALTEX*.
- KUEMPEL, E. D. 1997. *Development of a biomathematical lung model to describe respirable particle retention and to investigate exposure, dose, and disease in United States coal miners*, University of Cincinnati.
- KUEPFER, L., NIEDERALT, C., WENDL, T., SCHLENDER, J. F., WILLMANN, S., LIPPERT, J., BLOCK, M., EISSING, T. & TEUTONICO, D. 2016. Applied Concepts in PBPK Modeling: How to Build a PBPK/PD Model. *CPT: Pharmacometrics & Systems Pharmacology*, 5, 516-531.
- KUMAR, A., TERAKOSOLPHAN, W., HASSOUN, M., VANDERA, K.-K., NOVICKY, A., HARVEY, R., ROYALL, P. G., BICER, E. M., ERIKSSON, J. & EDWARDS, K. 2017. A biocompatible synthetic lung fluid based on human respiratory tract lining fluid composition. *Pharmaceutical research*, 34, 2454-2465.

- KUNCHAROENWIRAT, N., CHATUPHONPRASERT, W. & JARUKAMJORN, K. 2021. Factors influencing cell differentiation and expressions of cytochrome P450s and transporters in Caco-2 cells. *Songklanakarin Journal of Science & Technology*, 43.
- KÜRTI, L., VESZELKA, S., BOCSIK, A., OZSVÁRI, B., PUSKÁS, L. G., KITTEL, A., SZABÓ-RÉVÉSZ, P. & DELI, M. A. 2013. Retinoic acid and hydrocortisone strengthen the barrier function of human RPMI 2650 cells, a model for nasal epithelial permeability. *Cytotechnology*, 65, 395-406.
- KWON, H. C., SOHN, H., KIM, D. H., SHIN, D. M., JEONG, C. H., CHANG, Y. H., YUNE, J. H., KIM, Y. J., KIM, D.-W. & KIM, S. H. 2021. In Vitro and In Vivo Study on the Toxic Effects of Propiconazole Fungicide in the Pathogenesis of Liver Fibrosis. *Journal of Agricultural and Food Chemistry*, 69, 7399-7408.
- LAIRD, W. J. D., GLEDHILL, A. J. & LAPPIN, G. J. 2003. Metabolism of methyl-(E)-2-[2-[6-(2-cyanophenoxy)pyrimidin-4-yl]oxy]phenyl]-3-methoxyacrylate (azoxystrobin) in rat. *Xenobiotica*, 33, 677-690.
- LAKE, B. G. 2018. Human relevance of rodent liver tumour formation by constitutive androstane receptor (CAR) activators. *J Toxicology research*, 7, 697-717.
- LANKAS, G. R., CARTWRIGHT, M. E. & UMBENHAUER, D. 1997. P-glycoprotein deficiency in a subpopulation of CF-1 mice enhances avermectin-induced neurotoxicity. *Toxicology & applied pharmacology*, 143, 357-365.
- LARREGIEU, C. A. & BENET, L. Z. 2013. Drug discovery and regulatory considerations for improving in silico and in vitro predictions that use Caco-2 as a surrogate for human intestinal permeability measurements. *The AAPS journal*, 15, 483-497.
- LARSEN, S. T., DA SILVA, E., HANSEN, J. S., JENSEN, A. C. Ø., KOPONEN, I. K. & SØRLI, J. B. 2020. Acute Inhalation Toxicity After Inhalation of ZnO Nanoparticles: Lung Surfactant Function Inhibition In Vitro Correlates With Reduced Tidal Volume in Mice. *International Journal of Toxicology*, 39, 321-327.
- LAVÉ, T., COASSOLO, P. & REIGNER, B. 1999. Prediction of Hepatic Metabolic Clearance Based on Interspecies Allometric Scaling Techniques and In Vitro-In Vivo Correlations. *Clinical Pharmacokinetics*, 36, 211-231.
- LAW, V., KNOX, C., DJOUMBOU, Y., JEWISON, T., GUO, A. C., LIU, Y., MACIEJEWSKI, A., ARNDT, D., WILSON, M., NEVEU, V., TANG, A., GABRIEL, G., LY, C., ADAMJEE, S., DAME, Z. T., HAN, B., ZHOU, Y. & WISHART, D. S. 2014. DrugBank 4.0: shedding new light on drug metabolism. *Nucleic acids research*, 42, D1091-D1097.
- LÁZNÍČEK, M., KVĚTINA, J., MAZÁK, J. & KRCH, V. 1987. Plasma protein binding-lipophilicity relationships: interspecies comparison of some organic acids. *J Pharm Pharmacol*, 39, 79-83.
- LÁZNÍČEK, M. & LÁZNÍČKOVÁ, A. 1995. The effect of lipophilicity on the protein binding and blood cell uptake of some acidic drugs. *J Pharm Biomed Anal*, 13, 823-8.
- LEA, T. 2015. Caco-2 cell line. *The impact of food bioactives on health*, 103-111.
- LECHNER, J. F. & LAVECK, M. A. 1985. A serum-free method for culturing normal human bronchial epithelial cells at clonal density. *Journal of tissue culture methods*, 9, 43-48.
- LEE, B.-M., & KACEW, S. 2012. *Lu's Basic Toxicology: Fundamentals, Target Organs, and Risk Assessment*, Sixth Edition CRC Press.
- LEE, J.-Y. J., MILLER, J. A., BASU, S., KEE, T.-Z. V. & LOO, L.-H. 2018. Building predictive in vitro pulmonary toxicity assays using high-throughput imaging and artificial intelligence. *Archives of Toxicology*, 92, 2055-2075.
- LEE, J. B., ZGAIR, A., TAHA, D. A., ZANG, X., KAGAN, L., KIM, T. H., KIM, M. G., YUN, H.-Y., FISCHER, P. M. & GERSHKOVICH, P. 2017. Quantitative analysis of lab-to-lab variability in Caco-2 permeability assays. *European Journal of Pharmaceutics and Biopharmaceutics*, 114, 38-42.

- LEHMANN, A. D., DAUM, N., BUR, M., LEHR, C.-M., GEHR, P. & ROTHEN-RUTISHAUSER, B. M. 2011. An in vitro triple cell co-culture model with primary cells mimicking the human alveolar epithelial barrier. *European Journal of Pharmaceutics and Biopharmaceutics*, 77, 398-406.
- LEHR, C.-M. 15 June 2021. RE: *In vitro models of the human airblood-barrier for developing novel anti-infectives*.
- LEVINE, S. L., ORIS, J. T. & DENISON, M. S. 1999. Modulation of CYP1A expression in rainbow trout by a technical grade formulation of propiconazole. *Environmental Toxicology Chemistry: An International Journal*, 18, 2565-2573.
- LEWIS, J. 1985. The birth of EPA. *Environmental Protection Agency*, 11, 6.
- LI, L., CARRATT, S., HARTOG, M., KOVALCHUK, N., JIA, K., WANG, Y., ZHANG, Q.-Y., EDWARDS, P., VAN WINKLE, L. & DING, X. 2017. Human CYP2A13 and CYP2F1 Mediate Naphthalene Toxicity in the Lung and Nasal Mucosa of CYP2A13/2F1-Humanized Mice. *Environmental Health Perspectives*, 125, 067004.
- LI, X., YAO, Y., WANG, S. & XU, S. 2020. Resveratrol relieves chlorothalonil-induced apoptosis and necroptosis through miR-15a/Bcl2-A20 axis in fish kidney cells. *Fish & Shellfish Immunology*, 107, 427-434.
- LIANG, Y., DONG, B., PANG, N. & HU, J. 2019. ROS generation and DNA damage contribute to abamectin-induced cytotoxicity in mouse macrophage cells. *Chemosphere*, 234, 328-337.
- LIN, H., LI, H., CHO, H.-J., BIAN, S., ROH, H.-J., LEE, M.-K., KIM, J. S., CHUNG, S.-J., SHIM, C.-K. & KIM, D.-D. 2007. Air-Liquid Interface (ALI) Culture of Human Bronchial Epithelial Cell Monolayers as an in vitro Model for Airway Drug Transport Studies. *Journal of Pharmaceutical Sciences*, 96, 341-350.
- LIN, Y.-W., ZHOU, Q. T., HU, Y., ONUFRAK, N. J., SUN, S., WANG, J., FORREST, A., CHAN, H.-K. & LI, J. 2017. Pulmonary Pharmacokinetics of Colistin following Administration of Dry Powder Aerosols in Rats. *Antimicrobial Agents and Chemotherapy*, 61, e00973-17.
- LINDER, A., FRIEDEL, G., FRITZ, P., KIVISTÖ, K. T., MCCLELLAN, M. & TOOMES, H. 1996. The Ex-Vivo Isolated, Perfused Human Lung Model: Description and Potential Applications. *Thorac Cardiovasc Surg*, 44, 140-146.
- LIU, G., BETTS, C., CUNOOSAMY, D. M., ÅBERG, P. M., HORNBERG, J. J., SIVARS, K. B. & COHEN, T. S. 2019. Use of precision cut lung slices as a translational model for the study of lung biology. *Respiratory Research*, 20, 162.
- LIU, X., COOPER, D. E., CLUNTUN, A. A., WARMOES, M. O., ZHAO, S., REID, M. A., LIU, J., LUND, P. J., LOPES, M., GARCIA, B. A., WELLEN, K. E., KIRSCH, D. G. & LOCASALE, J. W. 2018. Acetate Production from Glucose and Coupling to Mitochondrial Metabolism in Mammals. *Cell*, 175, 502-513.e13.
- LIU, Y.-J., HUANG, P.-L., CHANG, Y.-F., CHEN, Y.-H., CHIOU, Y.-H., XU, Z.-L. & WONG, R.-H. 2006. GSTP1 Genetic Polymorphism Is Associated with a Higher Risk of DNA Damage in Pesticide-Exposed Fruit Growers. *Cancer Epidemiology Biomarkers & Prevention*, 15, 659.
- LIU, Y., NUSRAT, A., SCHNELL, F. J., REAVES, T. A., WALSH, S., POCHET, M. & PARKOS, C. A. 2000. Human junction adhesion molecule regulates tight junction resealing in epithelia. *Journal of Cell Science*, 113, 2363-2374.
- LOMBRY, C., EDWARDS, D. A., PRÉAT, V. & VANBEVER, R. 2004. Alveolar macrophages are a primary barrier to pulmonary absorption of macromolecules. *American Journal of Physiology-Lung Cellular and Molecular Physiology*, 286, L1002-L1008.
- LOURENÇO, R. V. & COTROMANES, E. 1982. Clinical Aerosols: I. Characterization of Aerosols and Their Diagnostic Uses. *Archives of Internal Medicine*, 142, 2163-2172.
- MACDONALD, N. & GLEDHILL, A. 2007. Potential impact of ABCB1 (p-glycoprotein) polymorphisms on avermectin toxicity in humans. *Archives of toxicology*, 81, 553-563.



- MADDEN, J. 2010. Introduction to QSAR and other in silico methods to predict toxicity. *In silico toxicology: Principles and applications*. Cambridge (UK): Royal Soc Chemistry. p, 11-30.
- MAGGI, F., TANG, F. H. M., LA CECILIA, D. & MCBRATNEY, A. 2019. PEST-CHEMGRIDS, global gridded maps of the top 20 crop-specific pesticide application rates from 2015 to 2025. *Scientific Data*, 6, 170.
- MAINA, J. N. 2002. Structure, function and evolution of the gas exchangers: comparative perspectives. *Journal of anatomy*, 201, 281-304.
- MAIOLI, M. A., DE MEDEIROS, H. C., GUELFI, M., TRINCA, V., PEREIRA, F. T. & MINGATTO, F. E. 2013. The role of mitochondria and biotransformation in abamectin-induced cytotoxicity in isolated rat hepatocytes. *Toxicology in Vitro*, 27, 570-579.
- MAIRINGER, S., SAKE, J. A., LOZANO, I. H., FILIP, T., SAUBERER, M., STANEK, J., WANEK, T., EHRHARDT, C. & LANGER, O. 2020. Assessing the Activity of Multidrug Resistance-Associated Protein 1 at the Lung Epithelial Barrier. *Journal of Nuclear Medicine*, 61, 1650.
- MAMANE, A., BALDI, I., TESSIER, J.-F., RAHERISON, C. & BOUVIER, G. 2015. Occupational exposure to pesticides and respiratory health. *European Respiratory Review*, 24, 306.
- MAN, D. K., KANNO, T., MANZO, G., ROBERTSON, B. D., LAM, J. K. W. & MASON, A. J. 2018. Rifampin- or Capreomycin-Induced Remodeling of the Mycobacterium smegmatis Mycolic Acid Layer Is Mitigated in Synergistic Combinations with Cationic Antimicrobial Peptides. *mSphere*, 3.
- MANTAJ, J., ABU-SHAMS, T., ENLO-SCOTT, Z., SWEDROWSKA, M. & VLLASALIU, D. 2018. Role of the basement membrane as an intestinal barrier to absorption of macromolecules and nanoparticles. *Molecular pharmaceuticals*, 15, 5802-5808.
- MARIASSY, A. T. 1992. Epithelial cells of trachea and bronchi. *Comparative biology of the normal lung*, 1, 63-76.
- MARK LAFRANCONI, W. & HUXTABLE, R. J. 1984. Hepatic metabolism and pulmonary toxicity of monocrotaline using isolated perfused liver and lung. *Biochemical Pharmacology*, 33, 2479-2484.
- MARTIN, F. & JULIAN, S. 2020. Industrial Chemicals in the Regulatory Laboratory: Self-responsibility and Inclusive Governance Research Handbook on EU Environmental Law. Cheltenham, UK: Edward Elgar Publishing.
- MATIDA, E. A., FINLAY, W. H., BREUER, M. & LANGE, C. F. 2006. Improving Prediction of Aerosol Deposition in an Idealized Mouth Using Large-Eddy Simulation. *Journal of Aerosol Medicine*, 19, 290-300.
- MAZUR, C. S., MARCHITTI, S. A. & ZASTRE, J. 2015. P-glycoprotein inhibition by the agricultural pesticide propiconazole and its hydroxylated metabolites: Implications for pesticide-drug interactions. *Toxicology Letters*, 232, 37-45.
- MCKENZIE, Z., KENDALL, M., MACKAY, R.-M., TETLEY, T. D., MORGAN, C., GRIFFITHS, M., CLARK, H. W. & MADSEN, J. 2015. Nanoparticles modulate surfactant protein A and D mediated protection against influenza A infection in vitro. *Philosophical Transactions of the Royal Society B: Biological Sciences*, 370, 20140049.
- MEHENDALE, H. M., ANGEVINE, L. S. & OHMIYA, Y. 1981. The isolated perfused lung — A critical evaluation. *Toxicology*, 21, 1-36.
- MEINDL, C., STRANZINGER, S., DZIDIC, N., SALAR-BEHZADI, S., MOHR, S., ZIMMER, A. & FRÖHLICH, E. 2015. Permeation of Therapeutic Drugs in Different Formulations across the Airway Epithelium In Vitro. *PLOS ONE*, 10, e0135690.
- MENSCH, J., MELIS, A., MACKIE, C., VERRECK, G., BREWSTER, M. E. & AUGUSTIJNS, P. 2010. Evaluation of various PAMPA models to identify the most discriminating method for the prediction of BBB permeability. *European journal of pharmaceuticals and biopharmaceuticals*, 74, 495-502.

- MERCIER, C., PEREK, N. & DELAVENNE, X. 2018. Is RPMI 2650 a Suitable In Vitro Nasal Model for Drug Transport Studies? *European Journal of Drug Metabolism and Pharmacokinetics*, 43, 13-24.
- METZ, J. K., WIEGAND, B., SCHNUR, S., KNOTH, K., SCHNEIDER-DAUM, N., GROß, H., CROSTON, G., REINHEIMER, T. M., LEHR, C.-M. & HITTINGER, M. 2020. Modulating the barrier function of human alveolar epithelial (hAELVi) cell monolayers as a model of inflammation. *Alternatives to Laboratory Animals*, 48, 252-267.
- MILLER, C., GEORGE, S. & NIKLASON, L. 2010. Developing a tissue-engineered model of the human bronchiole. *Journal of tissue engineering and regenerative medicine*, 4, 619-627.
- MIN, K. A., ZHANG, X., YU, J.-Y. & ROSANIA, G. R. 2014. Computational approaches to analyse and predict small molecule transport and distribution at cellular and subcellular levels. *Biopharmaceutics & Drug Disposition*, 35, 15-32.
- MINCHIN, R. F. & BOYD, M. R. 1983. Localization of Metabolic Activation and Deactivation Systems in the Lung: Significance to the Pulmonary Toxicity of Xenobiotics. *Annual Review of Pharmacology and Toxicology*, 23, 217-238.
- MISRA, B. B. 2019. Metabolomics Tools to Study Links Between Pollution and Human Health: an Exposomics Perspective. *Current Pollution Reports*, 5, 93-111.
- MITCHELL, L. A., WARD, C., KWON, M., MITCHELL, P. O., QUINTERO, D. A., NUSRAT, A., PARKOS, C. A. & KOVAL, M. 2015. Junctional Adhesion Molecule A Promotes Epithelial Tight Junction Assembly to Augment Lung Barrier Function. *The American Journal of Pathology*, 185, 372-386.
- MOHAMMED, H., ROBERTS, D. L., COPLEY, M., HAMMOND, M., NICHOLS, S. C. & MITCHELL, J. P. 2012. Effect of sampling volume on dry powder inhaler (DPI)-emitted aerosol aerodynamic particle size distributions (APSDs) measured by the Next-Generation Pharmaceutical Impactor (NGI) and the Andersen eight-stage cascade impactor (ACI). *Aaps Pharmscitech*, 13, 875-882.
- MORIN, J.-P., BASTE, J.-M., GAY, A., CROCHEMORE, C., CORBIÈRE, C. & MONTEIL, C. 2013. Precision cut lung slices as an efficient tool for in vitro lung physio-pharmacotoxicology studies. *Xenobiotica*, 43, 63-72.
- MOVIA, D., BRUNI-FAVIER, S. & PRINA-MELLO, A. 2020. In vitro Alternatives to Acute Inhalation Toxicity Studies in Animal Models—A Perspective. *Frontiers in Bioengineering and Biotechnology*, 8.
- MROZ, M. S. & HARVEY, B. J. 2019. Ursodeoxycholic acid inhibits ENaC and Na/K pump activity to restore airway surface liquid height in cystic fibrosis bronchial epithelial cells. *Steroids*, 151, 108461.
- MSIBI, S. S., CHEN, C.-Y., CHANG, C.-P., CHEN, C.-J., CHIANG, S.-Y. & WU, K.-Y. 2021. High pesticide inhalation exposure from multiple spraying sources amongst applicators in Eswatini, Southern Africa. *Pest Management Science*, n/a.
- MUDWAY, I. S., KELLY, F. J. & HOLGATE, S. T. 2020. Oxidative stress in air pollution research. *Free radical biology & medicine*, 151, 2-6.
- MURALIDHARAN, P., MALAPIT, M., MALLORY, E., HAYES, D. & MANSOUR, H. M. 2015. Inhalable nanoparticulate powders for respiratory delivery. *Nanomedicine: Nanotechnology, Biology and Medicine*, 11, 1189-1199.
- MURGIA, X., YASAR, H., CARVALHO-WODARZ, C., LORETZ, B., GORDON, S., SCHWARZKOPF, K., SCHAEFER, U. & LEHR, C.-M. 2017. Modelling the bronchial barrier in pulmonary drug delivery: A human bronchial epithelial cell line supplemented with human tracheal mucus. *European Journal of Pharmaceutics and Biopharmaceutics*, 118, 79-88.
- MUTCH, E., BLAIN, P. G. & WILLIAMS, F. M. 1999. The role of metabolism in determining susceptibility to parathion toxicity in man. *Toxicology Letters*, 107, 177-187.

- NATH, A. & ATKINS, W. M. 2008. A Quantitative Index of Substrate Promiscuity. *Biochemistry*, 47, 157-166.
- NATSCH, A., LANDSIEDEL, R. & KOLLE, S. N. 2021. A triangular approach for the validation of new approach methods for skin sensitization. *ALTEX-Alternatives to animal experimentation*.
- NAVE, R., FISHER, R. & MCCRACKEN, N. 2007. In vitro metabolism of beclomethasone dipropionate, budesonide, ciclesonide, and fluticasone propionate in human lung precision-cut tissue slices. *Respiratory Research*, 8, 65.
- NAVE, R., FISHER, R. & ZECH, K. 2006. In vitro metabolism of ciclesonide in human lung and liver precision-cut tissue slices. *Biopharmaceutics & drug disposition*, 27, 197-207.
- NAWROTH, J. C., ROTH, D., VAN SCHADEWIJK, A., RAVI, A., MAULANA, T. I., SENGER, C. N., VAN RIET, S., NINABER, D. K., RYAN, A. L., HIEMSTRA, P. S. & VAN DER DOES, A. M. 2021. Breathing on Chip: Biomechanical forces change airway epithelial cell biology in a human Airway Lung-Chip. *bioRxiv*, 2021.05.07.443164.
- NAZAROFF, W. W. & SINGER, B. C. 2004. Inhalation of hazardous air pollutants from environmental tobacco smoke in US residences. *Journal of Exposure Science & Environmental Epidemiology*, 14, S71-S77.
- NESNOW, S., GRINDSTAFF, R. D., LAMBERT, G., PADGETT, W. T., BRUNO, M., GE, Y., CHEN, P.-J., WOOD, C. E. & MURPHY, L. 2011. Propiconazole increases reactive oxygen species levels in mouse hepatic cells in culture and in mouse liver by a cytochrome P450 enzyme mediated process. *Chemico-Biological Interactions*, 194, 79-89.
- NEUHAUS, V., SCHAUDIEN, D., GOLOVINA, T., TEMANN, U.-A., THOMPSON, C., LIPPMANN, T., BERSCH, C., PFENNIG, O., JONIGK, D., BRAUBACH, P., FIEGUTH, H.-G., WARNECKE, G., YUSIBOV, V., SEWALD, K. & BRAUN, A. 2017. Assessment of long-term cultivated human precision-cut lung slices as an ex vivo system for evaluation of chronic cytotoxicity and functionality. *Journal of Occupational Medicine and Toxicology*, 12, 13.
- NICHOLS, S., BROWN, D. & SMURTHWAITE, M. 1998. New concept for the variable flow rate Andersen cascade impactor and calibration data. *Journal of aerosol medicine*, 11, S-133-S-138.
- NIGAM, S. K. 2015. What do drug transporters really do? *Nature reviews. Drug discovery*, 14, 29-44.
- OECD 2017. Test No. 433: Acute inhalation toxicity-fixed concentration procedure. . OECD Guidelines for the testing of chemicals, Section 4.
- OESCH, F., FABIAN, E. & LANDSIEDEL, R. 2019. Xenobiotica-metabolizing enzymes in the lung of experimental animals, man and in human lung models. *Archives of Toxicology*, 93, 3419-3489.
- OH, S. M., KIM, H. R., PARK, Y. J., LEE, S. Y. & CHUNG, K. H. 2011. Organic extracts of urban air pollution particulate matter (PM2.5)-induced genotoxicity and oxidative stress in human lung bronchial epithelial cells (BEAS-2B cells). *Mutation Research/Genetic Toxicology and Environmental Mutagenesis*, 723, 142-151.
- OLESTI, E., GONZÁLEZ-RUIZ, V., WILKS, M. F., BOCCARD, J. & RUDAZ, S. 2021. Approaches in metabolomics for regulatory toxicology applications. *Analyst*, 146, 1820-1834.
- OLIVEIRA, P., FORTUNA, A., ALVES, G. & FALCAO, A. 2016. Drug-metabolizing enzymes and efflux transporters in nasal epithelium: influence on the bioavailability of intranasally administered drugs. *Current drug metabolism*, 17, 628-647.
- OLSSON, B. & BÄCKMAN, P. Mimetikos Preludium™: A New Pharma-friendly Aerosol Drug Deposition Calculator. *Respiratory Drug Delivery*, 2018. 103-111.
- OLSSON, B., BONDESSON, E., BORGSTRÖM, L., EDSBÄCKER, S., EIREFELT, S., EKELUND, K., GUSTAVSSON, L. & HEGELUND-MYRBÄCK, T. 2011. Pulmonary Drug Metabolism, Clearance, and Absorption. In: SMYTH, H. D. C. & HICKEY, A. J. (eds.) *Controlled Pulmonary Drug Delivery*. New York, NY: Springer New York.

- PARASURAMAN, S. 2011. Toxicological screening. *Journal of pharmacology & pharmacotherapeutics*, 2, 74.
- PARK, H. S., KIM, S. R. & LEE, Y. C. 2009. Impact of oxidative stress on lung diseases. *Respirology*, 14, 27-38.
- PARKER, S., FOAT, T. & PRESTON, S. 2008. Towards quantitative prediction of aerosol deposition from turbulent flows. *Journal of Aerosol Science*, 39, 99-112.
- PARKINSON, O. T., TEITELBAUM, A. M., WHITTINGTON, D., KELLY, E. J. & RETTIE, A. E. 2016. Species Differences in Microsomal Oxidation and Glucuronidation of 4-*Ipomeanol*: Relationship to Target Organ Toxicity. *Drug Metabolism and Disposition*, 44, 1598.
- PATLEWICZ, G. & FITZPATRICK, J. M. 2016. Current and future perspectives on the development, evaluation, and application of in silico approaches for predicting toxicity. *Chemical research in toxicology*, 29, 438-451.
- PATTON, J. S. & BYRON, P. R. 2007. Inhaling medicines: delivering drugs to the body through the lungs. *Nature Reviews Drug Discovery*, 6, 67-74.
- PAULUHN, J. 2005. Overview of inhalation exposure techniques: Strengths and weaknesses. *Experimental and Toxicologic Pathology*, 57, 111-128.
- PAULUHN, J. 2008. Inhalation toxicology: Methodological and regulatory challenges. *Experimental and Toxicologic Pathology*, 60, 111-124.
- PELKONEN, O., BENNEKOU, S. H., CRIVELLENTI, F., TERRON, A. & HERNANDEZ, A. F. 2019. Integration of epidemiological findings with mechanistic evidence in regulatory pesticide risk assessment: EFSA experiences. *Archives of Toxicology*, 93, 1779-1788.
- PHALEN, R. F., CUDDIHY, R. G., FISHER, G. L., MOSS, O. R., SCHLESINGER, R. B., SWIFT, D. L. & YE, H. C. 1991. Main Features of the Proposed NCRP Respiratory Tract Model. *Radiation Protection Dosimetry*, 38, 179-184.
- PRESCOTT, M. J. & LIDSTER, K. 2017. Improving quality of science through better animal welfare: the NC3Rs strategy. *Lab Animal*, 46, 152-156.
- PRIMAVERSSY, D., METZ, J., SCHNUR, S., SCHNEIDER, M., LEHR, C.-M. & HITTINGER, M. 2021. Pulmonary in vitro instruments for the replacement of animal experiments. *European Journal of Pharmaceutics and Biopharmaceutics*, 168, 62-75.
- QUINLAN, G. J., LAMB, N. J., TILLEY, R., EVANS, T. W. & GUTTERIDGE, J. M. 1997. Plasma hypoxanthine levels in ARDS: implications for oxidative stress, morbidity, and mortality. *American Journal of Respiratory and Critical Care Medicine*, 155, 479-484.
- RADENAC, G., COTEUR, G., DANIS, B., DUBOIS, P. & WARNAU, M. 2004. Measurement of EROD Activity: Caution on Spectral Properties of Standards Used. *Marine Biotechnology*, 6, 307-311.
- RADIVOJEV, S., ZELNITZ, S., PAUDEL, A. & FRÖHLICH, E. 2019. Searching for physiologically relevant in vitro dissolution techniques for orally inhaled drugs. *International Journal of Pharmaceutics*, 556, 45-56.
- RANGAN, S. 1972. A new human cell line (FaDu) from a hypopharyngeal carcinoma. *Cancer*, 29, 117-121.
- RANI, M. & SHANKER, U. 2018. Degradation of traditional and new emerging pesticides in water by nanomaterials: recent trends and future recommendations. *International Journal of Environmental Science and Technology*, 15, 1347-1380.
- RAYNER, R. E., MAKENA, P., PRASAD, G. L. & CORMET-BOYAKA, E. 2019. Optimization of Normal Human Bronchial Epithelial (NHBE) Cell 3D Cultures for in vitro Lung Model Studies. *Scientific Reports*, 9, 500.
- REDDY, B. B. K. & KARUNAKAR, A. 2011. Biopharmaceutics classification system: A regulatory approach. *Dissolution Technologies*, 18, 31-37.
- REN, C., KONG, D., NING, C., XING, H., CHENG, Y., ZHANG, Y., LU, Y., LI, N., CHEN, X. & ZHAO, D. 2021. Improved Pharmacokinetic Characteristics of Ursolic Acid in Rats Following

- Intratracheal Instillation and Nose-Only Inhalation Exposure. *Journal of Pharmaceutical Sciences*, 110, 905-913.
- RIM, K.-T. 2020. Adverse outcome pathways for chemical toxicity and their applications to workers' health: a literature review. *Toxicology and Environmental Health Sciences*, 12, 99-108.
- RÖSCH, A., GOTTARDI, M., VIGNET, C., CEDERGREEN, N. & HOLLENDER, J. 2017. Mechanistic Understanding of the Synergistic Potential of Azole Fungicides in the Aquatic Invertebrate *Gammarus pulex*. *Environmental Science & Technology*, 51, 12784-12795.
- ROSNER, E., KLOS, C. & DEKANT, W. 1996. Biotransformation of the Fungicide Chlorthalonil by Glutathione Conjugation. *Fundamental and Applied Toxicology*, 33, 229-234.
- ROSTAMI, A. A. 2009. Computational Modeling of Aerosol Deposition in Respiratory Tract: A Review. *Inhalation Toxicology*, 21, 262-290.
- ROSTAMI, M. R., LEBLANC, M. G., STRULOVICI-BAREL, Y., ZUO, W., MEZEY, J. G., O'BEIRNE, S. L., KANER, R. J., LEOPOLD, P. L. & CRYSTAL, R. G. 2021. Smoking shifts human small airway epithelium club cells toward a lesser differentiated population. *npj Genomic Medicine*, 6, 73.
- ROTH, R. A. In vitro Toxicology of the Respiratory System. In: GALLI, C. L., MARINOVICH, M. & GOLDBERG, A. M., eds. *Modulation of Cellular Responses in Toxicity*, 1995// 1995 Berlin, Heidelberg. Springer Berlin Heidelberg, 331-371.
- ROTHEN-RUTISHAUSER, B., CLIFT, M. J., JUD, C., FINK, A. & WICK, P. 2012. Human epithelial cells in vitro—Are they an advantageous tool to help understand the nanomaterial-biological barrier interaction? *EURO NanoTox Letters*, 4, 1-20.
- RUBIN, K., EWING, P., BÄCKSTRÖM, E., ABRAHAMSSON, A., BONN, B., KAMATA, S. & GRIME, K. 2020. Pulmonary Metabolism of Substrates for Key Drug-Metabolizing Enzymes by Human Alveolar Type II Cells, Human and Rat Lung Microsomes, and the Isolated Perfused Rat Lung Model. *Pharmaceutics*, 12.
- RYRFELDT, Å., COTGREAVE, I. A. & MOLDÉUS, P. 1990. In Vitro Models to Study Mechanisms of Lung Toxicity. *Alternatives to Laboratory Animals*, 18, 267-281.
- SAFORO, D., OMER, L., SMOLENKOV, A., BARVE, A., CASSON, L., BOYD, N., CLARK, G., SISKIND, L. & BEVERLY, L. 2019. Primary lung cancer samples cultured under microenvironment-mimetic conditions enrich for mesenchymal stem-like cells that promote metastasis. *Scientific Reports*, 9, 4177.
- SAITO, S., OGAWA, J.-I. & MINAMIYA, Y. 2005. Pulmonary reexpansion causes xanthine oxidase-induced apoptosis in rat lung. *American Journal of Physiology-Lung Cellular and Molecular Physiology*, 289, L400-L406.
- SAKAGAMI, M. 2006. In vivo, in vitro and ex vivo models to assess pulmonary absorption and disposition of inhaled therapeutics for systemic delivery. *Advanced Drug Delivery Reviews*, 58, 1030-1060.
- SAKAGAMI, M. 2020. In vitro, ex vivo and in vivo methods of lung absorption for inhaled drugs. *Advanced Drug Delivery Reviews*, 161-162, 63-74.
- SAKAGAMI, M., OMIDI, Y., CAMPBELL, L., KANDALRAFT, L. E., MORRIS, C. J., BARAR, J. & GUMBLETON, M. 2006. Expression and Transport Functionality of FcRn within Rat Alveolar Epithelium: A Study in Primary Cell Culture and in the Isolated Perfused Lung. *Pharmaceutical Research*, 23, 270-279.
- SAKAMOTO, A., MATSUMARU, T., YAMAMURA, N., SUZUKI, S., UCHIDA, Y., TACHIKAWA, M. & TERASAKI, T. 2015. Drug Transporter Protein Quantification of Immortalized Human Lung Cell Lines Derived from Tracheobronchial Epithelial Cells (Calu-3 and BEAS2-B), Bronchiolar-Alveolar Cells (NCI-H292 and NCI-H441), and Alveolar Type II-like Cells (A549) by Liquid Chromatography-Tandem Mass Spectrometry. *Journal of Pharmaceutical Sciences*, 104, 3029-3038.

- SALOMON, J. J., MUCHITSCH, V. E., GAUSTERER, J. C., SCHWAGERUS, E., HUWER, H., DAUM, N., LEHR, C.-M. & EHRHARDT, C. 2014. The Cell Line NCI-H441 Is a Useful in Vitro Model for Transport Studies of Human Distal Lung Epithelial Barrier. *Molecular Pharmaceutics*, 11, 995-1006.
- SAMBUY, Y., DE ANGELIS, I., RANALDI, G., SCARINO, M. L., STAMMATI, A. & ZUCCO, F. 2005. The Caco-2 cell line as a model of the intestinal barrier: influence of cell and culture-related factors on Caco-2 cell functional characteristics. *Cell Biology and Toxicology*, 21, 1-26.
- SAPBAMRER, R. & THAMMACHAI, A. 2020. Factors affecting use of personal protective equipment and pesticide safety practices: A systematic review. *Environmental Research*, 185, 109444.
- SCIUBBA, E. 2016. A Critical Reassessment of the Hess–Murray Law. *Entropy*, 18, 283.
- SELG, E., EWING, P., ACEVEDO, F., SJÖBERG, C.-O., RYRFELDT, Å. & GERDE, P. 2012. Dry Powder Inhalation Exposures of the Endotracheally Intubated Rat Lung, Ex Vivo and In Vivo: The Pulmonary Pharmacokinetics of Fluticasone Furoate. *Journal of Aerosol Medicine and Pulmonary Drug Delivery*, 26, 181-189.
- SELO, M. A., AL-ALAK, H. H. & EHRHARDT, C. 2019. Lung transporters and absorption mechanisms in the lungs. *Inhalation Aerosols*. CRC Press.
- SELO, M. A., SAKE, J. A., KIM, K.-J. & EHRHARDT, C. 2021. In vitro and ex vivo models in inhalation biopharmaceutical research — advances, challenges and future perspectives. *Advanced Drug Delivery Reviews*, 113862.
- SEO, P. R., TEKSIN, Z. S., KAO, J. P. & POLLI, J. E. 2006. Lipid composition effect on permeability across PAMPA. *European journal of pharmaceutical sciences*, 29, 259-268.
- SHI, H., KLEINSTREUER, C. & ZHANG, Z. 2007. Modeling of inertial particle transport and deposition in human nasal cavities with wall roughness. *Journal of Aerosol Science*, 38, 398-419.
- SHIN, S.-I. & VAN DIGGELEN, O. P. 1978. Phenotypic alterations in mammalian cell lines after mycoplasma infection. *Mycoplasma infection of cell cultures*. Springer.
- SIBINOVSKA, N., ŽAKELJ, S. & KRISTAN, K. 2019. Suitability of RPMI 2650 cell models for nasal drug permeability prediction. *European Journal of Pharmaceutics and Biopharmaceutics*, 145, 85-95.
- SIBINOVSKA, N., ŽAKELJ, S., ROŠKAR, R. & KRISTAN, K. 2020. Suitability and functional characterization of two Calu-3 cell models for prediction of drug permeability across the airway epithelial barrier. *J International Journal of Pharmaceutics*, 585, 119484.
- SIEGEL, M. R. 1970. Reactions of certain trichloromethyl sulphenyl fungicides with low-molecular-weight thiols. In vivo studies with cells of *Saccharomyces pastorianus*. *Journal of Agricultural and Food Chemistry*, 18, 823-826.
- SINGH, A. V., ROSENKRANZ, D., ANSARI, M. H. D., SINGH, R., KANASE, A., SINGH, S. P., JOHNSTON, B., TENTSCHEIT, J., LAUX, P. & LUCH, A. 2020. Artificial intelligence and machine learning empower advanced biomedical material design to toxicity prediction. *Advanced Intelligent Systems*, 2, 2000084.
- SINGH, K. N. & MERCHANT, K. 2012. The Agrochemical Industry. In: KENT, J. A. (ed.) *Handbook of Industrial Chemistry and Biotechnology*. Boston, MA: Springer US.
- SINGH, S., KUMAR, V., SINGH, P., THAKUR, S., BANERJEE, B. D., RAUTELA, R. S., GROVER, S. S., RAWAT, D. S., PASHA, S. T., JAIN, S. K. & RAI, A. 2011. Genetic polymorphisms of GSTM1, GSTT1 and GSTP1 and susceptibility to DNA damage in workers occupationally exposed to organophosphate pesticides. *Mutation Research/Genetic Toxicology and Environmental Mutagenesis*, 725, 36-42.
- SLIFER, Z. M. & BLIKSLAGER, A. T. 2020. The Integral Role of Tight Junction Proteins in the Repair of Injured Intestinal Epithelium. *International Journal of Molecular Sciences*, 21, 972.

- SON, Y.-J. & MCCONVILLE, J. T. 2009. Development of a standardized dissolution test method for inhaled pharmaceutical formulations. *International Journal of Pharmaceutics*, 382, 15-22.
- SONWANI, S. & SAXENA, P. J. I. 2016. Identifying the sources of primary air pollutants and their impact on environmental health: a review. *International Journal of Engineering and Technical Research*, 6, 111-130.
- SØRLI, J. B., HUANG, Y., DA SILVA, E., HANSEN, J. S., ZUO, Y. Y., FREDERIKSEN, M., NØRGAARD, A. W., EBBEHØJ, N. E., LARSEN, S. T. & HOUGAARD, K. S. 2018. Prediction of acute inhalation toxicity using in vitro lung surfactant inhibition. *ALTEX-Alternatives to animal experimentation*, 35, 26-36.
- SOSNOWSKI, T. R., MOSKAL, A. & GRADOŃ, L. 2006. Dynamics of Oropharyngeal Aerosol Transport and Deposition With the Realistic Flow Pattern. *Inhalation Toxicology*, 18, 773-780.
- SPORTY, J. L., HORÁLKOVÁ, L. & EHRHARDT, C. 2008. In vitro cell culture models for the assessment of pulmonary drug disposition. *Expert Opinion on Drug Metabolism & Toxicology*, 4, 333-345.
- SRINIVASAN, B., KOLLI, A. R., ESCH, M. B., ABACI, H. E., SHULER, M. L. & HICKMAN, J. J. 2015. TEER measurement techniques for in vitro barrier model systems. *Journal of laboratory automation*, 20, 107-126.
- STAHLHOFEN, W., RUDOLF, G. & JAMES, A. 1989. Intercomparison of experimental regional aerosol deposition data. *Journal of Aerosol Medicine*, 2, 285-308.
- STEIMER, A., HALTNER, E. & LEHR, C.-M. 2005. Cell culture models of the respiratory tract relevant to pulmonary drug delivery. *Journal of aerosol medicine*, 18, 137-182.
- STEINBERG, G. & GURR, S. J. 2020. Fungi, fungicide discovery and global food security. *Fungal Genetics and Biology*, 144, 103476.
- STONE, K. C., MERCER, R. R., GEHR, P., STOCKSTILL, B. & CRAPO, J. D. 1992. Allometric Relationships of Cell Numbers and Size in the Mammalian Lung. *American Journal of Respiratory Cell Molecular Biology*, 6, 235-243.
- STUCKI, A. O., STUCKI, J. D., HALL, S. R. R., FELDER, M., MERMOUD, Y., SCHMID, R. A., GEISER, T. & GUENAT, O. T. 2015. A lung-on-a-chip array with an integrated bio-inspired respiration mechanism. *Lab on a Chip*, 15, 1302-1310.
- SUDSAKORN, S., BAHADDURI, P., FRETLAND, J. & LU, C. 2020. 2020 FDA Drug-drug interaction guidance: a comparison analysis and action plan by pharmaceutical industrial scientists. *Current Drug Metabolism*, 21, 403-426.
- SUN, G., THAI, S.-F., TULLY, D. B., LAMBERT, G. R., GOETZ, A. K., WOLF, D. C., DIX, D. J. & NESNOW, S. 2005. Propiconazole-induced cytochrome P450 gene expression and enzymatic activities in rat and mouse liver. *Toxicology letters*, 155, 277-287.
- SUN, H., NGUYEN, K., KERNS, E., YAN, Z., YU, K. R., SHAH, P., JADHAV, A. & XU, X. 2017. Highly predictive and interpretable models for PAMPA permeability. *Bioorganic & medicinal chemistry*, 25, 1266-1276.
- TAN, Y.-M., CHAN, M., CHUKWUDEBE, A., DOMORADZKI, J., FISHER, J., HACK, C. E., HINDERLITER, P., HIRASAWA, K., LEONARD, J. & LUMEN, A. 2020. PBPK model reporting template for chemical risk assessment applications. *Regulatory Toxicology and Pharmacology*, 115, 104691.
- TANG, V. W. & GOODENOUGH, D. A. 2003. Paracellular ion channel at the tight junction. *Biophysical journal*, 84, 1660-1673.
- TATE, R. M., VANBENTHUYSEN, K. M., SHASBY, D. M., MCMURTRY, I. F. & REPINE, J. E. 1982. Oxygen-Radical-Mediated Permeability Edema and Vasoconstriction in Isolated Perfused Rabbit Lungs. *American Review of Respiratory Disease*, 126, 802-806.

- TATENO, C., ITO, S., TANAKA, M. & YOSHITAKE, A. 1993. Effects of pyrethroid insecticides on gap junctional intercellular communications in Balb/c3T3 cells by dye-transfer assay. *Cell Biology and Toxicology*, 9, 215-221.
- TAULBEE, D. B. & YU, C. P. 1975. A theory of aerosol deposition in the human respiratory tract. *Journal of Applied Physiology*, 38, 77-85.
- TEHLER, U., FRANSSON, R., THORN, H., FRANEK, F. & WESTERGREN, J. 2018. Lung-Sim: a physiologically based biopharmaceutical prediction tool. *Journal of Aerosol Medicine and Pulmonary Drug Delivery*.
- TERAKOSOLPHAN, W., HASSOUN, M., KUMAR, A. & FORBES, B. Solubility of fluticasone propionate and beclomethasone dipropionate in simulated lung lining fluids. *JOURNAL OF AEROSOL MEDICINE AND PULMONARY DRUG DELIVERY*, 2017. MARY ANN LIEBERT, INC 140 HUGUENOT STREET, 3RD FL, NEW ROCHELLE, NY 10801 USA, A27-A27.
- TICE, C. M. 2001. Selecting the right compounds for screening: does Lipinski's Rule of 5 for pharmaceuticals apply to agrochemicals? *Pest Management Science*, 57, 3-16.
- TICE, R. R., AUSTIN, C. P., KAVLOCK, R. J. & BUCHER, J. R. 2013. Improving the Human Hazard Characterization of Chemicals: A Tox21 Update. *Environmental health perspectives*, 121, 756-765.
- TILLMAN, R. W., SIEGEL, M. R. & LONG, J. W. 1973. Mechanism of action and fate of the fungicide chlorothalonil (2,4,5,6-tetrachloroisophthalonitrile) in biological systems: I. Reactions with cells and subcellular components of *Saccharomyces pastorianus*. *Pesticide Biochemistry and Physiology*, 3, 160-167.
- TIMBRELL, J. 1999. *Principles of biochemical toxicology 3rd ed. Ed. Timbrell JA*, CRC Press LLC, Taylor & Francis.
- TOGAMI, K., YAMAGUCHI, K., CHONO, S. & TADA, H. 2017. Evaluation of permeability alteration and epithelial–mesenchymal transition induced by transforming growth factor- $\beta$ 1 in A549, NCI-H441, and Calu-3 cells: Development of an in vitro model of respiratory epithelial cells in idiopathic pulmonary fibrosis. *Journal of Pharmacological and Toxicological Methods*, 86, 19-27.
- TONNELIER, A., COECKE, S. & ZALDÍVAR, J.-M. 2012. Screening of chemicals for human bioaccumulative potential with a physiologically based toxicokinetic model. *Archives of toxicology*, 86, 393-403.
- TRAN, V. N., VIKTOROVÁ, J. & RUMML, T. 2020. Mycotoxins: Biotransformation and Bioavailability Assessment Using Caco-2 Cell Monolayer. *Toxins*, 12, 628.
- TRAPP, S., ROSANIA, G. R., HOROBIN, R. W. & KORNHUBER, J. 2008. Quantitative modeling of selective lysosomal targeting for drug design. *European Biophysics Journal*, 37, 1317.
- TRONDE, A., BOSQUILLON, C. & FORBES, B. 2008. The Isolated Perfused Lung for Drug Absorption Studies. In: EHRHARDT, C. & KIM, K.-J. (eds.) *Drug Absorption Studies: In Situ, In Vitro and In Silico Models*. Boston, MA: Springer US.
- TRONDE, A., NORDÉN, B., JEPPSSON, A.-B., BRUNMARK, P., NILSSON<sup>†</sup>, E., LENNERNÄS, H. & BENGTSOON, U. H. 2003. Drug Absorption from the Isolated Perfused Rat Lung–Correlations with Drug Physicochemical Properties and Epithelial Permeability. *Journal of Drug Targeting*, 11, 61-74.
- UHLIG, S. & WOLLIN, L. 1994. An improved setup for the isolated perfused rat lung. *Journal of Pharmacological and Toxicological Methods*, 31, 85-94.
- UMACHANDRAN, M., HOWARTH, J. & IOANNIDES, C. 2004. Metabolic and structural viability of precision-cut rat lung slices in culture. *Xenobiotica*, 34, 771-780.
- UPHOFF, C. C. & DREXLER, H. G. 2002. Comparative PCR analysis for detection of mycoplasma infections in continuous cell lines. *In Vitro Cellular & Developmental Biology - Animal*, 38, 79-85.



- UPPSTAD, H., ØVREBØ, S., HAUGEN, A. & MOLLERUP, S. 2010. Importance of CYP1A1 and CYP1B1 in bioactivation of benzo[a]pyrene in human lung cell lines. *Toxicol Lett*, 192, 221-8.
- URQUHART, B. L., TIRONA, R. G. & KIM, R. B. 2007. Nuclear receptors and the regulation of drug-metabolizing enzymes and drug transporters: implications for interindividual variability in response to drugs. *The Journal of Clinical Pharmacology*, 47, 566-578.
- VACHON, P. H. & BEAULIEU, J.-F. 1992. Transient mosaic patterns of morphological and functional differentiation in the Caco-2 cell line. *Gastroenterology*, 103, 414-423.
- VALADAS, J., MOCELIN, R., SACHETT, A., MARCON, M., ZANETTE, R. A., DALLEGRAVE, E., HERRMANN, A. P. & PIATO, A. 2019. Propiconazole induces abnormal behavior and oxidative stress in zebrafish. *Environmental Science and Pollution Research*, 26, 27808-27815.
- VAN DEN BOGAARD, E. H., DAILEY, L. A., THORLEY, A. J., TETLEY, T. D. & FORBES, B. 2009. Inflammatory response and barrier properties of a new alveolar type 1-like cell line (TT1). *Pharmaceutical research*, 26, 1172-1180.
- VAN HAUTE, L., DE BLOCK, G., LIEBAERS, I., SERMON, K. & DE RYCKE, M. 2009. Generation of lung epithelial-like tissue from human embryonic stem cells. *Respiratory Research*, 10, 105.
- VILLENEUVE, D. L., CRUMP, D., GARCIA-REYERO, N., HECKER, M., HUTCHINSON, T. H., LALONE, C. A., LANDESMANN, B., LETTIERI, T., MUNN, S., NEPELSKA, M., OTTINGER, M. A., VERGAUWEN, L. & WHELAN, M. 2014. Adverse Outcome Pathway (AOP) Development I: Strategies and Principles. *Toxicological Sciences*, 142, 312-320.
- VINEIS, P., ROBINSON, O., CHADEAU-HYAM, M., DEGHAN, A., MUDWAY, I. & DAGNINO, S. 2020. What is new in the exposome? *Environment International*, 143, 105887.
- VINKEN, M. & BLAAUBOER, B. J. 2017. In vitro testing of basal cytotoxicity: Establishment of an adverse outcome pathway from chemical insult to cell death. *Toxicology in Vitro*, 39, 104-110.
- VISIOLI, F. 2015. Xenobiotics and human health: A new view of their pharma-nutritional role. *PharmaNutrition*, 3, 60-64.
- WALTER, E. & KISSEL, T. 1995. Heterogeneity in the human intestinal cell line Caco-2 leads to differences in transepithelial transport. *European journal of pharmaceutical sciences*, 3, 215-230.
- WANG, J. & URBAN, L. 2014. *Predictive ADMET: Integrated Approaches in Drug Discovery and Development*, John Wiley & Sons.
- WATSON, M. A., STEWART, R. K., SMITH, G., MASSEY, T. E. & BELL, D. A. 1998. Human glutathione S-transferase P1 polymorphisms: relationship to lung tissue enzyme activity and population frequency distribution. *Carcinogenesis*, 19, 275-280.
- WEI, Y., TONG, Y., YIN, Y. & CHEN, K. 2009. The variety of main air pollutants concentration and its relationship with meteorological condition in Nanjing City. *Transactions of Atmospheric Sciences*, 3.
- WEIBEL, E. R., COURNAND, A. F. & RICHARDS, D. W. 1963. *Morphometry of the human lung*, Springer.
- WIDDICOMBE, J. 1997. Airway liquid: a barrier to drug diffusion? *European Respiratory Journal*, 10, 2194-2197.
- WIEBE, B. M. & LAURSEN, H. 1995. Human lung volume, alveolar surface area, and capillary length. *Microscopy research and technique* 32, 255-262.
- WINDER, C., AZZI, R. & WAGNER, D. 2005. The development of the globally harmonized system (GHS) of classification and labelling of hazardous chemicals. *Journal of Hazardous Materials*, 125, 29-44.
- WINKLER, J., HOCHHAUS, G. & DERENDORF, H. 2004. How the Lung Handles Drugs. *Proceedings of the American Thoracic Society*, 1, 356-363.

- WISHART, D. S. 2016. Emerging applications of metabolomics in drug discovery and precision medicine. *Nature reviews Drug discovery*, 15, 473-484.
- WONG, H. L., GARTHWAITE, D. G., RAMWELL, C. T. & BROWN, C. D. 2018. Assessment of exposure of professional agricultural operators to pesticides. *Science of The Total Environment*, 619-620, 874-882.
- WU, B., WU, J., LIU, S., SHEN, Z., CHEN, L., ZHANG, X.-X. & REN, H.-Q. 2019. Combined effects of graphene oxide and zinc oxide nanoparticle on human A549 cells: bioavailability, toxicity and mechanisms. *Environmental Science: Nano*, 6, 635-645.
- WU, J.-J., CAO, Y.-F., FENG, L., HE, Y.-Q., HONG, J. Y., DOU, T.-Y., WANG, P., HAO, D.-C., GE, G.-B. & YANG, L. 2017. A naturally occurring isoform-specific probe for highly selective and sensitive detection of human cytochrome P450 3A5. *Journal of medicinal chemistry*, 60, 3804-3813.
- XIONG, Z., WANG, Y., LANG, L., MA, S., ZHAO, L., XIAO, W. & WANG, Y. 2018. Tissue metabolomic profiling to reveal the therapeutic mechanism of reduning injection on LPS-induced acute lung injury rats. *RSC Advances*, 8, 10023-10031.
- YAMANO, T. & MORITA, S. 1995. Effects of pesticides on isolated rat hepatocytes, mitochondria, and microsomes II. *Archives of Environmental Contamination and Toxicology*, 28, 1-7.
- YAN, Q., PAUL, K. C., WALKER, D. I., FURLONG, M. A., DEL ROSARIO, I., YU, Y., ZHANG, K., COCKBURN, M. G., JONES, D. P. & RITZ, B. R. 2021. High-Resolution Metabolomic Assessment of Pesticide Exposure in Central Valley, California. *Chemical Research in Toxicology*, 34, 1337-1347.
- YANAMALA, N., KISIN, E. R., MENAS, A. L., FARCAS, M. T., KHALIULLIN, T. O., VOGEL, U. B., SHURIN, G. V., SCHWEGLER-BERRY, D., FOURNIER, P. M. & STAR, A. 2016. In vitro toxicity evaluation of lignin-(un) coated cellulose based nanomaterials on human A549 and THP-1 cells. *Biomacromolecules*, 17, 3464-3473.
- YAO, H., XU, X., ZHOU, Y. & XU, C. 2018. Impacts of isopyrazam exposure on the development of early-life zebrafish (*Danio rerio*). *Environmental Science and Pollution Research*, 25, 23799-23808.
- YAQUB, N., WAYNE, G., BIRCHALL, M. & SONG, W. 2021. Recent advances in human respiratory epithelium models for drug discovery. *Biotechnology Advances*, 107832.
- YARPUZ-BOZDOGAN, N. 2018. The importance of personal protective equipment in pesticide applications in agriculture. *Current Opinion in Environmental Science & Health*, 4, 1-4.
- YE, M., BEACH, J., MARTIN, J. W. & SENTHILSELVAN, A. 2013. Occupational Pesticide Exposures and Respiratory Health. *Journal of Environmental Research and Public Health*, 10, 6442-6471.
- YILDIZ-PEKÖZ, A. & EHRHARDT, C. 2020. Advances in Pulmonary Drug Delivery. *Pharmaceutics*, 12, 911.
- YILMAZ, Y., WILLIAMS, G., WALLE, M., MANEVSKI, N., KRÄHENBÜHL, S. & CAMENISCH, G. 2019. Comparison of Rat and Human Pulmonary Metabolism Using Precision-cut Lung Slices (PCLS). *Drug Metabolism Letters*, 13, 53-63.
- YU, C. & DIU, C. 1982. A comparative study of aerosol deposition in different lung models. *American Industrial Hygiene Association Journal*, 43, 54-65.
- YUSOF, S. R., AVDEEF, A. & ABBOTT, N. J. 2014. In vitro porcine blood-brain barrier model for permeability studies: pCEL-X software pKaFLUX method for aqueous boundary layer correction and detailed data analysis. *European Journal of Pharmaceutical Sciences*, 65, 98-111.
- ZAJAC, M., DREANO, E., EDWARDS, A., PLANELLES, G. & SERMET-GAUDELUS, I. 2021. Airway Surface Liquid pH Regulation in Airway Epithelium Current Understandings and Gaps in Knowledge. *International Journal of Molecular Sciences*, 22, 3384.

- ZANOLI, J. C. C., MAIOLI, M. A., MEDEIROS, H. C. & MINGATTO, F. E. 2012. Abamectin affects the bioenergetics of liver mitochondria: A potential mechanism of hepatotoxicity. *Toxicology in vitro*, 26, 51-56.
- ZENG, Z., ANDREW, N. W., ARISON, B. H., LUFFER-ATLAS, D. & WANG, R. W. 1998. Identification of cytochrome P4503A4 as the major enzyme responsible for the metabolism of ivermectin by human liver microsomes. *Xenobiotica*, 28, 313-321.
- ZHANG, H., SLUTSKY, A. S. & VINCENT, J. L. 2000. Oxygen free radicals in ARDS, septic shock and organ dysfunction. *Intensive Care Medicine*, 26, 474-6.
- ZHANG, J. Y., FEN WANG, Y. & PRAKASH, C. 2006. Xenobiotic-metabolizing enzymes in human lung. *Current drug metabolism*, 7, 939-948.
- ZHANG, L., ZHANG, H., AI, H., HU, H., LI, S., ZHAO, J. & LIU, H. 2018. Applications of machine learning methods in drug toxicity prediction. *Current topics in medicinal chemistry*, 18, 987-997.
- ZHAO, G.-P., WANG, X.-Y., LI, J.-W., WANG, R., REN, F.-Z., PANG, G.-F. & LI, Y.-X. 2021a. Imidacloprid increases intestinal permeability by disrupting tight junctions. *Ecotoxicology and Environmental Safety*, 222, 112476.
- ZHAO, Y. H., ABRAHAM, M. H. & ZISSIMOS, A. M. 2003. Fast calculation of van der Waals volume as a sum of atomic and bond contributions and its application to drug compounds. *Journal of Organic Chemistry*, 68, 7368-73.
- ZHAO, Z., LUO, X.-S., JING, Y., LI, H., PANG, Y., WU, L., CHEN, Q. & JIN, L. 2021b. In vitro assessments of bioaccessibility and bioavailability of PM2.5 trace metals in respiratory and digestive systems and their oxidative potential. *Journal of Hazardous Materials*, 409, 124638.
- ZHU, C., JIANG, L., CHEN, T.-M. & HWANG, K.-K. 2002. A comparative study of artificial membrane permeability assay for high throughput profiling of drug absorption potential. *European journal of medicinal chemistry*, 37, 399-407.
- ZHU, W.-J., ZHANG, Z.-W., WANG, X.-S., XU, S.-W., LI, M. & LI, S. 2014. Effects of avermectin on microsomal cytochrome P450 enzymes in the liver and kidneys of pigeons. *Environmental Toxicology and Pharmacology*, 38, 562-569.
- ZHUANG, X. & LU, C. 2016. PBPK modeling and simulation in drug research and development. *Acta Pharmaceutica Sinica B*, 6, 430-440.
- ZUBROD, J. P., BUNDSCHUH, M., ARTS, G., BRÜHL, C. A., IMFELD, G., KNÄBEL, A., PAYRAUDEAU, S., RASMUSSEN, J. J., ROHR, J., SCHARMÜLLER, A., SMALLING, K., STEHLE, S., SCHULZ, R. & SCHÄFER, R. B. 2019. Fungicides: An Overlooked Pesticide Class? *Environmental Science & Technology*, 53, 3347-3365.
- ZULUAGA, M., ROBLEDO, S., OSORIO-ZULUAGA, G. A., YATHE, L., GONZALEZ, D. & TABORDA, G. 2016. Metabolomics and pesticides: systematic literature review using graph theory for analysis of references. *Nova*, 14, 121-138.

# Appendix

## Supplementary data (I)

MTT calibration curves, used to determine cell seeding density for MTT cytotoxicity assays

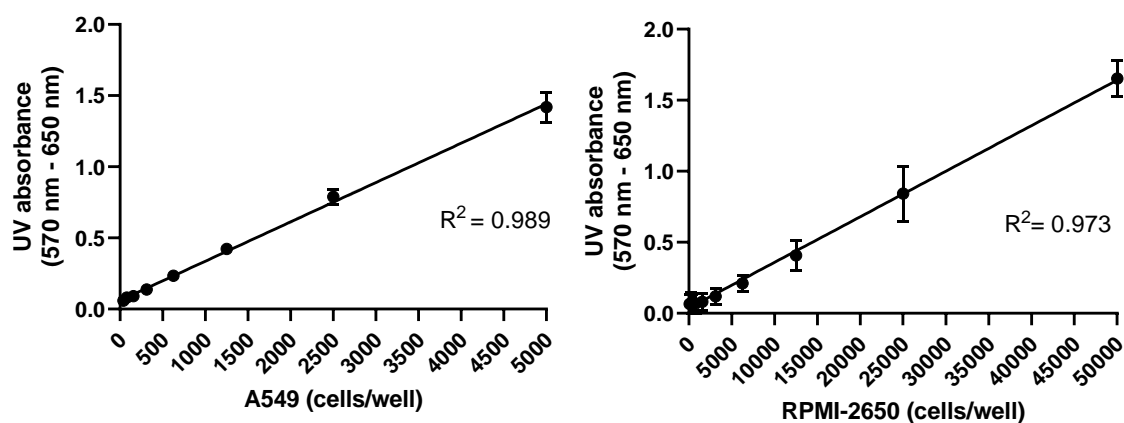


**Figure 0.1.** Calibration curves, plotting UV absorbance against cell number for (A) A549 or (B) RPMI-2650, following a 4 h incubation with MTT. Data represented as mean  $\pm$  SD (n=3).

Data for the other MTT assays is summarised in **Table 0.1**, the listed passage numbers were used for all experiments described in **Chapter 2-4**, with the exception of Calu-3 for which lower passage numbers (P20-25) and P7-10) were used in **Chapter 3** and **4** respectively. Caco-2 cells used in **Chapter 2-3**, were also of a low passage number (P20-25).

**Table 0.1.** Details for MTT calibration curves, including passage number, linear range and R<sup>2</sup> value (showing correlation between UV absorbance and cell number).

Cell line (Passage no.)	Linear range (cells/well)	R <sup>2</sup>
A549 (P50 – 60)	62.5 - 5000	0.989
BEAS-2B (P+3 – P+10)	313 - 20,000	0.995
Calu-3 (P50 – P60)	1563 – 50,000	0.994
RPMI-2650 (P+10 – P+20)	1563 - 50,000	0.973
TT1 (P+3 – P+10)	313 - 10,000	0.979
16HBE14o- (P25 – P34)	313 - 5,000	0.992

Human lung S9 fraction details, obtained commercially from Xenotech.

**Table 0.2. Human lung S9 fraction information. Donor details, serology information and enzyme activities, reported by XenoTech (Sample: H0610.PS9(NS)).**

Sample	Gender	Age	Race	Cause of Death	Smoked within past 10 years?
3	Male	75	Caucasian	Cerebrovascular accident	No
17	Female	37	Caucasian	Cerebrovascular accident	No
22	Female	49	African American	Head trauma	No
30	Male	22	Hispanic	Head trauma	No

**Serology information**

Cytomegalovirus: 3 donors tested positive and 1 donor tested negative.

All donors tested negative for Rapid Plasma Reagin, antibody to Human Immunodeficiency Virus, Hepatitis B Surface Antigen and antibody to Hepatitis C Virus.

Enzyme activities	Rate
NADPH-cytochrome c reductase	4.87 ± 0.00 (nmol/mg protein/min)
7-Ethoxyresorufin O-dealkylation	0.88 (pmol/mg protein/min)
Phenacetin O-dealkylation	1.46 ± 0.18 (pmol/mg protein/min)
Glucuronidation of 4-Methylumbelliferone	< 0.1 (nmol/mg protein/min)

The BCA assay was used to normal protein concentration for S9 fraction harvested from respiratory epithelial cell lines. Once diluted 1 mg/mL stocks were frozen, and later diluted to a final protein concentration of 0.5 mg/mL for the enzyme activity assays.

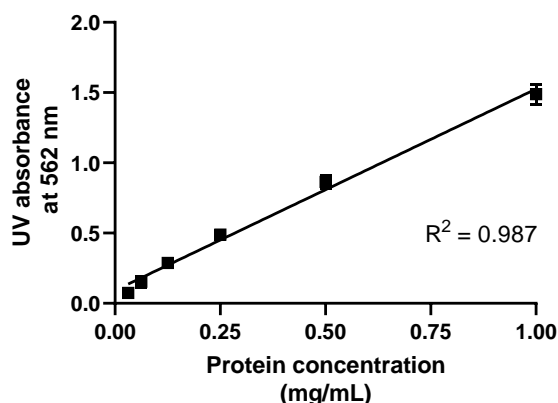
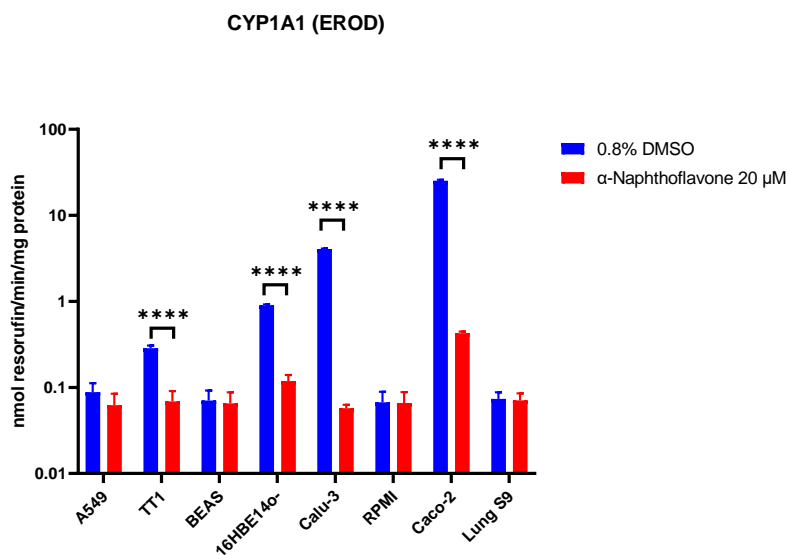


**Figure 0.2. Bicinchoninic acid (BCA) assay calibration curve, showing linearity between protein concentration and UV absorbance. Bovine serum albumin was used as the protein standard. Data represented as mean ± SD (n=3)**

### Functional activity data, for the individual xenobiotic metabolising enzymes

Commercially available human lung S9 was compared against S9 obtained from respiratory epithelial cell lines.

A



B

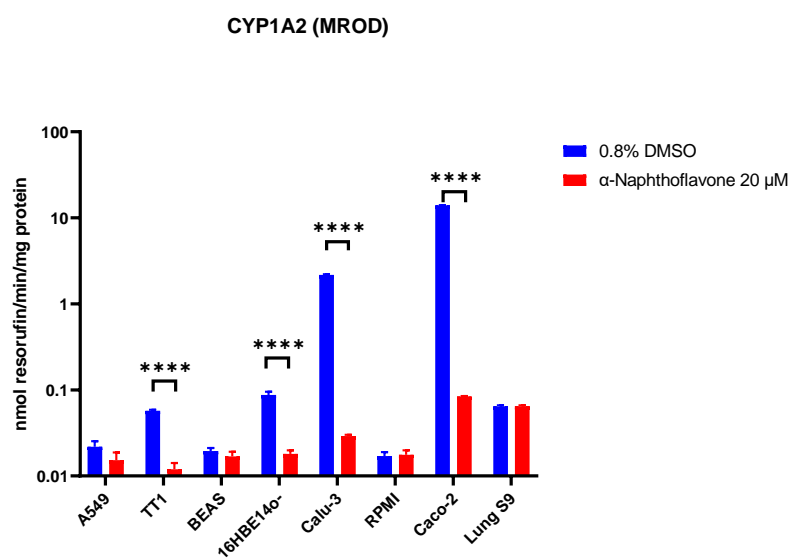
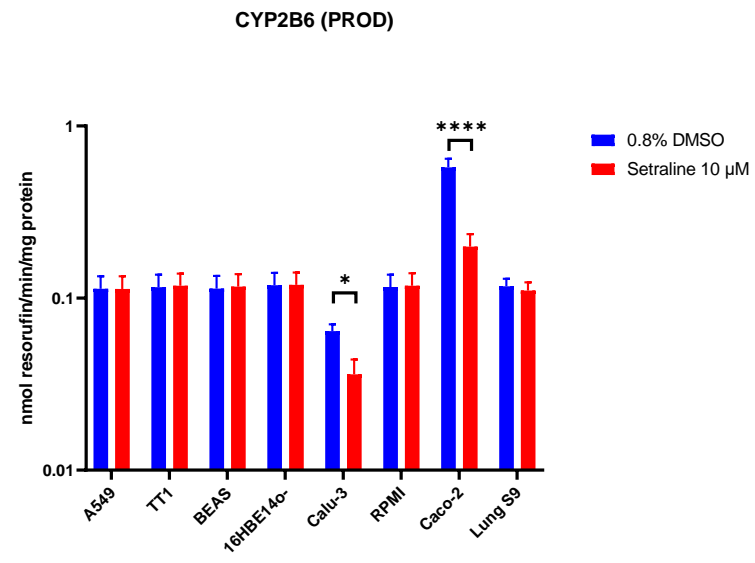


**Figure 0.3. (A) CYP1A1 and (B) CYP1A2 functional activity using the EROD and MROD assay, respectively. S9 fraction from respiratory epithelial cell lines or human lung S9 were used as the enzyme source. Data represented as mean  $\pm$  SD (n=3)**

**A**



**B**

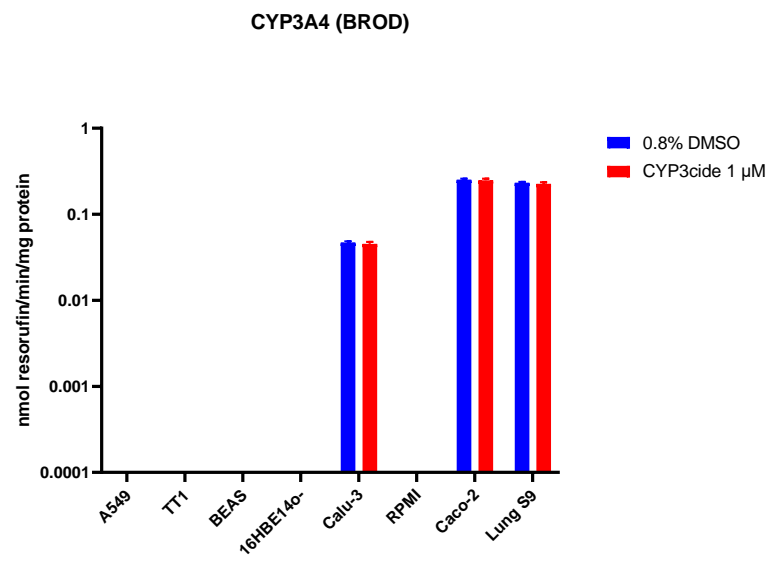
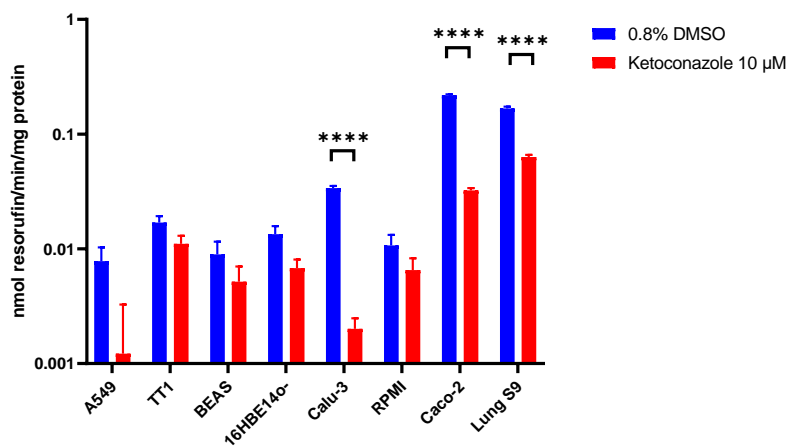


**Figure 0.4. (A) CYP2B6 and (B) CYP3A4 functional activity using the PROD and BROD assay, respectively. S9 fraction from respiratory epithelial cell lines or human lung S9 were used as the enzyme source. Data represented as mean  $\pm$  SD (n=3)**

A

CYP3A5 (BROD)



B

NQO1

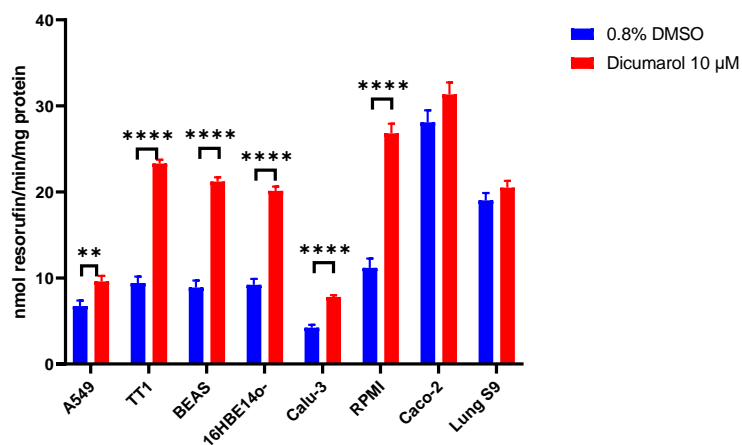
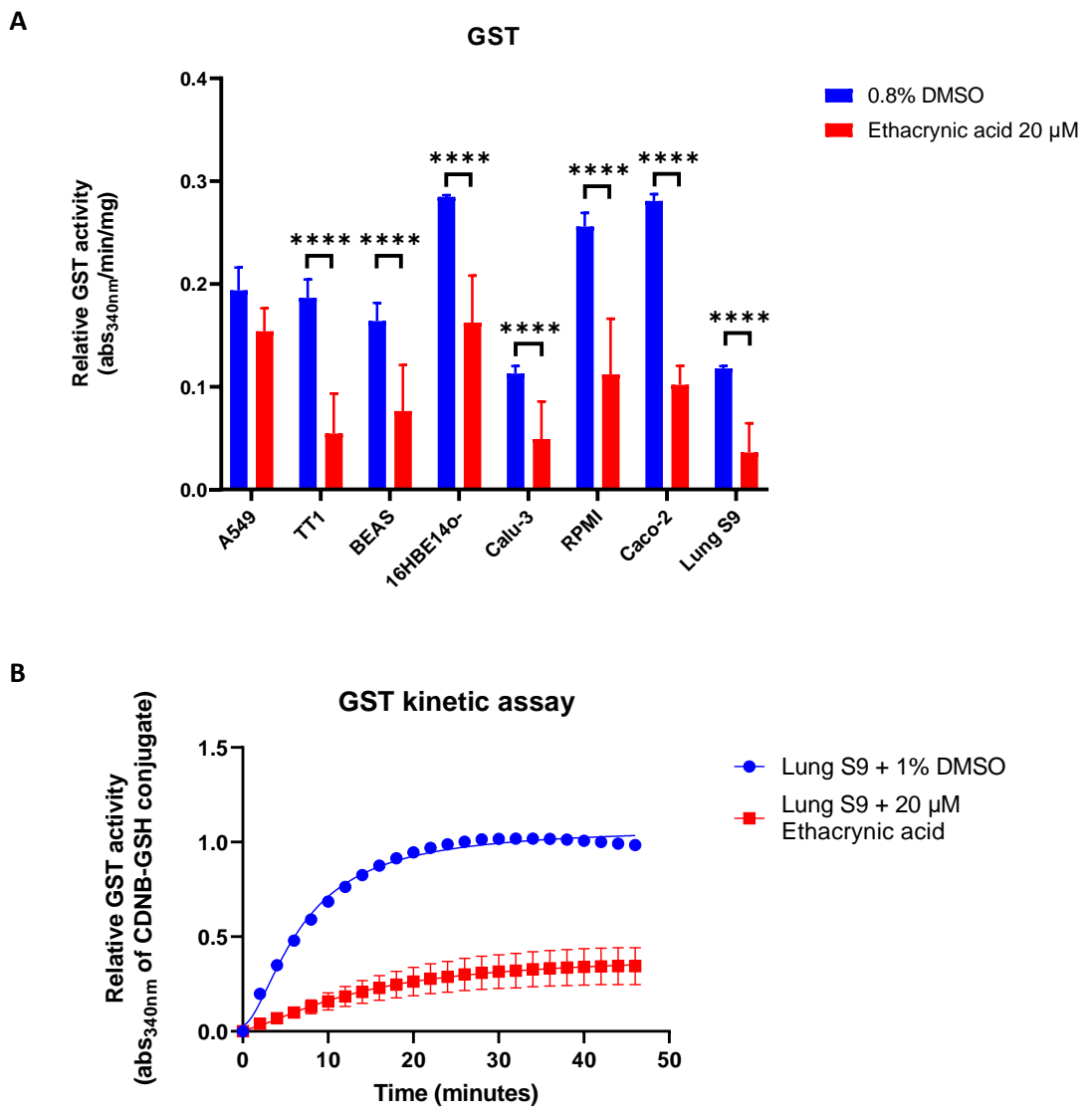


Figure 0.5. (A) CYP3A5 and (B) NQO1 functional activity using the BROD and resorufin assay, respectively. S9 fraction from respiratory epithelial cell lines or human lung S9 were used as the enzyme source. Data represented as mean  $\pm$  SD (n=3)



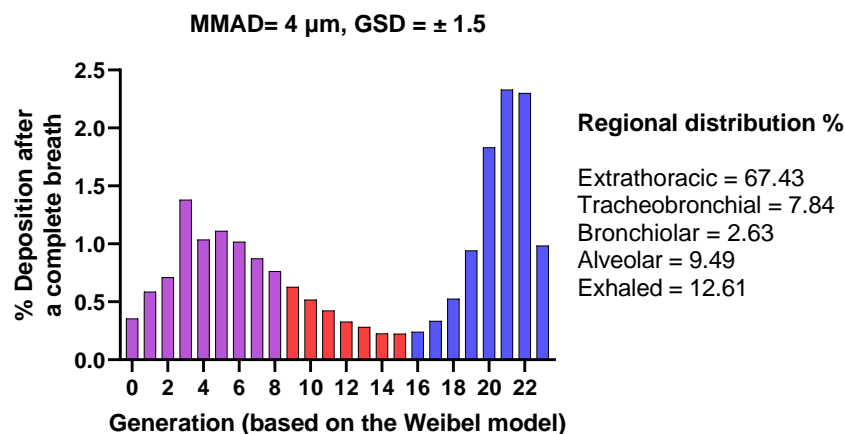


*Figure 0.6. GST functional activity using CDNB assay with and without the GST inhibitor ethacrynic acid 20 μM. (A) includes a comparison of the different S9 fractions, (B) highlights the kinetic assay for human lung S9. Data represented as mean ± SD (n=3)*

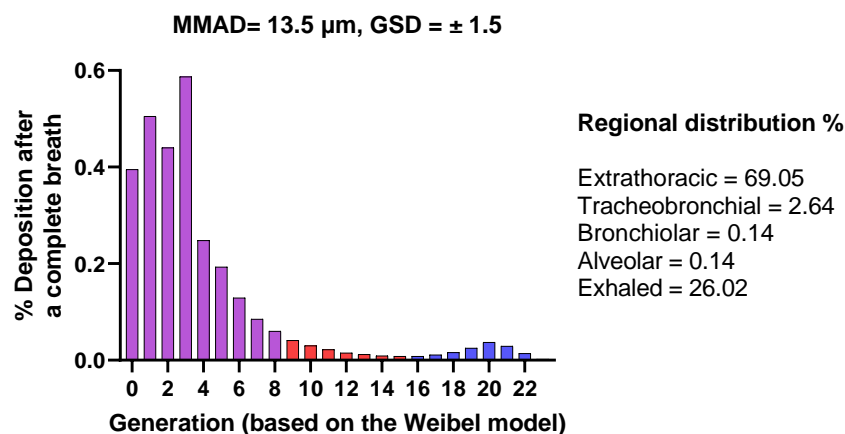
## Supplementary data (II)

Additional predicted aerosol deposition data (regional deposition in the respiratory tract)

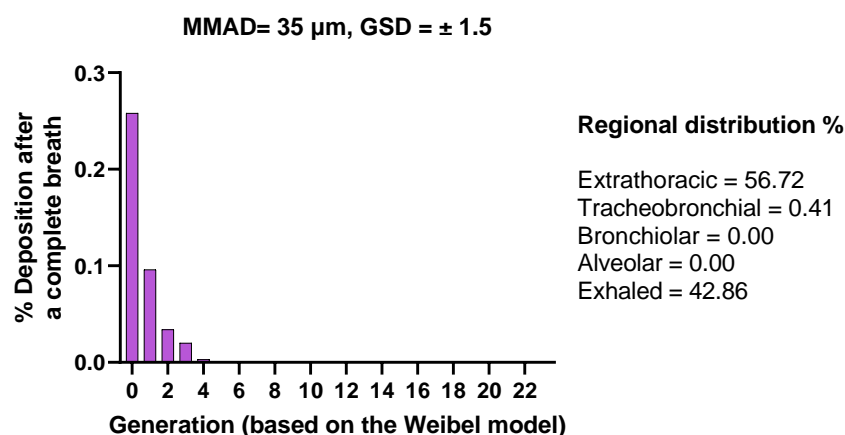
A



B



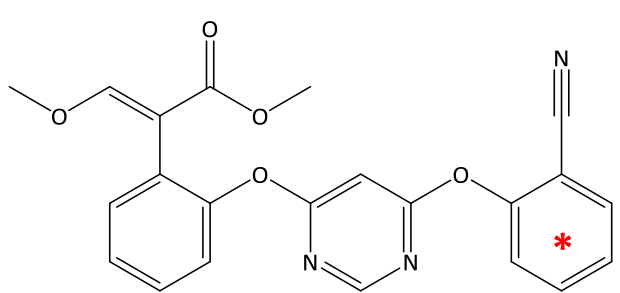
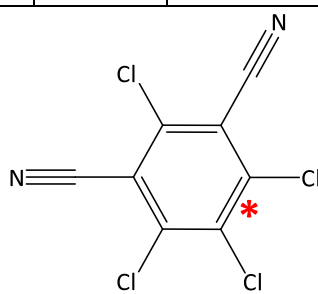
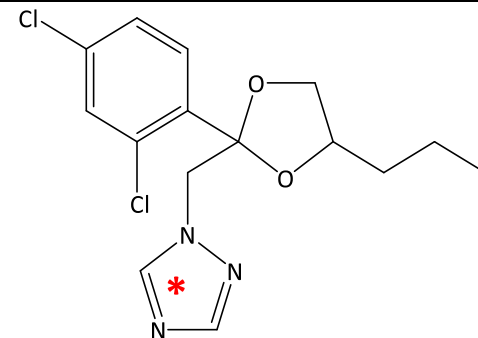
C



*Figure 0.7. Predicted regional lung deposition data for the generations of the tracheobronchial tree (based on the Weibel model) and also the % deposited in the extrathoracic region or exhaled. Data predicted using Mimetikos Preludium, for ambient aerosols with a median mass aerodynamic diameter of (A) 4  $\mu\text{m}$ , (B) 13.5  $\mu\text{m}$  or (C) 35  $\mu\text{m}$ . GSD = 1.5.*

**Activity and purity of radiolabelled pesticides used in Chapter 3.**

*Table 0.3. Summary of certificate of analysis data for the radiolabelled pesticides used within Chapter 3. <sup>14</sup>C position, activity (MBq), radiochemical purity (%), chemical purity (%) and supplier information are included.*

Radiochemical, [ <sup>14</sup> C]	Activity (MBq)	Radiochemical purity (%)	Chemical purity (%)	Supplier
<b>Azoxystrobin, [2-cyanophenyl ring-U-<sup>14</sup>C]</b>	10	100	99.84	Izotop, Institute of Isotopes Co. LTD (Budapest)
				
<b>Chlorothalonil, [<sup>14</sup>C(U)]-</b>	1.85	100	98.5	Moravek, (USA)
				
<b>Propiconazole, [triazol ring-U-<sup>14</sup>C]</b>	10	95.73	96.75	Izotop, Institute of Isotopes Co. LTD (Budapest)
				

Predicted maximum tissue concentrations following fungicide inhalation

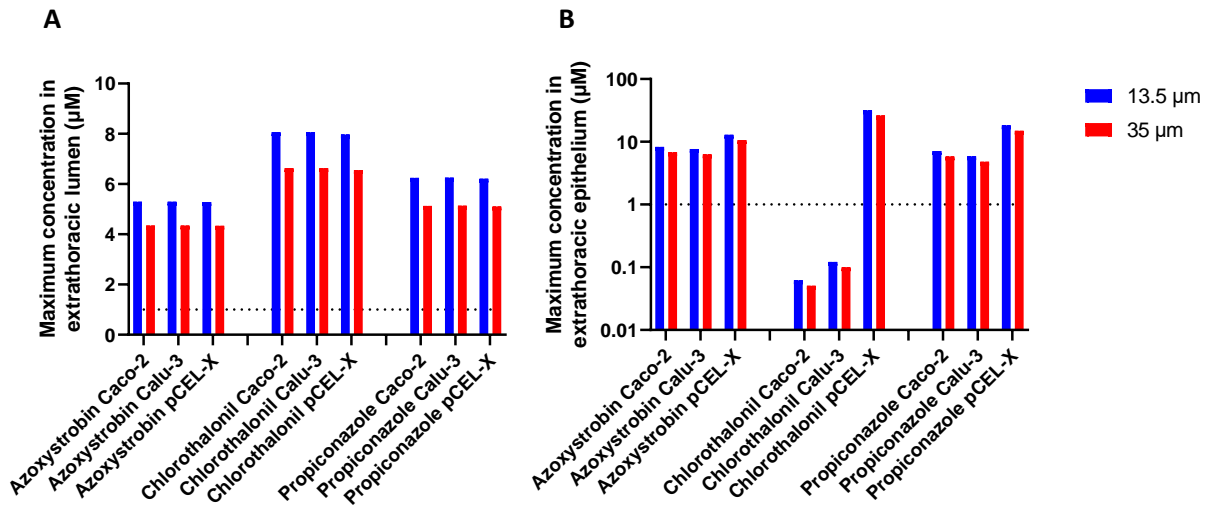


Figure 0.8. Predicted maximum fungicide concentration in (A) lumen or (B) epithelium of the extrathoracic region. Predicted using Mimetikos Preludium, with either in vitro or in silico data for aerosol exposures with an MMAD of 13.5 or 35 µm (GSD=1.5). The dotted line marks a fungicide concentration of 1 µM.

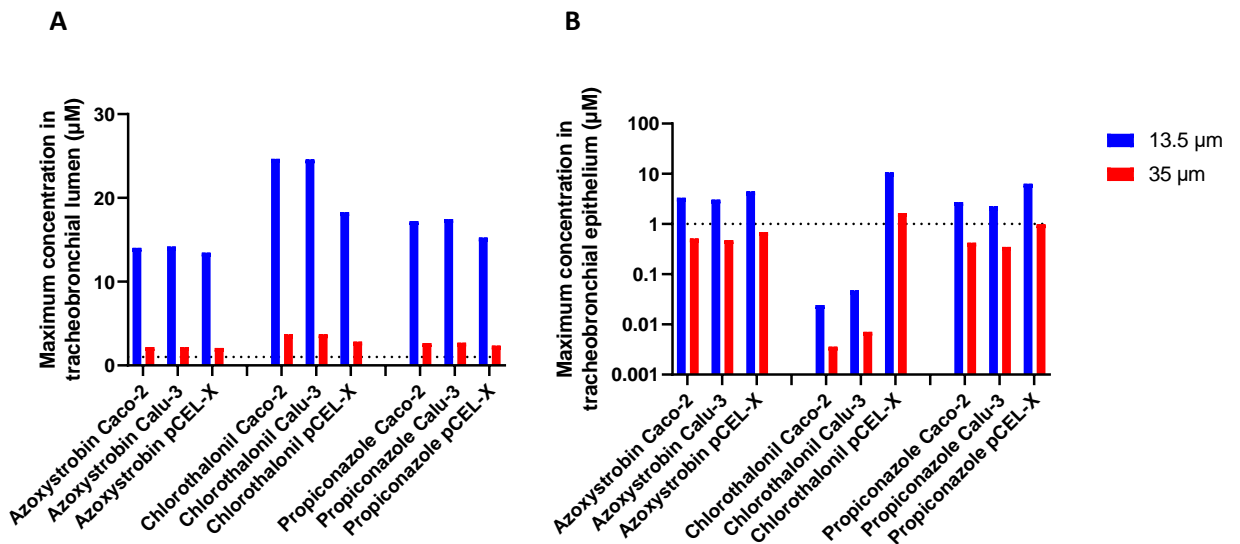


Figure 0.9. Predicted maximum fungicide concentration in (A) lumen or (B) epithelium of the tracheobronchial region. Predicted using Mimetikos Preludium, with either in vitro or in silico data for aerosol exposures with an MMAD of 13.5 or 35 µm (GSD=1.5). The dotted line marks a fungicide concentration of 1 µM.

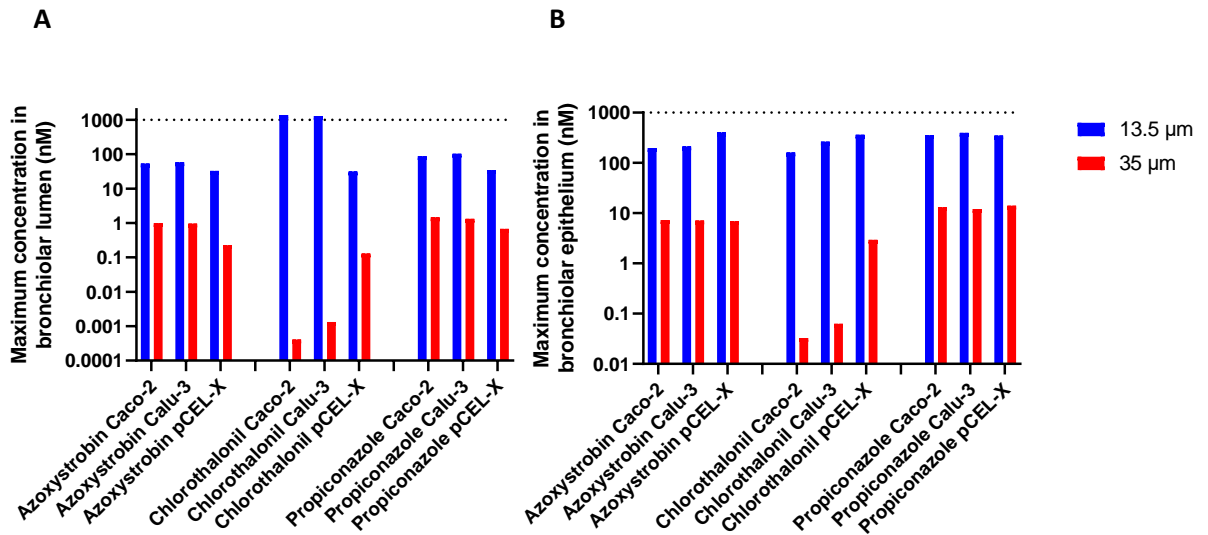


Figure 0.10. Predicted maximum fungicide concentration in (A) lumen or (B) epithelium of the bronchiolar region. Predicted using *Mimetikos Preludium*, with either *in vitro* or *in silico* data for aerosol exposures with an MMAD of 13.5 or 35  $\mu\text{m}$  (GSD=1.5). The dotted line marks a fungicide concentration of 1  $\mu\text{M}$ .

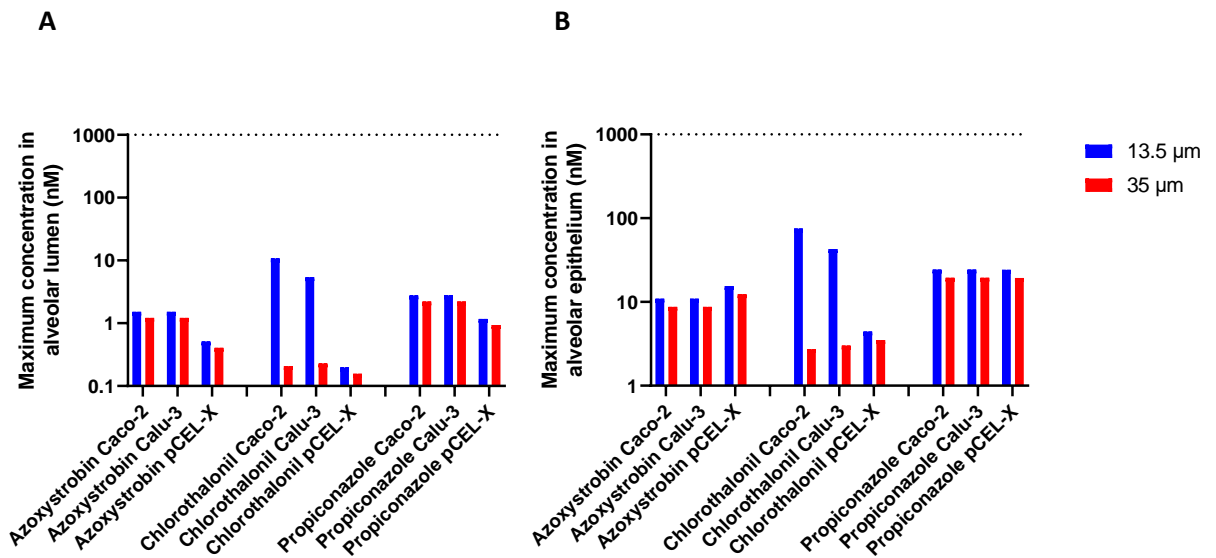


Figure 0.11. Predicted maximum fungicide concentration in (A) lumen or (B) epithelium of the alveolar region. Predicted using *Mimetikos Preludium*, with either *in vitro* or *in silico* data for aerosol exposures with an MMAD of 13.5 or 35  $\mu\text{m}$  (GSD=1.5). The dotted line marks a fungicide concentration of 1  $\mu\text{M}$ .

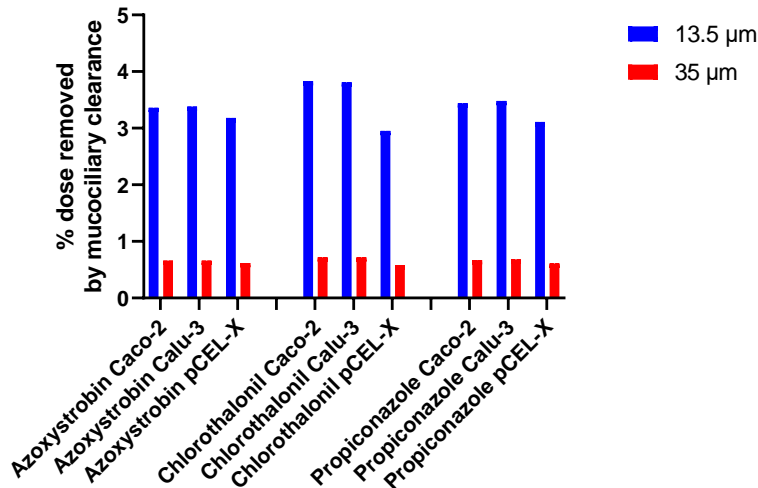


Figure 0.12. % Mucociliary clearance, predicted using *Mimetikos Preludium*, with either *in vitro* or *in silico* data for aerosol exposures with an MMAD of 13.5 or 35 µm (GSD=1.5).

In all cases, a lower MMAD resulted in greater mucociliary clearance due to increased deposition in the bronchial region of the respiratory tract (Figure 0.12). Mucociliary clearance was marginally higher when *in vitro* data was used, in comparison to *in silico* only predictions, this related to the inclusion of ASL binding data. Binding to ASL resulted in greater airway residence time, and increased the impact of mucociliary clearance.

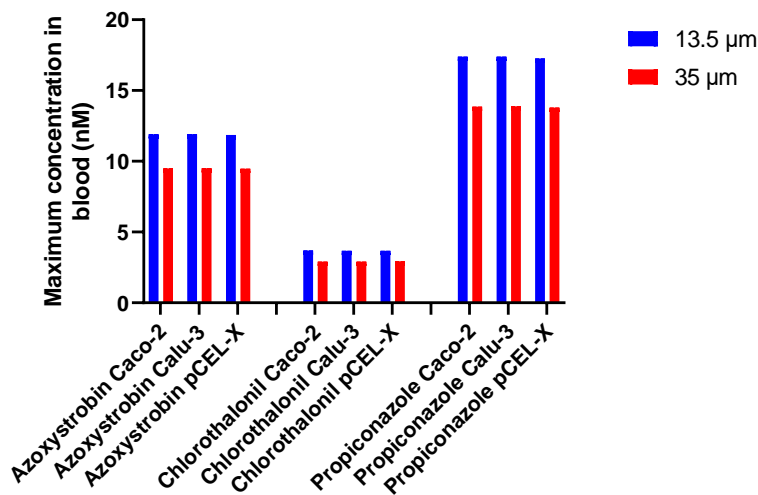


Figure 0.13. Maximum fungicide concentration in the blood, following an 8 h exposure to either an aerosol with an MMAD of 13.5 or 35 µm (GSD=1.5). Data was predicted using *Mimetikos Preludium* with either *in vitro* or *in silico* data for azoxystrobin, chlorothalonil or propiconazole, data includes the effect of both respiratory and oral bioavailability.

In all cases the maximum fungicide concentration in the blood (and overall bioavailability) was higher following exposure to an aerosol with an MMAD of 13.5 µm than 35 µm, due to greater deposition in the lower respiratory tract (Figure 0.13).

*Table 0.4. Summary of key toxicokinetic data predicted using Mimetikos Preludium, for the three fungicides and 3 different models. Data shown is based on for an 8 h exposure during mixing & loading (MMAD = 13.5  $\mu$ m). AUCt = Area under the Curve during the time modeled,  $C_{max}$  = maximum blood concentration, MCC% = % of total delivered dose cleared by mucociliary clearance,  $F_{pulm}$  % = % respiratory bioavailability (% absorbed of the total dose delivered to the lung),  $F_{tot}$  % = % total bioavailability (% absorbed of the total dose delivered to the body),  $C_{max_{LUMEN}}$  = maximum concentration dissolved in airway lumen,  $C_{max_{EPITHELIAL}}$  = maximum concentration in epithelial tissue.*

		Azoxystrobin	Chlorothalonil	Propiconazole
pCEL-X	AUCt (nM/h)	120.69	47.89	161.81
	$C_{max}$ (nM)	11.85	3.68	17.26
	Tmax (h)	9.47	10.30	9.22
	MCC %	3.18	2.95	3.11
	$F_{pulm}$ %	21.54	27.18	23.31
	$F_{tot}$ % (Oral + Respiratory)	80.17	20.88	91.09
	$C_{max_{LUMEN}}$ ( $\mu$ M)	13.46	18.30	15.26
	$C_{max_{EPITHELIAL}}$ ( $\mu$ M)	12.94	31.78	18.25
Caco-2	AUCt (nM/h)	121.12	46.38	162.18
	$C_{max}$ (nM)	11.91	3.69	17.38
	Tmax (h)	9.45	10.33	9.22
	MCC %	3.36	3.83	3.44
	$F_{pulm}$ %	17.21	5.61	15.24
	$F_{tot}$ % (Oral + Respiratory)	80.14	20.18	91.06
	$C_{max_{LUMEN}}$ ( $\mu$ M)	14.04	24.65	17.21
	$C_{max_{EPITHELIAL}}$ ( $\mu$ M)	8.26	0.06	7.08
Calu-3	AUCt (nM/h)	121.11	46.38	162.20
	$C_{max}$ (nM)	11.91	3.68	17.40
	Tmax (h)	9.45	10.32	9.22
	MCC %	3.38	3.81	3.48
	$F_{pulm}$ %	16.69	6.15	14.26
	$F_{tot}$ % (Oral + Respiratory)	80.14	20.2	91.05
	$C_{max_{LUMEN}}$ ( $\mu$ M)	14.18	24.59	17.47
	$C_{max_{EPITHELIAL}}$ ( $\mu$ M)	7.66	0.12	5.87

### Supplementary data (III)

NMR pre-analysis data (prior to metabolite annotation), highlighting extracellular metabolomic differences between the cell lines (DMSO controls).

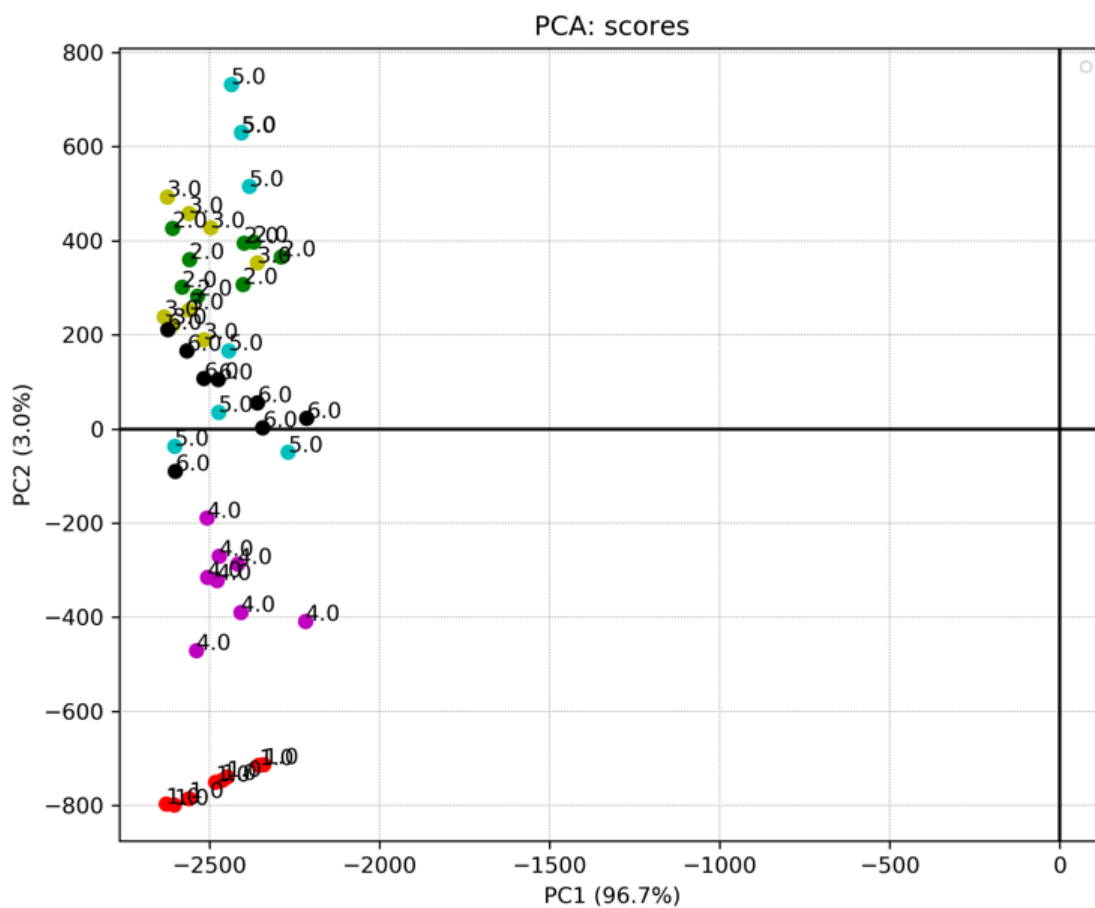


*Figure 0.14. Principal component analysis (PCA) plot comparing NMR metabolomics samples for (1) Fresh media, (2) A549, (3) TT1, (4) BEAS-2B, (5) 16HBE14o- and (6) Calu-3. All samples represent only media, with no pesticides added.*



OPLS-DA plots highlighting metabolomic differences between the tested cell lines. In all cases the differences between the compared groups were statistically significant ( $Q^2 > 0.5$ ).

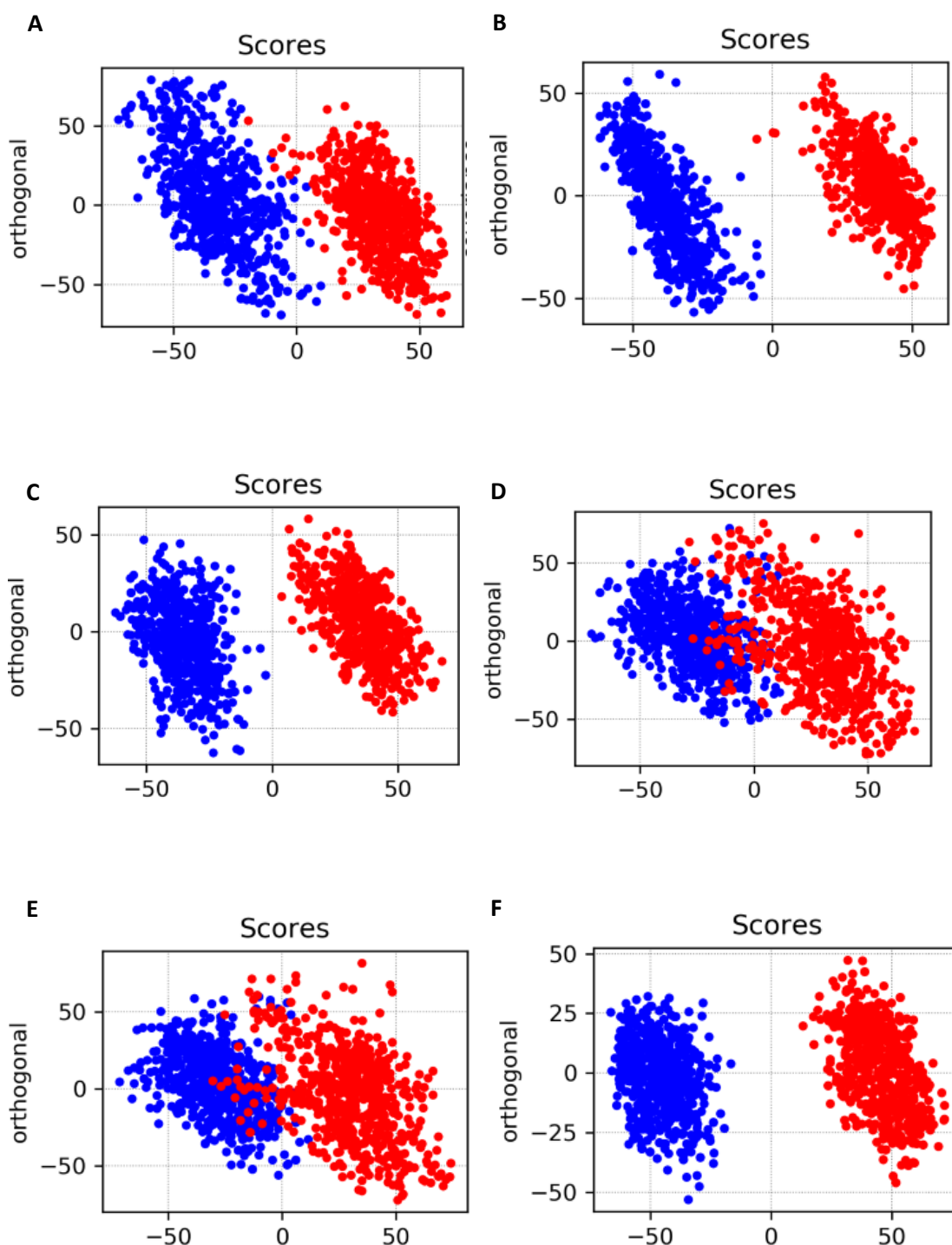


**Figure 0.15.** OPLS-DA plots illustrating discrimination between the metabolomic profiles of the DMSO control groups for the different cell lines, (A) A549\* vs TT1, (B) TT1\* vs 16HBE14o-, (C) TT1\* vs BEAS-2B, (D) A549\* vs Calu-3, (E) BEAS-2B\* vs Calu-3 and (F) BEAS-2B\* vs 16HBE14o-. Cell lines with \* are plotted in blue, those without are plotted in red. Data shown represents 4 individual experiments ( $n=4$ ) performed with duplicate samples to give a total of 8 replicates.